UNIVERSITÉ DU QUÉBEC À MONTRÉAL

ÉTUDE QUANTITATIVE DU CYCLE DE L'EAU À L'ÉCHELLE DES GRANDS BASSINS VERSANTS DE L'AMÉRIQUE DU NORD AVEC LE MODÈLE RÉGIONAL CANADIEN DU CLIMAT

THÈSE
PRÉSENTÉE
COMME EXIGENCE PARTIELLE
DU DOCTORAT EN SCIENCES DE L'ENVIRONNEMENT

PAR
BILJANA MUSIC

MARS 2008

À ma famille

REMERCIEMENTS

Je tiens d'abord et avant tout à remercier du fond du cœur mon directeur de recherche, Daniel Caya pour son encadrement, sa disponibilité, sa patience, sa flexibilité, sa gaieté et son soutien financier, mais surtout pour sa compréhension sans bornes dans des moments difficiles tout au long de cette thèse. Ce que j'apprécie énormément, c'est le soin qu'il a mis à me donner une perspective future. Merci beaucoup! Sur la même voie, j'adresse un merci très chaleureux à René Laprise, mon co-directeur, dont l'esprit rigoureusement scientifique n'a cessé de m'épater. Je lui suis particulièrement reconnaissante pour ses commentaires pertinents sur mon premier article. Enfin, je me sens privilégiée d'avoir eu la chance de côtoyer ces deux grands chercheurs qui m'ont grandement aidée et encouragée.

Aussi, je remercie le Groupe de Simulations Climatiques du consortium Ouranos pour son large apport en aide technique et scientifique : Sébastien Biner, Michel Giguère, surtout Anne Frigon, Hélène Côté et Dominique Paquin qui ont répondu à bon nombre de mes questions. Je suis également reconnaissante à Michel Slivitzky et à Ramón de Elía pour leurs conseils judicieux, à Richard Harvey pour sa discussion riche en informations sur CLASS, à Philippe Lucas-Picher pour son aide précieuse en informatique et ses corrections, à David Plummer, à Dorothée Charpentier et à Dominique Paquin qui ont également apporté quelques corrections d'orthographe et de syntaxe, à Mourad Labassi et à Georges Huard pour leurs soutien technique ainsi que à Dorina Surcel-Colan, à Kristina Stefanov et à Pascale Martineau pour le soutien moral qu'elles m'ont offert. Je remercie particulièrement ma collègue de bureau, Leticia Hernandez-Diaz, dont la personnalité si chaleureuse est venue à mon secours dans les moments les plus difficiles et qui a si bien su m'encourager. Aussi, je remercie mes compatriotes, Slavica Antic, Milena Dimitrijevic, Biljana

Bekcic et Radenko Pavlovic, car nous avons traversé ensemble les étapes d'adaptation suite à notre immigration.

Merci à Peter Zwack, qui faisait partie de mon comité d'encadrement, pour son encouragement sans limites. Le souvenir de cet homme exceptionnel et de sa grandeur d'âme, dont la mort m'a profondément touchée, garde une place importante dans mon coeur.

Je tiens aussi à exprimer ma profonde gratitude à tous les membres du jury : à Laxmi Sushama, à René Roy, à Alain Rousseau, à René Laprise et à Daniel Caya pour leurs commentaires pertinents sur la thèse.

Un grand merci à tous mes professeurs de l'Institut de Météorologie à l'Université de Belgrade grâce auxquels j'ai acquis mes premières connaissances en météorologie: à Mladjen Curic, à Borivoje Rajkovic, à Lazar Lazic, à Dejan Janc, à Fedor Mesinger et à Zavisa Janjic.

Je remercie également la Fondation canadienne pour les sciences du climat et de l'atmosphère (FCSCA) et Réseau canadien en modélisation et diagnostics du climat régional (MDCR) pour leur appui financier par l'intermédiaire de bourses de recherche doctorale.

Finalement, je dédie cette thèse à ma famille car sans elle, je ne serais pas allée bien loin. Un gros merci à mon époux, Nedzad Music, qui n'a jamais cessé de m'encourager, qui a vu passer mes vagues d'inquiétude et de mauvaise humeur et qui a été une grande source de motivation. Merci à mes enfants, mes cœurs, mes soleils, Sanela et Dino, qui ont éclairé mes journées et rempli mon cœur d'allégresse. Ma fille a même lu certaines parties de la thèse et y a apporté des corrections linguistiques. Merci à ma tante Dina Stoilkov, pour l'aide précieuse qu'elle m'a apportée tout au long de mes études. Merci à ma belle-mère, Remzija Music, qui a fait le voyage jusqu'au Canada plusieurs fois pour venir m'apporter son aide et enfin, merci à mon frère, Blaza Djordjev, qui m'a encouragée de loin, à mon père, Randjel Djordjev que j'espère avoir rendu fier, ainsi qu'à ma mère, Julka Djordjev, dont le souvenir me redonnait du courage.

TABLE DES MATIÈRES

LISTE DES TABLEAUX viii
LISTE DES FIGURES ix
RÉSUMÉ xvi
CHAPITRE I 3
INTRODUCTION GÉNÉRALE 3
1.1 Problématique et contexte de la recherche 3
1.2 Objectifs 9
1.3 Méthode générale 10
1.4 Plan 12
Bibliographie 14
CHAPITRE II 23
EVALUATION OF THE HYDROLOGICAL CYCLE OVER THE MISSISSIPPI RIVER BASIN AS SIMULATED BY THE CANADIAN REGIONAL CLIMATE MODEL (CRCM) 23
2.1 Introduction 25
2.2 Water budget analysis 27
2.2.1 Water budget equations 27
2.2.2 Validation methodology 29
2.3 CRCM description and experimental configuration 32
2.3.1 Model description 32
2.3.2 Experimental setup 35
2.4 Validation Datasets 36
2.4.1 Precipitation dataset 37
2.4.2 Runoff datasets 38
2.4.3 Reanalyses Datasets 40

2.5 Results and discussion....42
2.5.1 Analysis of the CRCM_V3.6 simulation: annual means of water budget components....42
2.5.2 Analysis of the CRCM_V3.6 simulation: climatological annual cycle of water budget components....45
2.5.3 Analysis of the CRCM_V4.0 simulation: annual mean of water budget components....49
2.5.4 Analysis of the CRCM_V4.0 simulation: climatological annual cycle of water budget components....50
2.5.5 Spatial distribution: validation of the CRCM_V3.6 simulated fields .52
2.5.6 Spatial distribution: validation of the CRCM_V4.0 simulated fields .53
2.6 Summary and conclusion....54
Acknowledgements....59
References....60
CHAPITRE III....78
INVESTIGATION OF THE SENSITIVITY OF WATER CYCLE COMPONENTS SIMULATED BY THE CANADIAN REGIONAL CLIMATE MODEL (CRCM) TO THE LAND SURFACE PARAMETERIZATION, THE LATERAL BOUNDARY DATA AND THE INTERNAL VARIABILITY....78
3.1 Introduction....81
3.2 Methodology and experimental setup....84
3.3 Results and discussion....87
3.3.1 Analysis of climatological means....87
3.3.2 Analysis of the climatological annual cycles....95
3.4 Summary and conclusion....102
Acknowledgements....105
References....806
CHAPITRE IV....131
CONCLUSION GÉNÉRALE....131

4.1 Conclusions principales de la recherche 131
4.2 Pertinence de la recherche, contribution à l'avancement des connaissances et originalité 136
4.3 Limites de la recherche 137
4.4 Travaux futurs et recommandations 140
Bibliographie 142
APPENDICE A 144
LAND-SURFACE PARAMETERISATION: A REVIEW 145
A.1 Introduction 146
A2. Radiative transfer between the land surface and the atmosphere 149
A3. Turbulent transfer between the land surface and the atmosphere 152
A3.1. Momentum turbulent flux 154
A3.2. Sensible heat fluxes 159
A3.3. Latent heat fluxes 163
A3.3.1. Bare soil evaporation 164
A3.3.2. Wet canopy evaporation and dry canopy transpiration 167
A4. Surface energy balance and soil and/or canopy temperature 169
A5. Surface water balance 176
A5.1. Prognostic equations for soil moisture 176
A5.2. Prognostic equations for canopy intercepted water 181
A6. Snow cover in Land Surface Models 182
A7. Validation and intercomparison of Land Surface Models 184
A8. Conclusion and point of view 190
Acknowledgement 193
References 194

LISTE DES TABLEAUX

Tableau 1.1 Moyennes spatiales de température et de précipitation pour les bassins du Mississippi, Saint-Laurent et Mackenzie, calculées à partir des données de CRU (Mitchell and Jones 2005). 19

Tableau 1.2 Paramétrages physiques utilisés dans le MRCC. 20

Tableau 3.1 Experimental configurations of the CRCM simulations. 111

Tableau 3.2 Change in climatological means (in mm day^{-1} and in %) of the water budget components for the period 1961-99 as a response to the change in land surface parameterisation (MAN vs CLASS), lateral boundary conditions (ERA40 vs NCEP) and internal variability (initial conditions). The error in closing the simulated water budget is also indicated. A star indicates a statistically significant change at the level $\alpha = 0.05$. 112

Tableau 3.3 Streamflow data sources 113

Tableau 3.4 Biases of simulated climatological means (in mm day^{-1} and in %) of precipitation (BIAS_P), evapotranspiration (BIAS_E), vertically integrated moisture flux convergence (BIAS_C) and runoff (BIAS_R). BIAS_P is calculated with respect to the mean observed precipitation; BIAS_E is calculated with respect to the average of the estimates based on terrestrial water budget; BIAS_R is calculated with respect to naturalized runoff (R_NAT) for the Mississippi basin, observed runoff (R_OBS) for the Mackenzie basin, and averaged runoff (observed, VIC and GRDC runoff, R_MEAN) for the St. Lawrence basin; BIAS_C is calculated with respect to the averaged NCEP/NCAR and ERA40 convergence. 114

LISTE DES FIGURES

Fig. 1.1 Les régions incluses dans les expériences « GEWEX CSEs » (source : Lawford et al. 2004) 21

Fig. 1.2 Fraction de canopée végétale dans CLASS : a) conifères ; b) feuillus ; c) terres arables ; d) herbes et toundra. 22

Fig. 2.1 Schematic illustration of combined atmospheric and terrestrial water balance. 66

Fig. 2.2 CRCM simulation domain with the topography (m). The Mississippi River basin outline is also indicated. 67

Fig. 2.3 Annual means (1988-1997) of the atmospheric and terrestrial water budget components, in mm/day, over the Mississippi River basin. 68

Figs. 2.4 Annual cycles of simulated and observed (quasi-observed) atmospheric water budget components averaged over the Mississippi River basin: (a) precipitation, P; (b) evapotranspiration, E; (c) vertically integrated horizontal moisture convergence, C; (d) atmospheric water storage tendency, $AWST$. 69

Fig. 2.5 The CRCM simulation biases of precipitation (BIAS_P), atmospheric moisture flux convergence (BIAS_C), atmospheric water storage tendency (BIAS_AWST). The error in closure of the water budget is also indicated (CLOSURE_ERROR) 70

Fig. 2.6 Annual cycle of simulated and quasi-observed terrestrial water budget components averaged over the Mississippi River basin: (a) runoff, R; $(P - E)$ forcing term (b) and of terrestrial water storage tendency, TWST(c). 71

Tableau 3.5 Change in interannual standard deviation (SWE) of the water budget components for the period 1961-99 as a response to the change in land surface parameterisation (MAN vs CLASS), lateral boundary conditions (ERA40 vs NCEP) and initial conditions (Internal variability). The error in closuring the simulated water budget is also indicated. A star indicates a statistically significant change at the level $\alpha = 0.05$ 115

Tableau A1. Summary of CHASM's experimental configurations (Desborough, 1999). 201

Fig. 2.7 The CRCM simulation biases of the terrestrial water cycle branch. 72
Fig. 2.8 Annual cycle of the CRCM simulated net radiative energy at the surface (RN), latent heat flux (LH) and sensible heat flux (SH) averaged over the Mississippi River basin. 73
Fig. 2.9 Annual cycle of the difference between the CRCM_V4.0 and CRCM_V3.6 evapotranspiration (DELTA_E), precipitation (DELTA_P), atmospheric moisture flux convergence (DELTA_C), atmospheric water storage tendency (AWST). The error in closure of the water budget is also indicated (CLOSURE_ERROR_CRCM_3.6, CLOSURE_ERROR_CRCM_4.0). 74
Fig. 2.10 CRCM annual mean precipitation and corresponding reference fields. 75
Fig. 2.11 CRCM annual mean runoff and corresponding reference fields. 76
Fig. 2.12 CRCM annual mean evapotranspiration and corresponding reference fields. 77
Fig. 3.1 CRCM simulation domain and topography. The Mississippi, St. Lawrence and Mackenzie River basins outlines are also indicated. 116
Fig. 3.2 Comparison of simulated and observed (quasi-observed) water budget components averaged in space over a basin and in time over a ten-year period. C: Convergence; P: Precipitation; E: Evapotranspiration; EST: Estimated; TB: Terrestrial Budget; AB: Atmospheric Budget. 117
Fig. 3.3 Difference between climatological monthly means of the atmospheric (left) and terrestrial (right) water budget components for the SS/RS simulation pair. Value on the curve identified by a star indicates statistically significant difference at the level a = 0.05. 118
Fig. 3.4 Difference between climatological monthly means of snow water equivalent for SS/RS simulation pair. 119
Fig. 3.5 Difference between climatological monthly means of the atmospheric and terrestrial water budget for the BC/RS simulation pair. A star indicates statistically significant difference at the level $\alpha = 0.05$. 120

Fig. 3.6 Difference between climatological monthly means of the atmospheric and terrestrial water budget for the IC/RS simulation pair.....121

Fig. 3.7 Annual cycles of simulated and observed (quasi-observed) water budget components over the Mississippi River basin for the period 1988-97: (a) precipitation, *P*; (b) evapotranspiration, *E*; (c) vertically integrated horizontal moisture convergence, *C*; (d) atmospheric water storage tendency, *AWST*; (e) runoff, *R*; (f) terrestrial water storage tendency, *TWST*; (g) difference between precipitation and evapotranspiration, *P-E*; (h) snow water equivalent, SWE...122

Fig. 3.8 The simulation biases for the atmospheric water budget components for the Mississippi basin: bias of simulated *P* with respect to the average of CCR, GPCP and CRU precipitation, BIAS_P(MEAN); bias of the simulated *C* with respect to the one of the NCEP/NCAR and ERA40, BIAS_C(NCEP/ERA40); bias of the simulated *AWST*, BIAS_AWST(NCEP/ERA40). The error in closuring the simulation water budget is also shown. 123

Fig. 3.9 The simulation biases for the terrestrial water budget components for the Mississippi basin: bias of simulated *R* with respect to the naturalized runoff, BIAS_R; bias of the simulated *TWST*, BIAS_TWST(NCEP/ERA40); bias of the simulated *P-E*, BIAS_P-E(NCEP/ERA40).....124

Fig. 3.10 Annual cycles of simulated and observed (quasi-observed) water budget components over the St. Lawrence basin for the period 1988-97. (a) precipitation, *P*; (b) evapotranspiration, *E*; (c) vertically integrated horizontal moisture convergence, *C*; (d) atmospheric water storage tendency, *AWST*; (e) runoff, *R*; (f) terrestrial water storage tendency, *TWST*; (g) difference between precipitation and evapotranspiration, *P-E*; (h) snow water equivalent, SWE...125

Fig. 3.11 The simulation biases for the St. Lawrence RB: bias of simulated *P* with respect to the CANGRID/GPCP/CRU precipitation, BIAS_P(CNGRD/GPCP/CRU); bias of the simulated C with respect to the averaged NCEP/NCAR and ERA40 moisture flux convergence, BIAS_C(MEAN); bias of the simulated AWST, with respect to the averaged

NCEP/NCAR and ERA40 AWST, BIAS_AWST(MEAN). The error in closuring the simulation water budget is also shown.....126

Fig. 3.12 The simulation biases for the terrestrial water budget components for the St. Lawrence basin: bias of simulated *R* with respect to the VIC runoff, BIAS_R; bias of the simulated *TWST* with respect to the averaged NCEP/NCAR and ERA40 *TWST*, BIAS_TWST(MEAN); bias of the simulated *P-E*, BIAS_P-E. 127

Fig. 3.13 Annual cycles of simulated and observed (quasi-observed) water budget components over the Mackenzie basin for the period 1987-96. (a) precipitation, *P*; (b) evapotranspiration, *E*; (c) vertically integrated horizontal moisture convergence, *C*; (d) atmospheric water storage tendency, *AWST*; (e) runoff, *R*; (f) terrestrial water storage tendency, *TWST*; (g) difference between precipitation and evapotranspiration, *P-E*; (h) snow water equivalent, SWE. 128

Fig. 3.14 The simulation biases for the Mackenzie basin: bias of simulated *P* with respect to the CANGRD/GPCP/CRU precipitation, BIAS_P(CNGRD/GPCP/CRU); bias of the simulated C with respect to the averaged NCEP/NCAR and ERA40 moisture flux convergence, BIAS_C(MEAN); bias of the simulated AWST, with respect to the averaged NCEP/NCAR and ERA40 AWST, BIAS_AWST(MEAN). The error in closuring the simulation water budget is also shown.....129

Fig. 3.15 The simulation biases for the terrestrial water budget components for the Mackenzie basin: bias of simulated *R* with respect to the VIC runoff, BIAS_R; bias of the simulated *TWST* with respect to the averaged NCEP/NCAR and ERA40 *TWST*, BIAS_TWST(MEAN); bias of the simulated *P-E*, BIAS_P-E. 130

Fig. A1. Turbulent transfer regimes considered in SiB2 (modified from Sellers et al., 1996): z_1-height of canopy bottom, z_2- height of canopy top, z_c- inflection height for leaf-area density, z_s- ground roughness length, z_r- reference height, z_o- canopy

roughness length, d- canopy zero plane displacement height, h_a- water vapour and sensible heat source height, u_1, u_2 and u_r- wind velocity at z_1, z_2 and z_r, respectively, r_d-aerodynamic resistance for heat (vapour) transfer between the ground and canopy air space, r_a- aerodynamic resistance between the canopy air space and the reference height, and r_b- aerodynamic resistance between the canopy surface and canopy air space. 203
Fig. A2. Transfer pathways for sensible heat as conceptualised in SiB2 (modified from Sellers et al., 1996).....204
Fig. A3. Transfer pathways for latent heat as conceptualized in the first-generation LSMs, modified from Pitman (2003) (a) and in SiB2, modified from Sellers et al. (1996) (b). 204
Fig.A4. Annual average (1980–1986) model-simulated net radiation (a), absorbed solar radiation (b), surface temperature (c), latent (d), sensible (e), and ground heat flux (f) over the Red-Arkansas River basin (Liang et al., 1998).....205
Fig. A5. Mean monthly evapotranspiration (1980–1986) over the Red-Arkansas River basin (Lohmann et al., 1998).....206
Fig. A6. Mean monthly runoff (1980–1986) over the Arkansas and Red River basins routed to respective basin outlets, compared to observed monthly mean naturalized streamflows summed at basin outlets (Lohmann et al., 1998).....207
Fig. A7. Model partitioning of runoff into surface and subsurface runoff, averaged over the years 1980–1986. Also shown are the runoff from the Cogley (1991) climatology and from the naturalized streamflow data (Lohmann et al., 1998).....207
Fig. A8. Mean monthly (1980–1986) water balances: soil moisture tendency (dS/dt), evapotranspiration (E), runoff (R), precipitation (P) (Lohmann et al., 1998).....208
Fig. A9. Basin average snow water equivalent (SWE) for March (surrogate for maximum) for the period (1989–1998) (left panel) and model identifiers (right panel) (Bowling et al., 2003) 209

Fig. A10. Mean annual basin-wide turbulent heat fluxes. The dashed line shows the water balance based estimate of the latent heat flux over the basin (Nijssen et al., 2003). Model identifiers are the same as in Fig. 9. 209
Fig. A11. Mean annual basin-wide sublimation and melt (Nijssen et al., 2003). Model identifiers are the same as in Fig. 9. 210
Fig. A12. Total basin mean annual surface and subsurface runoff. The dashed horizontal line represents mean annual runoff at the mouths of the Torne and Kalix Rivers combined (Nijssen et al., 2003). Model identifiers are the same as in Fig. 9. 210
Fig. A13. Total mean monthly runoff (not routed streamflow) and mean monthly snow melt flux (Bowling et al., 2003). 211
Fig. A14. Monthly evaporation cycles for CHASM's SLAM and SIMP modes compared to results from the corresponding PILPS experiments for (TRF a) and HAP (b). A thick solid line is used for SLAM, a thick dashed line for SIMP with an aerodynamic stability correction and a thick dotted line for SIMP without a stability correction (SIMP-A). M69-PILPS simulations are indicated by stars (*) and the simulations of other PILPS models are represented as unmarked thin lines (Desborough, 1999). 212
Fig. A15. Daily evaporation for TRF (a) and HAP (b) in CHASM's RS-GI, RS-I and RS calibrated constant surface resistance modes compared to corresponding values in simulations with SLAM-1T (Desborough, 1999 212

RÉSUMÉ

Le Modèle Régional Canadien du Climat (MRCC) fait partie d'une grande variété de modèles climatiques développés à travers le monde. Basé sur les lois fondamentales de la physique et sur les techniques numériques les plus modernes et les plus performantes, il génère des variables avec une bonne résolution spatiale qui sont physiquement cohérentes entre elles. Dans le cadre de cette thèse, le MRCC est utilisé pour étudier une large gamme de processus liés au cycle de l'eau. Une approche intégrée d'analyse et de validation du cycle hydrologique du modèle a été développée. Cette approche comprend une analyse à l'échelle multi-annuelle pour l'ensemble d'un bassin versant et intègre les deux branches du cycle hydrologique : atmosphérique et terrestre. Cette façon de procéder nous a permis d'évaluer la capacité de trois versions du MRCC à simuler correctement chacune des composantes du bilan hydrologique. Parallèlement, la sensibilité de ces composantes aux différents paramétrages physiques a été examinée.

Dans un premier temps, les comosantes du cycles hydrologiques sur le bassin versant du Mississippi simulées par les versions 3.6 et 4.0 du MRCC ont été comparées et évaluées par les observations et quasi-observations (estimations basées sur les observations et sur une analyse du bilan de l'eau). Les changements entre la version 3.6 et 4.0 portent sur plusieurs éléments : le schéma de radiation solaire à deux bandes a été remplacé par un schéma à quatre bandes ; le schéma de surface de la première génération a été changé par un schéma beaucoup plus sophistiqué de la deuxième génération ; les traitements de couverture des nuages et du transfert turbulent dans la couche limite ont été également améliorés. L'effet net de tous ces changements dans les paramétrages physiques du MRCC est une réduction importante des biais moyens annuels d'évapotranspiration (de 42% à 10%) et de précipitation (de 17% à -6%) ainsi qu'une meilleure représentation de la distribution spatiale de ces variables. Les cycles annuels de précipitation, d'évapotranspiration, de convergence de flux d'humidité et de tendance dans le stockage de l'eau terrestre ont également montré une amélioration importante. Cependant, le biais annuel du ruissellement a légèrement augmenté (de -41% a -45%).

Dans un deuxième temps, une paire de simulations se distinguant seulement par le paramétrage de processus de surface a été analysée afin de mieux comprendre le rôle de ces processus dans le cycle hydrologique du modèle. Les résultats de l'analyse, effectuée sur trois grands bassins versants (Mississippi, Saint-Laurent et Mackenzie), montrent que le schéma simple de la première génération a d'importantes limitations dans la simulation des processus associés à l'évapotranspiration. Si les biais dans les moyennes annuelles des composantes principales du cycle de l'eau pour les simulations basées sur les deux schémas de surface sont plutôt similaires, les cycles annuels basés sur le schéma de la première génération montrent des biais très grands. L'analyse d'une autre paire de simulations, générées avec la même version du modèle, mais pilotées avec des réanalyses atmosphériques différentes, a mis en évidence la sensibilité du cycle hydrologique aux données utilisées pour piloter le modèle régional à ses frontières. La sensibilité aux données du pilote est en général plus faible que la sensibilité au schéma de surface et s'est montrée plus grande pour les bassins nordiques (Mackenzie et Saint-Laurent). L'analyse d'une troisième paire de simulations avec des conditions initiales différentes a montré que la variabilité interne du modèle à l'échelle multi-annuelle sur l'ensemble d'un bassin versant est négligeable par rapport aux modifications introduites par le changement du schéma de surface et du pilote.

Mots-clés: cycle hydrologique, bassin versant, modèle climatique, paramétrages physiques.

CHAPITRE I

INTRODUCTION GÉNÉRALE

1.1 Problématique et contexte de la recherche

Une grande quantité d'eau circule continuellement dans le système climatique. Sous l'effet du rayonnement solaire, l'eau s'évapore des océans, des lacs, des rivières, du sol, etc. pour rejoindre l'atmosphère. De l'eau est également transférée depuis la surface terrestre vers l'atmosphère par la transpiration de la végétation et la sublimation de la neige et de la glace. Dans l'atmosphère, l'eau est transportée d'un endroit à l'autre par la circulation atmosphérique sous forme de vapeur d'eau, de liquide ou solide dans les nuages. La précipitation de l'eau sous forme liquide ou solide retourne cette eau à la surface terrestre. Le transfert direct de la vapeur d'eau atmosphérique vers le sol peut aussi avoir lieu (rosée, givre). L'eau qui atteint la surface est soit ré-évaporée, soit infiltrée dans le sol, soit transportée par les écoulements de surface et souterrains jusqu'aux océans, et le cycle recommence.

Les effets du cycle hydrologique sur le système climatique sont multiples. Il joue un rôle important dans le bilan énergétique de la Terre. Du côté du rayonnement, les nuages prennent part de différentes façons en fonction de leur altitude et de leur composition au bilan radiatif, la vapeur d'eau est un des principaux absorbants du rayonnement infrarouge et solaire, tandis que la quantité de neige et de glace au sol ainsi que l'humidité du sol influence l'albédo de la surface terrestre. Le cycle hydrologique participe également au bilan énergétique du système climatique par l'effet de la chaleur latente : lorsque l'eau change de phase, la chaleur latente est libérée ou absorbée, l'atmosphère se refroidit ou se réchauffe, ce qui affecte la circulation atmosphérique. Ces processus contribuent de façon majeure au transfert méridien de chaleur sur la planète.

L'équation du bilan de l'eau dans une colonne atmosphérique est donnée comme (Peixoto et Oort, 1992) :

$$\frac{\partial W}{\partial t} + \nabla \bullet \boldsymbol{Q} = E - P \tag{1.1}$$

où W (kg/m^2) est la quantité d'eau précipitable dans la colonne; $C = -\nabla \bullet \boldsymbol{Q}$ (kg/m^{2}s) est la convergence de l'humidité, $\boldsymbol{Q}$est l'intégrale verticale du transport horizontal de la vapeur d'eau ($\boldsymbol{Q} = \int_0^{p_0} q\boldsymbol{V}\frac{dp}{g}$; q est l'humidité spécifique; $\boldsymbol{V}$est le vecteur du vent horizontal et p_o est la pression à la surface); P(kg/m^{2}s) est le taux de précipitation, E(kg/m^{2}s) est le taux d'évapotranspiration.

L'équation du bilan de l'eau dans le sol peut être écrite (Roads et al., 2002) :

$$\frac{\partial(M+S)}{\partial t} = P - E - R \tag{1.2}$$

où M (kg/m^{2}s) est le stockage de l'eau dans le sol; S (kg/m^{2}s) est le stockage dans le couvert nival ; R (kg/m^{2}s) est l'écoulement.

La grande complexité des processus impliqués dans le cycle de l'eau dont les échelles spatiales varient énormément (e.g. 10^{-6} m, nucléation des gouttelettes et des cristaux ; 10^7 m, circulation à l'échelle planétaire) et la nécessité de mieux comprendre ces processus et leurs interactions ont mené au lancement de l'expérience mondiale du cycle de l'eau et de l'énergie (GEWEX, http://www.gewex.org) en 1990. Le but principal de GEWEX est de comprendre, quantifier et fermer les bilans d'eau et d'énergie. Durant sa première phase (1990-2002), le développement de nouvelles bases de données (régionales et globales) à haute résolution, ainsi que le développement de modèles constituaient le cœur des efforts. Afin d'assurer un fonctionnement efficace, les activités de GEWEX ont été divisées en trois secteurs : l'hydrométéorologie, l'énergie, ainsi que la modélisation et la prévision.

Les activités d'hydrométéorologie, coordonnées par le « GEWEX Hydrometeorology Panel » (GHP), sont concentrées sur l'étude de différents processus hydrologiques à l'échelle régionale (continentale). Le but visé est de mieux comprendre les processus clés du cycle hydrologique et de fermer le bilan de l'eau dans les grands bassins versants en combinant de nouvelles données d'analyse et de réanalyse d'observations avec celles des modèles. Un bassin versant peut être défini comme l'unité géographique où toutes les eaux souterraines et superficielles s'écoulent vers le point le plus bas en suivant la pente naturelle et se rejoignent pour former une rivière ou un fleuve ou un lac ou une nappe souterraine avant d'atteindre finalement la mer (http://www.cite-sciences.fr). Sur le continent américain, les études ont porté sur les bassins du Mississippi (Berbery and Rasmusson 1999; Berbery et al. 1999; Yarosh et al. 1999; Roads et Betts 2000; Maurer et al. 2001; Roads et al. 2002; Berbery et al. 2003; Ek et al. 2003; Roads et al. 2003), du Mackenzie (Stewart et al. 1998 ; Rouse, 2000 ; Stewart et al. 2002 ; Strong et al. 2002) et de l'Amazone (Betts

et al. 2005, Marengo 2005 ; Marengo 2006). En Europe, de nombreuses études ont été réalisées dans la région de la mer Baltique (Raschke et al. 1998 ; Jacob 2001 ; Graham et Bergström 2001 ; Bengtsson 2001). Les moussons asiatiques ont été étudiées dans les régions de la Thaïlande, du Tibet, de la Sibérie et de la Chine de l'Est. Récemment, des études ont été lancées dans les bassins d'Australie, de La Plata de l'Amérique du Sud et en Afrique de l'Ouest (voir Fig.1). Toutes ces expériences sont connues sous le nom «GEWEX Continental Scale Experiments (GEWEX CSEs)».

De nombreux modèles climatiques, globaux (MCG) et régionaux (MRC), sont utilisés dans le cadre de GEWEX CSEs. Ces modèles sont basés sur des lois fondamentales de la physique, représentés par des équations différentielles non-linéaires. La forte non-linéarité de ces équations empêche leur résolution analytique par les méthodes mathématiques classiques. Les équations originales, décrivant le spectre entier de la circulation atmosphérique, doivent être estimées par des techniques de discrétisation spatiales (différences finies, méthodes spectrales) et temporelles (explicites, implicites) et résolues numériquement. Les modèles climatiques peuvent donc êtres considérés comme des programmes informatiques utilisés pour obtenir une solution numérique du système d'équations décrivant l'évolution des variables météorologiques. Les modèles d'aujourd'hui exigent une grande puissance de calcul, offerte par les superordinateurs.

Un MCG se compose de deux parties principales: la dynamique et la physique. La « dynamique » correspond aux processus de la dynamique des fluides et traite la conservation de la quantité de mouvement, de la masse et de l'énergie dans l'atmosphère à l'échelle de la grille du modèle. Elle se compose d'équations du mouvement, d'équations de continuité pour l'air sec et la vapeur d'eau, d'une équation de la thermodynamique et d'une équation d'état du fluide atmosphérique. Les variables pronostiquées de la « dynamique » sont : la vitesse et la direction du

vent, la température, l'humidité de l'atmosphère et la hauteur géopotentielle (la pression). L'existence de la deuxième composante d'un MCG dite « physique » est imposée par la discrétisation spatiale. Elle correspond aux processus d'échelle inférieure à la grille du modèle, regroupées dans les termes sources (puits) des équations de conservation. Il s'agit ici des processus radiatifs, de transfert turbulent, de dissipations, des processus liés à la formation des nuages, etc. Ces processus sont décrits schématiquement en fonction des variables résolues du modèles (celle traitées par la dynamique). Les procédés mathématiques impliqué sont connus sous le nom de « paramétrage ». Peixoto et Oort (1992) expliquent la distinction entre la composante « dynamique » et la composante « physique » d'un MCG par des considérations historiques. Les premiers MCG, apparus dans les années soixante, étaient dérivés des modèles de prévision et résolvaient principalement la dynamique de l'atmosphère. La nécessité de prendre en compte de nombreux autres processus physiques, regroupés sous le terme « physique », devient évidente avec l'application des MCG dans les études de climat. Ainsi, l'utilisation de ces modèles pour simuler l'évolution du système climatique met en évidence la nécessité d'inclure non seulement le comportement de l'atmosphère, mais aussi le comportement des quatre autres composantes du système climatique : hydrosphère, cryosphère, lithosphère et biosphère. L'addition de sous-modèles qui décrivent les processus de ces composantes augmente beaucoup la quantité du calcul et limite la résolution spatiale. De nos jours, les GCM se caractérisent par une résolution d'environ 200 km.

Les simulations efficaces du climat à des résolutions spatiales beaucoup plus fines (d'environ 50 km) sur une région donnée sont possibles avec un modèle régional du climat (MRC) ou encore avec un GCM à résolution variable. Les MRC ont besoin de conditions frontières latérales provenant d'une simulation de GCM ou d'une réanalyse d'observations dont la résolution spatiale est inférieure à celle du MRC. Les simulations avec un MRC sont donc contrôlées par les flux venant de leur pilote et sont sensibles à la dimension du domaine, aux saisons et à la circulation

atmosphérique de grande échelle dans le domaine (Giorgi et Bi 2000). Les détails de fines échelles développés par le MRC doivent se superposer à la grande échelle du pilote pour produire des champs cohérents à hautes résolutions.

Vu la nature chaotique de la dynamique de l'atmosphère que les GCM et les RCM tentent de représenter ainsi que les nombreux processus de rétroaction prenant place dans le système climatique, la circulation atmosphérique simulée (de même que la circulation réelle) est sensible à de petites perturbations dans les conditions initiales. Ceci implique un phénomène dit « variabilité interne » qui rend possible plusieurs solutions de la circulation atmosphérique malgré des forçages externes identiques. La variabilité interne est donc considérée comme une propriété intrinsèque des modèles climatiques (et du système climatique réel) responsable de la divergence de simulations réalisées avec les mêmes forçages externes mais avec des conditions initiales différentes. Afin de couvrir le spectre des solutions possibles, les scientifiques génèrent des ensembles d'un certain nombre de simulations en introduisant une source de perturbation, habituellement dans les conditions initiales. Le degré de dispersion (d'écart) entre les membres d'un ensemble représente une mesure de la variabilité interne.

La variabilité interne dans un GCM, mesurée avec la dispersion entre les membres d'un ensemble, devrait être similaire à la variabilité interannuelle présentée dans une longue simulation de MCG. Cette association est permise par l'application de l'hypothèse d'ergodicité selon laquelle l'évolution d'un signal aléatoire et stationnaire dans le temps apporte la même information et a la même variabilité qu'un ensemble de réalisations. L'étude de la variabilité interne d'un MCG peut donc être faite à partir d'une seule, mais assez longue, simulation. L'hypothèse d'ergodicité ne s'applique pas dans le cas d'un MRC parce que les conditions aux frontières agissent comme un forçage (Lucas-Picher 2007). Pour étudier la variabilité interne d'un MRC, il convient donc de lancer plusieurs simulations avec des conditions initiales

différentes. Puisque le climat est défini par la moyenne des conditions atmosphériques pour une période assez longue, l'ordre des événements météorologiques, qui change avec le changement des conditions initiales, ne doit pas influencer le climat simulé de manière significative.

Par contre, les nombreuses études ont démontré que le climat simulé par les MCG et MRC est sensible à des propriétés de la surface terrestre et au paramétrage des processus y prenant place. Par exemple, la modification de l'albédo et de la rugosité a des conséquences significatives sur la circulation simulée à grande échelle ainsi que sur l'évaporation et la précipitation (Charney et al. 1977 ; Sud et al. 1986 ; Mintz 1982 ; Sato et al. 1989 ; Viterbo and Beljars, 1996; Twine et al. 2004; Jiao et Caya 2006). Des effets semblables se produisent lorsque le paramétrage de l'hydrologie du sol ou la représentation de la végétation (implicite, explicite, pas inclus) est changé. Une revue des principaux schémas de surface utilisés dans les modèles climatiques qui décrivent les échanges d'eau et d'énergie prenant place à l'interface sol-végétation-atmosphère est présentée à l'appendice A.

L'application des MCG et des MRC pour les projections du climat futur a mis en évidence la nécessité de quantifier l'incertitude associée aux projections climatiques. Un des principaux facteurs d'incertitude vient du fait que les changements projetés du climat régional par différents modèles peuvent être divergents, malgré les mêmes scénarios de forçage anthropogène. La stratégie adoptée par la communauté scientifique pour aborder ce problème est d'utiliser un ensemble des simulations, produites par différents modèles ou par un seul modèle en différentes configurations expérimentales (différents schémas de paramétrages, différentes bases de données de champ géophysique, différentes données du pilote dans le cas d'un MRC, etc.). Le signal du changement climatique pour une région donnée et l'incertitude associée doivent donc être basés sur des informations venant d'un ensemble de simulations. Pour extraire les informations les plus fiables de

chacune des simulations d'ensemble et pour minimiser la contribution des modèles dont les performances sont faibles (les biais pour le climat actuel), l'utilisation d'une moyenne pondérée des résultats des simulations est parfois retenues. Une des méthodes pour calculer la moyenne pondérée d'un ensemble de simulations, ainsi que l'incertitude et la fiabilité des changements climatiques à l'échelle régionale, a été proposée par Giorgi and Mearns (2002, 2003). Elle est connue sous le nom de « reliability ensemble averaging (REA) method » et tient compte de deux critères : (i) critère de fiabilité, basé sur les performances des modèles pour le climat actuel et (ii) le critère de convergence des changements simulés à travers les modèles.

L'évaluation des modèles est donc primordiale pour établir le niveau de fiabilité des projections climatiques, ainsi que pour leur développement. Malheureusement, certaines variables sont difficiles à mesurer et sont rarement disponibles à l'échelle des MRC actuels. De plus, les observations sont elles mêmes associées à des erreurs qui généralement ne sont pas négligeables. Dans ce contexte, un des objectifs principaux de la deuxième phase de GEWEX (2003-2013) est la production de bases de données d'observations, incluant une évaluation des erreurs, qui vont servir dans l'analyse du bilan de l'eau et de l'énergie ainsi que dans la validation et le développement des modèles (Lawford et al. 2004).

Le présent travail s'insère dans cette optique. Il utilise le Modèle Régional Canadien du Climat (MRCC; Caya et Laprise 1999) pour étudier de façon quantitative les processus liés au cycle de l'eau. Une approche intégrée d'analyse et de validation du cycle hydrologique simulé par les modèles a été développée. La validation de certaines composantes du cycle de l'eau du MRCC a été faite par plusieurs chercheurs en utilisant différentes approches (p.ex., Sushama et al. 2006 ; Frigon et al. 2006 ; Brochu et Laprise 2007). La méthode devrloppée dans cette thèse comprend une analyse à l'échelle multi-annuelle faite à l'échelle d'un bassin

versant et intègre les deux branches du cycle hydrologique (atmosphérique et terrestre). Cette approche intégrée nous a permis d'évaluer la performance de trois versions du MRCC (MRCC_V3.6, MRCC_V3.7 et MRCC_V4.0) pour simuler les composantes principales du cycle hydrologique. L'analyse porte sur trois grand bassins versants d'Amérique du Nord se retrouvant dans des régions avec des climats très différents : le Mississippi, le Mackenzie et le Saint Laurent (voir Tableau 1.1). La sensibilité des composantes du cycle hydrologique aux différents paramétrages physiques des processus de sous-échelle, aux données utilisées pour piloter le modèle et aux conditions initiales a aussi été examinée.

1.2 Objectifs

L'objectif général de cette thèse et d'affiner la compréhension du cycle hydrologique à l'échelle régionale et de développer une méthode d'analyse et de validation permettant une évaluation la plus complète possible du cycle hydrologique simulé par des modèles climatiques. Dans ce contexte, les objectifs spécifiques suivants ont été définis :

- Évaluer la capacité du MRCC à simuler correctement chacune des composantes du bilan hydrologique dans des régions se caractérisant par des conditions climatiques différentes ;
- Évaluer la sensibilité du cycle hydrologique simulé à la formulation des processus de surface afin de mieux comprendre les effets des interactions prenant place à l'interface sol-végétation-atmosphère ;
- Évaluer la sensibilité du cycle hydrologique du MRCC aux données utilisées pour piloter le modèle et aux conditions initiales ;
- Préciser, autant que l'on peut, l'origine des biais du cycle hydrologique du MRCC et orienter les efforts futurs pour diminuer ces biais.

1.3 Méthode générale

La méthode utilisée dans la présente étude est décrite en détail aux chapitres *II* et *III* de la thèse. Pour cette raison, seule la méthode générale est brièvement décrite dans la présente section.

Tel que mentionné plus tôt, trois versions du MRCC, soit MRCC_V3.6, MRCC_V3.7 et MRCC_V4.0, sont utilisées dans cette étude. Le MRCC est un modèle à aire limitée (Caya et Laprise, 1999) piloté soit par des ré-analyses pour les simulations du climat présent, soit par un Modèle de Circulation Générale (MCG) pour les simulations du climat futur. La formulation dynamique du MRCC provient du modèle MC2 (Bergeron et al. 1994), tandis que les paramétrages constitutant la physique proviennent du MCG Canadien (MCGC) développé par le Centre Canadien de la Modélisation et de l'Analyse Climatique. La physique du MRCC_V3.6 est basée sur les paramétrages physiques du MCGC II (McFarlane et al. 1992), ajustés à la résolution plus fine du MRCC, alors que le MRCC_V4.0 utilise le module physique du MCGC III. Les modifications principales entre ces deux versions du modèle portent sur les éléments suivants : (a) le schéma de radiation ; (b) le traitement de nuages ; (c) le schéma de transfert turbulent dans la couche limite ; et (d) le schéma de surface. Quant à la version intermédiaire du modèle (MRCC_V3.7), elle se distingue de la version 4.0 seulement par le paramétrage des processus de surface (voir Tableau 1.2). Notez aussi qu'il existe une différence dans les champs géophysiques. Les caractéristiques du sol (texture, couleur, porosité, capacités hydrique et thermique, etc.), ainsi que de la végétation (primaire et secondaire) dans les versions 3.6 et 3.7 du MRCC sont tirées de la base de données de Wilson and Henderson-Sellers (1985). Le MRCC_V4.0 utilise la même base de données pour définir les propriétés géophysiques de trois couches de sol, tandis que les principales classes de la végétation (conifères, feuillus, terres arables, herbes et toundra) et ses

nombreux paramètres (fraction de canopée végétale, masse de canopée végétale, LAI (« Leaf Area Index »), profondeur des racines, longueur de rugosité, albédo, etc.) sont basés sur GCL2000 (Global Land Cover 2000). Fig. 1.2 montre la fraction de canopée végétale (analogue de l'usage des sols) dans CLASS (MRCC_V4.0).

La sensibilité aux différents paramétrages physiques, aux données utilisées pour piloter le modèle et aux conditions initiales a été évaluée en se concentrant sur les moyennes climatologiques des composantes du bilan de l'eau (moyennées spatialement sur un bassin versant), leurs cycles annuels et leurs variabilités interannuelles. Le domaine d'intégration nommée AMNO est commun pour toutes les simulations utilisées dans cette étude et couvre la totalité de l'Amérique du Nord.

Étant donné qu'aucun des ensembles de données présentement disponibles ne permet une évaluation complète de toutes les composantes du cycle hydrologique simulées par les modèles, nous proposons ici une approche d'analyse à l'échelle multi-annuelle pour l'ensemble d'un bassin versant qui intègre les deux branches du cycle hydrologique (atmosphérique et terrestre). Basée sur la loi de conservation de la masse d'eau appliquée sur la totalité d'un bassin versant, cette approche permet l'estimation des composantes du cycle hydrologique pour lesquelles les données d'observation sont rares ou absentes. Un des avantage de l'analyse à l'échelle du bassin versant est la possibilité de profiter de données historiques de débits fluviaux. Lorsque le débit mesuré (m^3/s) est divisé par la superficie du bassin ((m^2), il peut être directement comparé avec le ruissellement simulé (kg m^{-2} s^{-1}) par le modèle. Ainsi, la quantité d'eau qui sort d'un bassin versant par le ruissellement (moyennée sur une ou plusieurs années) donne une mesure de quantité d'humidité qui entre dans ce bassin par la circulation atmosphérique. Finalement, le bilan effectué sur un bassin assez grand devrait être moins sensible aux erreurs des champs observés et simulés. La technique d'estimation des variables difficilement mesurables est détaillée au *chapitre II.*

1.4 Plan

La thèse comporte quatre chapitres dont deux correspondent à des articles soumis pour publication. Le présent chapitre présente l'étude réalisée d'une façon plutôt générale. Le *chapitre II* est constitué d'un article intitulé «Evaluation of the Hydrological Cycle over the Mississippi River Basin as Simulated by the Canadian Regional Climate Model (CRCM)», il a été publié dans le «*Journal of Hydrometeorology*» (Music and Caya, 2007). Le *chapitre III* est constitué d'un article intitulé « Investigation of Sensitivity of the CRCM Water Cycle Components to the Land Surface Parameterization, the Lateral Boundary Data and the Internal Variability » par Biljana Music et Daniel Caya, et il a été soumis pour publication dans le «*Journal of Hydrometeorology*». Le *chapitre IV* conclut l'étude réalisée au cours de cette thèse.

Les aspects plus théoriques de la recherche sont présentés au chapitre II. Tout d'abord, ce chapitre présente d'une façon générale les bilans de l'eau dans l'atmosphère ainsi qu'à l'interface terre-atmosphère et il présente en détail une approche d'analyse et de validation du cycle hydrologique simulé par les modèles climatiques. Les données observées qui servent dans l'analyse sont également présentées. De plus, les techniques impliquées dans la construction de ces bases de données ainsi que la fiabilité de celles-ci sont discutées. L'approche est appliquée à l'évaluation du cycle hydrologique du bassin versant du Mississippi simulé par les versions 3.6 et 4.0 du MRCC. L'évaluation a été faite pour une période de dix ans (1988-1997). Dans un premier temps, l'analyse porte sur les moyennes annuelles du bassin. Dans un deuxième temps, les cycles annuels de toutes les composantes du bilan simulé par les deux versions du modèle ont été comparés avec les cycles provenant d'observations. Finalement, les distributions spatiales de la précipitation, du ruissellement et de l'évapotranspiration sur le bassin ont été évaluées. Étant donné que les modifications entre les versions 3.6 et 4.0 du modèle portent sur plusieurs

éléments, l'effort a été mis pour distinguer les effets de ces changements sur les composantes principales du cycle hydrologique.

Le *chapitre III* présente une étude de sensibilité du cycle hydrologique au paramétrage des processus de surface et aux conditions latérales et initiales du modèle. Cette étude a été réalisée sur trois grands bassins se caractérisant par des conditions climatiques différentes : le Mississippi, le Saint-Laurent et le Mackenzie. Plus particulièrement, les sensibilités des moyennes climatologiques pour une période couvrant 39 ans, des cycles annuels climatologiques et de la variabilité interannuelle des composantes principales du cycle de l'eau ont été évaluées. Les effets du changement de paramétrage de surface ont été mis en contexte en faisant la comparaison de deux simulations, l'une réalisée avec le MRCC 4.0 et l'autre avec le MRCC_V3.7. Notons ici que la seule différence entre ces deux versions du modèle est dans leur représentation de la surface. L'analyse et la comparaison d'une deuxième paire de simulations effectuées avec la même version du modèle (MRCC_V4.0) mais pilotées avec des réanalyses atmosphériques différentes, nous ont permis d'évaluer la sensibilité aux données du pilote. Une troisième paire de simulations se distinguant seulement par les conditions initiales a été analysée pour estimer la variabilité interne du modèle. De plus, les biais de toutes les simulations par rapport aux observations ont été évalués et comparés.

Le *chapitre IV* conclut l'étude réalisée en présentant les contributions, les applications, les limites et les perspectives de la recherche.

Bibliographie

Bechtold, P., J.S. Kain, E. Bazile, F. Guichard, P. Mascart, et E. Richard, 2001: A Mass Flux Convection Scheme for Regional and Global Models. *Quart. J. Roy. Meteor. Soc.*, **127**, 869-886.

Bengtsson, L., 2001: Numerical modelling of the energy and water cycle of the Baltic Sea, *Meteor. Atmos. Phys.*, 77, 9-17.

Bergeron, G., R. Laprise, et D. Caya, 1994: Formulation of the Mesoscale Compressible Community (MC2) model. Internal Report, Cooperative Centre for Research in Mesometeorology, Montreal, PQ, Canada, 165 pp.

Betts, A. K., Ball, J. H., Viterbo, P., Dai, A. et J. A. Marengo, 2005: Hydrometeorology of the Amazon in ERA-40., *J. Hydrometeor. 6*, 764-774.

Berbery, E. H., K.E. Mitchell, S. Benjamin, T. Smirnova, H. Ritchie, R. Hogue, et E. Radeva, 1999: Assessment of land-surface energy budgets from regional and global models. *J. Geophys. Res.*, **104**, D16, 19329-19348.

Berbery, E. H., et E. M. Rasmusson, 1999: Mississippi moisture budgets on regional scales, *Mon. Wea. Rev.*, **127**, 2654-2673.

Berbery, E. H., Y. Luo, K. E. Mitchell, et A. K. Betts, 2003: Eta model estimated land surface processes and the hydrologic cycle of the Mississippi basin, *J. Geophys. Res.*, **108**, D22, 8852, doi:10.1029/2002JD003192.

Brochu, R. and R. Laprise. 2007 : Surface water and energy budgets over the Mississippi and Columbia river basins as simulated by two generations of the Canadian Regional Climate Model. *Atmos-Ocean*, **45**, 19 - 35.

Caya, D., et R. Laprise, 1999: A semi-implicit semi-Lagrangian regional climate model: The Canadian RCM. *Mon. Wea. Rev.*, **127**, 341-362.

Charney, J.G., 1975: Dynamics of deserts and droughts over the Sahel. *Quart. J. Roy. Meteor. Soc.*, **101**, 193-202.

Ek, M. B., K. E. Mitchell, Y. Lin, E. Rogers, P. Grunmann, V. Koren, G. Gayno, et J. D. Tarpley, 2003: Implementation of Noah land surface model advances in the National

Centers for Environmental Prediction operational mesoscale Eta model, *J. Geophys. Res.*, **108,** D22, 8851, doi:10.1029/2002JD003296.

Fritz, S., E. Bartholomé, A. Belward, A. Hartley, H-J. Stibig, H. Eva, P. Mayaux, S. Bartalev, R. Latifovic, S. Kolmert, P. S. Roy, S. Agrawal, W. Bingfang, X. Wenting, M. Ledwith, J-F Pekel, C. Giri, S. Mücher, E. de Badts, R. Tateishi, J-L Champeaux et P. Defourny, 2003 : Harmonisation, mosaicing and production of the Global Land Cover 2000 database (beta version), Report, European Commission, Joint Research Centre, 41pp.

Frigon A., Slivitzky M., Caya D., 2006 : Hydrology of Northern Quebec as seen by the Canadian Regional Climate Model . *WMO Research activities in Atmospheric and Oceanic Modelling, edited by J. Côté* . WMO/TD-No 1347, Report No. 36 : 7.09-7.10

Giorgi, F. et X. Bi, 2000: A Study of Internal Variability of a Regional Climate Model. *J. Geophys. Res.,* **105,** 29503-29521.

Giorgi, F., and R. Francisco, 2000: Evaluating uncertainties in the prediction of regional climate change. *Geophys. Res. Lett.,* **27,** 1295–1298.

Giorgi, F., and L. O. Mearns, 2002: Calculation of average, uncertainty range, and reliability of regional climate changes from AOGCM simulations via the "reliability ensemble averaging" (REA) method. *J. Climate,* **15,** 1141–1158.

Graham, L. P. et S. Bergström, 2001: Water balance modelling in the Baltic Sea drainage basin - analysis of meteorological and hydrological approaches. *Meteor. Atmos. Phys.,* **77,** 45-60.

Jacob, D., 2001: A note to the simulation of the annual and inter-annual variability of the water budg et over the Baltic Sea drainage basin. *Meteor. Atmos. Phys.,* **77,** 61-74.

Jiao, Y., et D. Caya, 2006: An investigation of the summer precipitation simulated by the Canadian Regional Climate Model. *Mon. Wea. Rev.,* **134,** 919-932.

Marengo. J. 2005: The chartacterisics and variability of the atmospheric water balance in the Amazon basin: Spatial and temporal variability. *Clim. Dyn.,* 24, 11-22.

Marengo, J. :2006 On the Hydrological Cycle of the Amazon basin**n**: A historical review and current State-of-the-art. Accepted, *Rev. Brasil. de Meteorologia.*

Maurer, E. P., G. M. O'Donnell, D. P. Lettenmaier, et J.O. Roads, 2001: Evaluation of the Land Surface Water Budget in NCEP/NCAR and NCEP/DOE Reanalyses using an Off-line Hydrologic Model, *J. Geophys. Res,* **106**, D16, 17841-17862.

McFarlane, N.A., G.J. Boer, J.-P. Blanchet, et M. Lazare, 1992: The Canadian Climate Centre second generation General Circulation Model and its equilibrium climate. *J. Climate*, **5**, 1013-1044.

Mintz, Y., 1984: The sensitivity of numerically simulated climates to land-surface boundary conditions. *Global Climate*, J. Houghton, Ed., 79-105.

Mitchell, T.D., and P.D. Jones 2005: An improved method of constructing a database of monthly climate observations and associated high-resolution grids. *Int. J. Climatol.,* **25**, 693-712.

Paquin, D., et R. Harvey, 2003: Les nuages dans gcmiii et MRCC_Version 3.7. Internal document of the CRCM Network (available from D. Paquin, Ouranos, 550 Sherbrooke st. west, 19 floor, Montreal, Quebec, Canada H3A 1B9).

Peixoto, J. P., and A. H. Oort, 1992: *Physics of Climate.* American Institute of Physics Press, 520 pp.

Puckrin, E., W. F. J. Evans, J. Li, et H. Lavoie, 2004: Comparison of clear-sky surface radiative fluxes simulated with radiative transfer models. *Can. J. Remote Sens.*, **30,** 903-912.

Raschke, E., U. Karstens, R. Nolte-Holube, R. Brandt, H.J. Isemer, D. Lohmann, M. Lobmeyer, B. Rockel et R. Stuhlmann, 1998: The Baltic Sea Experiment BALTEX: a brief overview and some selected results of the authors. *Surveys in Geophysics*, **19**, 1-22.

Roads, J., et A. Betts, 2000: NCEP/NCAR and ECMWF Reanalysis Surface Water and Energy Budgets for the Mississippi River Basin. *J. Hydrometeor.,* **1,** 88-94.

Roads, J., M. Kanamitsu, et R. Stewart, 2002: CSE Water and Energy Budgets in the NCEP-DOE Reanalysis II, *J. Hydrometeor.*, **3**, 128-165.

Roads, J., R., E.B. Lawford, H. Berbery, B. Fekete, K. Gallo, A. Grundstein, W. Higgins, J. Janowiak, M. Kanamitsu, V. Lakshmi, D. Leathers, D. Lettenmaier, Q. Li, L. Luo, E. Maurer, T. Meyers, D. Miller, K. Mitchell, T. Mote, R. Pinker, T. Reichler, D. Robinson, A. Robock, J. Smith, G. Srinivasan, K. Vinnikov, T. von der Haar, C. Vorosmarty, S. Williams, et E. Yarosh, 2003: GCIP Water and Energy Budget Synthesis (WEBS) *J. Geophys. Res.*, **108**, D16, 8609, doi:10.1029/2002JD002583.

Rouse, W.R., 2000: Progress in hydrological research in the Mackenzie GEWEX Study. *Hydrological Processes* **14**, 1667-1685.

Lawford, R. G., R. Stewart, J. Roads, H.-J.Isemer , M. Manton, J. Marengo, T. Yasunari, S. Benedict, T. Koike et S. Williams, 2004 : Advancing global and continental scale hydrometeorology: Contributions of the GEWEX Hydrometeorology Panel, *Bull. Amer. Meteor. Soc*, **85**, 1917-1930.

Sato, N., P.J. Sellers, D.A. Randall, E. K. Schneider, J.Shukla, J.L. Kinter III, Y.-Y. Hou, and E. Albertazzi, 1989: Effect of implementation of the Simple Biosphere Model (SiB) in general a circulation model. *J. Atmos. Sci.,* **46**, 2757-2782.

Stewart, R.E., H.G. Leighton, P. Marsh, G.W.K. Moore, H. Ritchie, W.R. Rouse, E.D. Soulis, G.S. Strong, R.W. Crawford, et B. Kochtubajda, 1998: The Mackenzie GEWEX Study: the water and energy cycles of a major North American river basin. *Bull. Amer. Meteor. Soc.*, **79**, 2665-2683.

Stewart, R.E., N. Bussieres, Z. Cao, H.R. Cho, D.R. Hudak, B. Kochtubajda, H. Leighton, P.Y.T. Louie, M.D. Mackay, P. Marsh, G.S. Strong, K.K. Szeto et J.E. Burford, 2002: Hydrometeorological features of the Mackenzie basin climate system during the 1994/1995 water year: a period of record low discharge. *Atmos-Ocean* **40**: 257-278.

Strong, G.S., B. Proctor, M. Wang, E.D. Soulis, C.D. Smith, F. Seglenieks, et K. Snelgrove, 2002: Closing the Mackenzie basin water balance budget, water-years 1994-95 through 1996-97. *Atmosphere-Ocean* **40**: 113-124.

Sud, Y.C., J. Shukla, and Y. Mintz, 1986 : Influence of land-surface on circulation and rainfall in a tropical model. *Quart. J. Roy. Met. Soc.*, **103**, 29-46.

Sushama, L., R. Laprise, D. Caya, A. Frigon, and M. Slivitzky. 2006 : Canadian RCM projected climate change signal and its sensitivity to model errors. *Int. J. Climat.*, 26, 2141-2159.

Twine T.E, Kucharik C.J, Foley J.A, 2004: Effects of land cover change on the energy and water balance of the Mississippi River basin. *J. Hydrometeor.*. **5**, 640–655.

Yarosh, E. S., C.F. Ropelewski, et E.H. Berbery, 1999: Biases of the observed atmospheric water budgets over the central United States. *J. Geophys. Res.*, **104**, D16, 19349-19360.

Verseghy, D.L., 1991: CLASS – A Canadian land surface scheme for GCMs. Part I: Soil model. *Int. J. Climatol.*, **11**, 111–133.

Verseghy, D.L., N.A. McFarlane, et M. Lazare, 1993: CLASS – A Canadian land surface scheme for GCMs. Part II: Vegetation model and coupledruns. *Int. J. Climatol.* **3**, 347–370.

Viterbo, P., and A.C.M. Beljaars, 1995: An improved land surface parameterization scheme in the ECMWF model and its validation. *J. Climate*, **8**, 2716-2748.

Tableau 1.1 Moyennes spatiales de température et de précipitation pour les bassins du Mississippi, Saint-Laurent et Mackenzie, calculées à partir des données de CRU (Mitchell and Jones 2005).

	Mississippi	Saint-Laurent	Mackenzie
Température moyenne annuelle (°C)	10,8	5,1	-3,9
Précipitation moyenne annuelle (mm/jour)	2,20	2,56	1,02

Tableau 1.2 Paramétrages physiques utilisés dans le MRCC.

	MRCC_V3.6	MRCC_V3.7	MRCC_V4.0
Schéma de surface	Première génération : « Beautified bucket » - capacité en eau du sol varie spatialement (McFarlane et al.1992)	Première génération : « Bucket »-capacité en eau du sol uniforme de 100 mm	Deuxième génération : CLASS (Verseghy 1991, Verseghy et al. 1993)
Schéma de radiation	Schéma à deux bandes de radiation solaire	Schéma à quatre bandes de radiation solaire et un continuum de vapeur plus détaillé (Puckrin et al. 2004)	Puckrin et al. (2004)
Nuages	Définition selon l'humidité relative critique et couplage avec le Bechtold-Kain-Fritsch (BKF) schéma (Bechtold et al. 2001)	Modification dans la formation des nuages : ajout de paramètre de stabilité (Paquin and Harvey 2003)	Paquin and Harvey (2003)
Transfert turbulent dans la couche limite	Distribution locale de flux de surface à travers la plus basse couche de modèle	Distribution de flux de surface à travers plusieurs niveaux de modèle, i.e. à travers la couche limite de l'atmosphère (Jiao and Caya 2006)	Jiao and Caya 2006

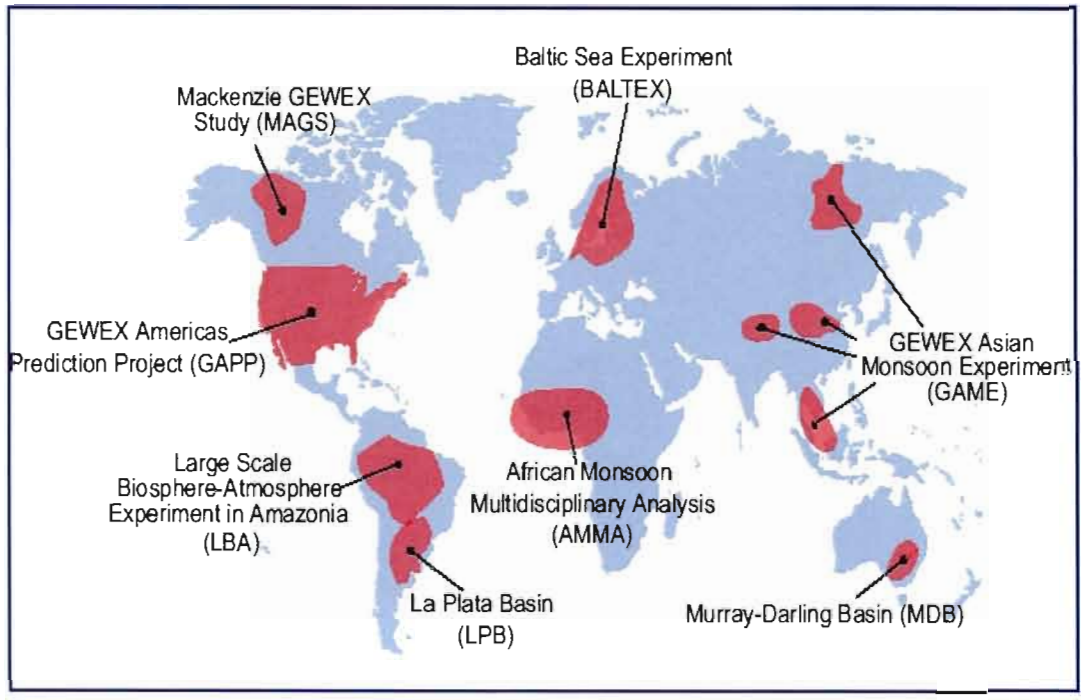

Fig. 1.1 Les régions incluses dans les expériences « GEWEX CSEs » (source : Lawford et al. 2004)

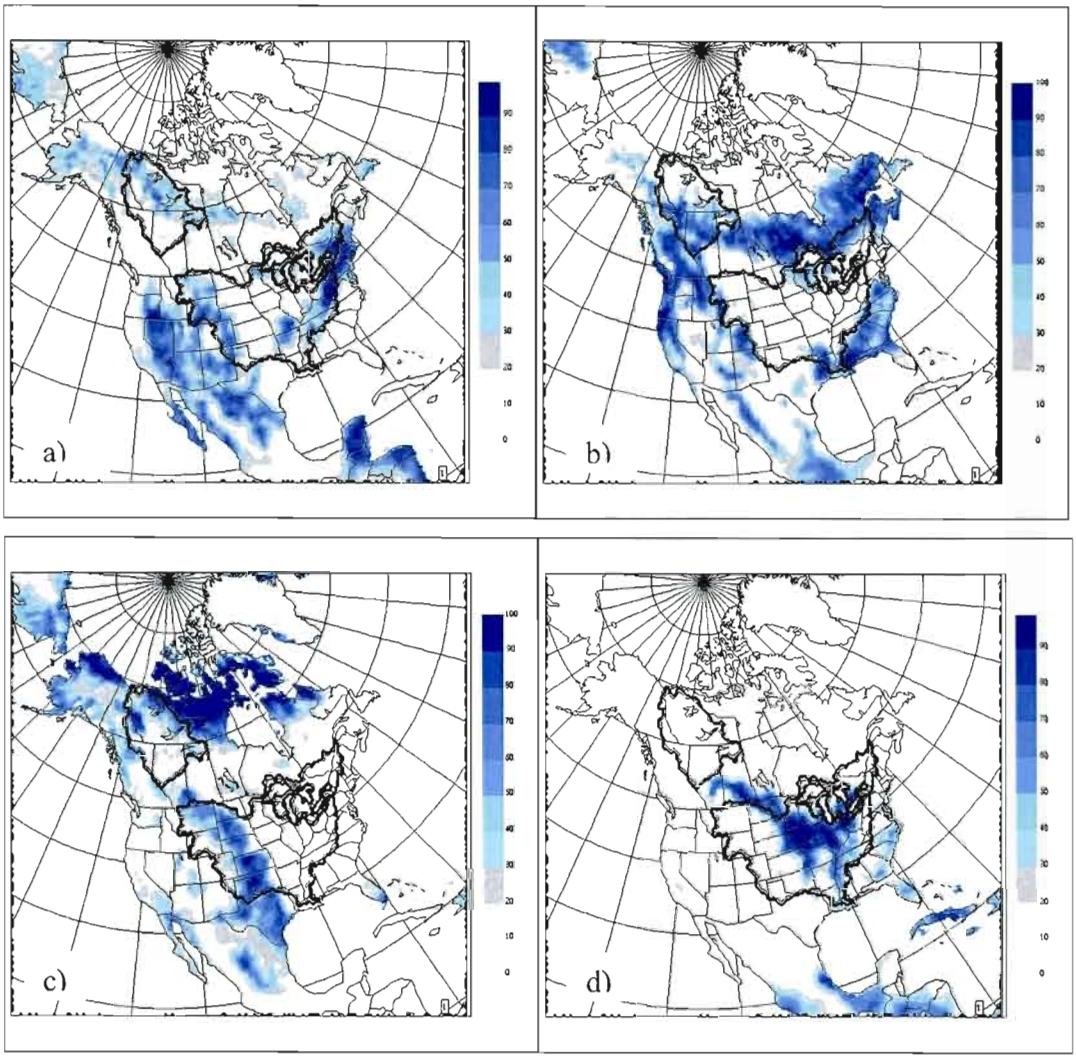

Fig. 1.2 Fraction de canopée végétale dans CLASS : a) conifères ; b) feuillus ; c) terres arables ; d) herbes et toundra.

CHAPITRE II

EVALUATION OF THE HYDROLOGICAL CYCLE OVER THE MISSISSIPPI RIVER BASIN AS SIMULATED BY THE CANADIAN REGIONAL CLIMATE MODEL (CRCM)

Biljana Music and Daniel Caya

pubilshed in

J. Hydrometeor. , 8(5), 969-988. DOI: 10.1175/JHM627.1.

Abstract

Water cycle over a given region is governed by many complex multi-scale interactions and feedbacks whose representation in climate models can vary in complexity. Evaluation and validation of all components of the simulated water cycle are required in order to understand which of the key processes require better representation, Adequate assessment of simulated hydrological cycle over a given region is not trivial because observations for various water cycle components are seldom available at regional scale.

In this paper, a comprehensive validation method of the water budget components over a river basin is presented. In addition, the sensitivity of the hydrological cycle in the Canadian Regional Climate Model (CRCM) to a more realistic representation of the land surface processes, as well as radiation, cloud cover and atmospheric boundary layer mixing is investigated. The changes to the physical parameterisations are assessed by evaluating the CRCM hydrological cycle over the Mississippi River Basin. The first part of the evaluation looks at the basin annual means. The second part consists in the analysis and validation of the annual cycle of all water budget components. Finally, the third part is directed toward the spatial distribution of the annual mean precipitation, evapotranspiration and runoff.

Results indicate a strong response of the CRCM evapotranspiration and precipitation biases to the physical parameterisation changes. Noticeable improvement was obtained in the simulated annual cycles of precipitation, evapotranspiration, moisture flux convergence and terrestrial water storage tendency when more sophisticated physical parameterisations are used. Some improvements are also observed for the simulated spatial distribution of precipitation and evapotranspiration. The simulated runoff is less sensitive to changes in the CRCM physical parameterisations.

2.1 Introduction

The hydrological cycle controls and regulates climate in a fundamental way through many complex interactions (Peixoto and Oort 1992). Inadequate understanding of the hydrological cycle and limited ability to model and predict the various hydrological cycle processes and their associated feedbacks contribute to many of the uncertainties associated with our understanding of long-term changes in the climate system (Watson et al. 2001). An international effort focusing on the understanding, measurement and modelling of water and energy cycles within the climate system at the continental scale has been undertaken within the framework of Continental-Scale Experiments (CSEs) of the Global Energy and Water Cycle Experiment (GEWEX) Hydrometeorological Panel (HP).

GEWEX initiated the Continental-Scale International Project (GCIP) in the early 1990s. The goals of GCIP were to understand the hydrology and water balance of the Mississippi River basin (Robock 2003). GCIP has recently transitioned into the GEWEX America Prediction Project, which aims to demonstrate skill in predicting changes in water resources at seasonal and annual timescales, as an integral part of the climate system. Many studies realised during GCIP have relied on global, regional mesoscale, land surface and hydrological models. Roads et al. (2003) provide a comprehensive description of GCIP water and energy budget synthesis (WEBS) by summarizing the estimates of several models as well as data of global and regional reanalyses. The models in their study include global circulation, regional climate and macroscale hydrologic models. They concluded that despite some agreement between the modelled and observed water budget components, there is still much quantitative uncertainty. Many other authors have undertaken water and energy budget studies over the region (e.g., Berbery and Rasmusson 1999, Berbery et al.

1999, Yarosh et al. 1999, Roads and Betts 2000, Maurer et al. 2001, Roads et al. 2002, Berbery et al. 2003, Ek et al. 2003). Effort is being carried out in these studies to understand improvements that are necessary in the models, reanalyses as well as observation products to better describe and eventually predict water and energy cycles.

Regional climate models (RCMs) can be powerful tools in quantitative studies of the hydrological cycle at the continental and sub-continental scales. These models, based on the fundamental laws of physics, can reproduce many of the complex processes in the hydrological cycle and can generate information about hydrological cycle components that are difficult to measure. Unfortunately, deficiencies in hydrological cycle modelling induce errors in RCMs simulations. These errors depend on the skill of the RCM itself, but also on the quality of the data used to drive the RCM at its boundaries. Model validation is therefore required to evaluate the magnitude of these errors. A thorough evaluation is also useful to identify errors in the model formulation and eventually correct them. Usually, only precipitation and river streamflow long-term observations are available at the regional scale. Surface flux measurements of latent and sensible heat that are very useful in model validations are extremely rare. Soil moisture and snow water equivalent, whose tendencies are important components of the water budget, are sporadically available in some regions. Therefore, we need to develop methodologies to carry out the validation of hydrological cycle components, takeing into account the available observations.

In the present study, we investigate the influence of changes in the physical parameterisation on the hydrological cycle of the Canadian Regional Climate (CRCM) by validating its water budget components using observations over the Mississippi River basin. Two model versions referred to here as CRCM_V3.6 and CRCM_V4.0 are used in this investigation. Atmospheric and terrestrial water budgets

are combined to estimate the components of the hydrological cycle that are not directly observed. These components are hence referred to as "quasi-observed" components and serve to validate the corresponding simulated fields. The paper is structured as follows: the water budget analysis and the validation approach are presented in section 2. Section 3 describes the CRCM and the experimental configuration. The datasets used for the validation of CRCM hydrological cycle are presented in section 4. Section 5 presents the validation of annual means of all water budget components for a 10-year period (1988-1997), the annual cycle validation and a comparison of the spatial distribution of some hydrological cycle components with the corresponding reference fields. The paper concludes in section 6.

2.2 Water budget analysis

The application of water mass conservation in a given control volume results in the water budget analysis. In this section, the atmospheric, terrestrial and combined water budget equations are presented as well as their application in the evaluation of the CRCM hydrological cycle.

2.2.1 Water budget equations

The water budget equation for an atmospheric column (per unit area) may be written as:

$$\frac{\partial W}{\partial t} = -\nabla_H \cdot \boldsymbol{Q} - (P - E), \tag{2.1}$$

where W (kg m^{-2}) is the precipitable water in the atmosphere, which represents the amount of water that would precipitate if all the water vapor in a column of the

atmosphere were condensed E (kg m^{-2} s^{-1}) is evapotranspiration, and P (kg m^{-2} s^{-1}) is precipitation. Note that the contribution of cloud water in the column can be neglected (see Paquin and Laprise 2003). The operator "$\nabla_H \cdot$" represents the horizontal divergence and $\boldsymbol{Q}$ is the vertically integrated horizontal water vapour flux:

$$\boldsymbol{Q} = \int_{p_{top}}^{p_s} q\boldsymbol{V}\frac{dp}{g}, \tag{2.2}$$

where q, $\boldsymbol{V}$ and g represent specific humidity, horizontal velocity vector, and gravitational acceleration, respectively. The lower limit in the integral (p_s) is the surface pressure and p_{top} is the pressure at the model lid.

Let us now consider the water balance requirement for the terrestrial branch of the hydrological cycle. Applying the water conservation law to a land column, the terrestrial water budget can be expressed as:

$$\frac{\partial(M+S)}{\partial t} = (P-E) - R, \tag{2.3}$$

where $M+S$ (kg m^{-2}) represents the storage of soil moisture (M) and the accumulated snowpack (S), and R (kg m^{-2} s^{-1}) is the total runoff, which includes the surface runoff and recharge from the ground water reservoir (subsurface runoff).

The term $(P-E)$ is common for equations (2.1) and (2.3) and it establishes the connection between the terrestrial and atmospheric branches of the hydrological cycle. Elimination of $(P-E)$ between these two equations yields a combined budget equation:

$$-\frac{\partial W}{\partial t} + C = \frac{\partial (M+S)}{\partial t} + R, \tag{2.4}$$

with $C = -\nabla_H \cdot \boldsymbol{Q}$. Equation (2.3) links the two branches of the hydrological cycle (Peixoto and Oort 1992). A schematic illustration of the combined water balance is shown in Fig. 2.1.

2.2.2 Validation methodology

An integrative analysis approach is used in the validation of the CRCM hydrological cycle. This approach links both the terrestrial and atmospheric branches and involves a long-term time mean of the hydrological cycle components, spatially averaged over a large area; in our case, the Mississippi River basin.

1) Annual means analysis approach

Taking time and spatial averages of the atmospheric and terrestrial water budget equations (2.1) and (2.3) over a multiyear period and over the whole basin leads to the following equations:

$$\left[\overline{C}\right] = \left[\overline{P}\right] - \left[\overline{E}\right], \tag{2.5}$$

and

$$\left[\overline{R}\right] = \left[\overline{P}\right] - \left[\overline{E}\right], \tag{2.6}$$

where $\overline{X}$ represents the time average of component X, and $\left[X\right]$ is the spatial average (over the entire Mississippi River basin). Annual mean tendencies of atmospheric and

terrestrial water storage ($\left[\frac{\partial \overline{W}}{\partial t}\right]$ and $\left[\frac{\partial(\overline{M}+\overline{S})}{\partial t}\right]$) can safely be neglected because they tend towards zero when averaged over long period of time.

In order to validate the various components of equations (2.5) and (2.6) from the simulation, the corresponding observed values must be known. An estimation of annual mean precipitation for the basin ($\left[\overline{P}\right]_{OBS}$) can be obtained from existing gridded precipitation analysis data sets. River streamflows observed at gauging stations are available for many river basins, so a fairly good accuracy can be obtained for the annual mean runoff for the Mississippi River basin $\left[\overline{R}\right]_{OBS}$.

Evapotranspiration observations are seldom available at the regional scale and evapotranspiration must be estimated as a residual using the water budget analysis. We used the time- and space- averaged terrestrial water budget equation (2.6) to obtain the "quasi-observed" evapotranspiration:

$$\left[\overline{E}\right]_{QOBS} = \left[\overline{P}\right]_{OBS} - \left[\overline{R}\right]_{OBS}. \tag{2.7}$$

The model-simulated atmospheric water vapour convergence over the basin can be compared with the convergence computed from reanalysis data ($\left[\overline{C}\right]_{REAN}$). It must be emphasized that the characteristics of reanalysis data, such as spatial and temporal sampling, vertical resolution, and treatment of the lower boundary layer in the computation, limit the accuracy of estimated water vapour convergence.

2) Annual cycle analysis approach

The validation of the annual cycle of water budget components is more complex and involves larger uncertainties. While terrestrial and atmospheric water storage components can be neglected for multi-year means, they cannot be neglected for monthly means, as these terms can be particularly large during spring and fall (Rasmusson 1968). For the annual cycle analysis, the averaged water budget equations become:

$$\left[\frac{\partial \overline{W}_i}{\partial t}\right] = \left[\overline{C}_i\right] + \left[\overline{E}_i\right] - \left[\overline{P}_i\right], \tag{2.8}$$

$$\left[\frac{\partial (\overline{M} + \overline{S})_i}{\partial t}\right] = \left[\overline{P}_i\right] - \left[\overline{E}_i\right] - \left[\overline{R}_i\right], \tag{2.9}$$

where $\overline{X}_i = \frac{1}{J}\sum_{j=1}^{J} X_{i,j}$ is the climatological monthly mean for month "i", based on J years, with $X_{i,j}$ the monthly mean for month "i" and year "j".

Quasi-observed climatological monthly evapotranspiration can now be obtained as a residual of the atmospheric water balance as:

$$\left[\overline{E}_i\right]_{QOBS} = \left[\frac{\partial \overline{W}_i}{\partial t}\right]_{REAN} - \left[\overline{C}_i\right]_{REAN} + \left[\overline{P}_i\right]_{OBS}. \tag{2.10}$$

Finally, climatological monthly values of quasi-observed terrestrial water storage tendencies can be computed as residuals from the combined water budget equation (2.4):

$$\left[\frac{\partial(\overline{M}+\overline{S})_i}{\partial t}\right]_{QOBS} = \left[\overline{C}_i\right]_{REAN} - \left[\frac{\partial \overline{W}_i}{\partial t}\right]_{REAN} - \left[\overline{R}_i\right]_{OBS} \qquad (2.11)$$

The terms $\left[\overline{P}_i\right]_{OBS}$, $\left[\overline{R}_i\right]_{OBS}$, $\left[\frac{\partial \overline{W}_i}{\partial t}\right]_{REAN}$ and $\left[\overline{C}_i\right]_{REAN}$ can be obtained from one of the existing datasets based on in situ observations (first two terms) and from reanalysis (last two terms). The accuracy of atmospheric water balance estimations depends on the investigated domain area. Seneviratne et al. (2004) have shown that the critical domain size for the water-balance estimation for terrestrial water storage using water vapour flux convergence from high-resolution ECMWR reanalysis (ERA-40) is $2\times10^5\ km^2$. Earlier studies (Rasmusson 1968, 1977) based on raw radiosonde data over North America, recommended even larger regions, larger than 10^6 km^2. The surface of the Mississippi River basin is approximately 3.2×10^6 km^2, thus satisfying both criteria.

2.3 CRCM description and experimental configuration

2.3.1 Model description

The CRCM is a limited-area nested model, originally developed at Université du Québec à Montréal, based on the fully elastic non-hydrostatic Euler equations. These equations are solved by non-centred semi-implicit and semi-Lagrangian numerical algorithm (Caya 1996; Laprise et al. 1998; Caya and Laprise 1999). The CRCM horizontal grid is uniform in a polar stereographic projection, with a typical 45 km grid mesh (true at 60° N) and its vertical resolution is variable using a Gal-Chen scaled-height terrain-following coordinate. In this study, two versions of the

CRCM referred to as CRCM_V3.6 and CRCM_V4.0 are used. In the following paragraphs, some model characteristics, pertaining to the hydrological cycle are described.

The CRCM_V3.6 shares most of the subgrid-scale physical parameterisation package of the second generation Canadian Coupled General Circulation Model (CGCM2, Flato and Boer 2001; McFarlane et al. 1992). The stratiform precipitation is parameterized as a simple supersaturation-based condensation scheme, while the convective processes are described by the Bechtold-Kain-Fritsch (BKF) mass flux scheme (Bechtold et al. 2001), adapted to the CRCM resolution.

The land surface processes in the CRCM_V3.6 are described by Manabe-based (1969) land surface scheme originally presented in McFarlane and Laprise (1985) and McFarlane et al. (1992). This scheme treats soil moisture storage as a single layer, with gains and losses occurring only at the surface via infiltration and evapotranspiration (drainage from the bottom of the layer is neglected). Infiltration is assumed to equal rainfall until the soil moisture exceeds the soil water-holding capacity, the excess water is assigned to runoff. The surface evapotranspiration rate is defined as a product of potential evapotranspiration and the factor of moisture availability (β-function), which is a simple function of the total soil moisture amount and soil water holding capacity. As discussed by McFarlane et al. (1992), the use of β function is appropriate when dealing with bare soil alone. To take into account - to some extent - the effects of vegetation on surface evaporation (the canopy is not modelled explicitly), the soil water holding capacity is made to vary with both vegetation and bare soil characteristics of the surface. The Wilson and Henderson-Sellers (1985) land-surface global dataset is used to specify soil properties and to determine the most frequently occurring primary and secondary vegetation classes.

The updated version of the model (CRCM_V4.0) is an important evolution from the previous version. The parameterisation package of the CRCM_V4.0 includes change to: the radiation scheme; the treatment of cloud cover; the boundary layer mixing scheme; and the land surface parameterisation scheme. A new radiation scheme uses four bands in the visible and near infrared region, replacing an earlier two-band parameterisation, to describe solar radiation heating. The treatment of the terrestrial radiation uses broad-band emissivities and a more detailed vapour continuum (Puckrin et al. 2004). A new cloud scheme adds layer stability to relative humidity as a parameter for triggering cloud formation (Paquin and Harvey 2003). The boundary layer mixing scheme has been modified to include non-local mixing of heat and moisture. Instead of mixing surface fluxes only with the lowest model layer, the new mixing scheme evenly adds fluxes to whole boundary layers so as to mimic the vertical profiles of water vapour and potential temperature in a well-mixed planetary boundary layer (Jiao and Caya 2006). The Manabe-based formulation of the land surface processes is replaced by a state of the art land surface scheme (Canadian LAnd Surface Scheme, CLASS_2.7, Verseghy 1991; Verseghy et al. 1993) in order to provide a more realistic description of water and energy exchange between the land surface and the atmosphere. The soil column in CLASS comprises a 10-cm surface layer, 25-cm vegetation root zone and a 3.75-m deep soil layer. The layers' liquid and frozen moisture contents as well as temperature are prognostic variables. They evolve following energy and moisture fluxes at the top and bottom of each layer. CLASS uses Darcy's equations to evaluate water fluxes between the layers. Water infiltration into the upper soil layer is treated as a downward propagation square wave (Mein and Larson 1973). When the infiltration capacity is exceeded, water is allowed to pond on the surface up to a maximum surface retention capacity, which varies according to land cover. The overflow of the surface retention capacity is assumed to be surface runoff. The subsurface runoff refers to the drainage of water from the deep soil column and is parameterized as $Q_d = k_{sat}(w_d / w_{sat})^{2b+3}$, where w_d is the volumetric

water content ($m^3\ m^{-3}$) in the deep soil layer, w_{sat} is the saturation soil water content, k_{sat} is the saturation hydraulic conductivity. The b, w_{sat} and k_{sat} depend on soil type. Vegetation canopy in CLASS is treated explicitly. The vegetation properties are determined based on the following vegetation types: coniferous trees deciduous trees, crops and grass. The leaf area index, roughness length, area mass, and rooting depth of each of those groups are considered as varying over seasonal timescale. Evapotranspiration over land originates from the following sources: bare soil evaporation from the topsoil layer, potential evaporation of the canopy intercepted water and transpiration from the root zone. The canopy interception capacity is a function of the leaf area index and varies for liquid or solid precipitation. Transpiration is controlled by the bulk canopy stomatal resistance, which is a function of leaf area index, incoming solar radiation, atmospheric vapour pressure deficit, temperature, and soil moisture tension.

As mentioned above, the CRCM uses the semi-Lagrangian numerical scheme, which results in a slight non-conservation of transported fields. A corrective factor that takes into account this inaccuracy is introduced in the CRCM_V4.0 and is applied to the specific humidity values at each grid point. The calculation of the corrective factor is presented in Paquin and Laprise (2003).

Finally, it should be noted that, in both the CRCM_V3.6 and the CRCM_V4.0, the atmospheric moisture flux is calculated on each model level (Gal-Chen) and vertically integrated at each time step. Moisture flux convergence is derived from accumulated (during 6-hour time interval) vertically integrated atmospheric moisture flux.

2.3.2 Experimental setup

Two model simulations will be analyzed in this study; one performed using CRCM_V3.6, while the other one uses CRCM_V4.0. The computational domain for both models covers the whole of North America (AMNO domain; Amérique du Nord, in French), and parts of the adjacent Pacific, Atlantic and Arctic Oceans. The simulations were driven by 6-hourly NCEP/NCAR reanalyses over the 1959-1999 period, linearly interpolated in time to the model's 15-minute time step. The sea-surface temperature and sea-ice coverage are taken from the AMIP-II database (Fiorino 1997). In addition to the nesting method of Davies (1976) used in most regional climate models to specify their lateral boundaries and to ensure coherence between the large-scale circulations of the driving and driven models over the large AMNO domain, the large-scale (length scale longer than 1400 km) horizontal wind field from the CRCM was nudged toward the large-scale wind of the driving data (Riette and Caya 2002). The nudging coefficient increases linearly above 500 hPa to reach 0.05 at the top level. The simulations were performed at a 45-km horizontal resolution using 29 unequally spaced Gal-Chen levels. The lowest thermodynamic level is at about 170 m above the surface, and the computational lid is near 29 km. Most of the vertical levels are assigned to the lower troposphere in order to allow the planetary boundary layer and lower troposphere to be well resolved. Fig. 2.2 presents the domain where the analysed region over the Mississippi River basin is indicated. A discretization of major river basins at 5' resolution by Graham et al. (1999) is used as a template to define the Mississippi basin.

2.4 Validation Datasets

The components derived directly from observations or closely connected to them, can be used as reference fields in the validation of model simulated hydrological cycle components. In this section, we describe the datasets used to supply some of the observations to validate the hydrological cycle components.

2.4.1 Precipitation dataset

Precipitation estimates, both global and regional, can be derived from either surface gauge measurements or satellite sensors. Satellite measurements provide complete spatial coverage, but their main disadvantage is that only relatively short records exist, accompanied with discontinuities occurring from sensor and platform changes and orbital variations. On the other hand, precipitation gauges provide records covering the entire twentieth century, however their disadvantage is that they cover only about 25% of Earth's surface (New et al. 2001). The most important source of error in gauge measurements arises because of gauge undercatch, which usually occurs during snowfall in colder area. Legates and Willmott (1990) estimated a global mean undercatch of total precipitation (rain and snow) to about 11%. Undercatch also varies with gauge type, therefore instrumental changes can result in non-homogeneities in the records. The correction of individual records requires detailed local meteorological and station meta-information.

For climate model evaluation, the use of gridded dataset of precipitation is preferred. Gridding is a necessary preliminary step that helps to reduce biases arising from the irregular station distribution. Several gridded datasets of monthly precipitation have been developed in recent years by groups such as the Climatic Research Unit (CRU; Hulme 1994; New et al. 2000; Mitchell and Jones 2005), the Global Precipitation Climatology Project/Centre (GPCP; Rudolf et al. 1999, Adler et al. 2003), the Center for Climatic Research (CCR: Willmott and Matsuura 2004), and the Global Historical Climatology Network (Peterson and Vose 1997). New et al. (2000) specify that the major sources of difference in gridded precipitation datasets are due to insufficient station coverage as well as by using different interpolation methods. The Mississippi River basin has good station coverage (see Fig. 2.2c in Roads et al. 2003), as such, there should not be significant differences between existing precipitation gridded datasets for this region.

The data of three available gridded monthly precipitation datasets were used in this study: CRU (Mitchell and Jones 2005), CCR (Willmott and Matsuura 2004) and GPCP (Adler et al. 2003). The CRU gridded dataset, already available for 1901-1995 (New et al. 2000), has recently extended to 2000 by Mitchell and Jones (2005). The primary variables (precipitation, mean temperature and diurnal temperature range) were interpolated directly from station observations to a regular 0.5° latitude x 0.5° longitude grid following a method adapted from Piper and Stewart (1996). The correction for undercatch of precipitation was not carried out. The CCR (Willmott and Matsuura 2004) precipitation dataset covers the 1950-1999 period. Surface station observations were interpolated to a 0.5° lat x 0.5° lon grid using a spherical version of Sherpard's method (Shepard 1968, Willmott et al. 1985). As for CRU, CCR precipitation data did not correct for undercatch of precipitation. The approach used by Adler et al. (2003) in the production of GPCP dataset (for 1979-2003 period) involved combining the precipitation information available from different sources into a final merged product. The surface rain gauge data were corrected for undercatch of precipitation using Legates' (1987) method. The station data were first interpolated using Wilmott et al. (1985) method to a regular 0.5° latitude x 0.5° longitude grid and then averaged to provide area mean precipitation on 2.5° grid cells. A gauge analysis is merged to precipitation data obtained from low-orbit microwave and geosynchronous orbit satellite infrared measurements. The higher accuracy of the low-orbit microwave observations is used to calibrate the more frequent geosynchronous infrared observations.

2.4.2 Runoff datasets

The total runoff from a drainage basin can be estimated from streamflow observations at gauging stations, where the direct observation of the stream water level is transformed to discharge via a rating curve. The rating curve is constructed by fitting discrete coincident observations of water level and discharge. For the Mississippi River basin, the observed data can be obtained from the US Geological Survey (USGS) measurements (http://waterdata.usgs.gov/nwis/sw), which routinely collect streamflow data at numerous gauging stations (see Fig. 2.2d in Roads et al. 2003). Since the Mississippi River basin is affected by water management practices, the so-called naturalized runoff (removing the effect of water management) is preferred for model validation purpose. Maurer and Lettenmaier (2001) estimated naturalized runoff using streamflow at the USGS gauge at Vicksburg MS and extrapolated this value to the entire Mississippi River basin. The dataset contains monthly and annual series for the period 1988-2000. We used this dataset for validation of the CRCM runoff averaged over basin. This is also used for estimations of mean annual evapotranspiration over the basin and monthly tendencies of terrestrial water storage (see Eqs 2.7 and 2.11).

In order to validate the spatial distribution of simulated runoff (Sections 2.5.5 and 2.5.6), the composite grided runoff dataset, developed by the Global Runoff Data Center (GRDC) can be used. It has a high resolution (0.5° latitude x0.5° longitude), however the water management effect is neglected. The dataset is constructed using USGS observation data and data from other National Hydrological Services, along with GRDC climate-driven water balance model (Fekete et al. 2000). The observation data covers mid-1960s to the mid-1980s period. We also use the Variable Infiltration Capacity (VIC) model runoff data at 1/8 degree resolution (Maurer et al. 2002). As suggested by Roads et al. (2003), VIC may actually provide a realistic geographic distribution of Mississippi runoff. It must be emphasized however, that the VIC model is tuned to reproduce observed runoff at the outlet of major tributaries of the

Mississippi and its pattern is not realistic in the central, northern part of the basin (Roads et al. 2003).

2.4.3 Reanalyses Datasets

The global and regional reanalysis products, such as those from the National Centers for Environmental Prediction/National Center for Atmospheric Research (NCEP/NCAR), National Centers for Environmental Prediction/U.S. Department of Energy (NCEP/DOE), European Centre for Medium Range Weather Forecasting (ECMWF) as well as NCEP North American Regional Reanalysis (NARR) provide long time series of optimal estimations of the 4-dimensional state of the atmosphere. The motivation for the reanalysis projects was the apparent "climate change" detected in the standard analysis data resulting from many changes introduced into data assimilation systems in order to improve the forecasts. The basis of these projects was to use a frozen version of a numerical weather prediction model retrospectively and perform data assimilation using an observed database as completely as possible. In this regard, the reanalyses can provide an excellent source for the estimation of variables that are closely linked to assimilated variables.

In the present study, we use the vertically integrated moisture convergences and precipitable water tendencies computed from NCEP/NCAR and ECMWF 40-yr reanalyses (ERA-40). The NCEP/NCAR system is based on a numerical weather prediction model with T62 spectral resolution (≈200 km) and 28 sigma levels in the vertical with five of those levels in the atmospheric boundary layer. Kalnay et al. (1996) classify the quality of NCEP/NCAR reanalysis variables based on how closely related an archived variable is to assimilated observations. All variables are separated into three classes: A to C, where A class variables are directly influenced by observations; B class variables are partly influenced by the reanalysis model; and

variables assigned to class C are completely determined by the model. Under this scheme, variables required for moisture flux convergence calculations (atmospheric profiles of wind and moisture) are assigned to classes A and B, respectively. The precipitable water, which is a variable of interest in the current study, belongs to class B. Satellite data of moisture have been made available to the global analysis systems since 1979, from TIROS (**T**elevision **I**nfra-**R**ed **O**bserving **S**atellite) Operational Vertical Sounder (TOVS). After July 1987, the fields of precipitable water and other quantities from Special Sensor Microwave/ Imager (SSM/I) became available.

Trenberth (1997) discusses the apparent differences when the computations of budget components from the reanalyses are performed on the model (sigma) and on pressure coordinates. He emphasized how the best possible accuracy of the budget products is obtained when the full-resolution 4-time daily data on model coordinates are used in calculations. This is particularly important for the moisture flux calculation since the moisture transport in the lower troposphere cannot be well resolved when pressure level fields are used.

The monthly series of vertical integrated moisture convergence and precipitable water tendencies, derived from NCEP/NCAR full-resolution data are obtained from UCAR Climate and Global Dynamics Division (http://www.cgd.ucar.edu/cas/catalog/newbudgets/index.html). This dataset spans the 1979-2001 period, and incorporates TOVS reruns in addition to the grid correction implemented by NCEP for reanalysis data covering the period of March 1979 through October 2001. For the moisture flux calculations, the fields of eastward and northward wind components and specific humidity at a 6-hour interval on each model (sigma) level are used. The monthly mean of the basic (u, v, q) and derived variables (uq, vq) are computed from the 6–hour data before any vertical integration is performed.

The ERA-40 model has a T159 spherical harmonic representation of the atmospheric dynamical and thermodynamical fields, and a gridpoint representation of humidity and cloud variables (Hortal and Simmons 1991). In the horizontal, the so-called reduced Gaussian grid is used with a grid spacing of about 112 km. A vertical coordinate is a hybrid sigma-pressure coordinate with 60 levels in the vertical (15 of those levels are in the first 2000m). The monthly series of moisture flux convergence and precipitable water tendency, derived from ERA-40 full resolution has been provided by ECMWF. For a detailed description of the computation of moisture flux convergence, the reader is referred to Seneviratne et al. (2004).

2.5 Results and discussion

The annual and monthly means of the CRCM-simulated hydrological cycle components over the Mississippi River basin are analyzed and compared with the available reference fields. The analysis is restricted to the 1988-1997 period for which monthly series of the naturalized runoff, ERA-40 moisture flux convergence and precipitable water tendency were available.

2.5.1 Analysis of the CRCM_V3.6 simulation: annual means of water budget components

Water mass conservation, when applied to the annual scale over the basin, requires that the atmospheric moisture flux convergence balances the difference between precipitation and evapotranspiration ($P - E$) and therefore the runoff (see Eqs. 2.5 and 2.6). As can be seen from Fig. 2.3, where the summary of the annual-

mean analysis is presented, the CRCM_V3.6 moisture flux convergence ($C_{CRCM\_V3.6} = 0.28$ mm day^{-1}) does not exactly balance the simulated $(P - E)$ ($P_{CRCM\_V3.6} - E_{CRCM\_V3.6} = 0.39$ mm day^{-1}) and runoff ($R_{CRCM\_V3.6} = 0.39$ mm day^{-1}) i.e., the model hydrological cycle is closed with an error of about 0.1 mm day^{-1}. Because the moisture flux convergence is calculated within the model using all levels and time steps, a fair part of this error in the atmospheric budget is related to the semi-Lagrangian numerical scheme, which induces a slight non-conservation of the prognostic variables (Paquin and Laprise 2003).

Comparing the moisture flux convergence calculated from the NCEP/NCAR reanalysis ($C_{NCEP} = 0.50$ mm day^{-1}) to the naturalized runoff ($R_{NAT} = 0.66$ mm day^{-1}), an error in the closure of the quasi-observed water budget of $\varepsilon_{QOBS} = 0.16$ mm day^{-1} is also seen in our analysis. This lack of balance could be related to inaccuracies in the atmospheric moisture flux convergence calculated from NCEP/NCAR reanalysis data, or in the runoff data and gives an approximation of the error bars on our observations. The coarse horizontal and vertical resolutions and the time sampling for calculating the fluxes of NCEP/NCAR reanalysis as well as NCEP model physics can introduce errors in atmospheric moisture and wind vertical profiles. As well, the estimation of water management effects can introduce errors to the naturalized runoff value. In addition, the streamflow measurements at the outlet of streams are an imperfect measure of complete runoff. An evaluation of the uncertainties in the moisture flux convergence calculated from the reanalysis data could be undertaken by comparing the NCEP/NCAR convergence to those calculated from ERA40. The difference between annually averaged moisture flux convergences from the ERA40 and NCEP/NCAR reanalyses for the Mississippi River basin is 0.2 mm day^{-1}. The ERA40 moisture flux convergence ($C_{ERA40} = 0.70$ mm day^{-1}) balances much better the naturalized runoff, while the NCEP/NCAR convergence is closer to the observed

runoff, derived from streamflow observations at Vicksburg, MS ($R_{OBS} = 0.57$ mm day^{-1}).

Mean annual precipitation over the basin simulated by the CRCM is compared to precipitation obtained from three observation datasets (CRU2, GPCP and CCR). The uncertainty of observed precipitation, which is annually averaged over the basin, is much smaller than the uncertainty associated with the reanalysis moisture convergence: the maximum difference between precipitation datasets used for this analysis is 0.08 mm day^{-1} (see Fig. 2.3).

The CRCM_V3.6 annual mean precipitation ($P_{CRCM\_V3.6} = 2.63$ mm day^{-1}) is higher than observed by about 0.4 mm day^{-1} (+17%). The comparison of the CRCM_V3.6 simulated evapotranspiration ($E_{CRCM\_V3.6} = 2.24$ mm day^{-1}) to quasi-observed ($E_{QOBS} = 1.58$ mm day^{-1}) indicates a positive bias in the model of about 0.7 mm day^{-1} (+42%). Since the quasi-observed evapotranspiration is estimated from the multi-year observed precipitation (average of three datasets) and from the naturalized runoff (see Eq. 2.7), it should be relatively realistic. The simulated annual mean runoff $R_{CRCM\_V3.6} = 0.39$ mm day^{-1} is smaller than the naturalized runoff by about 0.3 mm day^{-1} (-41%). This discrepancy is related to the excess in evapotranspiration bias with respect to the precipitation bias. When the simulated atmospheric moisture flux convergence ($C_{CRCM\_V3.6} = 0.28$ mm day^{-1}) is compared to the NCEP/NCAR and ERA40 convergences, the model biases of –0.2 (-44%) and –0.4 mm day^{-1} (-60%) are obtained.

The results presented above show that the hydrological cycle over the Mississippi River basin as simulated by the CRCM_V3.6 basin is characterized by a relatively large deficit of moisture convergence and by excess evapotranspiration. Hence, the simulated moisture convergence cannot be the cause of the excess of the mean annual

precipitation over the basin. Therefore, the excessive evapotranspiration could be a major source of the error in the precipitation.

The CRCM_V3.6 evapotranspiration is conditioned by its simple single-layer surface scheme. The prescribed soil water-holding capacity in this model version seems to be very large (average value over the basin is 528 kg m^{-2}). The soil water-holding capacity is an important parameter affecting evapotranspiration: a too small water-holding capacity will favour more runoff (the soil rapidly reaching is saturated value) thus reducing the water available for evaporation; a too large value allows for a larger fraction of precipitation to be stored and later released for evaporation therefore reducing the runoff. As such, the large CRCM_V3.6 water-holding capacity can be linked to the excessive evapotranspiration and inadequate runoff. An additional reason for the excessive evapotranspiration rate is the lack of vegetation stomatal resistance, which could reduce the evapotranspiration considerably.

2.5.2 Analysis of the CRCM_V3.6 simulation: climatological annual cycle of water budget components

Figure 2.4 presents the mean annual cycles for all components of the monthly averaged atmospheric water budget equations (Eqs. 2.8 and 2.9). In Fig. 2.4a, the observed and simulated annual cycles of precipitation are compared. Since the uncertainty of observed monthly mean precipitation is small, we can safely take an average of our three precipitation datasets to represent observed precipitation over the basin. The CRCM_V3.6 slightly underestimates observed precipitation during November to March, but largely overestimates it during summertime. The positive precipitation bias (BIAS_P) of the CRCM_V3.6 on the annual time-scale is therefore caused mainly by an extensive over-estimation of the precipitation from June to August.

The simulated annual cycles of evapotranspiration are compared to the quasi-observed values in Fig. 2.4b. The monthly mean of quasi-observed evapotranspirations are derived as a residual from the atmospheric water budget using mean observed precipitation and NCEP/NCAR (ERA40) moisture convergences and precipitable water tendencies (see Eq. 2.10). An estimation of the uncertainty in the quasi-observed evapotranspiration derived from the atmospheric water budget could be obtained by comparing its annual mean to the one derived from the land water budget using Eq. 2.7. The annual mean evapotranspiration derived from the atmospheric water budget using NCEP/NCAR (ERA40) data is higher (smaller) by 0.2 mm day^{-1} (0.02 mm day^{-1}) than residual evapotranspiration derived from the terrestrial water budget. The major differences in the quasi-observed evapotranspiration derived from the atmospheric water budget appear during spring (see Fig. 2.4b).

The CRCM_V3.6 evapotranspiration is larger than both quasi-observed evapotranspirations throughout the year. The positive evapotranspiration bias (BIAS_E) increases during spring and reaches its maximum in June, which is related to the warm air temperature and large soil moisture available for evapotranspiration during this period of the year.

The NCEP/NCAR, ERA40 and CRCM_V3.6 annual cycles of the atmospheric moisture flux convergence are compared in Fig. 2.4c. The NCEP/NCAR shows atmospheric moisture flux convergence during October to May, reaching a maximum in January and moisture flux divergence during June to September with a maximum in July. As discussed by Roads (2002), the large summertime divergence seen in the reanalysis is disconcerting since it occurs at a time when the low-level jet is usually active and thought to be a strong contributor to moisture convergence in the region. However, the ERA40 reanalysis also shows a moisture flux divergence in summer,

which is even slightly higher than that of NCEP/NCAR. On the other hand, NCEP/NCAR moisture flux convergence from October to May is smaller than the ERA40. The most significant difference between the two reanalyses appears during March to May, reaching a maximum of 0.54 mm day^{-1} in May. Despite this uncertainty, it can be seen that the increasing observed precipitation during spring over the Mississippi River basin is related only to the increasing evapotranspiration because moisture flux convergence derived from NCEP/NCAR (ERA40) slightly decreases (remain similar) from March to May.

Similar to the reanalyses, the CRCM_V3.6 shows atmospheric moisture flux divergence over the Mississippi River basin during the summer and at the beginning of the fall, and a moisture flux convergence during the rest of year. However, the simulated annual cycle amplitude is smaller compared to those from the reanalyses: while the moisture flux divergences from the reanalyses are strong during July to August and drop in September, the CRCM_V3.6 moisture divergence keeps a similar magnitude from July to September. In addition, the simulated atmospheric moisture convergence, which appears over the basin in October and lasts until May, is smaller than those from the reanalyses.

The quasi-observed monthly tendencies of the atmospheric water storage (Fig. 2.4d) are relatively small and CRCM_V3.6 captures them well.

In order to better understand the model behaviour, we compared the CRCM_V3.6 simulation biases of the atmospheric water budget components to each other in Fig. 2.5a. Since precipitation removes moisture from the atmosphere and evapotranspiration represents a source of atmospheric humidity, the negative difference between BIAS_P and BIAS_E from September to May could generate a positive bias of simulated atmospheric specific humidity, which in turn could be compensated by the decreasing moisture flux convergence over the basin. It is

interesting to note that the underestimation of the moisture flux divergence (with respect to the one computed from NCEP/NCAR and ERA40), from July to August, is linked to the excess in precipitation bias with respect to the evapotranspiration bias. The error in closure of the simulated atmospheric water budget is also shown in Fig. 2.5a and has a maximum value in summer.

Figs. 2.6 and 2.7 present mean annual cycles of the terrestrial water budget components and corresponding CRCM biases. The naturalized, observed and the CRCM_V3.6 runoff are compared in Fig. 2.6a: runoff is underestimated by the model, throughout the year, particularly in the first three months, when the negative bias reaches 0.4 mm day^{-1}. There are two sources of runoff underestimation by this model version. The first is related to the deficiencies in the "bucket" surface scheme: runoff is generated only when soil moisture content exceeds the prescribed water-holding capacity, which is too large. The second one is related to the biases of simulated precipitation and evapotranspiration. The negative bias in the difference between precipitation and evapotranspiration i.e., the underestimation of the $(P - E)$ term (simulated and quasi-observed $(P - E)$ are compared in Fig. 2.6b), which moistens the soil during September to May, contributes to the runoff underestimation throughout the year by the model.

The annual cycle of the CRCM terrestrial water storage tendency and the quasi-observed one (derived from naturalized runoff and moisture convergences and precipitable water tendencies of the reanalyses, see Eq. 2.11) are compared in Fig. 2.6c. It should be emphasized that the quasi-observed monthly tendencies of the terrestrial water storage are not free from errors. Rough error estimation by calculating quasi-observed annual mean tendency, gives -0.2 mm day^{-1} (with NCEP/NCAR moisture flux convergence) and 0.08 mm day^{-1} (with ERA40 moisture flux convergence). These errors are linked to the error in the closure of quasi-

observed water balance. Unfortunately, the seasonal error distribution in water balance estimates is unknown.

The terrestrial water tendencies simulated by the CRCM_V3.6 are relatively close to the quasi-observed, except during summer, when the evapotranspiration exceeds precipitation and hence the soil dries. In summer, the positive bias in precipitation exceeds bias in evapotranspiration, which is consistent with the summer soil drying underestimation. In addition, the negative runoff bias contributes to the summer soil drying underestimation.

2.5.3 Analysis of the CRCM_V4.0 simulation: annual mean of water budget components

The changes in the physical parameterisation between model versions 3.6 and 4.0, described in Section 2.3.1, result in a significant decrease of 0.50 mm day^{-1} in the annual mean evapotranspiration over the Mississippi River basin. As can be seen from Fig. 2.3, the annual mean of simulated evapotranspiration by the updated model version ($E_{CRCM\_V4.0} = 1.74$ mm day^{-1}) is closer to the quasi-observed. Implementation of CLASS in the CRCM provides a more realistic parameterisation of the evapotranspiration including the stomatal resistance effect in its vegetation. This resistance restricts transpiration of water extracted from the soil by vegetation roots. Modifications of the radiative scheme and treatment of the cloud cover result in an increased atmospheric absorption of the incoming solar radiation and an increased planetary albedo. As a consequence, the net radiative energy at the surface (R_{net}), which is mainly partitioned between latent and sensible heat fluxes, is decreased. This can be seen in Fig. 2.8, which also shows how R_{net} is partitioned between latent and

sensible heat in both model versions: latent heat of the CRCM_V 4.0 is smaller than the one from the CRCM_V3.6, while the sensible heat is larger.

Another water budget component that has changed significantly is the annual mean precipitation: the decrease of the annual mean evapotranspiration of 0.50 mm day^{-1} over the basin is associated with a decrease of annual mean precipitation of 0.47 mm day^{-1}. Simulated precipitation is now much closer to the observed: precipitation bias is reduced from 0.4 to -0.1 mm day^{-1}. Changes in the annual mean moisture flux convergence and runoff are smaller than the error in closure of the annual mean water budget of the CRCM_V3.6 (0.1 mm day^{-1}). The annual mean of the CRCM_V4.0 moisture flux convergence ($C_{CRCM\_V4.0} = 0.36$ mm day^{-1}) exactly balances the difference between precipitation and evapotranspiration ($(P-E)_{CRCM\_V4.0} = 0.36$ mm day^{-1}) as well as runoff ($R_{CRCM\_V4.0} = 0.36$ mm day^{-1}). Elimination of the water budget closure error is provided by introducing a small correction to the specific humidity values at each grid point (Paquin and Laprise 2003).

2.5.4 Analysis of the CRCM_V4.0 simulation: climatological annual cycle of water budget components

Figure 2.5b shows the CRCM_V4.0 biases of the monthly averaged atmospheric water budget components. These biases are noticeably smaller compared to those of CRCM_V3.6. Although the simulated annual cycle of precipitation by the updated model version matches the observed precipitation better, it is now underestimated throughout most of the year (July to March), especially from July to October. The negative bias in precipitation is mainly related to the underestimation of evapotranspiration (see also Fig. 2.4).

As discussed in the previous section, the significant change in the simulated annual mean evapotranspiration does not noticeably affect the annual mean simulated moisture flux convergence; the change being smaller than the error in closure of the CRCM_V3.6 annual water budget. However, from Fig. 2.9 (where the difference between the atmospheric water budget components of the CRCM_V4.0 and CRCM_V3.6 is shown) it can be seen that the moisture flux convergence (as well as precipitation) actually responds to the evapotranspiration change: a decrease of the evapotranspiration is associated with an increase in the moisture flux convergence from September to May. Despite this change, the moisture flux convergence over this period remains smaller than those from the reanalyses. Summer moisture flux divergence from the CRCM_V4.0 is larger than the one from CRCM_V3.6 and matches those of the reanalyses better. The bias in the precipitation is now almost equal to the bias in evapotranspiration because of the larger decrease in precipitation than in evapotranspiration. Such a large decrease in summer precipitation is related to the combined effects of the evapotranspiration reduction and stronger mixing in the CRCM_V4.0 boundary layer water vapour. The new vertical diffusion scheme distributes the water vapour on more levels within the boundary layer and therefore avoids the excessive accumulation of moisture in the near surface boundary layer. Jiao and Caya (2006) demonstrated how the accumulation of moisture in the lower boundary layers with the old scheme provides favourable conditions for triggering the convection. The new vertical diffusion scheme implemented in CRCM_V4.0 together with the reduced evapotranspiration, results in less favourable conditions for convection, therefore reducing condensation and precipitation.

Figure 2.7b shows the CRCM_V4.0 biases of the monthly averaged terrestrial water budget components. Despite some improvement in the simulated annual cycle of the moisture storage tendency as well as the *(P-E)* term (see also Fig. 2.6), the CRCM_V4.0 runoff remains underestimated throughout most of the year. The

negative runoff bias (BIAS_R) of the CRCM_V4.0 is even larger than the one of the CRCM_V3.6, from May to December.

2.5.5 Spatial distribution: validation of the CRCM_V3.6 simulated fields

In the previous sections, the hydrological cycle components averaged in time (1988-97) and in space (over the entire Mississippi River basin) have been discussed. The spatial distribution of precipitation, runoff and evapotranspiration over the basin is now investigated when averaged over the same period.

The precipitation fields simulated by the CRCM are compared to those of CRU, CCR and GPCP in Fig. 2.10. There is generally good agreement between the observed precipitation patterns: precipitation is largest at the outlet of the basin and decreases northwestward. Note that CRU and CCR precipitation fields are better spatially correlated to each other than with GPCP. Both CRU and CCR datasets have not been corrected for gauge biases by undercatch of solid precipitation. The GPCP precipitation dataset is a merged product of the surface gauge, low-orbit microwave and geosynchronous infrared measurements.

The CRCM_V3.6 precipitation, which is largely influenced by the abundant summertime precipitation, does not reproduce the observed dry area west of the basin. Precipitation is overestimated almost everywhere over the basin with the exception of the southern part of the basin where it is underestimated.

As discussed in Section 2.4.2, a relatively good estimate of the spatial distribution of the Mississippi runoff can be obtained from the VIC model, which is tuned to reproduce the observed Mississippi runoff. Therefore, the VIC monthly data series provided by Maurer et al. (2002) are used to calculate a runoff field

representative of the 1988-1997 period. Additional information on the spatial distribution of the Mississippi runoff based on observations can be obtained from the GRDC gridded composite runoff dataset. It should be kept in mind that the GRDC dataset is climatology from the mid-1960s to the mid 1980s, which does not match the 1988-97 period analysed in our study. In Fig. 2.11, the two runoff fields are used to validate runoff simulated by the CRCM. As can be seen, runoff is largely underestimated by the CRCM_V3.6 in the southeast part of the basin and overestimated in the mountainous region to the west.

Figure 2.12 shows the simulated evapotranspiration fields together with two quasi-observed fields. The first is derived as the difference between averaged precipitation (average of all three datasets) and the VIC runoff, while the second is the difference between averaged precipitation and the GRDC runoff. Despite some discrepancies between the two quasi-observed fields, which are more apparent in the southeast region of the basin, they provide useful information on the evapotranspiration pattern over the Mississippi River basin. Similar to the observed precipitation, the northwest-southeast gradient in the quasi-observed evapotranspiration fields is simulated, but it is weaker. The simulated evapotranspiration by the CRCM_V3.6 is overestimated throughout the basin except at its outlet, which is consistent with the precipitation overestimation.

2.5.6 Spatial distribution: validation of the CRCM_V4.0 simulated fields

As can be seen in Fig. 2.10, the CRCM_V4.0 shows a noticeable improvement in the simulated precipitation pattern. Although slightly underestimated, the northwest-southeast gradient is well captured by CRCM_V4.0. However, the precipitation is still underestimated in the southeast basin region and overestimated in the mountainous region to the northwest. Some improvement is obtained also in the

spatial distribution of the simulated evapotranspiration over the basin (see Fig. 2.12). However, the simulated runoff by the updated model version (see Fig. 2.11) is relatively similar to the runoff simulated by the CRCM_V3.6, despite the important changes in the simulated evapotranspiration and precipitation.

2.6 Summary and conclusion

Current inability of climate models to adequately simulate many of the complex multi-scale processes involved in the water cycle is a major source of uncertainty in long-term climate-change projections. Model evaluation and development are therefore crucial for improvement of the reliability of climate projection. Once models will be capable to successfully simulate present water cycle behavior, it is likely that they can more accurately assess potential changes due to changes in greenhouse gas concentration in the atmosphere.Various studies performed with different climate models have demonstrated better agreement of simulated and observed hydrological variables when more realistic physical parameterisations are used (e.g., Viterbo and Beljaars 1995, Beljaars et al. 1996, Ducharne et al. 2000, Ek et al. 2003, Hagemann et al. 2004, Anderson et al. 2004, Hagemann et al. 2006). The incentive to create a model that realistically represents many of the complex subgrid-scale processes involved in the water cycle has to comply with the need to have computationally fast enough models so that ensemble of multi-year integrations can be performed. The optimal level of complexity in physical parameterisations designed for use in climate models is still an unresolved issue. The only way to address this question is to evaluate simulated water budget components by comparison with observations wherever possible. The high complexity of the multi-scale processes involved in the hydrological cycle and their associated feedbacks as well as scarcity of observations for some water cycle components contribute to the problem of assessing simulated hydrological cycle over

a given region. Usually, for regional scale studies, only simulated precipitation and runoff are evaluated.

In this paper, a comprehensive validation of all water budget components over the Mississippi River basin as simulated by the Canadian Regional Climate Model (CRCM) was performed. In addition, the sensitivity of simulated hydrological cycle to a more realistic representation of the land surface processes, as well as radiation, cloud cover and atmospheric boundary layer mixing is investigated. Two simulations using different model versions (CRCM_V3.6 and CRCM_V4.0) were analyzed and compared with the corresponding values derived from observations or quasi-observations. The analysis was first performed for the annual means where the contributions of water budget components were integrated in space over the entire basin, and in time over the 1988-1997 period. The analysis highlighted a closure error in the CRCM_V3.6 simulated water budget: the simulated annual mean atmospheric moisture flux convergence does not balance the simulated runoff exactly. Since the moisture flux convergence is calculated within the model using all levels and time steps, a fair part of this error in the atmospheric budget is related to the semi-Lagrangian numerical transport scheme, that does not ensure conservation of the prognostic variables (Paquin and Laprise 2003).

Comparing the annual mean observed to the simulated precipitation over the Mississippi River basin, a large positive bias is found in the CRCM_V3.6. It is thought that the positive precipitation bias is mainly caused by an overestimation of the annual mean evapotranspiration. The CRCM_V3.6 has a single-layer Manabe-based land surface scheme, which cannot adequately represent many of the effects of vegetative control on evapotranspiration. The prescribed water-holding capacity appears excessive resulting in an excessive evapotranspiration. On the other hand, the annual means of the runoff and atmospheric moisture flux convergence are

underestimated, which is linked to the excess in evapotranspiration bias with respect to the precipitation bias.

Implementation of the Canadian Land Surface Scheme (CLASS) in the CRCM_V4.0 as well as changes to the radiation, cloud cover and boundary-layer mixing treatment have resulted in significant improvements to the simulated annual mean evapotranspiration over the basin. As a consequence, the annual mean bias of the CRCM_V4.0 precipitation is strongly reduced. Simulated annual mean of the atmospheric moisture flux convergence is slightly increased and now balances annual mean runoff. Elimination of the water budget closure error is obtained by introducing a small correction to the specific humidity values at each grid point, which takes into account the inaccuracy related to the semi-Lagrangian numerical scheme.

The annual cycle analysis shows that the annual positive precipitation bias of the CRCM_V3.6 is caused mainly by an excessive overestimation of the precipitation during summer. Such a large positive precipitation bias is related to the combined effects of an excessive summer evapotranspiration and inadequate moisture distribution in the CRCM_V3.6 lower boundary layer. Similarly to the NCEP/NCAR and ERA40 reanalyses, the CRCM_V3.6 shows a moisture flux convergence (divergence) over the Mississippi River basin from October to May (in summer), but the model underestimates this. The CRCM_V3.6 underestimates runoff throughout the year, and underestimates soil drying in summer. As well, the absolute value of the difference between precipitation and evapotranspiration, $|P - E|$, is underestimated by the CRCM_V3.6 throughout the year. This is consistent with the underestimation of summer soil drying and summer moisture flux divergence: the $(P\text{-}E)$ term dries the soil in summer but moistens the atmosphere because during this time evapotranspiration exceeds precipitation. Similarly, the negative bias in the difference between precipitation and evapotranspiration is linked to the underestimation of the

atmospheric moisture flux convergence and runoff from September to May when the *(P-E)* term dries the atmosphere and moistens the soil.

The comparison of the annual cycles of the water budget components simulated by the CRCM_V3.6 and CRCM_V4.0 demonstrated that the atmospheric moisture flux convergence (as well as precipitation) responds to changes in the evapotranspiration. A decrease in the evapotranspiration is associated with an increase in the atmospheric moisture flux convergence from September to May. Inversely, precipitation is decreased throughout most of the year. In summer, the decrease in precipitation is larger than the decrease in evapotranspiration because of the combined effect of the evapotranspiration reduction and stronger mixing of the water vapour in the CRCM_V4.0 boundary layer, which means less favourable conditions for triggering convection. As a consequence, summer moisture flux divergence is increased and matches those of reanalyses more accurately.

Analysis of the spatial distribution has shown that the CRCM_V4.0 captures observed precipitation patterns better then the CRCM_V3.6. As well, some improvement is obtained in simulated spatial distribution of evapotranspiration. However, the simulated runoff of the updated model version is relatively similar to the runoff simulated by the CRCM_V3.6, despite the important changes in the simulated evapotranspiration and precipitation.

In summary, implementation of a four-band instead of the two-band radiation scheme in the CRCM and an improved treatment of cloud cover results in reduction of the net radiation at the surface and therefore in decreased latent and sensible heat fluxes. Replacing the Manabe-based parameterisation with a state-of-the-art land surface scheme, which provides more realistic land-surface processes by taking into account stomatal resistance of vegetation results in an important reduction of simulated evapotranspiration. Finally, stronger mixing of the water vapour in the new

boundary-layer scheme results in less favorable conditions for convection, therefore reducing condensation and precipitation. Overall effect of the changes to the physical parameterisation of the CRCM is an improved annual cycle (and annual mean) of simulated precipitation, evapotranspiration, moisture flux convergence and terrestrial water storage tendency. Despite these improvements, simulated runoff remains underestimated throughout the year (except for March). In a continuing effort to improve parameterisation of subgrid processes in the CRCM, work is underway to improve runoff generation and water transfer in soil.

Acknowledgements

This research was financially supported by the Canadian Network for Regional Climate Modelling, funded by the Canadian Foundation for Climate and Atmospheric Sciences (CFCAS) and the Ouranos Consortium on Regional Climatology and Adaptation to Climate Change. Authors are grateful to the Climatic Research Unit, the Global Precipitation Climatology Project/Centre and the Centre for Climatic Research for precipitation data, UCAR Climate and Global Dynamics Division for atmospheric moisture flux convergence and precipitable water tendency data, Dr. Edwin P. Maurer and Dr. Dennis P. Lettenmaier for providing naturalized runoff for the GCIP Region and data from the VIC model. Monthly mean integrated water vapor products from ERA40 at their original resolution were kindly provided by Dr. Pedro Viterbo. A special thanks goes out to all members of the Climate Simulations Team of the Ouranos Consortium for their valuable help. The helpful comments provided by Dr. René Laprise are deeply appreciated. The authors wish to thank the three anonymous reviewers for their constructive comments on the original version of this manuscript. Finally, we are grateful to Ms. Bano B. Mehdi for her careful revision of the manuscript.

References

Adler, R.F., G.J. Huffman, A. Chang, R. Ferraro, P. Xie, J. Janowiak, B. Rudolf, U. Schneider, S. Curtis, D. Bolvin, A. Gruber, J. Susskind, and P. Arkin, 2003: The Version-2 Global Precipitation Climatology Project (GPCP) Monthly Precipitation Analysis (1979–Present). *J. Hydrometeor.*, **4,** 1147-1167.

Anderson, J. L., V. Balaji, A. J. Broccoli, W. F. Cooke, T. L. Delworth, K. W. Dixon, L. J. Donner, K. A. Dunne, S. M. Freidenreich, S. T. Garner, R. G. Gudgel, C. T. Gordon, I. M. Held, R. S. Hemler, L. W. Horowitz, S. A. Klein, T. R. Knutson, P. J. Kushner, A. R. Langenhorst, N.-C. Lau, Z. Liang, S. L. Malyshev, P. C. D. Milly, M. J. Nath, J. J. Ploshay, V. Ramaswamy, M. D. Schwarzkopf, E. Shevliakova, J. J. Sirutis, B. J. Soden, W. F. Stern, L. A. Thompson, R. John Wilson, A. T. Wittenberg, and B. L. Wyman, 2004: The new GFDL global atmosphere and land model AM2-LM2: Evaluation with prescribes SST simulation. *J. Climate*, **17**, 4641-4673.

Bechtold, P., J.S. Kain, E. Bazile, F. Guichard, P. Mascart, and E. Richard, 2001: A Mass Flux Convection Scheme for Regional and Global Models. *Quart. J. Roy. Met. Soc.,* **127**, 869-886.

Beljaars, A. C. M., P. Viterbo, M. J. Miller, and A. K. Betts, 1996: The anomalous rainfall over the United States during July 1993: Sensitivity to land surface parameterisation and soil moisture anomalies. *Mon. Wea. Rev.,* **124,** 362–383.

Berbery, E. H., K.E. Mitchell, S. Benjamin, T. Smirnova, H. Ritchie, R. Hogue, and E. Radeva, 1999: Assessment of land-surface energy budgets from regional and global models. *J. Geophys Res.*, **104**, D16, 19329-19348.

Berbery, E. H., and E. M. Rasmusson, 1999: Mississippi moisture budgets on regional scales, *Mon. Wea. Rev.,* **127**, 2654-2673.

Berbery, E. H., Y. Luo, K. E. Mitchell, and A. K. Betts, 2003: Eta model estimated land surface processes and the hydrologic cycle of the Mississippi basin, *J. Geophys. Res.,* **108**, D22, 8852, doi:10.1029/2002JD003192.

Caya, D., 1996: Le modèle régional de climat de l'UQAM. PhD thesis, Doc. Sc. Env., Université du Québec à Montréal, Canada, 134 pp.

Caya, D., and R. Laprise, 1999: A semi-implicit semi-Lagrangian regional climate model: The Canadian RCM. *Mon. Wea. Rev.*, **127**, 341-362.

Davies, H. C., 1976: A lateral boundary formulation for multi-level prediction models. *Quart. J. R. Meteor. Soc.*, **102**, 405-418.

Ducharne A, R.D. Koster, M.J. Suarez, K. Praveen, and M. Stieglitz, 2000: A catchment-based approach to modeling land surface processes in a GCM - Part 2: Parameter estimation and model demonstration, *J. Geophys. Res.*, **105**, D20, 24823-24838.

Ek, M. B., K. E. Mitchell, Y. Lin, E. Rogers, P. Grunmann, V. Koren, G. Gayno, and J. D. Tarpley, 2003: Implementation of Noah land surface model advances in the National Centers for Environmental Prediction operational mesoscale Eta model, *J. Geophys. Res.*, **108,** D22, 8851, doi:10.1029/2002JD003296.

Fekete, B. M., C. J. Vorosmarty, and W. Grabs, 2000: Global, composite runoff fields based on observed river discharge and simulated water balances, Documentation for UNH-GRDC Composite Runoff Fields, v.1.0, Global Runoff Data Center, Koblenz, Germany, pp 120.

Fiorino, M., cited 2001: AMIP II sea surface temperature and sea ice concentration observations. [Available online at http://www-pcmdi.llnl.gov/projects/amip/AMIP2EXPDSN/BCS_OBS/amip2_bcs.htm.]

Flato, G. M., and G. J. Boer, 2001: Warming Asymmetry in Climate Change Simulations. *Geophys. Res. Lett.*, **28**, 195-198.

Graham, S. T., J. S. Famiglietti, and D. R. Maidment, 1999: Five-minute, 1/2° and 1° data sets of continental water sheds river networks for use in regional and global hydrologic and climate system modeling studies. *Water Resour. Res.*, **35**, 583-587.

Hagemann, S., B. Machenhauer, R. Jones, O.B. Christensen, M. Déqué, D. Jacob, and P.L. Vidale, 2004: Evaluation of water and energy budgets in regional climate models applied over Europe, *Climate Dyn.*, **23**, 547-567.

Hagemann, S., K. Arpe, and E. Roeckner, 2006: Validation of the hydrological cycle simulated by the GCM ECHAM5 model. *J. Climate,* **19**, 3810-3827.

Hortal, M., and A. J. Simmons, 1991: Use of reduced Gaussian grids in spectral models. *Mon. Wea. Rev.,* **119,** 1057–1074.

Hulme M., 1994: Validation of large-scale precipitation fields in General Circulation Models. In *Global Precipitation and Climate Change*, NATO ASI Series I, 26, Springer Verlag., 387-405.

Jiao, Y., and D. Caya, 2006: An investigation of the summer precipitation simulated by the Canadian Regional Climate Model. *Mon. Wea. Rev.* **134,** 919-932.

Kalnay E., M. Kanamitsu, R. Kistler, W. Collins, D. Deaven, L. Gandin, M. Iredell, S. Saha, G. White, J. Woollen, Y. Zhu, M. Chelliah, W. Ebisuzaki, W. Higgins, J. Janowiak, K. C. Mo, C. Ropelewski, J. Wang, A. Leetmaa, E. Reynolds, R. Jenne, D. Joseph, 1996: The NCEP/NCAR 40-year reanalysis project. *Bull. Amer. Meteor. Soc.*, 77, 437-471.

Laprise, R., D. Caya, M. Giguère, G. Bergeron, H. Côté, J.-P. Blanchet, G. J. Boer, and N. McFarlane, 1998: Climate and Climate Change in Western Canada as Simulated by the Canadian Regional Climate Model. *Atmos.-Ocean*, **36**, 119-167.

Legates, D. R., 1987: *Climatology of Global Precipitation.* Publications in Climatology, Vol. 40, University of Delaware, 85 pp.

Legates D.,R., C. J. Willmott, 1990: Mean seasonal and spatial variability in gauge-corrected, global precipitation. *Int. J. Climatol.*, 10, 111–127.

Manabe, S., 1969: Climate and ocean circulation. I. The atmospheric circulation and the hydrology of the Earth's surface. *Mon. Wea. Rev.,* **97**, 739-774.

Maurer, E. P., and D. P. Lettenmaier, cited 2004: Calculation of undepleted runoff for the GCIP region, 1988–2000. [Available online at http://www.ce.washington.edu/pub/HYDRO/edm/WEBS_runoff/.]

Maurer, E. P., G. M. O'Donnell, D. P. Lettenmaier, and J. O. Roads, 2001: Evaluation of the Land Surface Water Budget in NCEP/NCAR and NCEP/DOE Reanalyses using an Off-line Hydrologic Model, *J. Geophys. Res,* **106**, D16, 17841-17862.

Maurer, E.P., A.W. Wood, J.C. Adam, D.P. Lettenmaier, and B. Nijssen, 2002: A Long-Term Hydrologically-Based Data Set of Land Surface Fluxes and States for the Continental United States, *Bull. Amer. Meteor. Soc.,* **15**, 3237–3251.

Mein, R. G., and C. L. Larson, 1973: Modeling infiltration during a steady rain. *Water Resour. Res.*, **9**, 384-394.

McFarlane, N.A., and R. Laprise, 1985: Parameterization of Sub-grid Scale processes in the AES/CCC Spectral GCM, Atmospheric Environment Service, Downsview, Ontario, no. 85-12 CCRN 17, 70 pp.

McFarlane, N.A., G.J. Boer, J.-P. Blanchet, and M. Lazare, 1992: The Canadian Climate Centre second generation General Circulation Model and its equilibrium climate. *J. Climate*, **5**, 1013-1044.

Mitchell, T.D., and P.D. Jones 2005: An improved method of constructing a database of monthly climate observations and associated high-resolution grids. *Int. J. Climatol.,* **25**, 693-712.

New, M., M. Hulme, and P.D. Jones, 2000: Representing twentieth century space-time climate variability. Part 2: development of 1901–96 monthly grids of terrestrial surface climate. *J. Climate* **13**, 2217-2238.

New, M., M. Hulme, and P.D. Jones, 2001: Precipitation measurements and trend in twentieth century. *Int. J. Climatol.*, **21**, 1899–1922.

Paquin, D., and R. Harvey, 2003: Les nuages dans gcmiii et MRCC_Version 3.7. Internal Document of the CRCM Network, 7 pp. [Available from Ouranos Consortium, 550 Sherbrooke St. West, 19th Floor, Montreal, Quebec, Canada H3A 1B9.]

Paquin, D., and R. Laprise, 2003: Traitement du bilan d'humidité interne au MRCC. Internal Document of the CRCM Network, 26 pp. [Available from Ouranos Consortium, 550 Sherbrooke St. West, 19th Floor, Montreal, Quebec, Canada H3A 1B9.]

Peixoto, J. P., and A. H. Oort, 1992: *Physics of Climate.* American Institute of Physics, 520 pp.

Peterson T.C, and R.S. Vose, 1997: An overview of the global historical climatology

network temperature database. *Bull. Amer. Meteor. Soc.,* **78**, 2837–2849.

Piper, S. C., and E. F. Stewart, 1996: A gridded global data set of daily temperature and precipitation for terrestrial biosphere modeling. *Global Biogeochem. Cycles,* **10,** 757–782.

Puckrin, E., W. F. J. Evans, J. Li, and H. Lavoie, 2004: Comparison of clear-sky surface radiative fluxes simulated with radiative transfer models. *Can. J. Remote Sens.*, **30,** 903-912.

Rasmusson, E. M., 1977: Hydrological application of atmospheric vapor flux analyses. *Hydrology rep.* 11, WMO.

Rasmusson, E. M., 1968: Atmospheric water vapor transport and the water balance of North America. II. Large-scale water balance investigations. *Mon. Wea. Rev.,* **96,** 720–734.

Riette, S., and D. Caya, 2002: Sensitivity of short simulations to the various parameters in the new CRCM spectral nudging. Research activities in Atmospheric and Oceanic Modeling, edited by H. Ritchie, *WMO/TD* - No 1105, Report No. 32: 7.39-7.40.

Robock, A., 2003: Preface to special section: GEWEX Continental-Scale International Project (GCIP)-3, *J. Geophys. Res,* **108**, D16, 8605, doi:10.1029/2003JD003924.

Rudolf B., A. Gruber, R. Adler, G. Huffman, J. Janowiak, and P. P. Xie, 1999: GPCP precipitation analyses based on observations as a basis for NWP and climate model verification. *Proceedings of WCRP 2nd International Reanalysis Conference*, Reading, UK, 23–27th August, 1999, WCRP-Report.

Roads, J., and A. Betts, 2000: NCEP/NCAR and ECMWF Reanalysis Surface Water and Energy Budgets for the Mississippi River Basin. *J. Hydrometeor.,* **1,** 88-94.

Roads, J., M. Kanamitsu, and R. Stewart, 2002: CSE Water and Energy Budgets in the NCEP-DOE Reanalysis II, *J. Hydrometeor.*, **3**, 128-165.

Roads, J., R., E.B. Lawford, H. Berbery, B. Fekete, K. Gallo, A. Grundstein, W. Higgins, J. Janowiak, M. Kanamitsu, V. Lakshmi, D. Leathers, D. Lettenmaier, Q. Li, L. Luo, E. Maurer, T. Meyers, D. Miller, K. Mitchell, T. Mote, R. Pinker, T. Reichler, D. Robinson, A. Robock, J. Smith, G. Srinivasan, K. Vinnikov, T. von der Haar, C.

Vorosmarty, S. Williams, and E. Yarosh, 2003: GCIP Water and Energy Budget Synthesis (WEBS) *J. Geophys. Res.*, **108**, D16, 8609, doi:10.1029/2002JD002583.

Seneviratne S., P. Viterbo, D. Lüthi, and C. Schär, 2004: Inferring Changes in Terrestrial Water Storage Using ERA-40 Reanalysis Data: The Mississippi River Basin. *J. Climate,* **17**, 2039-2057.

Shepard, D., 1968: A two-dimensional Interpolation function for irregularly-spaced Data. *Proceedings, 1968 ACM National Conference*, 517-523.

Trenberth, K. E., 1997: Using atmospheric budgets as a constraint on surface fluxes. *J. Climate*, 10, 2796-2809.

Verseghy, D.L., 1991: CLASS – A Canadian land surface scheme for GCMs. Part I: Soil model. *Int. J. Climatol.,* **11**, 111–133.

Verseghy, D.L., N.A. McFarlane, and M. Lazare, 1993: CLASS – A Canadian land surface scheme for GCMs. Part II: Vegetation model and coupledruns. *Int. J. Climatol.* **3**, 347–370.

Viterbo, P., and A.C.M. Beljaars, 1995: An improved land-surface parameterization in the ECMWF model and its validation. *J. Climate*, **8**, 2716-2748.

Watson, R. T., and the Core Writing Team, Eds., 2001: *Climate Change 2001: Synthesis Report.* Cambridge University Press,398 pp. [Available online at http://www.ipcc.ch.]

Wilson, M.F., and A. Henderson-Sellers, 1985: A global archive of the land cover and soils data for use in general circulation climate models. *J. Climatol.,* **5**, 119-143.

Willmott, C. J., C. M. Rowe and W. D. Philpot, 1985: Small-Scale Climate Maps: A Sensitivity Analysis of Some Common Assumptions Associated with Grid-point Interpolation and Contouring. *American Cartographer*, **12**, 5-16.

Willmott, C. J., and K. Matsuura, cited 2004: Terrestrial air temperature and precipitation: Monthly and annual time series (1950–1999), version 1.02. [Available online at http://climate.geog.udel.edu/_climate/html_pages/download.html.]

Yarosh, E. S., C.F. Ropelewski, and E.H. Berbery, 1999: Biases of the observed atmospheric water budgets over the central United States. *J. Geophys. Res.*, **104**, D16, 19349-19360.

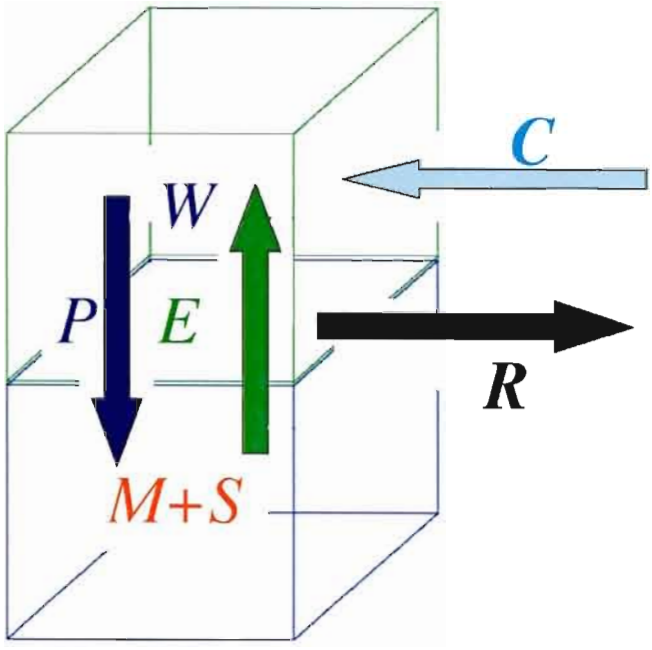

Fig. 2.1 Schematic illustration of combined atmospheric and terrestrial water balance.

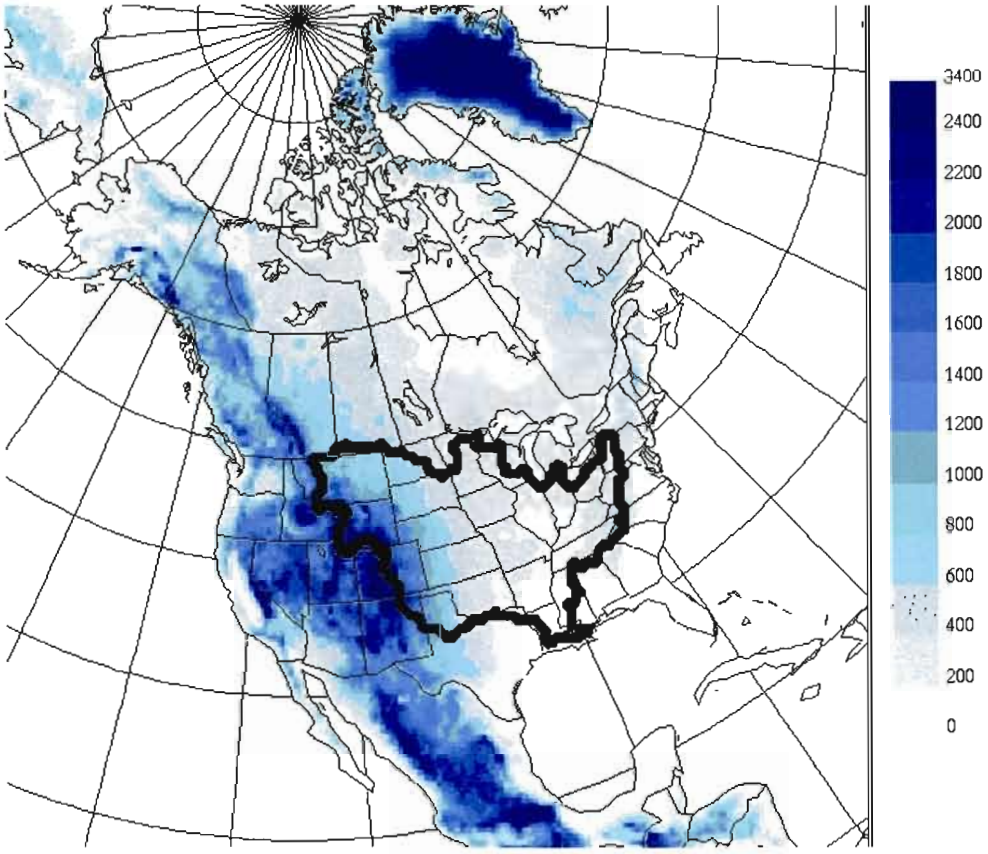

Fig. 2.2 CRCM simulation domain with the topography (m). The Mississippi River basin outline is also indicated.

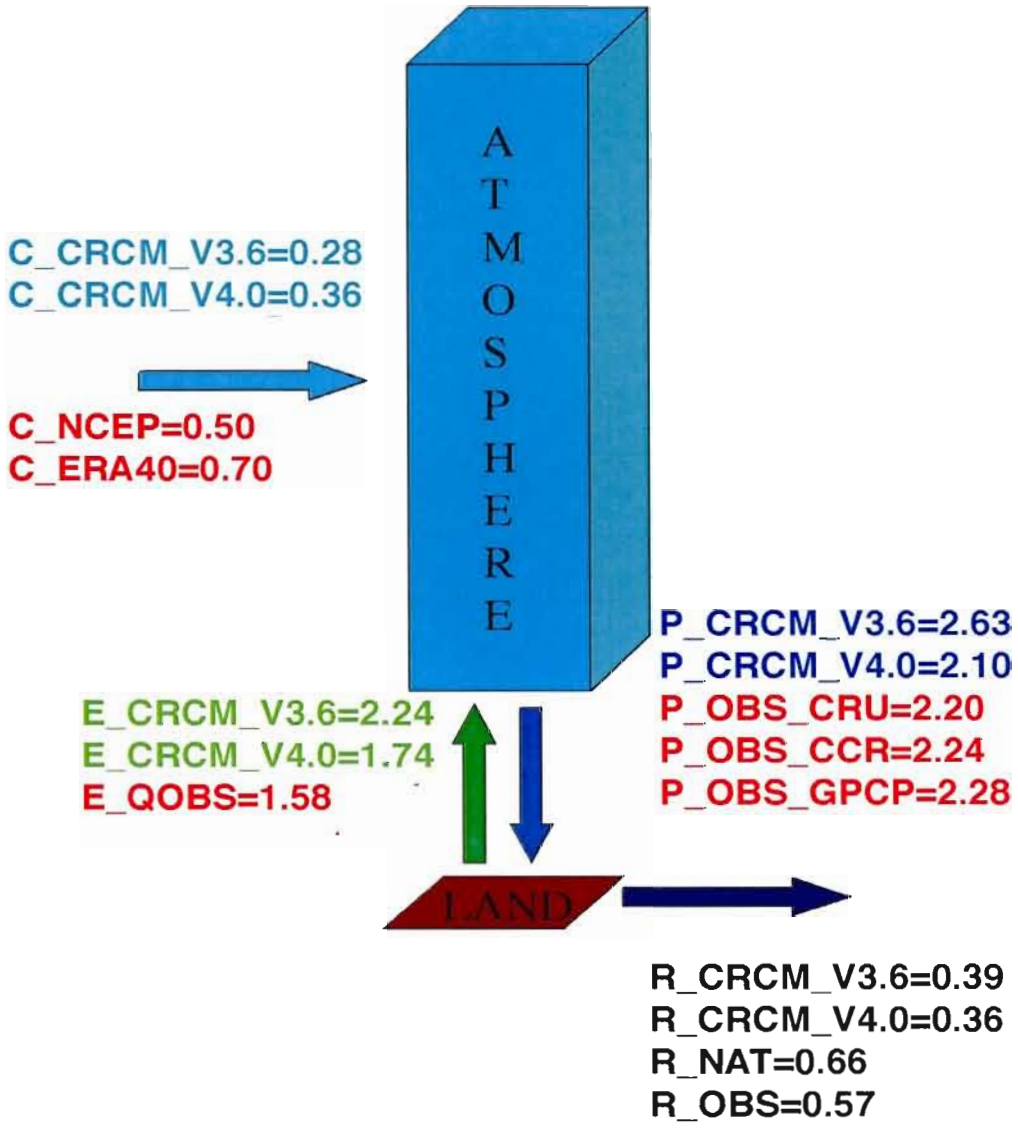

Fig. 2.3 Annual means (1988-1997) of the atmospheric and terrestrial water budget components, in mm/day, over the Mississippi River basin.

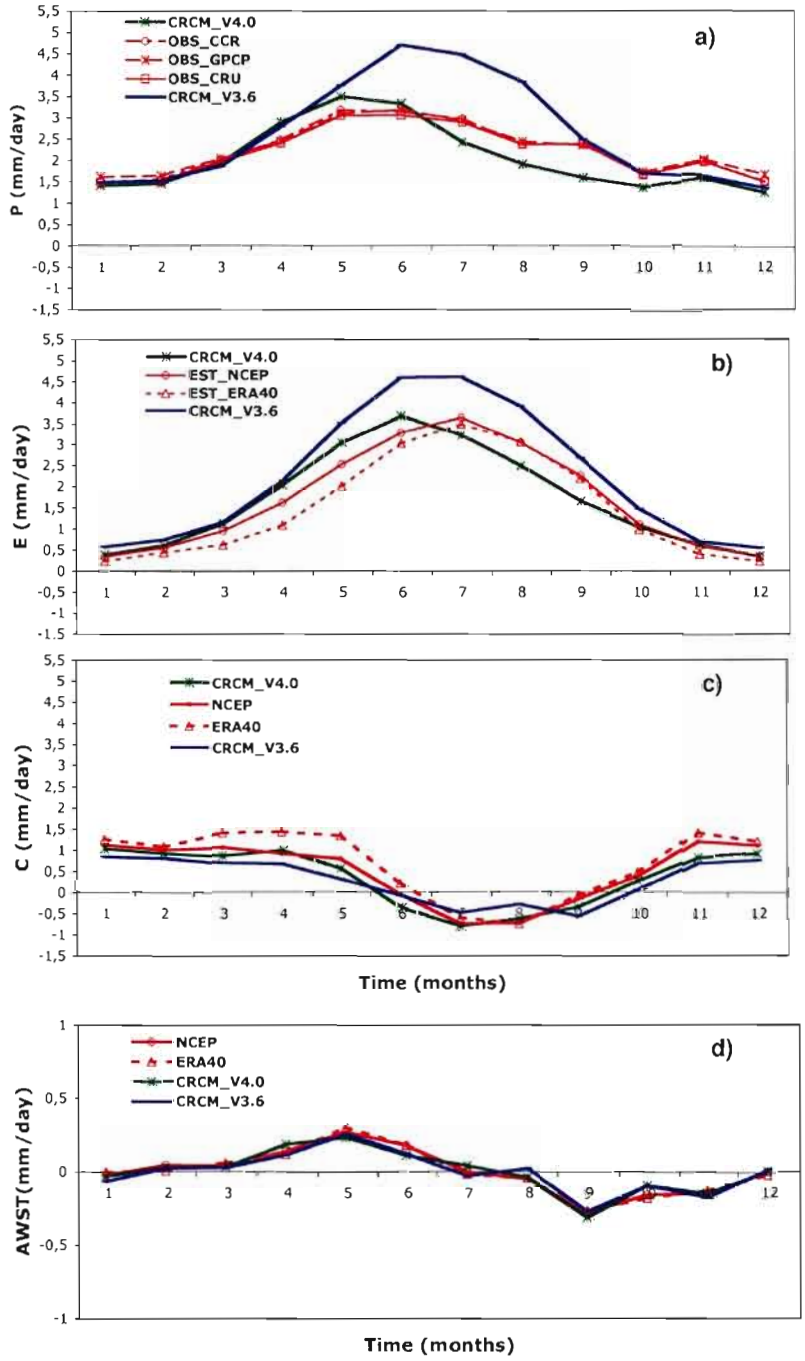

Figs. 2.4 Climatological annual cycles of simulated and observed (quasi-observed) atmospheric water budget components averaged over the Mississippi River basin: (a) precipitation, *P*; (b) evapotranspiration, *E*; (c) vertically integrated horizontal moisture convergence, *C*; (d) atmospheric water storage tendency, *AWST*.

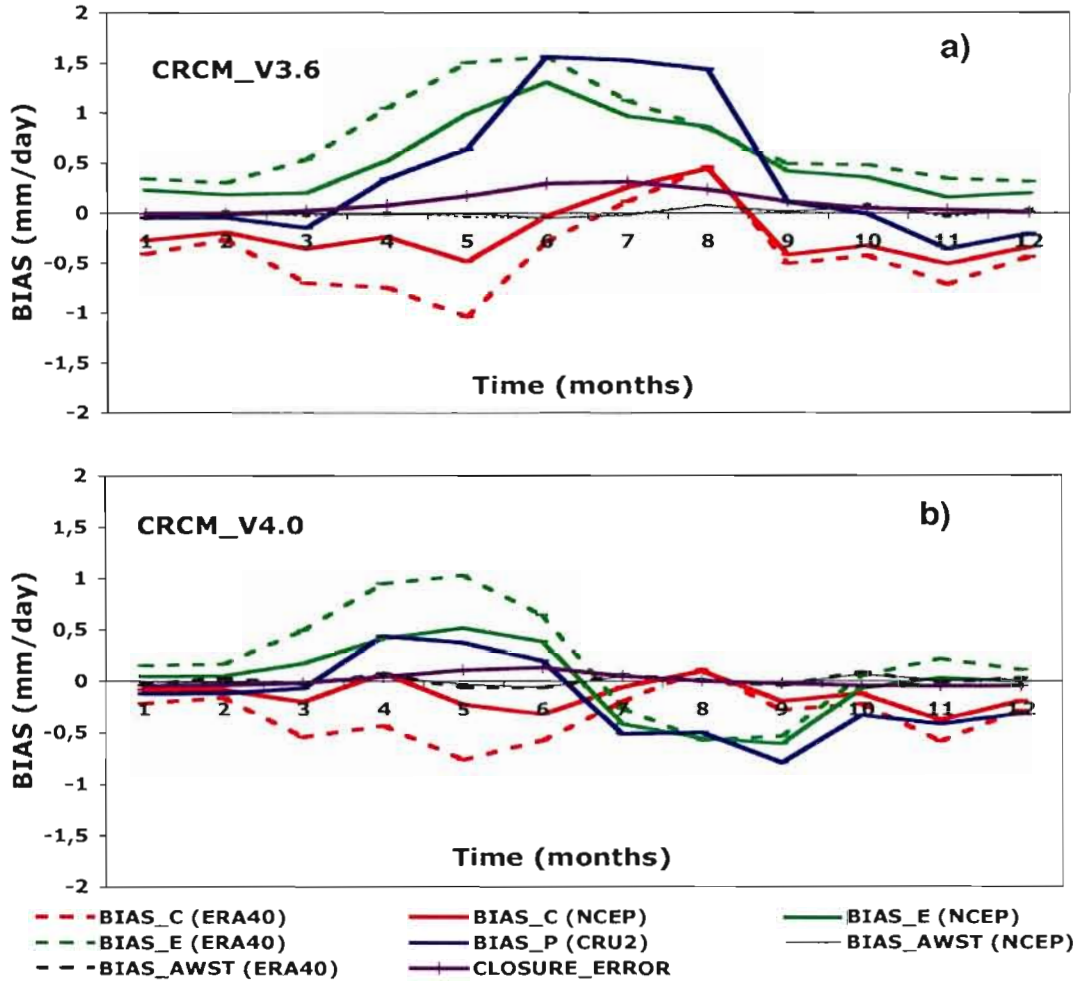

Fig. 2.5 The CRCM simulation biases of precipitation (BIAS_P), atmospheric moisture flux convergence (BIAS_C), atmospheric water storage tendency (BIAS_AWST). The error in closure of the water budget is also indicated (CLOSURE_ERROR).

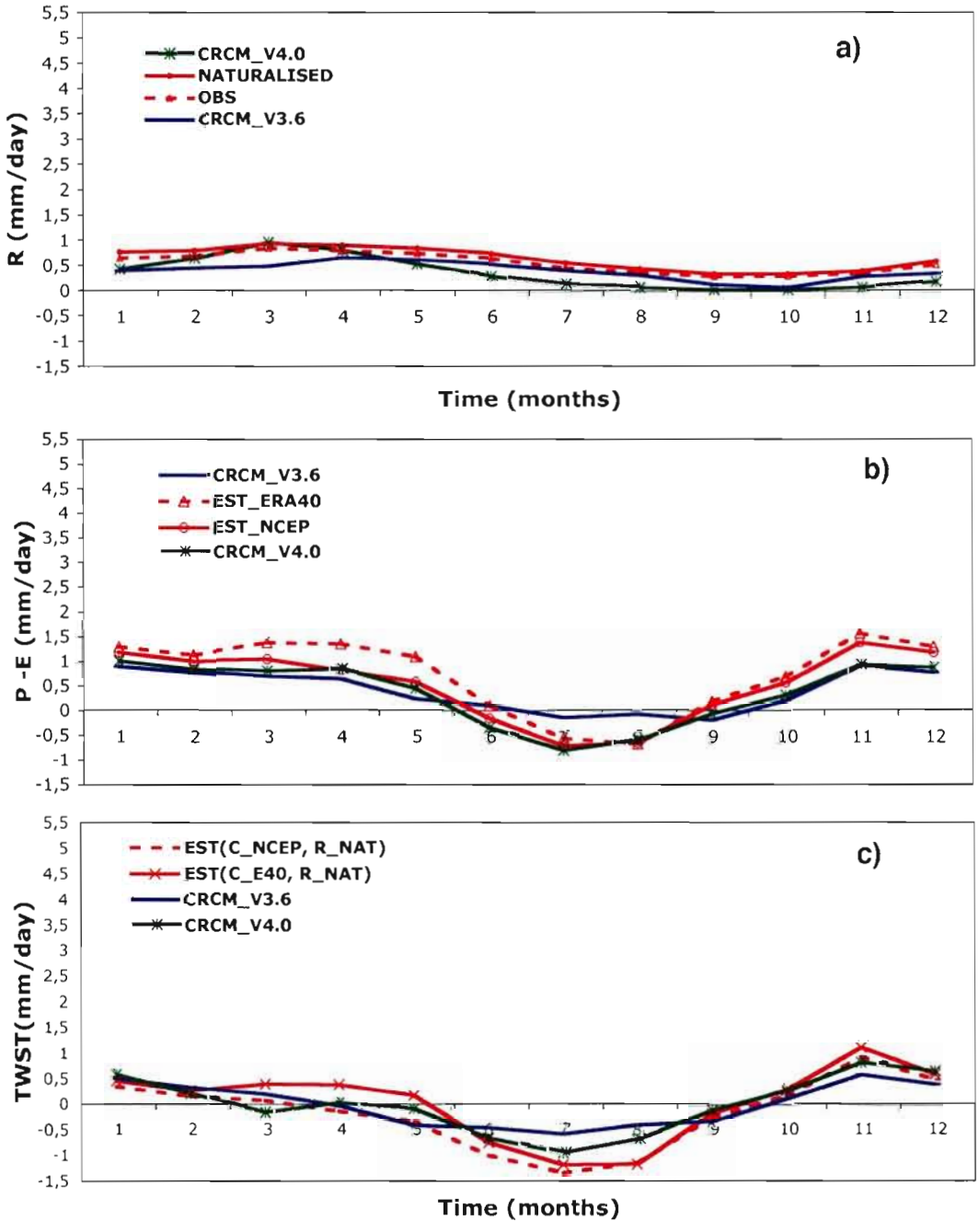

Fig. 2.6 Annual cycle of simulated and quasi-observed terrestrial water budget components averaged over the Mississippi River basin: (a) runoff, R; $(P-E)$ forcing term (b) and of terrestrial water storage tendency, TWST(c).

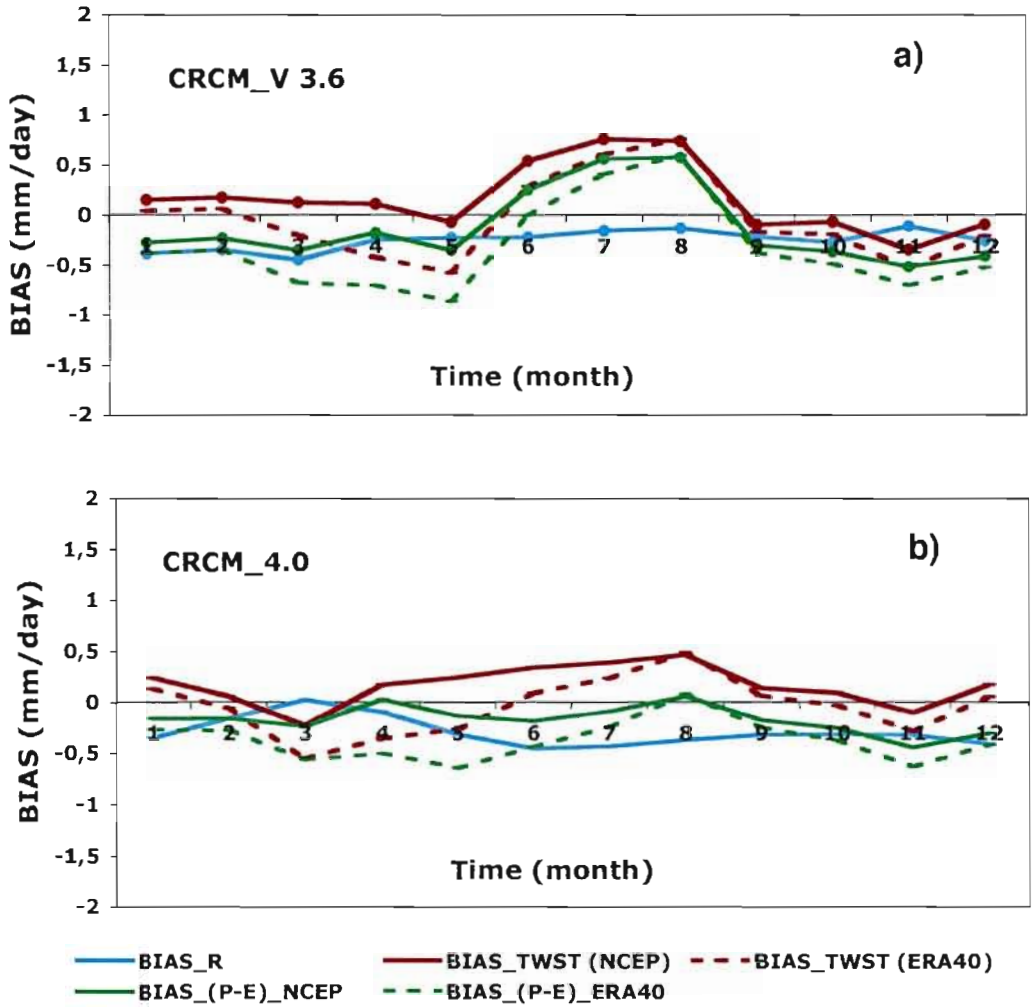

Fig. 2.7 The CRCM simulation biases of the terrestrial water cycle branch.

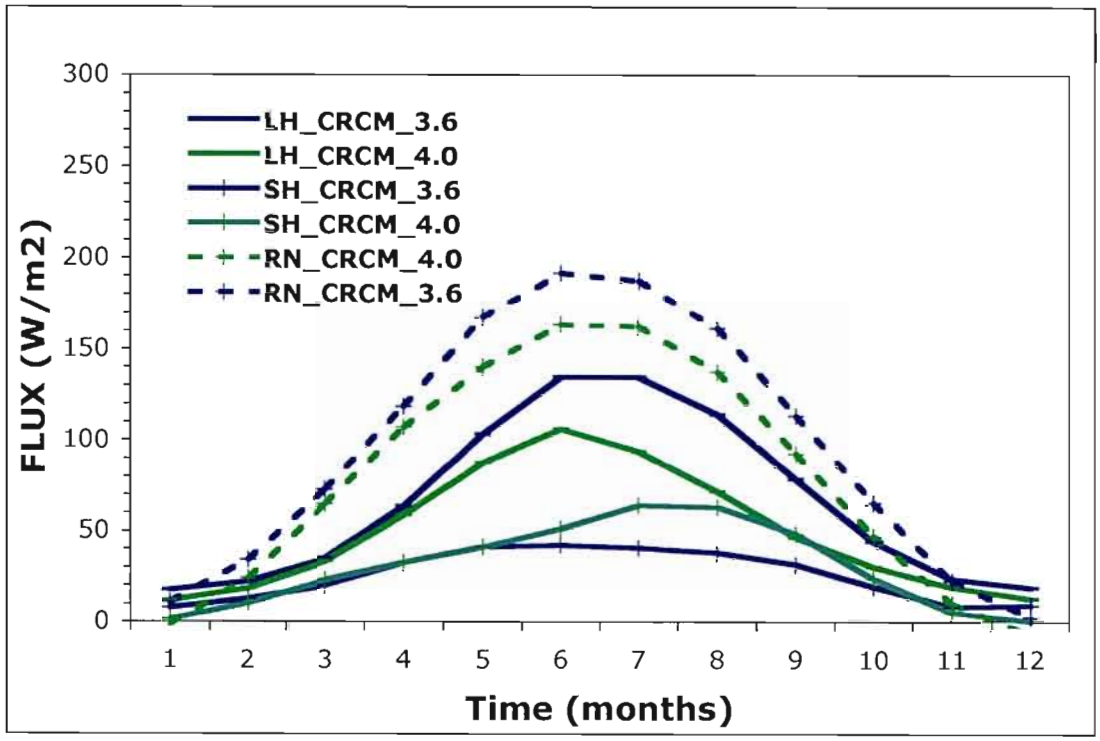

Fig. 2.8 Annual cycle of the CRCM simulated net radiative energy at the surface (RN), latent heat flux (LH) and sensible heat flux (SH) averaged over the Mississippi River basin.

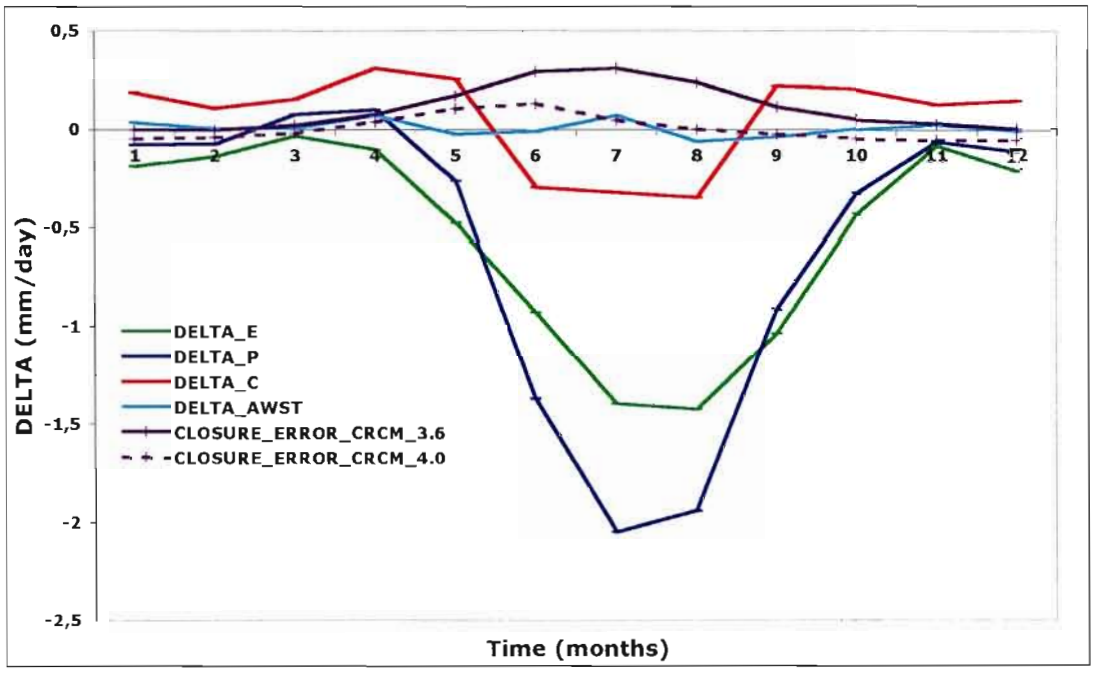

Fig. 2.9 Annual cycle of the difference between the CRCM_V4.0 and CRCM_V3.6 evapotranspiration (DELTA_E), precipitation (DELTA_P), atmospheric moisture flux convergence (DELTA_C), atmospheric water storage tendency (AWST). The error in closure of the water budget is also indicated (CLOSURE_ERROR_CRCM_3.6, CLOSURE_ERROR_CRCM_4.0).

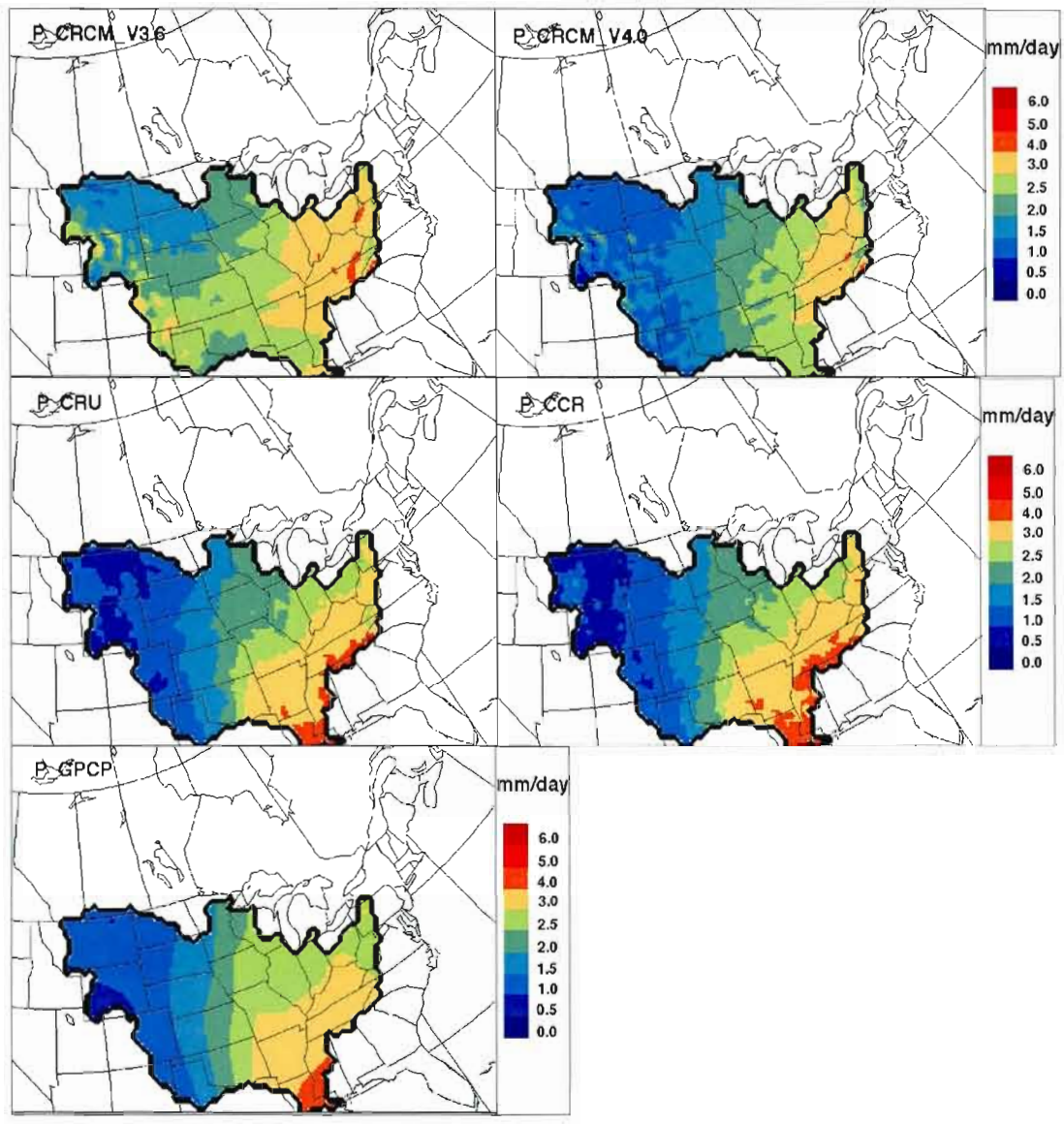

Fig. 2.10 CRCM annual mean precipitation and corresponding reference fields.

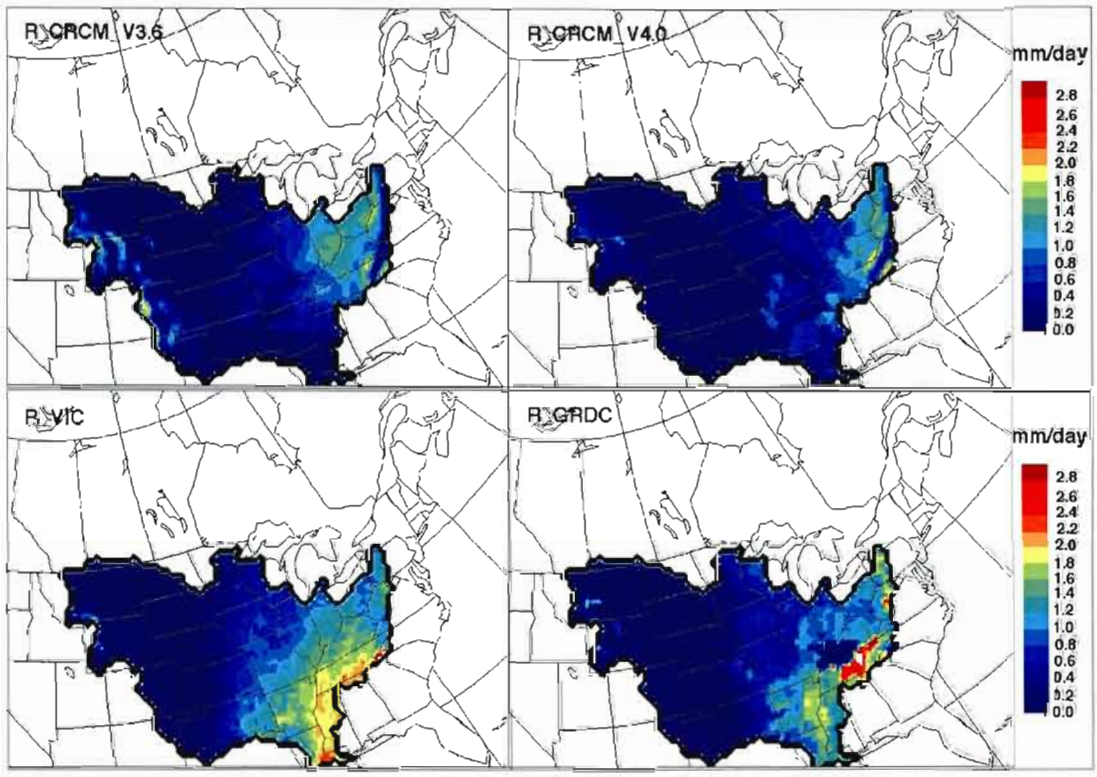

Fig. 2.11 CRCM annual mean runoff and corresponding reference fields.

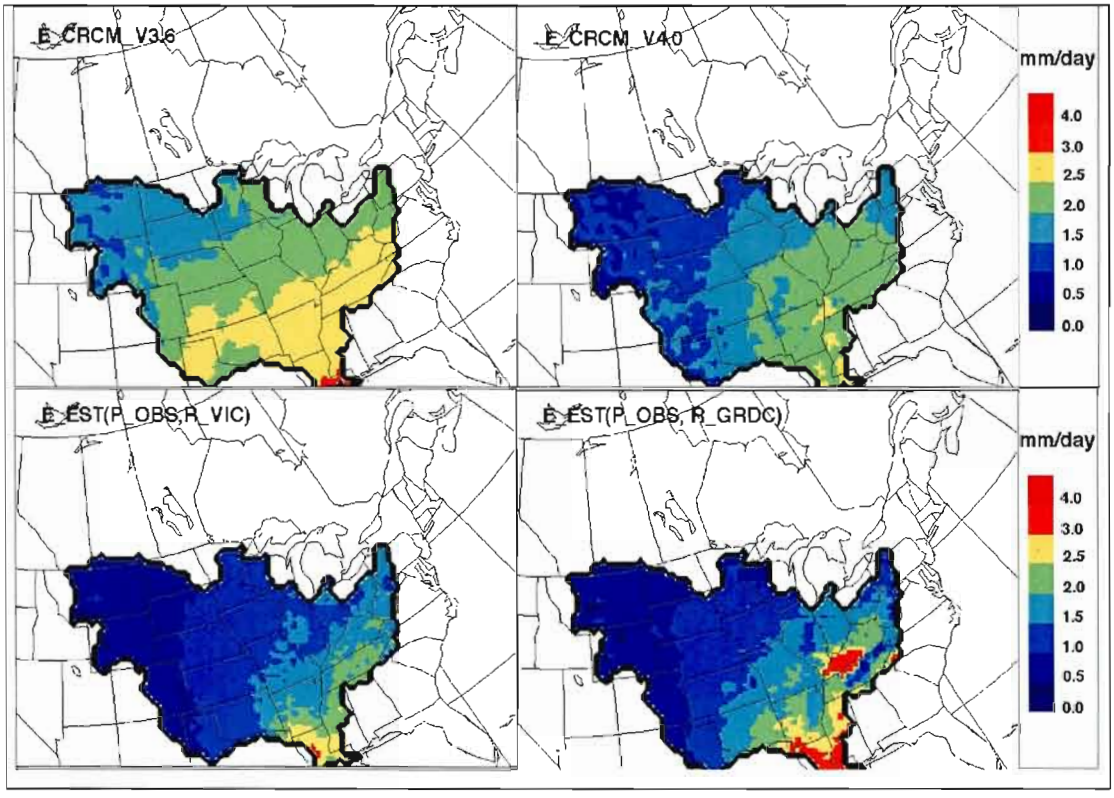

Fig. 2.12 CRCM annual mean evapotranspiration and corresponding reference fields.

CHAPITRE III

INVESTIGATION OF THE SENSITIVITY OF WATER CYCLE COMPONENTS SIMULATED BY THE CANADIAN REGIONAL CLIMATE MODEL (CRCM) TO THE LAND SURFACE PARAMETERIZATION, THE LATERAL BOUNDARY DATA AND THE INTERNAL VARIABILITY

Biljana Music and Daniel Caya

Submitted to *J. Hydrometeor.*

Abstract

Regional Climate Models (RCMs) allow about one-order higher spatial resolution than Global Climate Models (GCMs). Credible climate-change projections from RCMs can only come from detailed assessment of their performance at simulating the components of the climate system. RCM simulations require to be continuously forced by lateral boundary conditions, usually taken from a low-resolutions reanalysis or a GCM simulation, and are therefore affected by these lateral boundary conditions. The land surface scheme provides time-dependent lower boundary conditions over land surface, also affects RCM simulations. The non-linear nature of the climate system implies that simulations initialised with different initial conditions result in different sequences of weather events.

The present study investigates the sensitivity of the components of the hydrological cycle simulated by the Canadian Regional Climate Model (CRCM) to the formulation of land surface processes (LSS), lateral boundary and initial conditions. This helps in estimating the uncertainty associated to RCMs' climate-change projections. Sensitivity analysis was carried out for climatological means, climatological annual cycles and interanual variability, over the period 1961-1999 for three North American River basins, selected to cover a wide range of climate conditions: the Mississippi, the St.-Lawrence and the Mackenzie River basins. Three pairs of simulations have been used: the first one was generated using two different LSSs (a simple Manabe-based and complex second-generation scheme); the simulations in the second pair differing in driving data (NCEP/NCAR vs ERA40 reanalysis); and simulations in the third pair were started at different times. An evaluation of the simulated water budget components with respect to the observations is presented.

Results indicate that changes in climatological means and annual cycles of the water budget components resulting from different land surface parameterisations and

from different lateral boundary conditions vary from basin to basin. Sensitivity to lateral boundary conditions was in general smaller than sensitivity to the LSS and tended to be stronger for the northern basins (Mackenzie and St. Lawrence). Interannual variability was not much affected by the change in LSS and driving data. Internal variability triggered by the non-linear nature of the climate model (i.e. change in initial conditions) does not significantly affect neither 39-year climatology nor climatological annual cycles and interanual variability. Comparison with observation pointed out that while simple Manabe-based LSS may be adequate for simulations of climatological means, skilful simulation of annual cycles require the use of second-generation LSS.

3.1 Introduction

A large number of models are available today to simulate the evolution of the climate system. The growth in their complexity and physical realism follows development in computer technology. For climate simulations on decadal to century time scales, the so-called coupled Global Climate Models (GCMs) are the most complete and accurate representation of the physical processes taking place in the climate system. These models have full four-dimensional (3 in space and one in time) representation of the atmosphere and the ocean circulations in addition to sea-ice and land-surface modules. However, long climate integrations with coupled GCMs at a high resolution are still computationally prohibitive. For that reason, the horizontal resolution of coupled GCMs is typically limited to a few hundred kilometers.

In the last two decades, there has been a growing need by the climate impact community for climate simulations at higher spatial resolutions. This is particularly important for the variables related to the water cycle because of their important spatial variability. Nested limited-area regional climate models (RCMs) represent an appealing approach to achieve finer spatial resolution simulation at an affordable computational cost (Laprise et al. 2003). An alternative to nested limited-area RCMs is the use of stretched-grid global models (Déqué et al. 1998, Fox-Rabinovitz et al. 2001).

Because of their limited area, RCMs require time-dependent lateral boundary conditions. Low-resolution reanalyses or GCM simulations usually provide these conditions that force the RCM simulations. Recent studies showed that, when driven by accurate boundary conditions, regional climate models are capable of capturing the overall observed regional climate evolution and can add realistic spatial and temporal information to the information provided by the driving model (Denis et al.,

2002, Giorgi et al., 2001; Frei et al., 2003). However, it should not be expected that the large-scale errors in the global model circulation to be corrected by a RCM.

RCMs also require time-dependent lower boundary conditions for the land and sea surfaces. In most RCMs, sea surface temperature and sea-ice amount are taken from a climatological database for present climate or from GCM simulations for future climate. The fluxes of radiation, momentum, sensible and latent heat across the land surface - atmosphere interface are provided by the land-surface scheme. These fluxes are governed by the low-level atmospheric humidity, as well as by the surface albedo, aerodynamic roughness length and soil moisture availability, which depends on soil type, moisture content, vegetation type and density, fractional snow cover and snow age. Therefore, the land-surface scheme has a strong influence on the water cycle in the simulated climate through the control of land evaporation.

There are three main generations of land-surface scheme. The first generation was based on Manabe's (1969), the so-called bucket approach. A single soil layer, with a constant moisture holding capacity is used to represent the soil moisture regime and any moisture in excess is considered as runoff. The surface fluxes are parameterized in terms of a simple energy balance equation relating the energy fluxes to the surface temperature. Evaporation is expressed as a function of soil moisture availability (the so-called β function) and energy-driven potential evaporation. Vegetation is not considered explicitly.

The development of second-generation land-surface parameterisations was initiated by Deardorff (1978). He proposed an alternative approach in land surface modelling, introducing a greater emphasis of the role of vegetation in the regulation of land-surface interactions with the atmosphere. His model included an explicit foliage layer and multi-layer representation of soil moisture and temperature regimes.

Bare ground evaporation, canopy transpiration (water extracted by plants from the soil root zone), evaporation of canopy-intercepted water as well as the influence of a plant stomata on transpiration were parameterized explicitly. Soon after Deardorff's (1978) work, a large number of fairly sophisticated biophysically based land-surface models followed: BATS (Dickinson et al., 1986), SiB (Sellers et al., 1986), CLASS (Verseghy 1991; Verseghy et al. 1993), BEST (Pitman and Desborough 1996). Since the 1990s there has been a tendency in the climate community for implementation of biophysically-based land surface model into GCMs. Effects of replacing Manabe's approach by Deardorf's have been investigated by many authors. For example, Sato et al. (1989) and Chen et al. (1997) show that climate simulated by a GCM coupled to a biophysically-based land surface model is more realistic. Verseghy et al. (1993) demonstrated that implementation of CLASS within the Canadian GCM resulted in a reduction of the wet and cold surface biases that were present with the Manabe's based parameterization of land surface processes.

The third-generation land-surface parameterisations, published in late 1990s (Bonan 1995, Sellers et al. 1996, Dickinson et al. 1998), combine consistent description of the physical climate system transfer processes for energy, momentum, water and heat, with the biophysics of photosynthesis (IPCC 2001). Therefore, third generation land-surface parameterisations allow the carbon budget to be carried out along with conventional surface water and energy budget calculations.

An interesting twist on the evolution from the very simple Manabe (1969) land model to the complex schemes of today is that recent research seems to indicate that increase in complexity of land surface parameterisation does not directly leads to smaller biases in climate simulations (McGuffie and Henderson-Sellers 2001). For example, Desborough (1999) has shown that a simple surface parameterization with a suitably prescribed surface resistance is as appropriate as a more complex parameterisation for simulations of the annual, monthly and seasonally averaged

evapotranspiration. The impact of any "improved" paramererisation on climate model simulations should be assessed critically by carying out sensitivity studies. Moreover, for hydrological applications, the investigation should look at all components of the hydrological cycle and not only to the precipitation field.

The present study investigates the sensitivity of all the components of the hydrological cycle simulated by the Canadian Regional Climate Model (CRCM) to the formulation of land-surface processes, lateral boundary and initial conditions. Pairs of multi-year simulations were performed with the CRCM over North America in a way to assess the sole effect of the land-surface scheme and the lateral boundary driving data. Another pair of simulations was used to assess the internal variability associated with the selected CRCM configuration. The analysis is carried out over three North American River basins differing in their location, size and topography. The document is organized as follows: the next section describes the methodology and experimental setup. Section 3 presents the results of the analysis of simulated water budget components spatially averaged over a river basin and Section 4 summarizes the results of this study.

3.2 Methodology and experimental setup

All simulations used in the present investigation are generated over the same domain covering the whole of North America and parts of the adjacent Pacific, Atlantic and Arctic oceans (hereinafter referred to as the AMNO domain for "AMérique du NOrd" i.e. North America in French) as depicted in Figure 3.1. Table 3.1 describes the configuration of the CRCM simulations used to build the pairs of simulations mentioned in the previous section. The so-called Reference Simulation (RS) is carried out for the period January 1st 1959 to December 31st 1999. The same period is used for two other simulations with modifications in the model

configuration (change in the Surface Scheme SS, change in the Boundary Conditions BC), while the simulation IC (change in Initial Conditions) was initialised one year earlier. The CRCM is driven either by 6-hourly NCEP/NCAR (simulations RS, SS and IC) or ERA 40 (simulation BC) reanalysis, linearly interpolated in time to the model's 15-minute time step. A 45-km horizontal mesh on a polar-stereographic projection (true at 60° N) with 29 levels in the vertical is used. The one-way nesting method of Davies (1976) is applied over a nine grid-point wide buffer zone. In addition, to assure coherence between the large-scale circulations of the driving and driven models over the large AMNO domain, the large-scale (length scale longer than 1400 km) horizontal wind field from the CRCM is weakly nudged toward the large-scale wind of the driving data following Riette and Caya (2002). The sea-surface temperature and sea ice amount as well as the Great Lakes surface temperature and ice are taken from the AMIP II observations database (Fiorino, 1997).

Three simulations (RS, BC and IC) were generated with the CRCM_Version 4.0 (CRCM_V4.0), where the **C**anadian **LA**nd **S**urface **S**cheme (CLASS, Verseghy, 1991; Verseghy et al. 1993) was used to describe the exchange of water and energy at the land surface-atmosphere interface. The simulation SS used CRCM_Version 3.7 (CRCM_V3.7). This model version uses the same physical parameterisations as CRCM_V4.0, with the sole exception of the Manabe-based land-surface scheme (hereinafter MAN) being used instead of CLASS. In the original version of MAN, presented in McFarlane and Laprise (1985) and McFarlane et al. (1992), the soil water-holding capacity varied in space depending on both vegetation and bare soil characteristics. However, in the simulation SS, the water holding capacity was set to 100 mm because the former spatially varying values were found excessively high, resulting in large overestimation of evaporation and precipitation during summer (cf CRCM_V3.6 in Music and Caya 2007). Note that the value of 100 mm is somewhat low compared to a typically used soil water capacity of 150 mm and represents a

decrease of between a factor of two and eight from the soil water capacity used in Music and Caya (2007). This value was found to give the most accurate surface water vapour flux over the AMNO domain.

Comparison of SS and RS allows to investigate the sensitivity of the CRCM hydrological cycle variables on land surface processes parameterization. The pair BC-RS is used to estimate the sensitivity of the CRCM water cycle to the driving data used at the lateral boundary of the CRCM integration domain. As discussed in Caya and Biner (2004), any real influence of modification in the model configuration cannot be evaluated without previous estimation of model internal variability, which is a consequence of the chaotic nature of the climate system. In other words, it is necessary to determine if changes in simulated water budget components caused by modification of the CRCM configuration are significant compared to the changes due solely to the internal variability. An investigation of internal variability is desirable each time sensitivity studies are attempted because of the internal variability dependence on experimental configuration (Caya and Biner 2004; Lucas-Picher et al. 2004; de Elía et al. 2007). The appropriate assessment requires a sizeable ensemble of simulations, however given the cost in computer resources, only one pair of simulation (IC-RS) were used to obtain a crude estimate of the internal variability in the simulated climate; it is assumed here that this estimated internal variability is representative of all experiments carried out in this investigation.

3.3 Results and discussion

3.3.1 Analysis of climatological means

1) Sensitivity of the water budget components

This section analyses and compares climatological means for the period 1961-99 of simulated water budget components over the three North American river basins that were selected to cover a wide range of climate conditions (Mississippi, St. Lawrence and Mackenzie). Fig. 3.1 shows the CRCM integration domain; the three investigated river basins are outlined in black. The Mississippi and St. Lawrence basins represent the hydrology of central and northeast regions of North America, while the Mackenzie River basin characterizes the hydrological regime of a colder Northern region. In addition, an evaluation of the simulated climatological means, using various sets of observations is carried out.

There are four important terms in annual atmospheric and terrestrial water budgets: precipitation, evapotranspiration, vertically integrated atmospheric moisture flux convergence (sometimes identified as atmospheric run-in) and runoff. Table 3.2 summarizes simulated climatological means of the water budget components averaged over each basin and indicate their sensitivity to the land surface parameterisation, lateral boundary and initial conditions. Table 3.2 also indicates the error in closing the simulated water budget for each of the investigated basins, ranging from 0.01 mm day^{-1} (Mississippi River basin) to 0.04 mm day^{-1} (Mackenzie River basin). As discussed by Music and Caya (2007), this error is associated to the CRCM semi-Lagrangian numerical scheme, which is responsible for a slight non-conservation in prognostic variables. The smaller error is found over the Mississippi

basin and can be explained by the larger area ($\approx 3.2 \times 10^6$ km^2) compared to the areas of the Mackenzie ($\approx 1.7 \times 10^6$km^2) and St. Lawrence ($\approx 1.1 \times 10^6$ km^2) river basins.

In all simulations, the largest precipitation is simulated over the St. Lawrence River basin followed by the Mississippi River basin, while the Mackenzie River basin receives only half the St. Lawrence precipitation. It is interesting to partition the relative contributions from the evapotranspiration and atmospheric moisture convergence to the precipitation over each basin. The relative contribution of the evapotranspiration to the precipitation over the Mississippi River basin is 84% in the reference simulation (as well as in IC and BC), while in SS it is 78%. Such a large relative contribution in all simulations suggests that the rates of precipitation and evapotranspiration over the Mississippi River basin are linked through a strong positive feedback related to the local (regional) moisture recycling. Consequently, moisture flux convergence over the basin (averaged over 39 years) and the associated runoff are relatively small. The relative contributions of the evapotranspiration to the precipitation for the St. Lawrence and Mackenzie basins in RS (as well as in IC) are 60% and 53%, respectively. In simulation SS, it is 62% over both basins, while in BC, the contributions are similar as in reference simulation (61% and 52%). Overall, for all three river basins, moisture recycling is most affected by the change in the representation of the land surface (SS is characterized by the largest differences with respect to the reference simulation).

Since evapotranspiations in RS and SS simulations are governed by fundamentally different parameterisations of the land surface, differences in their climatological means are not surprising. As can be seen from Table 3.2, changes in evapotranspiration resulting from the use of CLASS or MAN differ in magnitude as well as in sign, from basin to basin. While climatological mean of simulated evapotranspiration over the Mississippi River basin decreased by 0.17 mm day^{-1}

(10%), it increased by 0.15 mm day^{-1} (25%) over the Mackenzie River Basin. Changes over both basins are statistically significant. The statistical significance was assessed with a Student's and Wilcoxon rank-sum test using a level of confidence of $\alpha = 0.05$. Climatological mean of evaporation over the St. Lawrence River basin was not much affected by the change in the land surface scheme, however climatological means of precipitation and moisture flux convergence (and runoff) are affected, although not statistically significant. The response of the investigated river basins to the land surface parameterisation change is investigated further by the analysis of the climatological annual cycles in Section 3.3.2.

Both atmospheric-moisture flux convergence and precipitation over the Mississippi and Mackenzie basins respond to the change in annual mean evapotranspiration induced by the modification of the land surface scheme. The decreased evapotranspiration over the Mississippi River basin by 0.17 mm day^{-1} results in an increase in the moisture flux convergence by 0.10 mm day^{-1} (statistically significant) and decreased precipitation by 0.07 mm day^{-1} (not statistically significant). This means that 41% of total evapotranspiration change goes to the precipitation decrease (for a small relative change of 4% in precipitation) and 59% to the moisture flux convergence increase (for a relative change of 32% in moisture flux convergence). The change in moisture flux convergence is reflected to the runoff generation that changes by the same amount (an analysis of the water budget equations shows that runoff must equals moisture flux convergence when integrated over long periods, see Music and Caya 2007 for details). For the Mackenzie River basin, where the change in the land surface parameterisation increased the overall evaporation, the situation is somewhat different. About half of the evapotranspiration increase is returned to the basin by increased precipitation while the other half reduces the moisture flux convergence. Changes in all components of the hydrological cycle over the Mackenzie River basin are statistically significant. Overall, the change in evapotranspiration (increase or reduction), induced by

modification in the land surface parameterisation, seems to affect somewhat equally both moisture flux convergence and precipitation.

Comparing BC with RS allows us to estimate the sensitivity of the simulated water budget components to specification of the lateral boundary conditions. Over the Mississippi River basin, the differences between climatological means of the BC and RS simulations are smaller than the one induced by the land surface scheme. However, the precipitation increase from RS to BC over Mackenzie River basin is slightly larger (0.10 mm day^{-1} or 9%) than the increase from RS to SS since both moisture flux convergence and evapotranspiration are increased (significantly) when NCEP/NCAR driving model is replaced by ERA40. The St. Lawrence River basin behaves similarly (climatological means of all water budget components are increased from RS to BC), but the changes are slightly smaller. Note that over the Mississippi River basin, the annual mean precipitation as well as the evapotranspiration are higher in simulation BC when compared to the reference simulation, however the differences are not statistically significant. The signal of the atmospheric moisture flux convergence over the Mississippi River basin to changes in the lateral boundary conditions, is equal to the closure error of the simulated water budget (0.01 mm day^{-1}).

Comparing IC with the reference simulation shows that differences in the climatological means of the water budget components are very small and not statistically significant.

2) Comparison with observations

Agreement between simulated and observed climatological means of the water budget components over each basin is assessed over a ten-year period for which observations were available (see Fig. 3.2). In order to evaluate uncertainty in

observed and quasi-observed values (interval in which estimated data vary), several datasets from different sources were used: for the Mississippi basin, gridded-precipitation analyses from the Center for Climate Research (CCR, Willmott and Matsuura 2004), Global Precipitation Climatology Project/Centre (GPCP, Adler et al. 2003) and Climate Research Unit (CRU, Mitchell et al. 2005); for the Mackenzie and St. Lawrence River basins, the Canadian Gridded-precipitation dataset (CANGRID, Louie et al. 2002; McKenney et al. 2005) as well as CRU and GPCP. The largest uncertainty in observed precipitation is over the Mackenzie River basin where differences between the 3 datasets can reach 0.21 mm day^{-1} (20%). This is mostly related to the density of precipitation gauge station, which is particularly low in the northern region of the Mackenzie River basin. Gauge undercatch, which is important in high-latitude regions (Legates and Willmott 1990), is also suspected. Over the St. Lawrence and Mississippi basins the differences are much smaller and less than 5%. Note that CANGRID and GPCP precipitation are corrected for gauge undercatch while CRU and CCR are not.

Vertically integrated moisture flux convergence has been obtained from two different sources: National Centers for Environmental Prediction/National Center for Atmospheric Research (NCEP/NCAR reanalysis) and European Centre for Medium Range Weather Forecasting (ERA40 reanalysis). The largest discrepancy in reanalysis moisture flux convergences is found over the Mississippi River basin where ERA40 is higher than NCEP/NCAR by 0.20 mm day^{-1} (40%). Over the St. Lawrence and Mackenzie basins, ERA40 convergence is also higher than that of NCEP/NCAR one, but the difference is much smaller: 0.07 mm day^{-1} (8%) and 0.05 mm day^{-1} (8%), respectively.

A ten-year average of observed runoff over each basin (R_OBS) is obtained using monthly streamflows observations from U.S. Geological Survey and from Canadian Hydrographic Service (see Table 3.3). For the Mississippi River basin, data

of naturalized runoff (Maurer and Lettenmaier 2001) were also available. St. Lawrence River basin is highly regulated, and to our best knowledge, there is no naturalized runoff data for this river basin. For that reason, two additional runoff datasets were used: (1) runoff simulated by the Variable Infiltration Capacity (VIC) hydrologic model driven by observed meteorological data (Maurer et al. 2002); and (2) gridded climatological runoff dataset provided by Global Runoff Data Center (GRDC, Fekete et al. 2000). GRDC runoff is obtained by combining streamflow observations (during 1965-85) with the simulated runoff from a climate-driven water balance model. As can be seen from Fig. 3.2, runoff climatology (for 1987-96) based on VIC, over the St. Lawrence basin, differs from observed by only 0.01 mm day^{-1} (1%). Larger difference is present between the GRDC and observed runoff (0.17 mm day^{-1} or 20%). Since the average of the observed, VIC and GRDC runoff (R_MEAN) agree well with averaged NCEP/NCAR and ERA40 moisture flux convergences (the difference is only 0.05 mm day^{-1} or 5%), biases in simulated runoffs over the St. Lawrence basin were calculated with respect to this average (see Table 3.4).

The climatological mean for evapotranspiration was estimated from the terrestrial water budget (labelled as E_EST_TB in Fig. 3.2) as a difference between the observed precipitation and runoff. For the Mississippi River basin, naturalized runoff (R_NAT) and averaged observed precipitation (P_MEAN) were used because of the relatively good agreement between the CCR, GPCP and CRU precipitations over this basin. For the Mackenzie and St. Lawrence basins, E_EST_TB is calculated separately from each of the three precipitation data sets (see Label Identifier in Fig. 3.2). A second estimate of evapotranspiration over each basin is computed from the atmospheric water budget (E_EST_AB) as a difference between the observed precipitation and atmospheric moisture flux convergence computed from both reanalyses data. Since NCEP/NCAR and ERA40 moisture flux convergences agree well over the St. Lawrence and Mackenzie basins, average from both reanalyses (C_MEAN) is used to estimate the quasi-observed evapotranspiration. The largest

uncertainty in quasi-observed evapotranspiration is found over the Mackenzie River basin, related to the uncertainty of observed precipitation as well as to the error in closing the quasi-observed water budget (observed runoff does not equal reanalysis moisture flux convergence). For example, evapotranspiration estimated as a difference between CRU precipitation and C_MEAN (E_EST_AB (CRU, C_MEAN)) is smaller than the one estimated using CANGRID precipitation and observed runoff (E_EST_TB (CANGRID, R_OBS)) by 0.38 mm day^{-1} (51%). For the Mississippi and St. Lawrence basins, the maximum differences between the values of quasi-observed evapotranspiration are 0.20 mm day^{-1} (12%) and 0.18 mm day^{-1} (10%).

Table 3.4 shows that precipitation over the Mississippi River basin is underestimated by all simulations reaching a maximum bias of -12% in simulation SS. Precipitation biases in RS and BC are –10% and –7%, respectively. Biases in simulated evapotranspiration and runoff however are smaller in SS (-4% and –33%) than in RS (+6% and -48%) and BC (+11% and -50%). For the St. Lawrence River basin, observed annual mean precipitation is underestimated in all simulations. Again, simulation SS is characterized by the largest precipitation bias of about -14%, while in simulations RS and BC, precipitation biases are about -12% and -8%, respectively. Runoff biases over the St. Lawrence basin are relatively small in all simulations ($\leq$ 8%), which is consistent with the underestimation of evapotranspiration in all simulations. Contrary to the Mississippi and St. Lawrence basins, simulated precipitations over the Mackenzie River basin are larger than the average of CANGIRD, GPCP and CRU precipitation. However, it should be kept in mind that there is relatively large uncertainty in observed precipitation over this basin. Simulations SS and BC have similar precipitation biases of about +14% (with respect to the observed average), however runoff simulated in BC is larger than observed by 22%, while runoff simulated in SS is equal to the observed one. This is consistent with the larger overestimation of evapotranspiration in SS than in BC.

Precipitation and runoff biases for the RS simulation are +8% and +14% respectively. Note that biases in simulated moisture flux convergence (calculated with respect to the average of NCEP/NCAR and ERA40 moisture flux convergence, see Table 3.4) differ from runoff biases, particularly over the Mackenzie River basin, where error in closing the quasi-observed water budget is the largest.

In summary, the above analysis suggests that the land surface scheme sensitivity (MAN with respect to CLASS) results in:

(1) Increase in bias of precipitation climatological mean over all three river basins;

(2) Relatively large increase in bias of climatological mean of evapotranspiration over the Mackenzie basin and some decrease in evapotranspiration bias over the Mississippi and St. Lawrence basins;

(3) Relatively large decrease in bias of climatological mean of runoff over the Mississippi and Mackenzie basins and some increase in runoff bias over the St. Lawrence basin.

Lateral boundary sensitivity (ERA40 with respect to NCEP/NCAR) results in:

(1) Some decrease in bias of climatological means of precipitation over the St. Lawrence and Mississippi river basins and some increase in bias over the Mackenzie basin;

(2) Some decrease in bias of climatological mean of evapotranspiration over the St. Lawrence basin and some increase in evapotranspiration bias over the Mississippi and Mackenzie basins;

(3) Some increase in bias of climatological mean of runoff over all three river basins.

3.3.2 Analysis of the climatological annual cycles

1) Sensitivity of the water budget components

An analysis of the climatological annual cycle of the water budget components was done to further investigate the sensitivity analysis carried out in the previous section. Differences in simulated mean annual cycle of the atmospheric water budget components for the SS-RS simulations pair are shown in Fig. 3.3a, 3.3c and 3.3e. As it can be seen, the significant reduction in evapotranspiration climatological mean over the Mississippi River basin from RS to SS resulted from a decrease in evapotranspiration from June to November. From February to May, however, evapotranspiration is larger in SS. Evaporation in MAN is strongly linked to the availability of soil water and is strongly impeded when soil moisture is low. During spring, soil is almost saturated (moisture is accumulated in the soil or in the snow pack from October to February) and MAN allows a larger evaporation than CLASS, for which canopy resistance limits excessive evapotranspiration. Large evaporation over the basin during spring in simulation SS, as well as a relatively small water-holding capacity (100 mm) of the bucket, results in very low soil water content during summer and early fall, and hence evaporation in SS is largely reduced in this period of the year.

The change in the atmospheric moisture convergence (from RS to SS) over the Mississippi basin behaved in opposition to the evapotranspiration change. The decrease in evapotranspiration from July to November is counteracted by an increased atmospheric moisture flux convergence over the basin and a decreased precipitation. For February and March, evapotranspiration and moisture flux convergence changes had the same sign (both are increased) and therefore both contributed to precipitation increase. A similar situation is seen in June, where evapotranspiration and moisture flux convergence changes are both negative,

decreasing precipitation.

In the previous section, it was shown that climatological mean water budget components over the St. Lawrence River had not changed significantly from RS to SS. However, Fig. 3.3c shows that changes in the climatological annual cycles of evapotranspiration and precipitation are as strong as over the Mississippi River basin: large evapotranspiration and precipitation increases are noted during spring and early summer, and decreases from July to October. As well, the changes of the atmospheric moisture convergence and evapotranspiration have opposite signs during most of the year. However, the relatively large increase in moisture flux convergence over the Mississippi basin from July to September is not present over the St. Lawrence basin despite a comparable decrease in evapotranspiration (moisture flux convergence only increases in August). During summer, the expanded Atlantic subtropical anticyclonic circulation largely influences the Mississippi basin (Roads et al. 2003) and the reduced low-level atmospheric humidity caused by the decreased evapotranspiration could be compensated by moisture from the Gulf of Mexico. It should be kept in mind that low-level atmospheric specific humidity over ocean is strongly influenced by sea-surface temperatures, which are the same in both (RS and SS) simulations.

The response of the Mackenzie basin to the change of land-surface scheme is somewhat different from the other two basins. From late summer to winter, the water budget components remain essentially unchanged. As shown later, the snowmelt over the Mackenzie basin generally begins one or two months later than over the other two basins. Therefore, the soil of the Mackenzie basin still contains relatively large amount of water in summer and fall, allowing evaporation in simulation SS in late summer and fall, and reducing the difference between SS and RS. Nevertheless, larger evaporation in MAN than in CLASS is clearly visible during spring and early summer

Changes in the terrestrial components of the water budget (simulated runoff and terrestrial water storage tendency) by replacing CLASS with MAN are shown in Figs. 3.3b, 3.3d and 3.3f. The figures also show the change in precipitation minus evapotranspiration *(P-E)* that gives information about the net amount of moisture that the soil gains or looses in its interaction with the atmosphere. Over the Mississippi River basin, simulated runoff in SS is larger than in RS, from November to May (see Fig. 3.3b), which is mainly related to the difference in simulated terrestrial water storage: relatively small water holding capacity of the bucket (in simulation SS) limits the amount of water that can be absorbed and stored in soil, and the bucket often overflows. During July to October, runoff over the Mississippi basin is nearly equal in both simulations despite significant difference in simulated *P-E*. In this period of the year, an important soil moisture deficit over the basin is present and almost all the precipitation is stored in the soil (runoff is close to zero in both simulations).

Runoff over the St. Lawrence basin is significantly decreased from June to October as a response to the replacement of CLASS with MAN, and significantly increased in March resulting from the snowmelt that is important enough to make the bucket to overflow with MAN. Over the Mackenzie basin, a large decrease of runoff in May is found, which is actually responsible for significant decrease in climatological runoff mean (see Table 3.2). Over the rest of the year, runoff over the Mackenzie basin remains similar in both simulations, except in March and July, when it is significantly increased. Such a large reduction in May runoff is partly related to decrease in simulated *(P-E)* (see Fig. 3.3f), but the main reason is a large decrease in simulated snow amount from RS to SS (Fig. 3.4). Note that over the Mackenzie River basin, snow generally melts in May. Fig. 3.4 shows that the use of MAN in lieu of CLASS results in snow-depth reduction over all three river basins, but the change over the Mackenzie basin is the largest. Smaller snow amount are simulated by the land surface schemes, that use composite snow-soil parameterization (as is the case in

MAN) compared to the schemes where snow is parameterized as a discrete layer (as in CLASS), has been reported in the Project for Intercomparison of Land-Surface Parameterization Schemes (PILPS; Bowling et al. 2003).

Change in climatological annual cycles of the water budget components due to replacing NCEP/NCAR by ERA40 driving data are shown in Fig. 3.5. In general, these changes are much smaller than those caused by the change of land surface scheme. Student's t-test and Wilcoxon rank-sum test, applied on data of each month separately, demonstrates that there is no statistically significant change in the water budget components over the Mississippi and St. Lawrence basins. The significant increase in climatological means of evapotranspiration over the St. Lawrence river basin (found in Section 3.3.1) is therefore related to the slight increase in evapotranspiration throughout the year. For the Mackenzie River basin, evapotranspiration is significantly increased during July to October when NCEP/NCAR is replaced by ERA40. As well, a significant increase in precipitation is present over Mackenzie basin in August and September.

The comparison of IC and RS simulations shows that the changes in climatologal annual cycle (due to internal variability) can reach 0.07 mm day^{-1} for some months. Spring and summer are the most affected seasons (see Fig. 3.6), while the most affected basin by internal variability is the St. Lawrence basin. However, changes in annual cycles of water budget components due to internal variability are much smaller than those resulted from alternation of land surface scheme and driving data and are not statistically significant.

2) Comparison with observations

Since internal variability has little impact on the climatological annual cycles, validation (over a ten year period) is performed only for the RS, SS and BC simulations.

Over the Mississippi River basin (see Fig. 3.7), precipitation and evapotranspiration are characterized in all simulations by positive biases during spring and negative biases during summer and fall. Note that annual cycles of quasi-observed evapotransipration are derived as a residual from the atmospheric water budget, using monthly time series of observed precipitation as well as moisture flux convergence and atmospheric water storage tendency (AWST) calculated from atmospheric reanalyses (see Music and Caya 2007 for details). Relatively large uncertainty in evapotranspiration estimation during spring is related to the discrepancy of ERA40 and NCEP/NCAR moisture flux convergence. Despite this uncertainty, it can be seen that the annual cycles of the atmospheric water budget components simulated in RS and BC are closer to quasi-observations than those simulated in SS (see also Fig. 3.8 and 3.9, for biases).

The runoff is underestimated throughout the whole year (with the exception of March and April) in RS and BC, and from May to November in SS (see Fig. 3.7e). Simulated snow water equivalent in SS is closer to the observations (Brown et al. 2003) than snow water equivalent simulated in RS and BC (see Fig. 3.7h).

The agreement between the various sources of precipitation observations for the St. Lawrence basin is not as good as for the Mississippi basin (see Fig. 3.10). However, all three observation datasets show that precipitation increases from March to July, then remains relatively constant from July to November, and then begins to decrease in winter. The simulated precipitation decreases from May to September in

SS and from June to September in RS and BC. This creates a negative bias in late summer and fall for all simulations. From April to June, precipitation is overestimated in all simulations. The biases in precipitation annual cycles seem to be linked to the out of phase reduction in the simulated evapotranspiration since the reanalysis moisture flux convergence and *AWST* are well captured in all simulations. As for Mississippi basin, simulated annual cycles of precipitation and evapotranspiration in RS and BC are in better agreement with observations (see also Fig. 3.11 and 3.12, for biases).

Simulated annual cycle of runoff over the St. Lawrence basin is compared to the observed, VIC and GRDC runoffs in Fig. 3.10e. Since observed monthly runoff is affected by water regulation activities and GRDC runoff is not wholly appropriate for the period studied here (1987-96), we believe that the hydrological model VIC forced with observed meteorological data actually provides the "best" estimate of the natural annual cycle of runoff over the St. Lawrence River basin. As can be seen, RS and BC runoffs are characterized by somewhat smaller biases (with respect to the VIC runoff) than SS runoff during June to October as well as in March. Biases in simulated runoff are partly related to the biases in simulated *(P-E)*. For example, negative biases in *(P-E)* from May to October in the SS simulation contribute to the runoff underestimation in this period of the year.

Simulated snow water equivalents over the St. Lawrence River basin are smaller than observed in all simulations and biases in SS are somewhat larger than in RS and BC (see Fig. 3.10h). Note that snow observations over the St. Lawrence basin show that an important amount of snow melts from March to April and hence runoff reaches its maximum in April. This is not seen in runoff derived from the streamflow observations, but VIC as well as GRDC runoff has a maximum in April.

Simulated and observed (quasi-observed) annual cycles of the water budget

components over the Mackenzie River basin are compared in Fig. 3.13, while simulation biases are shown in Figs. 3.14 and 3.15. As for the other two river basins, annual cycles of observed (quasi-observed) atmospheric water budget components are better captured in RS and BC than in SS simulation. In summer, simulated moisture flux convergences in RS and BC are somewhat smaller than those based on NCEP/NCAR and ERA40 reanalyses while evapotranspiration is slightly larger than the quasi-observation and therefore the simulated annual cycle of precipitation appears to be well captured. In simulation SS, an overestimation of precipitation and evapotranspiration is visible during spring and early summer. The atmospheric moisture flux convergence in SS is underestimated from April to October. Note that ERA40 and NCEP/NCAR annual cycles of the moisture flux convergence are very close, but it should kept in mind that their climatological means are overestimated when compared to climatological mean of observed runoff. Runoffs simulated in RS and BC reach their maxima in May as in the observations, but a large positive bias is present. This bias is related to the overestimation of observed snow water equivalent (see Fig. 3.13h). For the rest of the year, runoff in all simulations is underestimated, especially during summer, partly related to the to the *(P-E)* negative bias.

3.3.3 Investigation of inter-annual variability

In order to determine magnitudes of interannual variability of the water budget components over the investigated river basins and to assess its sensitivity to the change in land surface parameterisations, lateral boundary and initial conditions, the interannual standard deviation (SD) of the water budget components is computed for each simulation as:

$$SD_i = \left(\frac{1}{N-1} \sum_{j=1}^{N=39} (X_{ij} - \overline{X}_i)^2 \right)^{1/2} ; \qquad (3.1)$$

where $\overline{X}_i$ is climatological mean of variable X (spatially averaged over a basin) from simulation i (*RS, SS, BC or IC*), and X_{ij} is the annual mean for year j for simulation i. Table 3.5 presents the interannual standard deviations of the water budget components in the reference simulation and summarises their sensitivity to the model configuration change. A Fisher's test applied to the data of the SS-RS, BC-RS and IC-RS simulations pair shows that changes in interannual standard deviation are not statistically significant (except for SS-RS evapotranspiration for the St. Lawrence basin) at the level of $\alpha = 0.05$.

Table 3.5 also shows the coefficient of variations (CV) of the water budget components of the reference simulation, which is the ratio of standard deviation to the climatological mean and is a useful statistic for comparing the degree of variation of variables having different climatological means. Mississippi River basin has the largest coefficient of variation of all water budget components, meaning the largest interannual variability in its hydrological cycle.

3.4 Summary and conclusion

The goal of the present study was to assess the sensitivity of the water budget components of the Canadian Regional Climate Model (CRCM) to the formulation of land surface processes, lateral boundary and initial conditions. This helps in estimating the uncertainty in the simulated water budget components that is required to assess the signal to noise ratio (measure of signal strength relative to background noise) in climate change projections. An ensemble of multi-year simulations generated over North America was used. The first simulation pair (referred to as SS-RS) was built in a way to assess the sole effect of the land surface scheme: the

simulation RS was based on a state-of-the-art land surface scheme (CLASS, Verseghy et al. 1993), while in SS a Manabe-based land surface scheme (MAN) with a constant water holding capacity of 100 mm was used. The second pair (BC-RS) consists of simulations differing only in lateral boundary conditions: RS was driven by NCEP/NCAR and BC with ERA40 reanalyses. Internal variability of the selected CRCM configuration was evaluated using another pair of simulations (IC-RS) differing only in initial conditions. Sensitivity analyses were carried out for climatological means, climatological annual cycles and interanual variability over three North American River basins that were selected to cover a large range of climate conditions: Mississippi, St. Lawrence and Mackenzie River basins. In addition an evaluation of simulated water budget components from various sets of observations was done.

Change in climatological mean of the water budget components from the change in land-surface parameterisation varied from basin to basin. Over the Mississippi and Mackenzie River basins, there was a statistically significant change in climatological means of all water budget components, with the exception of precipitation over the Mississippi basin. Climatological means of the water budget components over the St. Lawrence basin due to change in land surface parameterisation were not affected by the in a statistically significant way.

Analysis of climatological annual cycles indicated that there was an important increase in evaporation from RS to SS during spring and early summer over all three river basins. In general, the increased spring evaporation was counteracted by decreased moisture flux convergence and increased precipitation. Snow dept was reduced over all three basins, but the change over the Mackenzie basin was the largest. During late summer and fall, there was a large reduction in evaporation and precipitation from RS to SS over the Mississippi and St. Lawrence river basins, while changes over the Mackenzie basin were relatively small. The larger availability of

soil water limits the summer reduction in evaporation and precipitation over this basin.

Comparison with observations indicated somewhat smaller biases of precipitation climatological means in simulation RS than in SS, over all three river basins. However, over the Mississippi and Mackenzie basins, climatological mean of simulated runoff in SS was in better agreement with observations. Biases in climatological mean of evaporation over the Mississippi and St. Lawrence basins were smaller in SS. The comparison of simulated with observed (derived from observations) annual cycles showed that the use of a state-of-the-art land surface scheme provide more realistic climatological annual cycles of the water budget components for all three river basins.

Sensitivity of the water budget components to the change in lateral boundary conditions was much smaller than sensitivity to the change in land-surface parameterisation. It is important to keep in mind that ERA40 and NCEP data are in much better agreement to each other than are model data obtained from different GCMs. The sensitivity from reanalysis data to GCM data will be investigated in a forthcoming paper together with the climate-change signal in all the water budget components. Mackenzie river basin is the most sensitive to the change in boundary conditions: climatological means for all water budget components were increased significantly. Over the St. Lawrence basin only evapotranspiration was increased significantly, while over the Mississippi river basin, the changes were not statistically significant. Changes in climatological annual cycles from RS to BC were relatively small.

Comparison of the IC to the reference simulation indicated that changes in climatological means over the investigated river basins were smaller or equal to 0.01 mm day^{-1}. The most sensitive seasons to internal variability were spring and summer

and the most affected basin was the St. Lawrence basin. None of these changes with IC were statistically significant.

Results of analysis of inter-annual variability demonstrated that there were no statistically significant changes in interannual standard deviation for SS-RS, BC-RS and IC-RS simulation pairs.

Acknowledgements

This research was financially supported by the Canadian Regional Climate Modelling and Diagnostics (CRCMD) Network, funded by the Canadian Foundation for Climate and Atmospheric Sciences (CFCAS) and the Ouranos Consortium on Regional Climatology and Adaptation to Climate Change. Authors are grateful to all members of the Climate Simulations Team of the Ouranos Consortium for their valuable help.

References

Adler, R.F., G.J. Huffman, A. Chang, R. Ferraro, P. Xie, J. Janowiak, B. Rudolf, U. Schneider, S. Curtis, D. Bolvin, A. Gruber, J. Susskind, and P. Arkin, 2003: The Version-2 Global Precipitation Climatology Project (GPCP) Monthly Precipitation Analysis (1979–Present). *J. Hydrometeor.*, **4,** 1147-1167.

Bonan, G.B., 1995: Land-atmosphere CO2 exchange simulated by a land surface process model coupled to an atmospheric general circulation model. *J. Geophys. Res.,* **100**, 2817-2832.

Bowling, L., D. Lettenmaier, B. Nijssen, J. Polcher, R. Koster, and D. Lohmann, 2003: Simulation of high-latitude hydrological processes in the Torne-Kalix basin: PILPS Phase 2(e) 3: Equivalent model representation and sensitivity experiments. *Global and Plan. Change*, **38**, 55-71.

Brown, R. D., B. Brasnett, and D. Robinson 2003: Gridded North American monthly snow depth and snow water equivalent for GCM evaluation. *Atmos.-Ocean*, **41**, 1-14.

Caya, D., and S. Biner, 2004: Internal Variability of RCM Simulations over an Annual Cycle. *Climate Dyn.,* **22**, 33-46.

Chen, T. H., A. Henderson-Sellers, P. C. D. Milly, A. J. Pitman, A. C. M. Beljaars, J. Polcher, F. Abramopoulos, A. Boone, S. Chang, F. Chen, Y. Dai, C. E. Desborough, R. E. Dickinson, L. Duemenil, M. Ek, J. R. Garratt, N. Gedney, Y. M. Gusev, J. Kim, R. Koster, E. Kowalczyk, K. Laval, J. Lean, D. Lettenmaier, X. Liang, J-F. Mahfouf, H.-T. Mengelkamp, K. Mitchell, O. N. Nasonova, J. Noilhan, A. Robock, C. Rosenzweig, J. Schaake, C. A. Schlosser, J.-P. Schulz, Y. Shao, A. B. Shmakin, D. L. Verseghy, P. Wetzel, E. F. Wood, Y. Xue, Z.-L. Yang, and Q. Zeng, 1997: Cabauw experimental results from the project for intercomparison of landsurface schemes (PILPS). *J. Climate*, **10**, 1194-1215.

Davies, H. C., 1976: A lateral boundary formulation for multi-level prediction models. *Quart. J. R. Meteor. Soc.*, **102**, 405-418.

de Elía, R. D. Caya, H. Côté, A. Frigon, S. Biner, M. Giguère, D. Paquin, R. Harvey, and D. Plummer, 2007: Evaluation of uncertainties in the CRCM-simulated North American climate. Accepted in *Climate Dyn.*

Deardorff, J.W., 1978: Efficient prediction of ground surface temperature and moisture, with inclusion of a layer of vegetation. *J. Geophys. Res.*, **83**, 1889-1903.

Dequé M.P., P. Marquet, R.G. Jones, 1998: Simulation of climate change over Europe using a global variable resolution general circulation model. *Climate Dyn.*, **14**, 173–189.

Denis, B., R. Laprise and D. Cava, 2002 : Downscaling ability of oneway nested regional climate models: the big-brother experiment. *Climate Dyn.*, **18**, 627–646.

Desborough C.E., 1999. Surface energy balance complexity in GCM land surface models. *Climate Dyn.*, **5**, 389–403.

Dickinson, R.E., M. Shaikh, R. Bryant, and L. Graumlich, 1998: Interactive canopies for a climate model. *J. Climate*, **11**, 2823-2836.

Giorgi, F., B. Hewitson, J. Christensen, M. Hulme, H. von Storch, P.Whetton, R. Jones, L. Mearns and C. Fu, 2001. Regional climate information – evaluation and projections. In: J.T. Houghton, Y. Ding, D.J. Griggs, M. Noguer, P.J. van der Linden, X. Dai, K. Maskell and C.A. Johnson (eds.), in Climate Change 2001: The Scientific Basis. Contribution of Working Group I to the Third Assessment Report of the Intergovernmental Panel on Climate Change. Cambridge University Press, pp. 583–638.

Fekete, B. M., C. J. Vorosmarty, and W. Grabs, 2000: Global, composite runoff fields based on observed river discharge and simulated water balances, Documentation for UNH-GRDC Composite Runoff Fields, v.1.0, Global Runoff Data Center, Koblenz, Germany, pp 120.

Fiorino, M., cited 2001: AMIP II sea surface temperature and sea ice concentration observations. [Available online at http://www-pcmdi.llnl.gov/projects/amip/AMIP2EXPDSN/BCS_OBS/amip2_bcs.htm.]

Frei, C., J.H. Christensen, M. Deque, D. Jacob, R.G. Jones and P.L. Vidale, 2003: Daily precipitation statistics in regional climate models: evaluation and intercomparison for the European Alps. *J. Geophys. Res*, **108**, doi: 10.1029/2002JD002287.

Fox-Rabinovitz M.S., L.L. Takacs, R. C. Govindaraju, M. J. Suarez, 2001: A variable resolution stretched grid GCM: regional climate simulation. *Mon. Wea. Rev.*, **129**, 453–469.

Legates D.,R., C. J. Willmott, 1990: Mean seasonal and spatial variability in gauge-corrected, global precipitation. *Int. J. Climatol.*, **10**, 111–127.

Louie, P.Y.T., W.D. Hogg, M.D. MacKay, Z. Zhang, R. F. Hopkinson, 2002: The Water Balance Climatology of the Mackenzie Basin with Reference to the 1994/95 Water Year, *Atmos.-Ocean*, **40**, 159–180.

Lucas-Picher, P., D. Caya and S. Biner, 2004: RCM's internal variability as function of domain size. *Research activities in Atmospheric and Oceanic Modelling*, WMO/TD, J. Côté, Ed., 1220 (34): 7.27-7.28.

Manabe, S., 1969: Climate and ocean circulation. I. The atmospheric circulation and the hydrology of the Earth's surface. *Mon. Weat. Rev.*, **97**, 739-774.

Maurer, E. P., and D. P. Lettenmaier, cited 2004: Calculation of undepleted runoff for the GCIP region, 1988–2000. [Available online at http://www.ce.washington.edu/pub/HYDRO/edm/WEBS_runoff/.]

Maurer, E.P., A.W. Wood, J.C. Adam, D.P. Lettenmaier, and B. Nijssen, 2002: A Long-Term Hydrologically-Based Data Set of Land Surface Fluxes and States for the Continental United States, *Bull. Amer. Meteor. Soc.*, **15**, 3237–3251.

Mitchell, T.D., and P.D. Jones 2005: An improved method of constructing a database of monthly climate observations and associated high-resolution grids. *Int. J. Climatol.*, **25**, 693-712.

McGuffie, K., A. Henderson-Sellers, 2001: Forty years of numerical climate modelling. *Int. J. Climatol.*, **21**, 1067-1109.

McKenney, D., P. Papadopol, K. Campbell, K. Lawrence, and M. Hutchinson, 2005: Spatial models of Canadian and North American-wide 1971/2000 minimum and

maximum temperature, total precipitation and derived bioclimatic variables. Frontline Technical note, pp 7.

McFarlane, N.A., and R. Laprise, 1985: Parameterization of Sub-grid Scale processes in the AES/CCC Spectral GCM, Atmospheric Environment Service, Downsview, Ontario, no. 85-12 CCRN 17, 70 pp.

McFarlane, N.A., G.J. Boer, J.-P. Blanchet, and M. Lazare, 1992: The Canadian Climate Centre second generation General Circulation Model and its equilibrium climate. *J. Climate*, **5**, 1013-1044.

Music, B., and D. Caya, 2007: Evaluation of the Hydrological Cycle over the Mississippi River Basin as Simulated by the Canadian RCM (CRCM). *J. Hydrometeor.*, **8**, 969-988.

Pitman, A.J., and C. Desborough, 1996: Brief description of bare essentials of surface transfer and results from simulations with the HAPEX-MOBILHY data. *Global and Plan. Change*, **13**, 135-143.

Riette, S., and D. Caya, 2002: Sensitivity of short simulations to the various parameters in the new CRCM spectral nudging. *Research activities in Atmospheric and Oceanic Modeling*, edited by H. Ritchie, *WMO/TD* - No 1105, Report No. 32: 7.39-7.40.

Roads, J., R., E.B. Lawford, H. Berbery, B. Fekete, K. Gallo, A. Grundstein, W. Higgins, J. Janowiak, M. Kanamitsu, V. Lakshmi, D. Leathers, D. Lettenmaier, Q. Li, L. Luo, E. Maurer, T. Meyers, D. Miller, K. Mitchell, T. Mote, R. Pinker, T. Reichler, D. Robinson, A. Robock, J. Smith, G. Srinivasan, K. Vinnikov, T. von der Haar, C. Vorosmarty, S. Williams, and E. Yarosh, 2003: GCIP Water and Energy Budget Synthesis (WEBS) *J. Geophys. Res.*, **108**, D16, 8609, doi: 10.1029/2002JD002583.

Sato, N., P.J. Sellers, D.A. Randall, E. K. Schneider, J.Shukla, J.L. Kinter III, Y.-Y. Hou, and E. Albertazzi, 1989: Effect of implementation of the Simple Biosphere Model (SiB) in general a circulation model. *J. Atmos. Sci.,* **46**, 2757-2782.

Sellers, P.J., Y. Mintz, Y.C. Sud, and A. Dalcher, 1986: A simple biosphere model (SiB) for use within general circulation models. *J. Atmos. Sci.*, **43**, 505-531.

Sellers, P.J., G.J. Collatz, J.A. Berry, C.B. Field, D.A. Dazlich, C. Zhang, G.D.Collelo, and L. Bounoua, 1996: A revised land surface parameterization (SiB2) for atmospheric GCMs. Part I: Model formulation. *J. Climate,* **9**, 676–705.

Verseghy, D.L., 1991: CLASS - A Canadian land surface scheme for GCMs. Part I: Soil model. *Int. J. Climatol.,* **11**, 111–133.

Verseghy, D.L., N.A. McFarlane, and M. Lazare, 1993: CLASS - A Canadian land surface scheme for GCMs. Part II: Vegetation model and coupled runs. *Int. J. Climatol.* **3**, 347–370.

Watson, R. T., and the Core Writing Team, Eds., 2001: *Climate Change 2001: Synthesis Report.* Cambridge University Press, 398 pp. [Available online at http://www.ipcc.ch.]

Willmott, C. J., and K. Matsuura, cited 2004: Terrestrial air temperature and precipitation: Monthly and annual time series (1950–1999), version 1.02. [Available online at http://climate.geog.udel.edu/_climate/html_pages/download.html.]

Table 3.1 Experimental configurations of the CRCM simulations.

Name	Model version	Nesting data	Period
RS	CRCM_4.0	NCEP/NCAR	1959-1999
SS	CRCM_3.7	NCEP/NCAR	1959-1999
BC	CRCM_4.0	ERA40	1959-1999
IC	CRCM_4.0	NCEP/NCAR	1958-1999

Table 3.2 Change in climatological mean (in mm day^{-1} and in %) of the water budget components for the period 1961-99 as a response to the change in land-surface parameterisation (MAN vs CLASS), lateral boundary conditions (ERA40 vs NCEP) and internal variability (initial conditions). The error in closing the simulated water budget is also indicated. A star indicates a statistically significant change at the level $\alpha = 0.05$.

		$\overline{X}_{RS}$ (mm/day)	$(\overline{X}_{SS} - \overline{X}_{RS})$ **MAN_vs_CLASS**	$(\overline{X}_{BC} - \overline{X}_{RS})$ **ERA40_vs_NCEP**	$(\overline{X}_{IC} - \overline{X}_{RS})$ **INTERNAL_VARIAB.**
P	Mississippi	1.96	-0.07 (-4%)	+0.04 (+2%)	0.00 (0%)
	St-Lawrence	2.30	-0.06 (-3%)	+0.08 (+3%)	-0.01 (-0.4%)
	Mackenzie	1.15	+0.08* (+7%)	+0.10* (+9%)	0.00 (0%)
E	Mississippi	1.64	-0.17* (-10%)	+0.03 (+2%)	0.00 (0%)
	St-Lawrence	1.39	0.00 (0%)	+0.05* (+4%)	0.00 (0%)
	Mackenzie	0.61	+0.15* (+25%)	+0.04* (+6%)	0.00 (0%)
C	Mississippi	0.31	+0.10* (+32%)	-0.01 (-3%)	0.00 (0%)
	St-Lawrence	0.94	-0.06 (-6%)	+0.03 (+3%)	-0.01 (-1%)
	Mackenzie	0.58	-0.07* (-12%)	+0.06* (+10%)	0.00 (0%)
R	Mississippi	0.32	+0.11* (+34%)	-0.01 (-3%)	0.00 (0%)
	St-Lawrence	0.91	-0.06 (-7%)	+0.03 (+3%)	-0.01 (-1%)
	Mackenzie	0.54	-0.08* (-15%)	+0.04* (+7%)	0.00 (0%)
Closure error (mm/d)	Mississippi	0.01	0.00	0.00	0.00
	St-Lawrence	0.03	0.00	0.00	0.00
	Mackenzie	0.04	0.00	0.00	0.00

Table 3.3 Streamflow data sources

Basin name	Station name	Data source	Drainage area (km^2)
Mississippi	Vicksburg	USGS[a]	2 868 901
St. Lawrence	Cornwall	HYDAT[b]	774 000
Mackenzie	Arctic Red River	HYDAT	1 680 000

[a] U.S. Geological Survey (for data download, see http://waterdata.usgs.gov/nwis/sw).

[b] HYDAT. 1999. Canadian hydrological data available on CD-ROM (version 99-2.00), National Water Data Archive, Environment Canada, available through the Environment Canada Web site at http://www.mscsmc.ec.gc.ca/climate/hydat/index_e.cfm.

Table 3.4 Biases of simulated climatological means (in mm day^{-1} and in %) of precipitation (BIAS_P), evapotranspiration (BIAS_E), vertically integrated moisture flux convergence (BIAS_C) and runoff (BIAS_R). BIAS_P is calculated with respect to the mean observed precipitation; BIAS_E is calculated with respect to the average of the estimates based on terrestrial water budget; BIAS_R is calculated with respect to naturalized runoff (R_NAT) for the Mississippi basin, observed runoff (R_OBS) for the Mackenzie basin, and averaged runoff (observed, VIC and GRDC runoff, R_MEAN) for the St. Lawrence basin; BIAS_C is calculated with respect to the averaged NCEP/NCAR and ERA40 convergence.

		RS	SS	BC
BIAS_P	Mississippi	-0.23 (-10%)	-0.28 (-12%)	-0.16 (-7%)
	St-Lawrence	-0.33 (-12%)	-0.36 (-14%)	-0.21 (-8%)
	Mackenzie	0.09 (8%)	0.16 (14%)	0.15 (14%)
BIAS_E	Mississippi	0.09 (6%)	-0.07 (-4%)	0.17 (11%)
	St-Lawrence	-0.35 (-20%)	-0.30 (-17%)	-0.29 (-17%)
	Mackenzie	0.02 (3%)	0.16 (26%)	0.04 (6%)
BIAS_R	Mississippi	-0.32 (-48%)	-0.22 (-33%)	-0.33 (-50%)
	St-Lawrence	0.00 (0%)	-0.07 (-8%)	0.06 (7%)
	Mackenzie	0.07 (14%)	0.00 (0%)	0.11 (22%)
BIAS_C	Mississippi	-0.27 (-45%)	-0.13 (-22%)	-0.27 (-45%)
	St-Lawrence	0.00 (0%)	-0.09 (-10%)	0.06 (6%)
	Mackenzie	-0.06 (-9%)	-0.13 (-19%)	-0.02 (3%)

Table 3.5 Change in interannual standard deviation (SD) of the water budget components for the period 1961-99 as a response to the change in land surface parameterisation (MAN vs CLASS), lateral boundary conditions (ERA40 vs NCEP) and initial conditions (Internal variability). The error in closing the simulated water budget is also indicated. A star indicates a statistically significant change at the level $\alpha = 0.05$.

		SD_{RS}	$SD_{SS} - SD_{RS}$ MAN_vs_CLASS	$SD_{BC} - SD_{RS}$ ERA40_vs_NCEP	$SD_{IC} - SD_{RS}$ INTERNAL_VARIAB	CV_{RS}
P	Mississippi	0.20	0.00	0.03	0.01	0.10
(mm/d)	St-Lawrence	0.19	0.03	0.00	0.00	0.08
	Mackenzie	0.08	0.09	0.00	0.00	0.07
E	Mississippi	0.12	-0.01	0.02	0.00	0.07
(mm/d)	St-Lawrence	0.05	0.05*	0.00	0.00	0.03
	Mackenzie	0.04	0.00	0.01	0.00	0.06
C	Mississippi	0.10	0.02	0.02	0.01	0.33
(mm/d)	St-Lawrence	0.19	-0.02	0.00	0.00	0.20
	Mackenzie	0.08	-0.01	0.01	0.00	0.14
R	Mississippi	0.10	0.02	0.01	0.00	0.31
(mm/d)	St-Lawrence	0.15	0.02	0.00	0.00	0.17
	Mackenzie	0.05	0.00	0.01	0.00	0.10

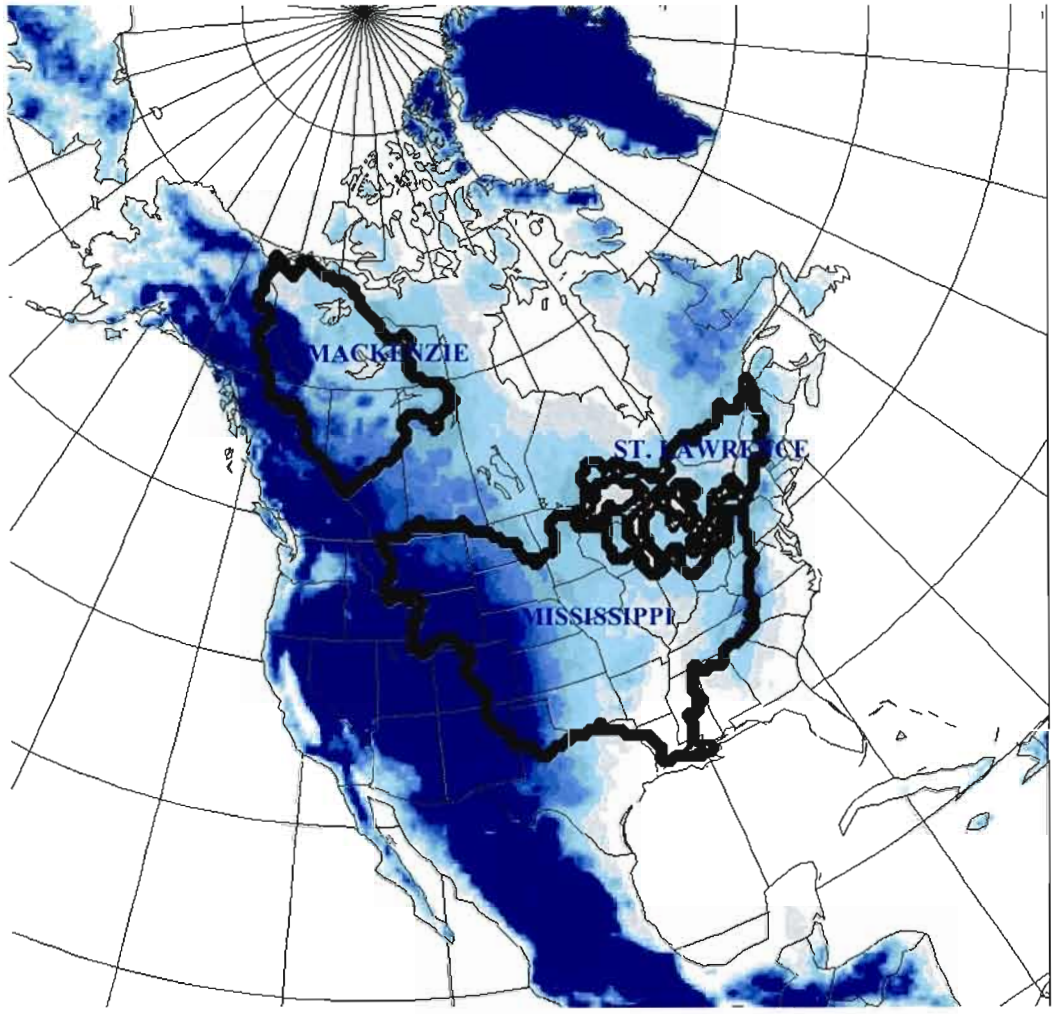

Fig. 3.1 CRCM simulation domain and topography. The Mississippi, St. Lawrence and Mackenzie River basins outlines are also indicated.

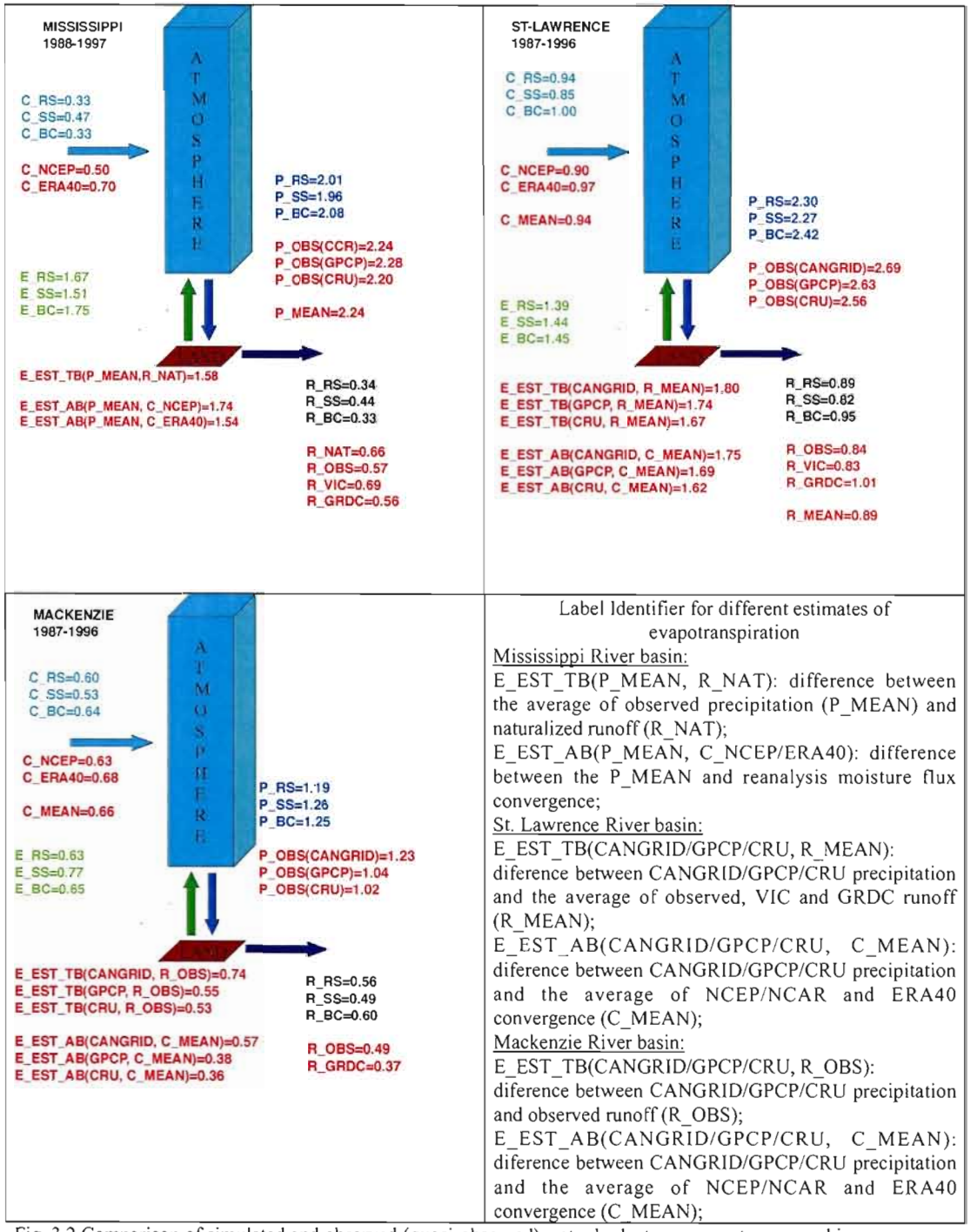

Fig. 3.2 Comparison of simulated and observed (quasi-observed) water budget components averaged in space over a basin and in time over a ten-year period. C: Convergence; P: Precipitation; E: Evapotranspiration; EST: Estimated; TB: Terrestrial Budget; AB: Atmospheric Budget.

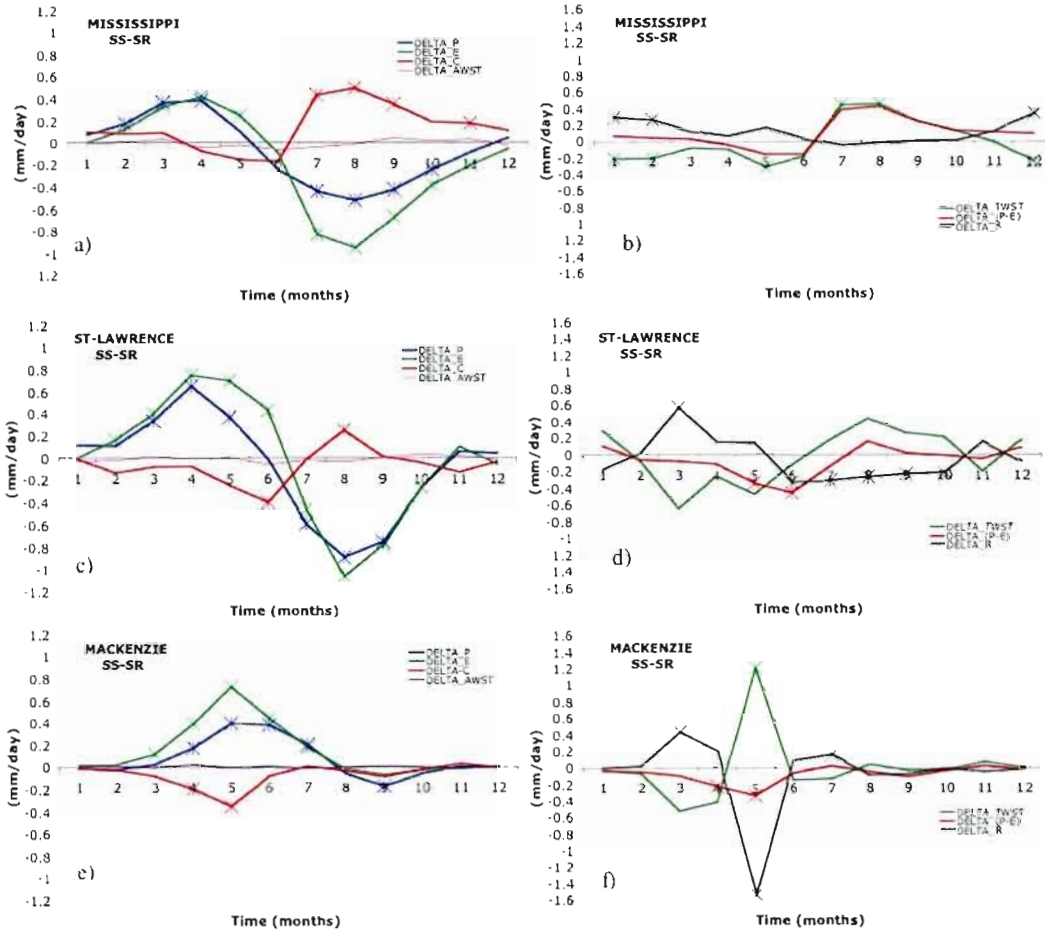

Fig. 3.3 Difference between climatological monthly means of the atmospheric (left) and terrestrial (right) water budget components for the SS/RS simulation pair. Value on the curve identified by a star indicates statistically significant difference at the level $\alpha = 0.05$.

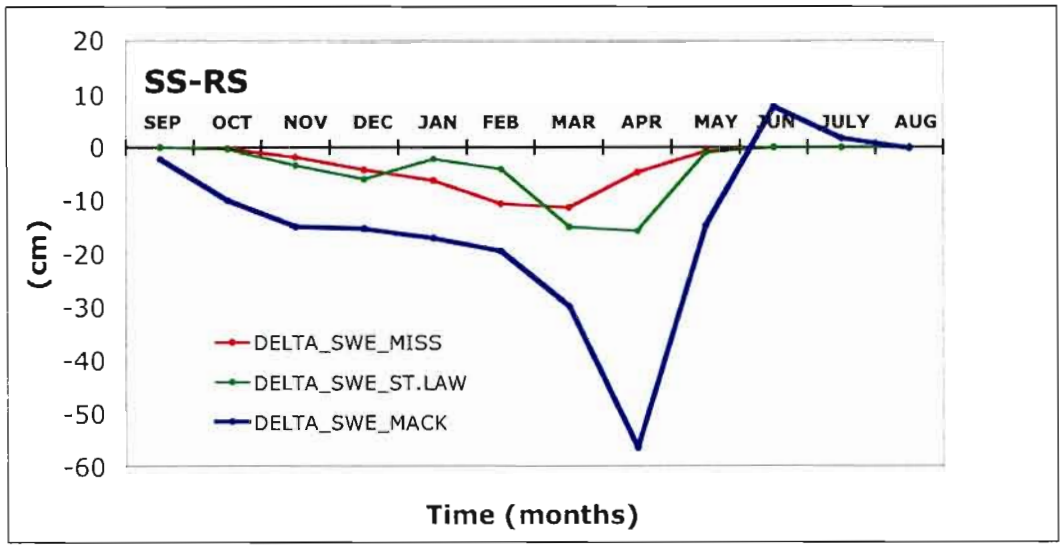

Fig. 3.4 Difference between climatological monthly means of snow water equivalent for SS/RS simulation pair.

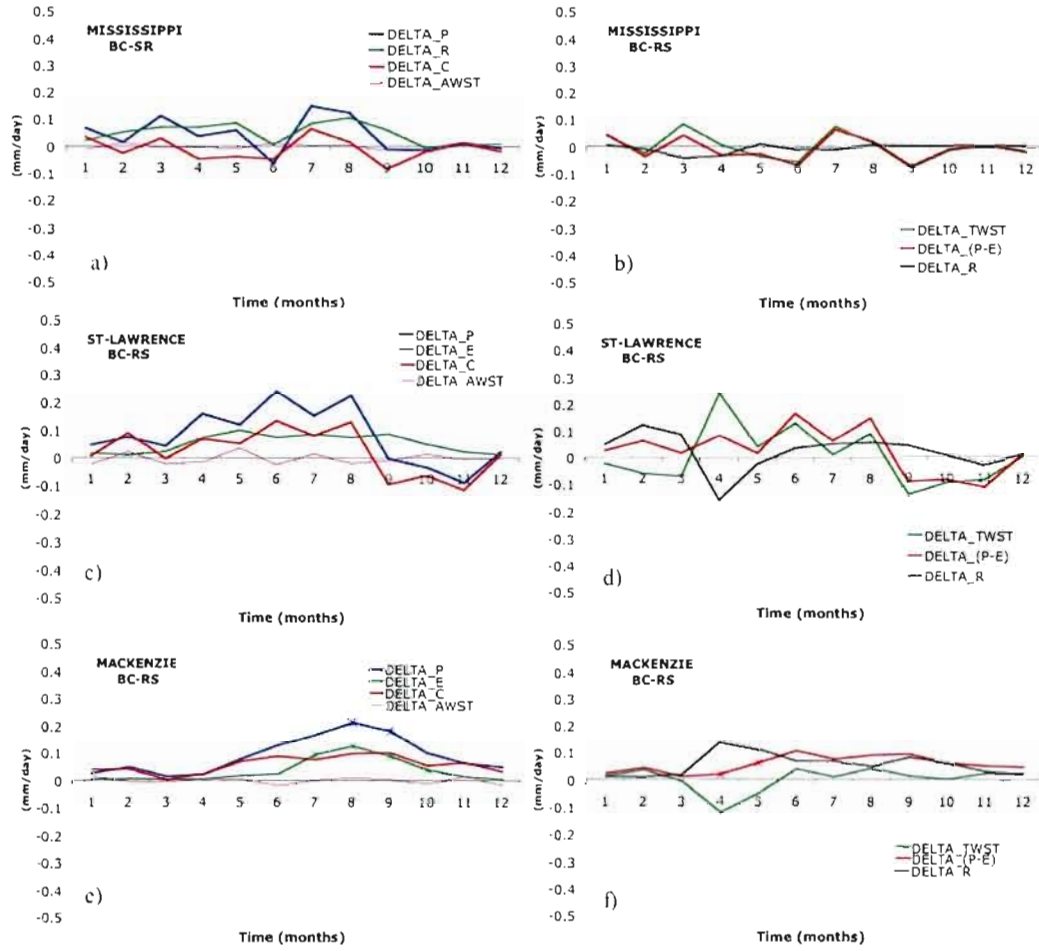

Fig. 3.5 Difference between climatological monthly means of the atmospheric and terrestrial water budgets for the BC/RS simulation pair. A star indicates statistically significant difference at the level $\alpha = 0.05$.

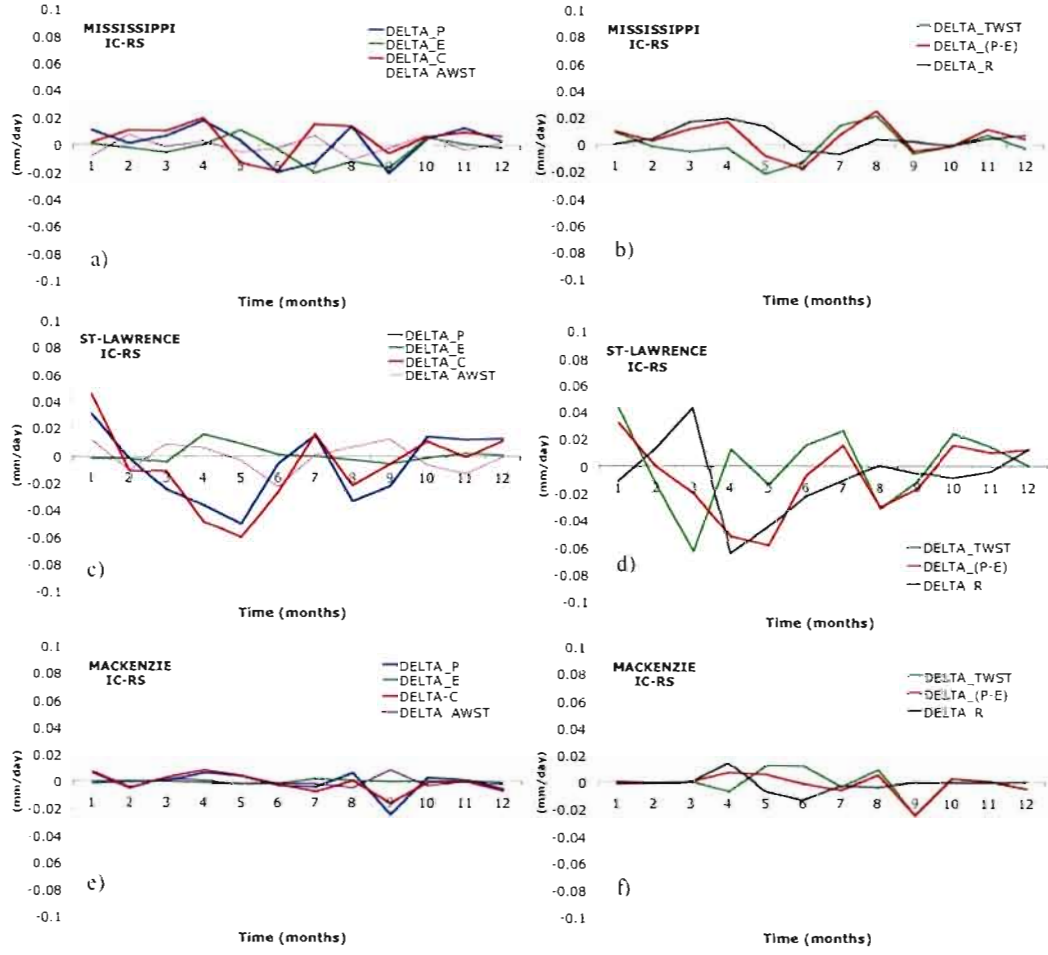

Fig. 3.6 Difference between climatological monthly means of the atmospheric and terrestrial water budgets for the IC/RS simulation pair.

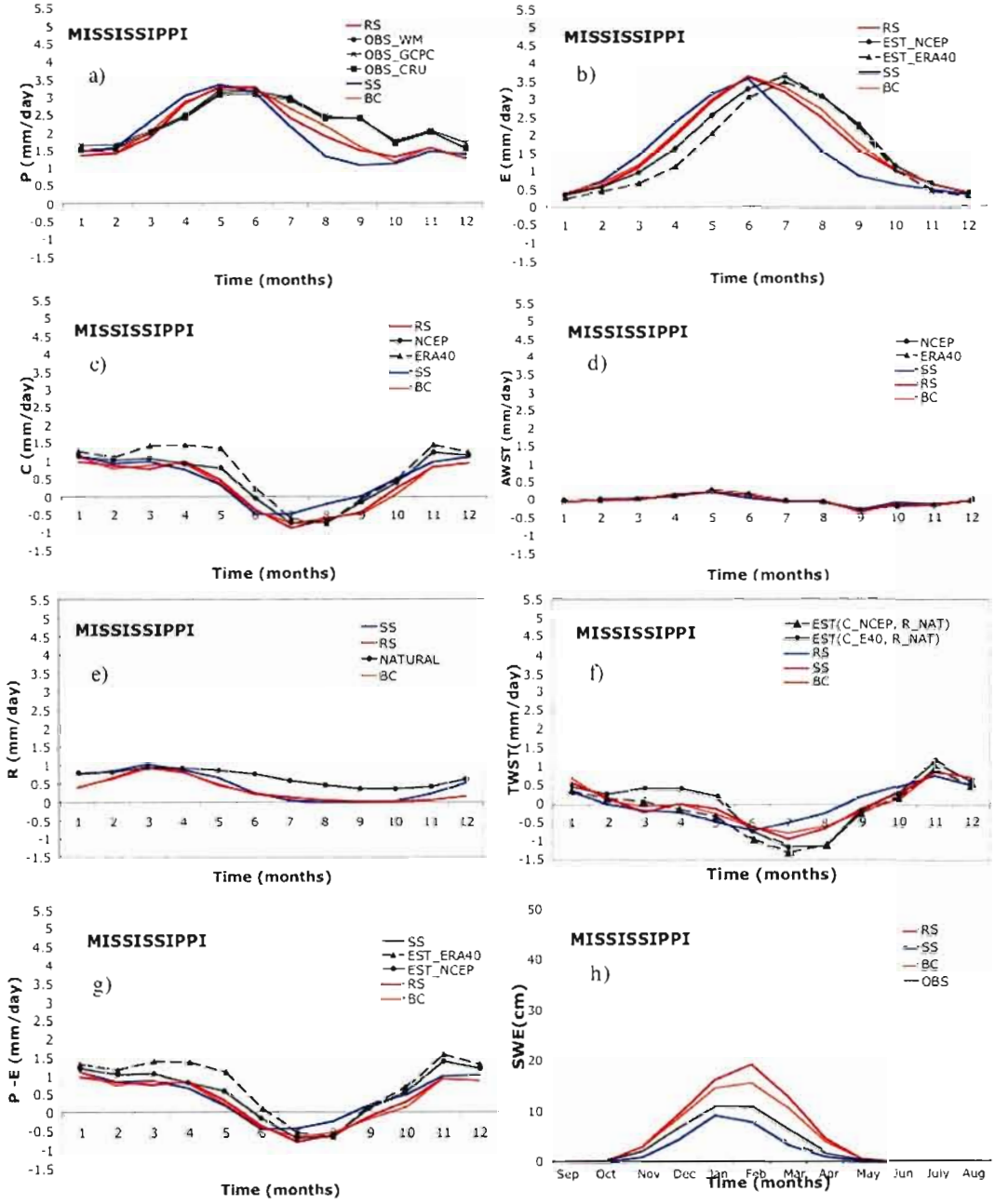

Fig. 3.7 Climatological annual cycle of simulated and observed (quasi-observed) water budget components over the Mississippi River basin for the period 1988-97: (a) precipitation, P; (b) evapotranspiration, E; (c) vertically integrated horizontal moisture convergence, C; (d) atmospheric water storage tendency, $AWST$; (e) runoff, R; (f) terrestrial water storage tendency, $TWST$; (g) difference between precipitation and evapotranspiration, P-E; (h) snow water equivalent, SWE.

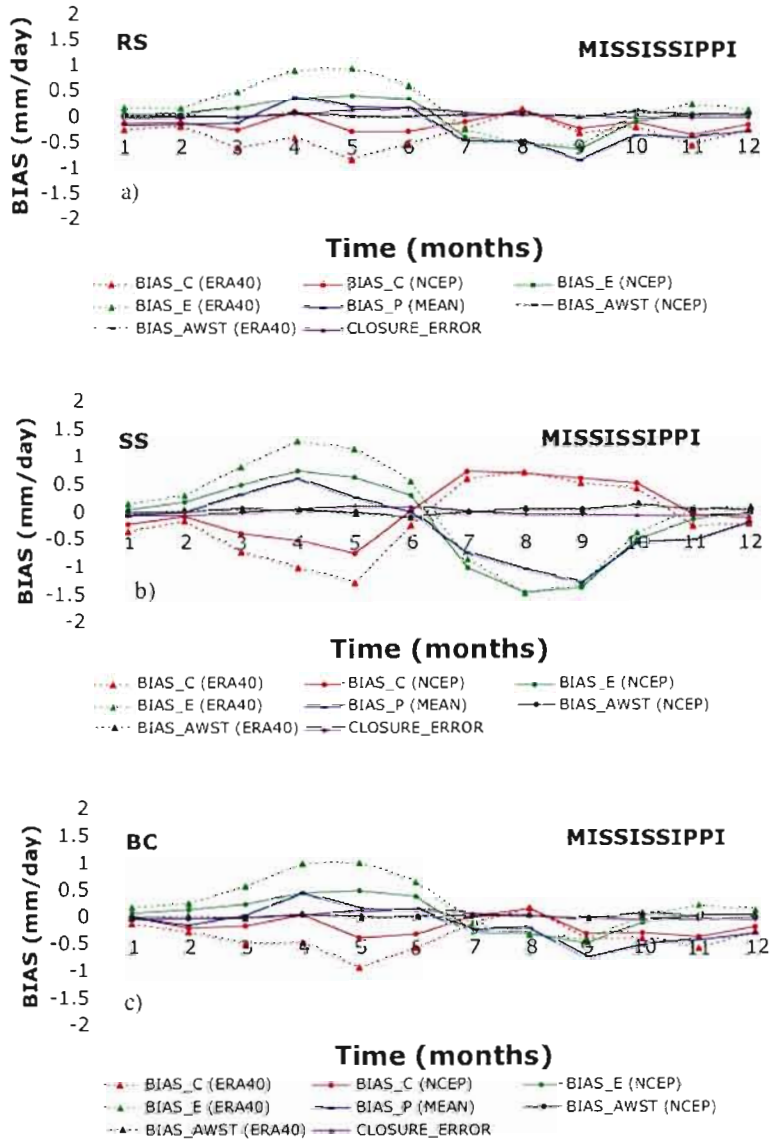

Fig. 3.8 The simulation biases for the atmospheric water budget components for the Mississippi basin: bias of simulated *P* with respect to the average of CCR, GPCP and CRU precipitation, BIAS_P(MEAN); bias of the simulated *C* with respect to the one of the NCEP/NCAR and ERA40, BIAS_C(NCEP/ERA40); bias of the simulated *AWST*, BIAS_AWST(NCEP/ERA40). The error in closing the simulation water budget is also shown.

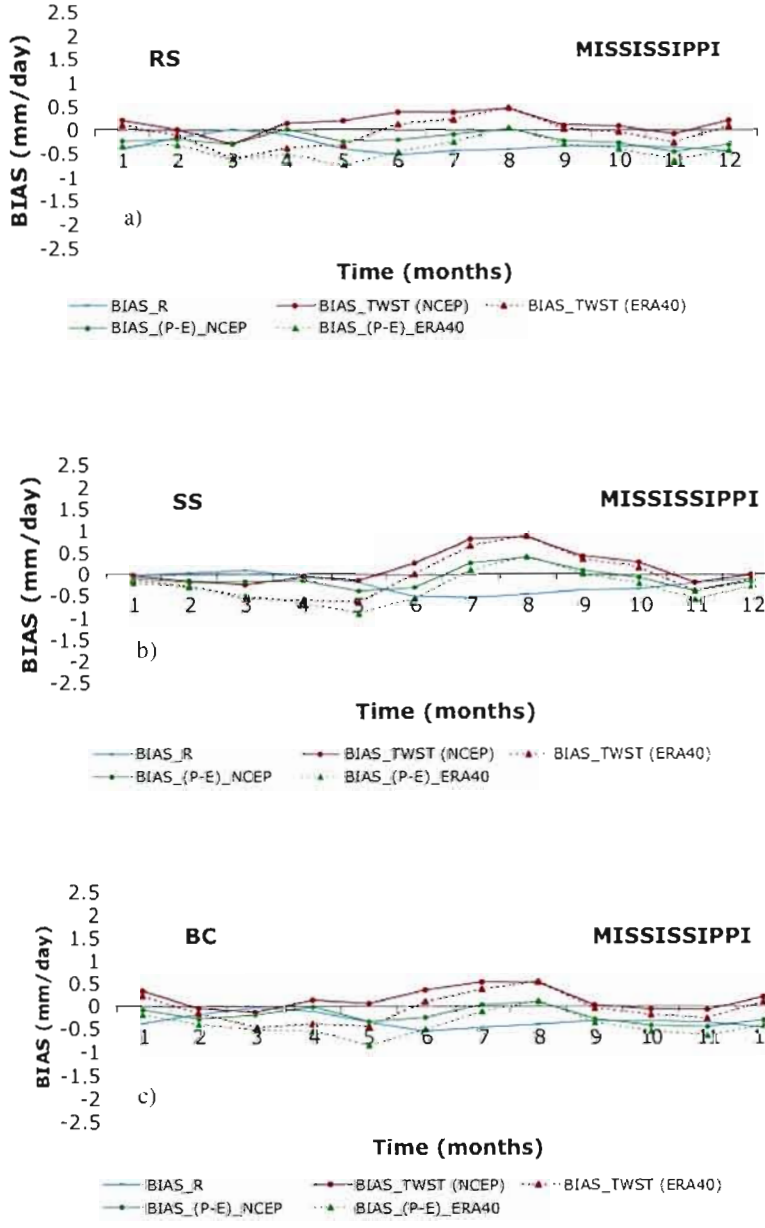

Fig. 3.9 The simulation biases for the terrestrial water budget components for the Mississippi basin: bias of simulated *R* with respect to the naturalized runoff, BIAS_R; bias of the simulated *TWST*, BIAS_TWST(NCEP/ERA40); bias of the simulated *P-E*, BIAS_P-E(NCEP/ERA40).

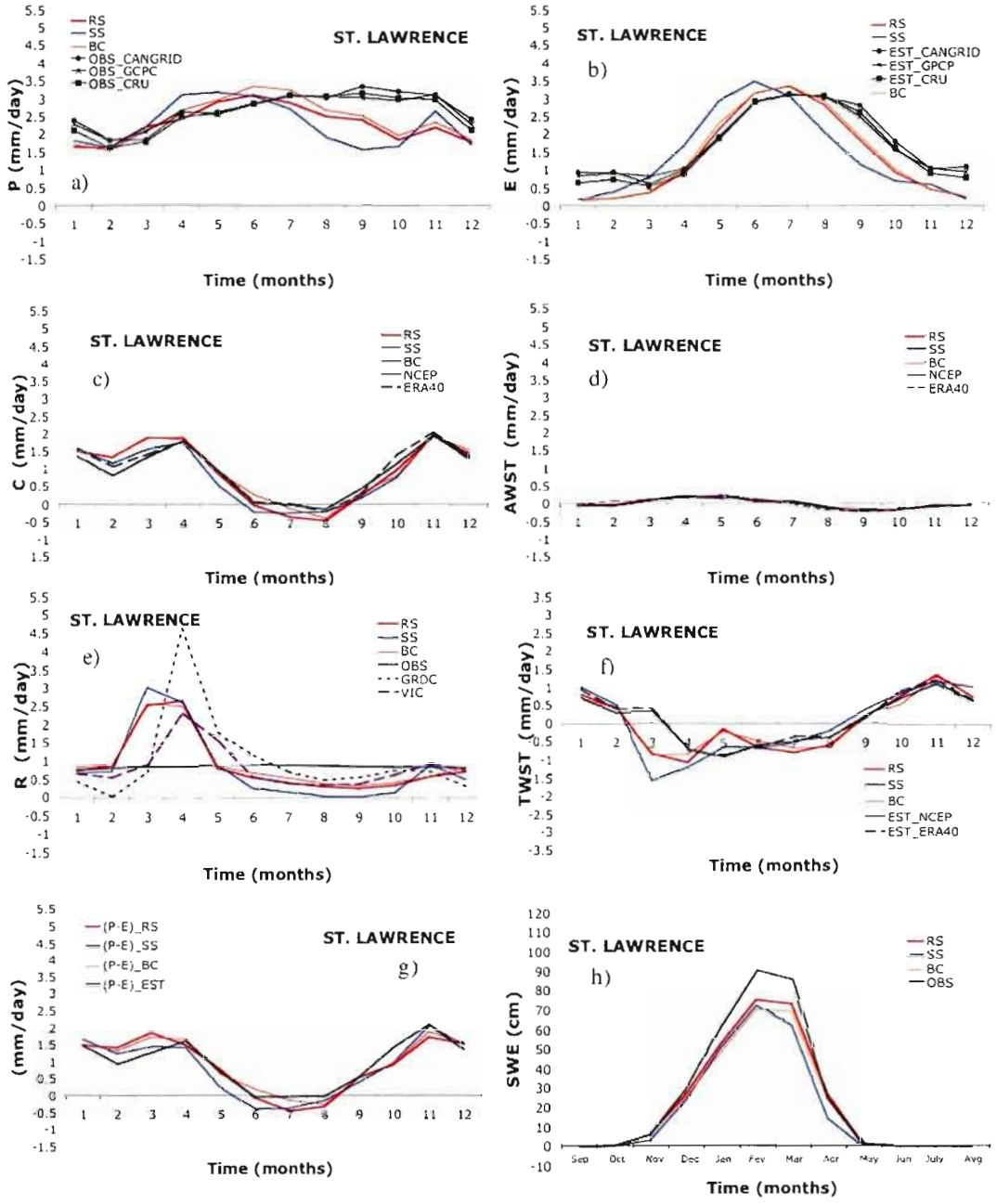

Fig. 3.10 Climatological annual cycle of simulated and observed (quasi-observed) water budget components over the St. Lawrence basin for the period 1988-97. (a) precipitation, *P*; (b) evapotranspiration, *E*; (c) vertically integrated horizontal moisture convergence, *C*; (d) atmospheric water storage tendency, *AWST*; (e) runoff, *R*; (f) terrestrial water storage tendency, *TWST*; (g) difference between precipitation and evapotranspiration, *P-E*; (h) snow water equivalent, SWE.

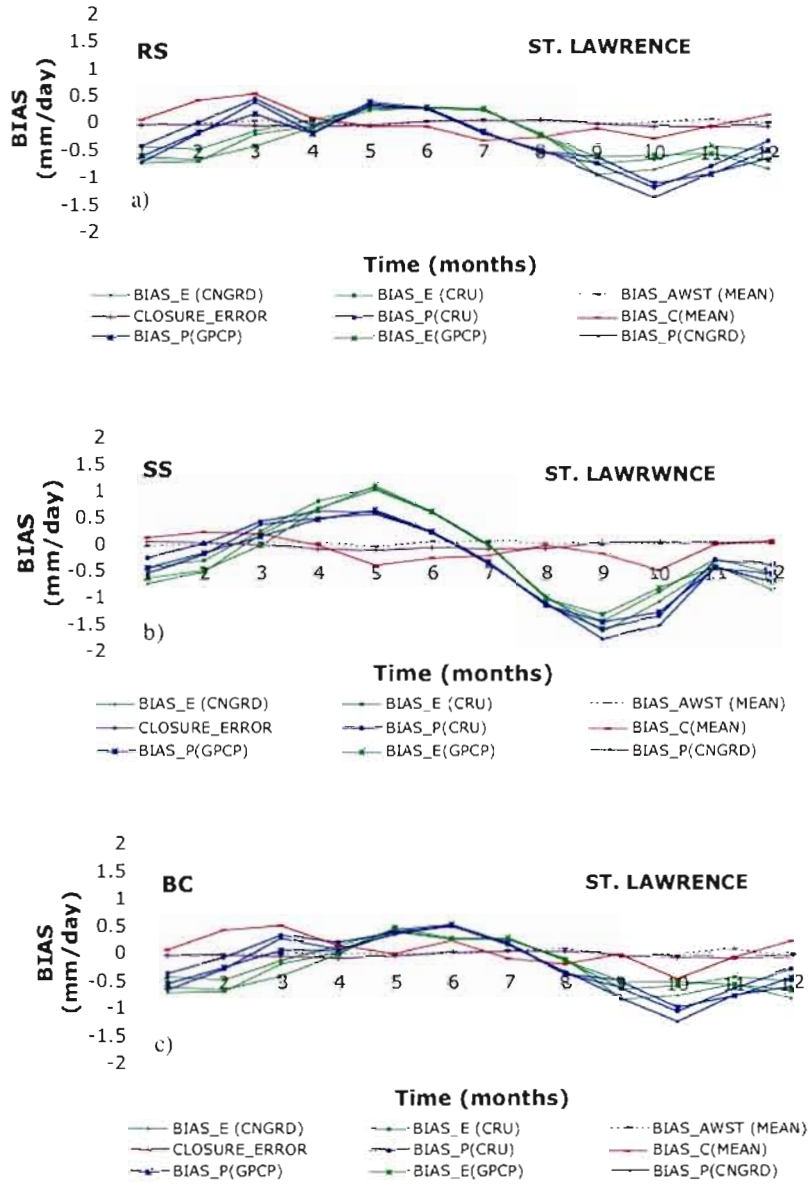

Fig. 3.11 The simulation biases for the St. Lawrence RB: bias of simulated *P* with respect to the CANGRID/GPCP/CRU precipitation, BIAS_P(CNGRD/GPCP/CRU); bias of the simulated C with respect to the averaged NCEP/NCAR and ERA40 moisture flux convergence, BIAS_C(MEAN); bias of the simulated AWST, with respect to the averaged NCEP/NCAR and ERA40 AWST, BIAS_AWST(MEAN). The error in closuring the simulation water budget is also shown.

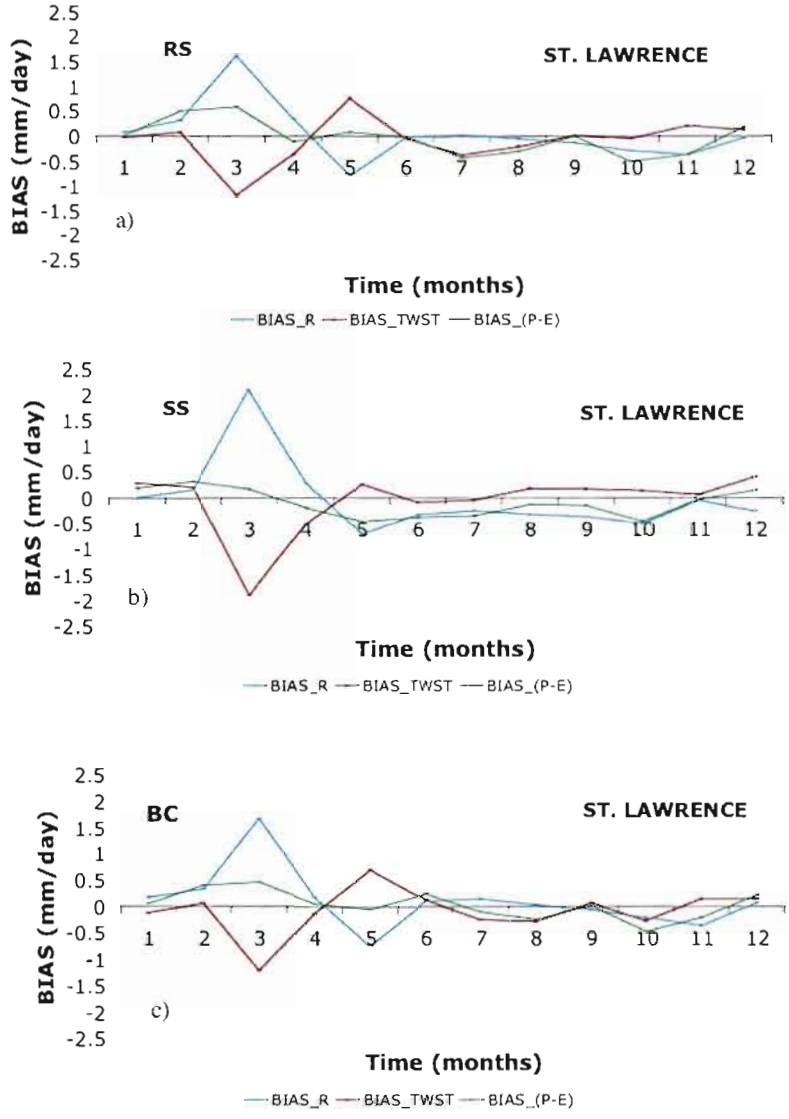

Fig. 3.12 The simulation biases for the terrestrial water budget components for the St. Lawrence basin: bias of simulated *R* with respect to the VIC runoff, BIAS_R; bias of the simulated *TWST* with respect to the averaged NCEP/NCAR and ERA40 *TWST*, BIAS_TWST(MEAN); bias of the simulated *P-E*, BIAS_P-E.

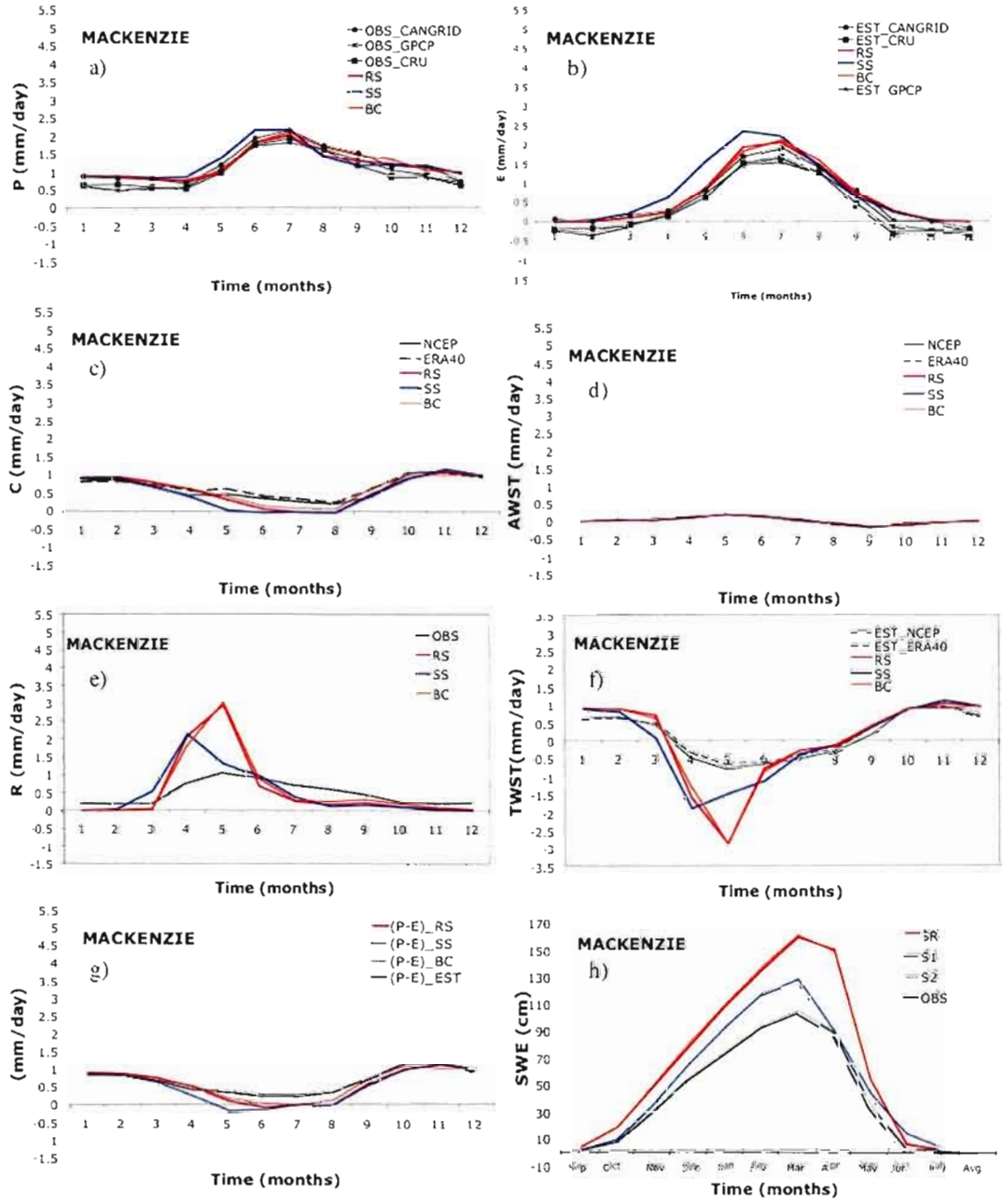

Fig. 3.13 Climatological annual cycle of simulated and observed (quasi-observed) water budget components over the Mackenzie basin for the period 1987-96. (a) precipitation, *P*; (b) evapotranspiration, *E*; (c) vertically integrated horizontal moisture convergence, *C*; (d) atmospheric water storage tendency, *AWST*; (e) runoff, *R*; (f) terrestrial water storage tendency, *TWST*; (g) difference between precipitation and evapotranspiration, *P-E*; (h) snow water equivalent, SWE.

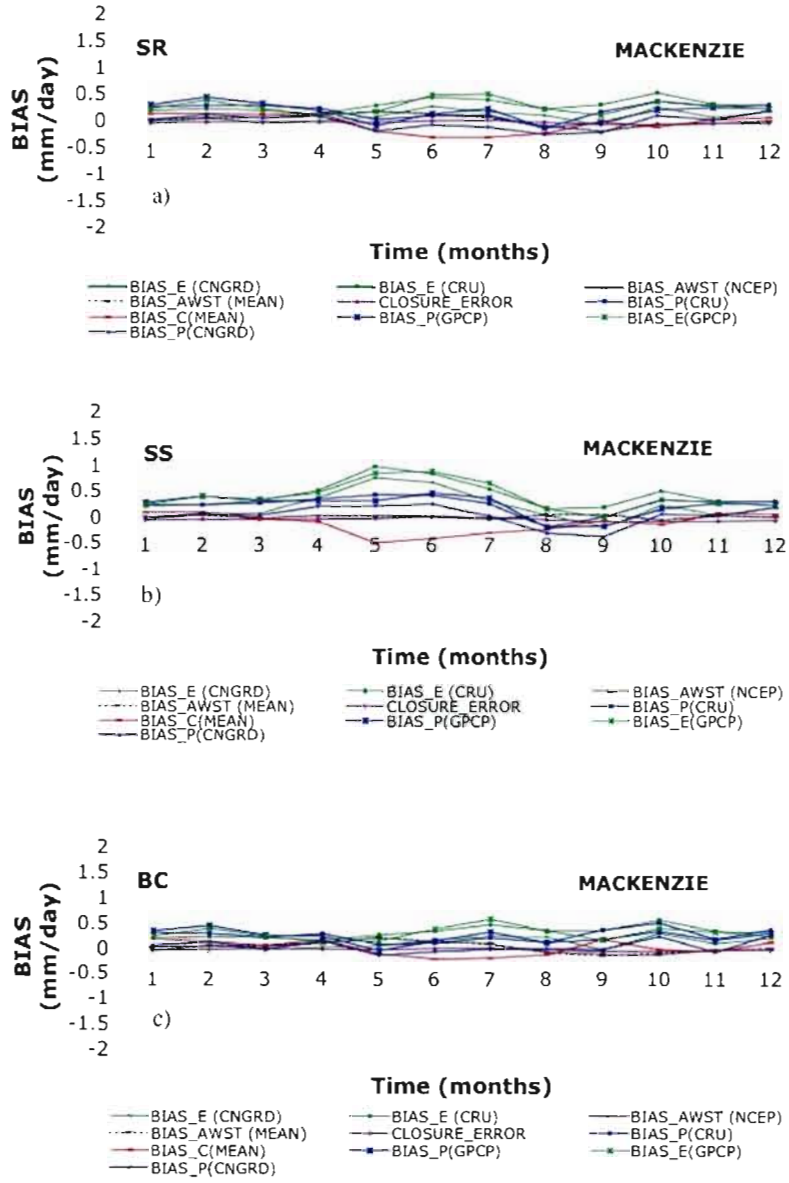

Fig. 3.14 The simulation biases for the Mackenzie basin: bias of simulated *P* with respect to the CANGRD/GPCP/CRU precipitation, BIAS_P(CNGRD/GPCP/CRU); bias of the simulated C with respect to the averaged NCEP/NCAR and ERA40 moisture flux convergence, BIAS_C(MEAN); bias of the simulated AWST, with respect to the averaged NCEP/NCAR and ERA40 AWST, BIAS_AWST(MEAN). The error in closuring the simulation water budget is also shown.

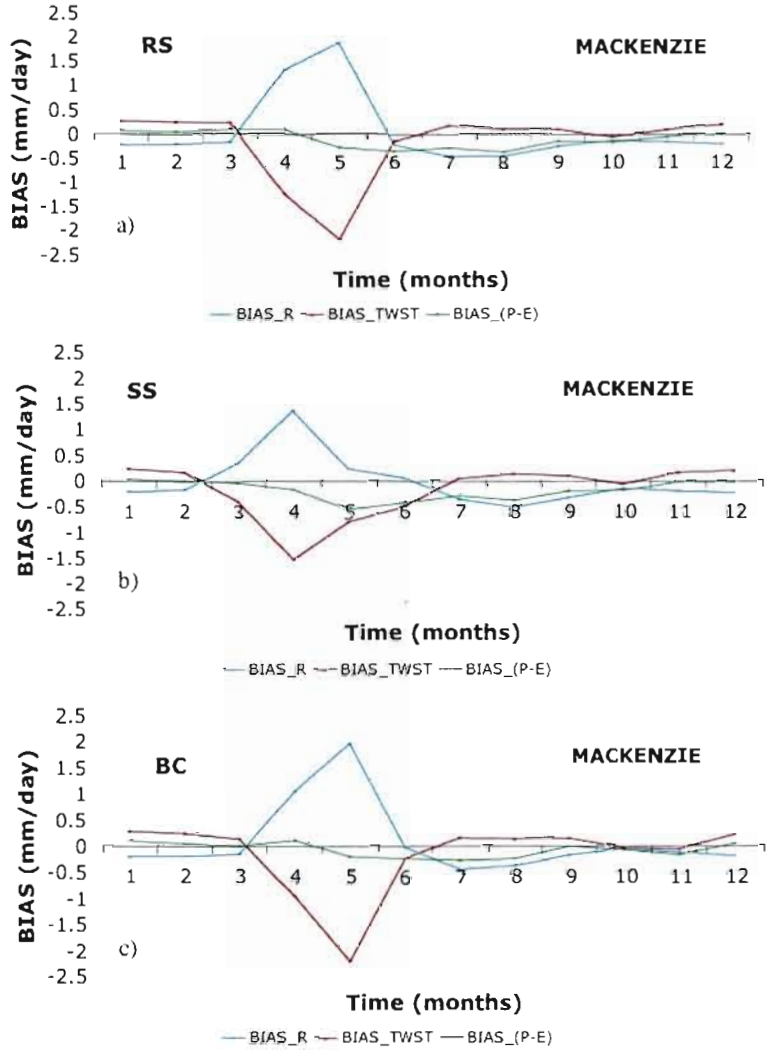

Fig. 3.15 The simulation biases for the terrestrial water budget components for the Mackenzie basin: bias of simulated *R* with respect to the VIC runoff, BIAS_R; bias of the simulated *TWST* with respect to the averaged NCEP/NCAR and ERA40 *TWST*, BIAS_TWST(MEAN); bias of the simulated *P-E*, BIAS_P-E.

CHAPITRE IV

CONCLUSION GÉNÉRALE

4.1 Conclusions principales de la recherche

Dans un cadre général, la présente recherche nous a permis d'affiner notre compréhension des différents processus reliés au cycle de l'eau en utilisant le Modèle Régional Canadien du Climat (MRCC). L'utilisation des modèles comme des outils permettant l'approfondissement de nos connaissances nous oblige à confronter leur réalité virtuelle avec le monde réel, que malheureusement nous ne comprenons que partiellement. De nombreuses incertitudes impliquées dans l'évaluation du cycle hydrologique simulé par un modèle sont donc inévitables et imposent d'une certaine manière les échelle spatiale et temporelle qui peuvent être traitées. L'approche développée dans cette thèse comprend une analyse à l'échelle multi-annuelle pour l'ensemble d'un bassin versant assez grand, permettant une évaluation par une réduction importante des erreurs dans les champs observés et simulés.

Un des volets importants de cette recherche était d'évaluer si tout le développement qui a eu lieu dans le module physique du MRCC de la version 3.6 vers la version 4.0 a changé son habileté à simuler les composantes principales du bilan de l'eau. Autrement dit, il a permi d'évaluer si une meilleure représentation des processus sous maille dans le MRCC_V4.0 ait rendu son cycle hydrologique plus réaliste. Notons ici que le MRCC_V3.6 utilise le module physique de la première version du MRCC développé vers le milieu des années 1990 (Caya et Laprise, 1999).

Les résultats d'évaluation du cycle hydrologique simulé par le MRCC_V3.6 sur le bassin versant du Mississippi (*chapitre II)* ont montré les limites de cette version du modèle à reproduire correctement les valeurs annuelles ainsi que le cycle annuel des composantes principales du bilan d'eau. Des biais importants dans les valeurs moyennes annuelles d'évapotranspiration (+0.7 mm jour^{-1} i.e. +42%), de la précipitation (+0,4 mm jour^{-1} i.e. +17%)) et du ruissellement (-0,3 mm jour^{-1} –41%)) ont été identifiés. L'analyse du cycle annuel a montré des surestimations de l'évapotranspiration et de la précipitation durant l'été. Par contre, la convergence d'humidité et le ruissellement sont sous-estimés pour la plupart de l'année. Une erreur de fermeture du bilan annuel de l'eau simulé de 0,1 mm jour^{-1} a été notée. Étant donné que la convergence de flux de l'humidité est calculée à chaque pas de temps pour tous les niveaux du modèle, cette erreur est attribuée au schéma numérique semi-lagrangien qui introduit une légère non-conservation des variables pronostiques. Notons ici que le schéma semi-lagrangien permet l'utilisation d'un pas de temps plus long par rapport au schéma eulérien et diminue le coût de calcul de façon importante.

La conclusion tirée de l'évaluation du cycle hydrologique du MRCC_V3.6 sur le basin du Mississippi est que la représentation simplifiée des processus de surface est à l'origine de ces biais. Le schéma de surface utilisé dans le MRCC_V3.6 est constitué d'une seule couche où la végétation est traitée implicitement. Dans les

années 1980, lors du développement de ce schéma, des valeurs de capacité de rétention de l'eau dans le sol (WCAP) plus élevées ont été retenues pour prendre en compte les effets de la végétation dont les racines, notamment celles des arbres, peuvent prélever de l'eau jusqu'à une profondeur de plusieurs mètres. Par conséquent, la capacité en eau du sol et le facteur d'évapotranspiration β ont été définis en fonction du type de sol et de la végétation. L'influence des stomates des plantes sur la transpiration n'est cependant pas considérée. Les valeurs assez grandes de capacité en eau (528 mm, moyenné sur le bassin du Mississippi) ainsi que l'absence des résistances des stomates et du drainage vertical du sol résulte en une grande quantité d'eau stockée dans le sol, prête à retourner dans l'atmosphère par évaporation lorsque suffisamment d'énergie est fournie par la radiation. En été, lorsque l'énergie radiative est importante, une forte surestimation de l'évaporation a été notée.

Les changements entre la version 3.6 et 4.0 du modèle ont été introduits afin de rendre l'évapotranspiration du modèle plus près de la réalité. Le remplacement du schéma de radiation solaire à deux bandes avec le schéma à quatre bandes (Puckrin et al. 2004) ainsi que le traitement amélioré de la couverture des nuages ont réduit le rayonnement net à la surface et par conséquence les flux de chaleur latente et sensible. L'utilisation d'un schéma de surface de la deuxième génération (CLASS, Verseghy 1991, Verseghy et al. 1993) qui, entre autres, introduit le paramétrage explicite de résistance des stomates de la végétation, contribue à la réduction d'évapotranspiration entre les versions 3.6 et 4.0. Finalement, un mélange plus efficace dans la couche limite (non-local mixing) de la chaleur et l'humidité introduit par un nouveau schéma de transfert turbulent (Jiao et Caya 2006) implique des conditions moins favorables à la convection, réduisant la précipitation. L'effet total de tous ces changements dans les paramétrages physiques du MRCC est une réduction importante des biais moyens annuels d'évapotranspiration (de 42% à 10%) et de

précipitation (de 17% à -6%) ainsi qu'une meilleure représentation de la distribution spatiale de ces variables. Les cycles annuels de précipitation, d'évapotranspiration, de convergence de flux d'humidité et de tendance dans le stockage de l'eau terrestre ont également montré une amélioration importante. Cependant, on n'a pas noté de changements significatifs de la convergence d'humidité atmosphérique ni du ruissellement annuel.

Afin de mieux comprendre le rôle de paramétrage des processus de surface dans le cycle hydrologique du MRCC, nous avons, au *chapitre III,* analysé une paire de simulations basée sur deux versions du modèle (MRCC_V3.7/MRCC_V4.0) où la seule différence était le paramétrage des processus de surface. La version 3.7 du MRCC utilise un schéma de type Manabe (« bucket ») qui est en fait le schéma utilisé dans la version 3.6, mais avec une capacité de rétention de l'eau du sol réduit et uniformisé à 100 mm. L'objectif de cette réduction importante de la capacité de rétention par rapport aux valeurs utilisées dans le MRCC_V3.6 était de réduire l'évaporation excessive pendant l'été à des valeurs plus près des observations. Cette réduction de l'évaporation par conservation a réduit également la précipitation. Notons ici que Manabe (1969) a proposé une valeur de 150 mm à partir des contraintes de son modèle (production de ruissellement à partir d'une certaine humidité) et non à partir d'observations. De l'analyse effectuée sur les trois grands bassins versants (Mississippi, Saint-Laurent et Mackenzie) nous concluons que le schéma simple basé sur Manabe (1969) a d'importante limitation dans la simulation des processus associés à l'évapotranspiration. Si les biais dans les moyennes annuelles des composantes principales du cycle de l'eau pour les simulations basées sur les deux schémas de surface sont plutôt similaires, les cycles annuels utilisant le schéma de Manabe montrent des biais très grands. Cependant, la simplicité du schéma de Manabe diminue le coût de calcul de façon importante et il est encore utilisé dans la construction d'ensemble de simulations nécessaires pour établir des projections climatiques.

Nous avons également analysé la sensibilité du cycle hydrologique du modèle face aux données utilisées pour le piloter à ses frontières. Sachant que le MRCC est un modèle régional, ses simulations sont contraintes par les informations provenant du pilote au travers de ses frontières. L'analyse de différences entre deux simulations générées avec le MRCC_V4.0 dont une pilotée par la réanalyse NCEP/NCAR et l'autre par la réanalyse ERA40 a mis en évidence cette sensibilité. Par exemple, sur le bassin de Mackenzie, les moyennes climatologiques de toutes les composantes du bilan de l'eau provenant de la simulation pilotée par la réanalyse NCEP/NCAR ont été significativement plus grandes que celles qui sont basées sur la simulation pilotée par la réanalyse ERA40.

L'analyse d'une troisième paire de simulations avec des conditions initiales différentes a montré que la variabilité interne du modèle à l'échelle des bassins versants est négligeable par rapport aux modifications introduites par le changement du schéma de surface et du pilote. Cette analyse de la variabilité interne permet de dire que les différences observées dans nos expériences sont réellement le fruit des modifications apportées dans la configuration du modèle et ne sont pas simplement liées au « bruit » généré par la variabilité interne.

En résumé, une méthode intégrée d'analyse et de validation du cycle hydrologique simulé par des modèles du climat a été développée au cours de cette thèse. Elle a permis l'évolution du cycle hydrologique simulé par trois versions du MRCC se caractérisant par des niveaux de complexité différents. La sensibilité des composantes principales du cycle de l'eau aux différents paramétrages physiques, aux données utilisées pour piloter le modèle et aux conditions initiales a également été examinée. L'ensemble des résultats a montré que l'introduction de nouveaux paramétrages dans le MRCC permet de minimiser les biais de son cycle hydrologique.

4.2 Pertinence de la recherche, contribution à l'avancement des connaissances et originalité

Une gestion appropriée des ressources en eau est primordiale. Les informations quantitatives sur les composantes principales du cycle hydrologique sont à la base de toutes réflexions au sujet de la gestion des eaux. Étant donné que les modèles régionaux peuvent fournir ces informations tant pour le climat actuel que pour le climat futur, il est de grande importance d'évaluer et d'améliorer leurs cycles hydrologiques. En effet, une évaluation compréhensive du cycle hydrologique ainsi qu'une bonne compréhension des processus y prenant place est primordiale au développement des modèles.

La présente thèse contribue à l'avancement des connaissances sur les capacités et limitations impliquées dans la quantification du cycle de l'eau par des simulateurs du climat, ainsi que par les observations disponibles. La méthodologie développée combine les simulations effectuées avec le MRCC avec diverses bases de données d'observations et de réanalyses et met l'accent sur leurs limitations inhérentes. Les résultats permettent de mieux comprendre le fonctionnement du climat et de quantifier divers termes du bilan hydrique ainsi que les incertitudes associées à l'échelle des bassins versants. Ces études sont essentielles pour cerner les incertitudes associées aux simulations du climat présent, ainsi que celles associées aux projections des changements climatiques.

L'originalité principale de la thèse consiste en: (i) la mise en commun de multiples sources d'informations, simulations et mesures, afin de « fermer » le bilan et d'obtenir une vision complète des divers termes contribuant à l'équilibre du bilan de l'eau à l'échelle de bassins versants ; (ii) la quantification de chacune des composantes du bilan de l'eau à l'échelle de bassins versants ; (iii) l'évaluation de la

sensibilité de chacune des composantes du bilan de l'eau à l'échelle des bassins versants au schéma de surface, aux données du pilote et aux conditions initiales.

La présente thèse doit beaucoup aux travaux des nombreux chercheurs de l'UQÀM et d'Ouranos qui ont participé au développement de trois versions du MRCC utilisé dans cette étude ainsi qu'à l'équipe Simulations climatiques d'Ouranos qui a effectué les longues simulations analysées. Ma contribution personnelle consiste principalement dans la recherche et la manipulation des vastes archives de données provenant des réanalyses et des observations. J'ai développé la méthodologie et accompli tous les calculs diagnostiques nécessaires pour quantifier le cycle de l'eau sur les trois bassins versants étudiés, ce qui requiert une application adéquate des méthodes de calcul et informatiques scientifiques avancées.

4.3 Limites de la recherche

La méthode intégrée d'analyse et de validation du cycle hydrologique simulé par un modèle du climat est attirante et raisonnable, cependant il est très important de reconnaître ses limites. Certaines de ces limites proviennent de l'incertitude sur les données observées. Premièrement, il faut mettre l'accent sur l'incertitude de la convergence de flux d'humidité atmosphérique calculé à partir des variables assimilées (l'humidité et la vitesse du vent) des réanalyses. La résolution spatiale (horizontale et verticale) et temporelle des données atmosphériques et le traitement des processus de surface dans le modèle de réanalyse peuvent avoir une influence importante sur le champ calculé du flux d'humidité. Plusieurs chercheurs ont attiré l'attention sur la différence qui apparaît quand le calcul est exécuté sur la coordonnée verticale du modèle de réanalyse et sur la coordonnée de pression (Trenberth, 1995; Trenberth and Guillemot 1995; Trenberth, 1997; Seneviratne et al. 2004). La meilleure estimation est atteinte si le calcul est effectué sur les coordonnées propres

du modèle et à sa résolution originale. Nous avons montré l'existence d'une différence assez importante entre la convergence de flux d'humidité provenant des deux réanalyses (NCEP/NCAR et ERA40) qui utilisent différents modèles et méthodes d'assimilation de données. Le plus grand désaccord a été trouvé sur le bassin du Mississippi où la différence entre les moyennes annuelles basées sur dix ans était 0.2 mm/jour ou 40%. Notons que la convergence du flux d'humidité a été calculée à partir des données de réanalyses NCEP/NCAR et ERA40 à leurs résolutions originales et sur les coordonnées des modèles.

Une autre façon d'évaluer la fiabilité de la convergence d'humidité des réanalyses consistait à comparer la moyenne annuelle sur un bassin donné avec la quantité d'eau qui sort du bassin par l'écoulement terrestre, le débit à l'exutoire. Toutefois, les mesures des débits des rivières sont aussi affectées par de nombreux facteurs tels : la régulation aux barrages, les détournements d'eau, la croissance de la glace fluviale au cours de la saison hivernale, etc. D'autres sources de données relativement fiables du ruissellement sont les modèles hydrologiques forcés avec des données météorologiques observées. Ces modèles doivent cependant êtres étalonnés ; ce qui demande une longue série d'observations journalières de précipitation et de débit.

Les estimations des précipitations à partir des données observées peuvent aussi être biaisées dans certaines régions. Les ensembles de données historiques de précipitation sont basés sur des mesures aux stations météorologiques avec des capteurs (précipitomètre) qui peuvent ne pas capturer toute la précipitation. En plus, les stations météorologiques sont distribuées de façon irrégulière et sont essentiellement centrées dans les zones densément peuplées et à basse altitude. Par conséquent, les estimations de taux de précipitation dans les régions où il y a peu de stations météorologiques se caractérisent par une fiabilité limitée.

Il faut aussi souligner que les contraintes reliées à la disponibilité des données d'observations nous avaient obligé d'effectuer la comparaison des bilans simulé et quasi-observé sur une periode de 10 ans. Les statistiques issues de cette periode relativement courte pourait gagner en fiabilité si la periode de reference était plus longue.

Finalement, il faut reconnaître que le cycle de l'eau est étroitement lié à celui de l'énergie et une évaluation intégrée de tous les termes impliqués dans les bilans d'eau et d'énergie est donc préférable. Cependant, les données historiques des différents termes du bilan radiatif et des flux énergétiques dans l'atmosphère et en surface ne sont pas disponibles. Récemment (en 1998), un programme de mesure des flux d'énergie, d'eau et de CO_2 sur plusieurs sites couvrant certaines régions du globe a été lancé dans le cadre de « Fluxnet Network » (Baldocchi et al. 2001). Les méthodes d'assimilation des données pour obtenir les meilleures estimations de flux à partir des ces observations (comme, par exemple, dans le cas des réanalyses) ne sont pas encore élaborées (Roads et al. 2003). Certains chercheurs comparent les flux énergétiques simulés par leurs modèles avec ceux des réanalyses, malgré le fait que les flux énergétiques des réanalyses soient purement les résultats du modèle de réanalyse (n'étant pas contraints par des observations). Ainsi, d'autres chercheurs entreprennent les inter-comparaisons des flux provenant de leurs modèles avec d'autres modèles (voir Bengtsson 2001, Jacob et al. 2001).

En résumé, on devrait porter une attention particulière aux limites de la fiabilité des résultats obtenus lorsque l'on évalue les cycles de l'eau et de l'énergie simulés par un modèle avec des données provenant d'observations et de « quasi-observations ».

4.4 Travaux futurs et recommandations

Les travaux réalisés dans le cadre de cette thèse nous ont permis de quantifier chacune des composantes du bilan de l'eau (branches atmosphérique et terrestre) sur trois grands bassins versants en Amérique du Nord pour le climat actuel ainsi que d'évaluer les performances des trois versions du MRCC. Un travail de très grande importance serait d'entreprendre un type similaire d'étude dans un contexte du changement climatique, c'est-à-dire de quantifier les composantes du bilan hydrique en utilisant les simulations du climat futur provenant de ces différentes versions du modèle. Ceci va permettre d'acquérir une meilleure compréhension de l'influence des biais du modèle sur les projections du changement des divers termes du bilan hydrologique, ainsi que de quantifier les incertitudes de ces projections. Dans les deux derniers rapports de l'IPCC, il a été souligné qu'en moyenne et à l'échelle du globe, le contenu en vapeur d'eau, l'évaporation et les précipitations devraient augmenter. Cependant, à l'échelle régionale, on prévoit à la fois des augmentations et des diminutions de la précipitation et de l'écoulement. Pour certaines régions, les changements projetés sont caractérisés comme probables ou très probables, mais pour d'autres régions, les changements projetés montrent une forte divergence. Il faut aussi souligner que ces projections ont été principalement basées sur les modèles globaux dont la résolution spatiale demeure faible pour des études des impacts des changements climatiques sur le régime hydrologique à l'échelle régionale. Dans ce contexte, les projections provenant des modèles régionaux du climat sont préférables.

Afin que les projections du changement du régime hydrique avec le MRCC soient considérées comme fiables, il est de très grande importance de continuer son développement ainsi que la validation sur d'autres régions (bassins versants). D'une part, nous estimons qu'un traitement adéquat de la variabilité sous maille de la précipitation, par exemple par l'application d'une distribution de probabilité appropriée, aurait comme effet une amélioration du réalisme du cycle hydrologique

simulé par le MRCC. Les paramétrages d'écoulement de surface et d'écoulement profond, de même que le paramétrage de la neige qui est particulièrement important pour l'hydrologie des régions froides, méritent également d'être révisés. D'autre part, la circulation générale (partie dynamique) du modèle devrait aussi être examinée pour une évaluation du transport d'humidité au-dessus des bassins étudiés.

Bibliographie

Caya, D., and R. Laprise, 1999: A semi-implicit semi-Lagrangian regional climate model: The Canadian RCM. *Mon. Wea. Rev.,* 127, 341-362

Baldocchi, D., E. Falge, L. Gu, R. Olson, D. Hollinger, S. Running, P. Anthoni, Ch. Bernhofer, K. Davis, R. Evans, J. Fuentes, A. Goldstein, G. Katul, B. Law, X. Lee, Y. Malhi, T. Meyers,W. Munger,W. Oechel, K. T. Paw U, K. Pilegaard, H. P. Schmid, R. Valentini, S. Verma, T.Vesala, K. Wilson, and S. Wofsyn 2001 FLUXNET: A new tool to study the temporal and spatial variability of ecosystem-scale carbon dioxide, water vapor, and energy flux densities, *Bull. Amer. Meteor. Soc.,* **82**, 2415–2433.

Bengtsson, L., 2001 : Numerical modelling of the energy and water cycle of the Baltic Sea, *Meteorology and Atmospheric Physics* 77, 9-17.

Jacob D, U. Andre, G. Elgered, C. Fortelius, L.P. Graham, S.D. Jackson, U. Karstens, C. Köpken, R. Lindau, R. Podzun, B. Rockel, F. Rubel, B.H. Sass, R.N.B. Smith, B.J.M. Van den Hurk, X. Yang, 2001 : A comprehensive model intercomparison study investigating the water budget during the BALTEX-PIDCAP period. *Meteorol. Atmos. Phys.*, 77, 19-43

Jiao, Y., and D. Caya, 2006: An investigation of the summer precipitation simulated by the Canadian Regional Climate Model. *Mon. Wea. Rev.,* **134,** 919-932.

Laprise, R., D. Caya, A. Frigon and D. Paquin, 2003: Current and perturbed climate as simulated by the second-generation Canadian Regional Climate Model (CRCM-II) over northwestern North America, *Clim. Dyn.*, **21**, 405-421.

Manabe, S., 1969: Climate and ocean circulation. I. The atmospheric circulation and the hydrology of the Earth's surface. *Mon. Wea. Rev.*, **97**, 739-774.

Puckrin, E., W. F. J. Evans, J. Li, and H. Lavoie, 2004: Comparison of clear-sky surface radiative fluxes simulated with radiative transfer models. *Can. J. Remote Sens.*, **30,** 903-912.

Roads, J., R., E.B. Lawford, H. Berbery, B. Fekete, K. Gallo, A. Grundstein, W. Higgins, J. Janowiak, M. Kanamitsu, V. Lakshmi, D. Leathers, D. Lettenmaier, Q. Li, L. Luo, E. Maurer, T. Meyers, D. Miller, K. Mitchell, T. Mote, R. Pinker, T. Reichler, D. Robinson, A. Robock, J. Smith, G. Srinivasan, K. Vinnikov, T. von der Haar, C. Vorosmarty, S. Williams, and E. Yarosh, 2003: GCIP Water and Energy Budget.

Seneviratne S, P. Viterbo, C.H. Lüthiand, 2004: Inferring Changes in Terrestrial Water Storage Using ERA-40 Reanalysis Data:The Mississippi River Basin. *J. Climate,* **17**: 2039-2057.

Trenberth, K. E., 1995: Truncation and use of model coordinate data. *Tellus,* **47A,** 287–303.

Trenberth and Guillemot 1995: Evaluation of the global atmospheric moisture budget as seen from analyses. *J. Climate,* **8,** 2255–2272.

Trenberth, K. E., 1997: Using atmospheric budgets as a constraint on surface fluxes. *J. Climate*, **10**, 2796-2809.

Verseghy, D.L., 1991: CLASS – A Canadian land surface scheme for GCMs. Part I: Soil model. *Int. J. Climatol.,* **11**, 111–133.

Verseghy, D.L., N.A. McFarlane, and M. Lazare, 1993: CLASS – A Canadian land surface scheme for GCMs. Part II: Vegetation model and coupledruns. *Int. J. Climatol.* **3**, 347–370.

APPENDICE A

LAND-SURFACE PARAMETERISATION: A REVIEW

Biljana Music

Abstract

Energy, momentum and water fluxes at the lower boundary of the atmosphere have notable effects on the physical climate system as simulated by climate models. As a consequence, the main objective of any land surface model (LSM) designed for use in a climate model is to supply the correct energy, momentum and water fluxes across the soil-biosphere-atmosphere interface.

The present paper aims to provide a reasonably comprehensive review of the land surface parameterizations developed within the most commonly used LSMs (BATS, SiB, CLASS, ISBA, etc.). Over the last few decades, land surface parameterizations have evolved from the very simple first generation of land surface schemes, where the exchanges from the vegetation canopy with the atmosphere was not considered explicitly, to fairly sophisticated second and third generation models that emphasize the role of vegetation in the regulation of land surface-atmosphere interactions. Incorporation of biophysics as well as multilayer representations of soil thermal and hydrological regimes into the second-generation LSMs made them more realistic and capable of calculating surface-atmosphere fluxes more accurately than their predecessor. Inclusion of biochemical models of leaf photosynthesis into the third generation LSMs allows the carbon balance to be performed along with conventional surface water and energy balance calculations. However it is not yet clear how detailed land surface parameterizations for use in climate models need to be. The impact of any "improved" parameterization on climate model simulations should be assessed critically.

Many aspects in land surface modeling remain to be addressed. Work is continuing to improve the realism of turbulent exchanges between the land surface and the atmosphere, water transfer in soil, the parameterization of snow processes as well as the parameterization of subgrid spatial variability of the land surface and its impact on surface turbulent and radiative fluxes and soil hydrology. Additionally, there is an effort now for developing interactive vegetation models (fourth generation LSMs) that will be able to simulate changes in vegetation parameters and carbon cycle variables in response to climate change.

A.1 Introduction

Atmospheric models used for climate simulations and weather forecasting require the fluxes of radiation, momentum, sensible and latent heat across the soil-vegetation-atmosphere (S-V-A) interface. These fluxes are provided by land surface parameterization schemes. Until 1980s, land-surface parametrization schemes within atmospheric models were based on Manabe's (1969) soil model, where vegetation was not considered explicitly. The radiative and turbulent fluxes were parameterized simply in terms of a single surface energy balance equation relating the energy fluxes to the surface temperature. Evaporation was expressed as a simple function of soil moisture availability (so-called β function) and energy-driven potential evaporation. Soil moisture holding capacity was assumed to be 150 mm globally and any moisture in excess was considered as runoff. The land-surface properties such as albedo and roughness, which regulate the exchange of radiation, momentum, moisture and heat at the S-V-A interface, were prescribed and often uniform. Although this early modeling approach was not very realistic, it was used in numerous climate sensitivity studies in which the influence of albedo, surface roughness and the surface hydrology (moisture availability for evaporation) were investigated separately. Thus, Charney et al. (1977) performed experiments with their General Circulation Model (GCM) by changing albedo of some land regions and observed significant consequence in the large-scale atmospheric circulation and rainfall. Mintz (1982) reviewed the climate sensitivity experiments related to land-surface boundary condition performed with different GCMs and highlighted that all experiments show large changes in simulated circulation and rainfall when the prescribed surface albedo or available soil moisture change. Sud et al. (1986) have shown that changing the land surface roughness changes the convergence of horizontal water vapor transport in the atmospheric boundary layer and produces large changes in the distribution of convective precipitation.

During 1980s, many problems have been identified with the use of Manabe's approach and oversimplification of land-surface processes. Sato et al. (1989) demonstrated that the concept of β-function is fundamentally in error for the calculation of land surface evapotranspiration. Verseghy et al. (1993) showed that using Manabe-based land surface scheme within the Canadian GCM model generates a land surface climate that is considerably too cold and too wet compared with observations.

Deardorff (1978) proposed an alternative approach to that of Manabe (1969), introducing a greater emphasis on the role of vegetation in the regulation of land surface interactions with the atmosphere. His model included an explicit foliage layer and multiple energy exchange sites. He differentiated between direct canopy evaporation (evaporation of canopy intercepted water), canopy transpiration (water extracted by plants from the soil root zone) and bare ground evaporation, and each of these evaporation components had their own resistance parameterization. Deardorff formulated an explicit parameterization of the influence of a plant's stomata on transpiration and included a multi-layer representation of soil temperature and moisture content.

Deardorff's (1978) work as well as Mintz's (1982) review of GCM sensitivity experiments stimulated development of sophisticated biophysically based, so-called second generation land surface models (LSMs), for use in GCMs such as BATS (Dickinson et al., 1986, 1993; Yang and Dickinson, 1996), SiB (Sellers et al., 1986), CLASS (Verseghy, 1991; Verseghy et al., 1993), BEST (Pitman and Desborough, 1996), etc. Some scientists have constructed their models on the basis of Deardorff's philosophy with a focus on decreased complexity such as ISBA (Noilhan and Platon, 1989) and SSIB (Xue et al., 1991). In all these models the effort was made to let the vegetation determine the way in which the land surface interacts with the atmosphere. These efforts can be summarized as follows:

(i) Vegetation changes the solar radiation absorbed by the land surface: Vegetation is highly absorbent in the visible wavelength interval (0.4-0.7 ìm), frequently referred to us as photosynthetically active radiation (PAR), and moderately reflective in the near-infrared region (0.7-4.0 ìm). In contrast, bare ground reflectivity generally increases with wavelength over the solar spectrum interval (0.0-4.0 ìm).

(ii*) Vegetation controls turbulent transfer (momentum, sensible heat and latent heat):* Vegetation canopy is usually a rough surface and enhances the transport of sensible and latent heat away from the surface, while a drag force may be significantly larger than that produced by bare ground.

(*iii) Vegetation controls the evapotranspiration and precipitation input in the soil:* Solar radiation energy absorbed by the plants is used to combine water and atmospheric carbon dioxide (CO_2) into sugars and organic compounds. This process is called photosynthesis. Plants allow the transfer of the CO_2 from the atmosphere to the cellular sites of photosynthesis located inside the leaves. This necessitates the maintenance of an open pathway between the atmosphere and the saturated tissues inside the leaf, which leads to an inevitable loss of water vapor over the same route. The plants regulate the amount of gas exchange, and hence water loss, by means of the valve-like structures on the leaf surface, called stomata. Under normal conditions, the stomata regulate gas exchange with the atmosphere in a way that maximises CO_2 influx and minimizes water loss. However, there are some additional effects that are induced as a leaf response to stress. For example, when the atmosphere becomes very dry, the stomata tend to close. A similar stomatal closure response appears when soil moisture decreases. Vegetation canopy can also intercept the precipitation, and this intercepted precipitation evaporates directly from the canopy. In this way the precipitation input to the soil is reduced.

(iv) Vegetation controls soil moisture availability: the depth and density of the vegetation root systems determines the amount of soil moisture available for evapotranspiration.

The biophysically based models are largely used to study the impact of land surface change on the regional and global climate. Lean and Warrilow (1989) showed that large scale Amazonian deforestation could lead to a decrease in regional evapotranspiration and precipitation, and an increase in surface temperature. Xue and Shukla (1991) investigated the influence of vegetation on precipitation patterns in the Sahelian Africa, and found that replacement of seasonal forest and grassland by desert led to a displacement of the seasonal rainfall patterns to the south.

The focus of this study is to review the main methods of modelling of water and energy fluxes at the soil-vegetation-atmosphere (S-V-A) interface, which are used in land surface schemes designed for climate models in the last few decades. The paper is structured as follows. The radiative transfer modelling at the S-V-A interface is presented in section 2. Section 3 describes the approaches used to describe turbulent transfer between the land surface and the atmosphere. Surface energy balance parameterizations and the governing equations for soil/vegetation/snow temperature are discussed in section 4, while the water balance parameterization methods are considered in section 5. Section 6 presents snow cover and its effects as parameterized in the land surface schemes. Finally, some results and aspects of validation and intercomparison between current land-surface models are discussed in section 7. The paper concludes in section 8.

A2. Radiative transfer between the land surface and the atmosphere

An adequate description of the radiative transfer at the S-V-A interface is an essential precursor to quantifying the net energy at the land surface available for transfer into other energy forms. Taking into account the radiative properties of the vegetation is important for an adequate calculation of the soil surface and canopy temperatures, which is in turn important for calculation of the surface fluxes. The net radiative

energy at the surface, R_n , is defined as the sum of the absorbed solar energy and the absorbed downward long-wave radiation emitted by the overlying atmosphere minus the long-wave radiation emitted by the surface:

$$R_n = R_s(1-\alpha\ ) + R_L - \varepsilon\sigma T_s^4 \qquad \text{(A2.1)}$$

where R_s is the solar radiation incident on the surface, R_L is the net downward longwave radiation absorbed by the surface, T_s is land surface (canopy-ground) temperature, α is the surface albedo (integrated reflectance of the surface over the solar spectrum, ε is the surface emissivity, and σ is Stefan-Boltzmann constant. The terms R_s and R_L represent forcing terms and are provided by the atmospheric model. On the other hand, the land surface scheme provides ε , α , and T_s .

In reality, the surface emissivity ε (both soil and vegetation) varies according to the surface type and is wavelength dependent; however, in practice it is assumed to be unity in almost all models. In contrast, there is a variety of approaches for the specification of surface albedo used in land surface modelling. Surface albedo of snow-free surface depends on the solar zenith angle, the spectral distribution of the incident solar radiation beam and whether that radiation is direct or diffuse, the soil type, the soil moisture, as well as on the type and density of the vegetation. Until the early 1980s, three basic approaches for surface albedo determination could be distinguished in land surface modelling (Carson, 1982): (i) single specified albedo value (usually $\alpha = 0.2$ or $\alpha = 0.14$ for all continental surfaces); (ii) latitudinal variation albedo based on Posey and Clapp (1964); (iii) specified geographical distribution of albedo for 12 natural surfaces (Holloway and Manabe, 1971). After Charney's (1975) work, which emphasized the importance of albedo variation on climate, much more attention has been paid to the calculation of albedo, especially with the introduction of vegetation within LSMs. Dickinson (1983) adapted the Meador and Weaver (1980) two-stream method used to describe solar ($0.0 - 4.0\ \mu$m) radiation fluxes in the atmosphere, in order to describe radiative transfer in vegetation

canopies. The two-stream approach forms the basis of solar radiative transfer packages in SiB and BATS and is briefly presented here.

In nature, the direct beam radiation intercepted by the leaves may be scattered (reflected and transmitted) into infinite number of radiances. A two-stream model considers only two integrated fluxes for the diffuse radiation, one upward and one downward. The original equations for the diffuse solar radiative fluxes as specified by Dickinson (1983) are:

$$-\bar{\mu}\frac{dI_{up}}{dL}+(1-(1-\beta)\omega)I_{up}-\omega\beta I_{down}=\omega\bar{\mu}K\beta_o e^{-KL} \qquad \text{(A2.2)}$$

$$-\bar{\mu}\frac{dI_{down}}{dL}+(1-(1-\beta)\omega)I_{down}-\omega\beta I_{up}=\omega\bar{\mu}K(1-\beta_o)e^{-KL} \qquad \text{(A2.3)}$$

where I_{up} and I_{down} are the upward and downward diffuse solar radiative fluxes, normalized by the incident beam, $K=G(\mu)/\mu$ is the optical depth of the direct beam per unit leaf area (μ is the cosine of the zenith angle of incident beam, $G(\mu)$ is the projected area of leaves in the direction μ), $\bar{\mu}$ is the average inverse diffuse optical depth per unit leaf area, β and β_o are the upscatter parameters for the diffuse and direct beams, ω is the scattering coefficient of leaves (reflectance plus transmission coefficient), and L is the leaf area index. These equations can be solved for the canopy-ground system using the incident solar radiative flux above the canopy and the upward diffuse flux reflected by the soil (upper and lower boundary conditions). In this way, the canopy reflectance, absorbance, and transmittance can be specified, and the solar radiation absorbed by the canopy and soil from each incident component supplied by the atmospheric model (four components in all: direct and diffuse beam of visible and near-infrared radiation) can be calculated. A weighted average of the resulting four reflectances provide an estimation of the albedo term as used in Eq. (A2.1). It should be noted that the parameters in Eqs. (A2.2) and (A2.3) depend on the leaf angle distribution function (canopy geometry) and incident beam

zenith angle (K, $G(\mu)$) as well as on the leaf optical properties (β and β_o). The parameter $\overline{\mu}$ is a function of canopy geometry only.

A3. Turbulent transfer between the land surface and the atmosphere

Because the wind velocity, temperature and humidity at the land surface are different from those in the layers of air above, there are exchanges of momentum, heat and water between them. The nature of this exchange is turbulent and its proper modeling is a complex process. The LSMs developed for use in climate models commonly use an eddy-diffusion approach to describe turbulent transfer between the land surface and the atmosphere. This approach is often called *K*-theory or first-order closure and is comprehensively described by Stull (1988) and Garratt (1992). More sophisticated treatments of turbulent transport are based on higher-order closure methods, which avoid the need to use eddy-diffusivity coefficients but are computationally expensive.

Considering that turbulent transfer is a process analogous to molecular diffusion, the vertical turbulent flux F_X of a conservative quantity X per unit area is written as:

$$F_X = -\rho(z) K_X(z) \frac{\partial X}{\partial z} \tag{A3.1}$$

where $\rho(z)$ is air density and $K_X(z)$ is the eddy-diffusion coefficient. Assuming that F_X is constant with height between $z = z_1$ and $z = z_2$, and integrating in vertical, Eq. (A3.1) becomes:

$$F_X = \frac{\rho_a}{r_a}\left[(X(z_2) - X(z_1)\right] \tag{A3.2}$$

where ρ_a is the average air density defined as :

$$(\rho_a)^{-1} = \frac{\int_{z_1}^{z_2} (\rho K_X)^{-1} dz}{\int_{z_1}^{z_2} K_X^{-1} dz} \tag{A3.3}$$

and the aerodynamic resistance for the transfer of quantity X between $z = z_1$ and $z = z_2$ can be defined as:

$$r_a = \int_{z_1}^{z_2} \frac{1}{K_X} dz \tag{A3.4}$$

Generally, $z_1 = 0$ is the ground and $z_2 = z_r$ is the lowest level in the atmospheric model (reference level).

The surface turbulent exchanges of momentum, heat and moisture are parameterized in such a way that they can be determined from values of wind, temperature and humidity at the lowest atmospheric level and from values of surface properties such as surface roughness, temperature and wetness. It is standard practice to express the mean vertical surface turbulent flux, F_X, of the quantity X (wind velocity, temperature or humidity) as:

$$F_X = \rho_a u_r C_X [X(z_r) - X(0)] \tag{A3.5}$$

where u_r is the wind speed at the reference level and C_X is the so-called bulk transfer coefficient. Numerous field and laboratory experiments show that C_X is different for each X. It is a complicated function of height, atmospheric stability, surface roughness and other physical and physiological characteristics of the surface vegetation. The relation between aerodynamic resistance and the bulk transfer coefficient can be obtained by comparing Eq. (A3.5) to Eq. (A3.2), which is written for $z_1 = 0$ (ground level) and $z_2 = z_r$ (reference level), and gives:

$$r_a = \frac{1}{u_r C_X} \tag{A3.6}.$$

A3.1. Momentum turbulent flux

The deceleration force exerted on the horizontal wind flow ($\mathbf{u}$) as it moves over a rough surface induces the transfer of momentum from the atmosphere to the surface. The bulk transfer coefficient (drag coefficient) for momentum transfer, C_D, can be parameterized in different ways. One of the approaches, widely used in many of the second-generation LSMs, is based on the Monin-Obukhov (MO) similarity theory (Monin and Obukhov, 1954). According to this theory, within the atmospheric surface layer (a layer of constant turbulent fluxes) under neutral atmospheric conditions one can write (see Eq. 3.1):

$$\frac{\partial F_M}{\partial z} = \frac{\partial}{\partial z}(\rho_a K_M \frac{\partial u}{\partial z}) = 0 \qquad \text{(A3.7)}$$

and hence,

$$\frac{\partial u}{\partial z} = \frac{const}{\rho_a K_M} \qquad \text{(A3.8).}$$

Here F_M is the vertical transfer of horizontal momentum (shear stress), K_M is the eddy-diffusion coefficient for momentum given as $K_M = lu_*$, where l is the mixing length scale ($l = kz$, $k = 0.41$ is the von Karman constant) and u_* is the so-called friction velocity. The constant in Eq. (A3.8) is the turbulent flux at the surface, i.e. $const = F_M(z=0) = \rho_a u_*^2$. Integration of Eq. (A3.8), from z_o (surface roughness length) to z, gives an expression for the logarithmic wind profile in the surface layer, i.e. $u(z) = \frac{u_*}{k}\ln\frac{z}{z_o}$. Since the atmospheric boundary layer can deviate from neutral stratification, Monin and Obukhov suggested a stability correction in the following form:

$$u(z) = \frac{u_*}{k}(\ln\frac{z}{z_o} - \psi(z/L)) \qquad \text{(A3.9)}$$

where L is MO length scale and $\Psi(\frac{z}{L})$ is an empirical function. The empirical nature of $\Psi(\frac{z}{L})$ has resulted in a great variety of possible formulations. Therefore, the bulk transfer coefficient for momentum transfer, C_D, can be parameterized as:

$$C_D = \frac{F_M(z=0)}{\rho_a(u(z))^2} = \frac{u_*^2}{(u(z))^2} = \left(\frac{k}{\ln(z/z_o) - \Psi(z/L)}\right)^2 \qquad \text{(A3.10).}$$

Another way to parameterize C_D is to define $\Phi^{-2} = (1 - \frac{\psi(z/L)}{\ln(z/z_o)})$, where Φ could be seen as a new empirical function. Louis (1979), Hack et al. (1993), Abdella and McFarlane (1996) and many others consider Φ as a function of the Richardson number R_i:

$$C_D(z) = \left(\frac{k}{\ln(z/z_o)}\right)^2 \Phi(R_i) = C_{D,n}\Phi(R_i) \qquad \text{(A3.11).}$$

Here $C_{D,n} = (k/\ln(z/z_o))^2$ describes transfer under neutral atmospheric conditions (neutral drag coefficient). Following Eq. (A3.5), the mean vertical transfer of horizontal momentum from the reference level to the surface can be expressed as:

$$F_M = \rho_a C_D u_r^2 \qquad \text{(A3.12).}$$

Under neutral atmospheric conditions it is therefore given as:

$$F_M = \rho_a\left(\frac{k\ u_r}{\ln(z_r/z_o)}\right)^2 \qquad \text{(A3.13).}$$

The roughness length, z_o, is different for bare soil and for vegetated surface and also depends on the vegetation type. Rough surfaces such as forests are more strongly coupled to the atmosphere via turbulent transfer than smooth surfaces such as bare-soil.

In BATS, roughness length for bare soil is taken to be $z_{o,b} = 0.01$ m, while the value for a vegetation canopy is specified for each vegetation type. In addition,

when a vegetation canopy is present, the logarithmic wind profile in the surface-layer is effectively shifted upward by a distance d, the so-called zero-plane displacement height, and thus the neutral drag coefficient over a canopy is:

$$C_{D,n} = k^2 / (\ln(z_r - d)/z_{o,c}))^2 \qquad \text{(A3.14)}$$

where $z_{o,c}$ is the roughness length for canopy. For a grid square, which is covered with several vegetation types, an effective (composite) canopy roughness length has to be determined. Assuming partial vegetation coverage, the neutral drag coefficient is calculated as:

$$C_{D,n} = A_v \left(\frac{k}{\ln((z_r - d)/z_{o,c})} \right)^2 + (1 - A_v) \left(\frac{k}{\ln((z_r)/z_{o,b})} \right)^2 \qquad \text{(A3.15)}$$

where A_v and $(1 - A_v)$ are the area fraction of the vegetation and the bare soil, respectively. The stability function, $\Phi(R_i)$, in BATS is defined following Hack et al. (1993).

In CLASS, the same formulation of the neutral drag coefficient is used, while the stability function is taken from Abdella and McFarlane (1996). The parameters z_o and d in CLASS are calculated from the canopy height Z, using the simple relations $z_o = 0.10Z$ and $d = 0.70Z$. In ISBA a similar formulation is used, while the stability function is taken from Louis (1979).

Sellers et al. (1986, 1996) developed more detailed formulations for momentum transfer where different turbulent regimes below a vegetation canopy, within the canopy and above the canopy are considered (see Fig. A1). Under neutral conditions, equations for the transfer of momentum below, above and within the canopy in SiB2 (Sellers et al. 1996) are given as:

(i) Below the canopy ($z < z_1$) it is assumed that a logarithmic wind profile is valid with the constant shear stress, given as:

$$F_{M_1} = \rho_a \left(\frac{k u_1}{\ln(z_1 / z_s)} \right)^2 \qquad \text{(A3.16)}$$

where $z_s = 0.05$ m is the ground roughness length and u_1 is the wind speed at z_1.

(ii) Above the canopy ($z > z_2$), two sub-layers are specified with different turbulent regimes:

(a) The upper sub-layer ($z_t < z < z_r$), where logarithmic wind profile is assumed to be valid with a constant shear stress, is described by the following equations:

$$z_t = z_2 + 11.785 z_o \tag{A3.17}$$

$$F_M = \rho_a K_M \frac{du}{dz} \tag{A3.18}$$

$$K_M = K_M^* = k u_*(z-d) = \frac{k^2 u(z-d)}{\ln \dfrac{z-d}{z_o}} \tag{A3.19}$$

where z_o is the roughness length, $K_M^* = k u_*(z-d)$ is the value of the eddy-diffusion coefficient for a logarithmic wind profile, d is zero-plane displacement height. The friction velocity is related to wind speed at the reference level as $u_* = ku / \ln(\frac{z_r - d}{z_o})$.

(b) The lower sub-layer ($z_2 < z < z_t$): Shear stress is assumed to be constant, but the eddy-diffusion coefficient K_M differs from K_M^* (it is assumed that K_M decreases linearly from its value at $z = z_2$ (higher than K_M^*) to K_M^* at $z = z_t$):

$$K_M = K_M^* \left[(1 + 0.449(\frac{z_t - z}{z_t - z_2}) \right] \tag{A3.20}.$$

Higher values of K_M in this sub-layer are introduced in order to take into account the intense local turbulence generated by roughness elements at the top of the canopy. To maintain constant shear stress throughout the same layer, the wind profile must differ from the logarithmic profile.

(iii) Within the canopy ($z_1 < z < z_2$), the momentum absorption is described by:

$$\frac{\partial F_M}{\partial z} = \rho_a \frac{C_l L_d}{p_s} u^2 \tag{A3.21}$$

where C_l is the leaf drag coefficient that can be specified empirically from field data (Monteith, 1973), p_s is the so-called shelter factor, and L_d is leaf area density given as:

$$L_d = a_i + b_i z \tag{A3.22}$$

where $i = 1$ or 2, depending on whether $z \lesseqgtr z_c$ (see Fig. A1). The constants a_i and b_i can be obtained from the total leaf area index ($L_T = \int_{z_1}^{z_2} L_d dz$, L_T is defined as the green leaf area per unit ground area, and is a time-varying vegetation-type-dependent parameter). The shelter factor p_s accounts for the observation that the drag coefficient of an ensemble of densely clustered phytoelements is less than the sum of their individual drag coefficients. Following observation of Thom (1971) it is given by:

$$p_s = 1 + L_d^{0.6} \tag{A3.23}.$$

The variation of K_M within the canopy air space is defined to be proportional to the local wind speed, u:

$$K_M = l\, u \tag{A3.24}$$

where l is the mixing length. The zero-plane displacement height is defined as the moment height for momentum absorption (Sellers et al., 1996) and is expressed as:

$$d = \frac{\int_{z_1}^{z_2} \frac{L_d C_l}{p_s} u^2 z dz}{\int_{z_1}^{z_2} \frac{L_d C_l}{p_s} u^2 dz + \frac{\tau_1}{\rho_a}} \tag{A3.25}.$$

Replacing Eq. (A3.22) in Eq. (A3.21), which is combined with (A3.18) and (A3.24) yields an expression for the wind profile within the canopy ($z_1 < z < z_2$):

$$\frac{d^2}{dz^2}(u^2) = (A_i + B_i z)u^2 \tag{A3.26}$$

where $A_i = 2a_i C_l / p_s l$ and $B_i = 2b_i C_l / p_s l$ ($i = 1$ or 2, depending on whether $z \lesseqgtr z_c$).

Manipulating Eqs. (A3.16) to (A3.26), with the specified boundary conditions at z_1, z_2 and z_r, allows the profiles of u and K_M (from the surface to the reference level) and the solution for z_o and d to be obtained. The parameters that must be specified are: z_1, z_2, z_c, L_T, C_l and z_s. The calculated profiles of u and K_M are then used to derive the aerodynamic resistances for heat (water) transfer, r_d, r_a and r_b (see Fig. A1), needed for calculation of sensible and latent heat fluxes. Note that the constants used in Eqs. (A3.17) and (A3.20), i.e. 11.785 and 0.449, are obtained by optimization of the calculated values of z_o and d, derived by this model, against values of z_o and d calculated by a second-order closure model (Sellers et al., 1996).

A3.2. Sensible heat fluxes

The net radiative flux at the surface is mainly partitioned between sensible and latent heat fluxes, which have profound effects on weather and climate. The sensible heat flux released from the land surface warms the overlying air, while the latent heat flux has a nonlocal impact on the atmosphere because water vapour is transported through the atmospheric circulation and warms the atmosphere where condensation occurs (sometimes very far away from its source region). The clouds formed during condensation have strong effects on the radiation budget. Thus, the turbulent transfer of heat and water vapor from the land surface (canopy and soil) to the air above should be very carefully modeled within a LSM. Fairly sophisticated models such as SiB (and SiB2) and BATS use comprehensive formulations for evaluating flux components from the soil beneath the canopy, from the canopy to the reference level as well as from open areas between the canopy elements. Some models such as ISBA and SSiB do not predict soil fluxes beneath the vegetation.

Transfer pathways for sensible heat as conceptualized in SiB2 are shown in Fig. A2 and are expressed as:

$$H_g = \frac{(T_s - T_{cas})\rho_a c_p}{r_d} \tag{A3.27}$$

$$H_c = \frac{(T_c - T_{cas})\rho_a c_p}{r_b} \tag{A3.28}$$

$$H_a = \frac{(T_{cas} - T_r)\rho_a c_p}{r_a} \tag{A3.29}$$

where c_p is the specific heat of air, H_g is the flux from the ground to the canopy air space, H_c is the flux from canopy to the canopy boundary layer, and H_a is the flux from the canopy air space to the reference level, T_s is the soil surface temperature (prognostic variable), T_{cas} is the canopy-air space temperature that is expressed in terms of the canopy temperature, T_c, (prognostic variable), the reference level temperature, T_r, and the soil surface temperature, T_s. The quantity r_d is the aerodynamic resistance for heat (vapour) transfer between the ground and canopy air space, r_b is the aerodynamic resistance between canopy surface and canopy air space (bulk canopy boundary layer resistance) and r_a is the aerodynamic resistance between the canopy air space and the reference height.

Given profiles of u and K_M under, within and above the canopy (the equation set for calculation of these profiles are shown in section 3.1), the aerodynamic resistances r_b, r_d and r_a (under neutral atmospheric conditions) are expressed by the following equations:

$$r_b = \left[\int_{z_1}^{z_2} \frac{L_d (u)^{1/2}}{90\sqrt{l_w}\, p_s} dz\right]^{-1} = \frac{C_1}{(u_2)^{1/2}} \tag{A3.30}$$

$$r_d = \int_{z_1}^{h_a} \frac{1}{K_M} dz = \frac{C_2}{u_2} \tag{A3.31}$$

$$r_a = \int_{h_a}^{z_r} \frac{1}{K_M} dz = \frac{C_3}{u_r} \tag{A3.32}$$

where L_d and p_s are the leaf area density and shelter factor, l_w is the leaf width, u_2 and u_r are the wind speed at the level z_2 and z_r, z_s (=0.01m) is the soil roughness length, h_a is the water vapour and sensible heat source height (see Fig 1), which is the center of action of r_b in the canopy (its formulation is similar to the Eq. (A3.25) for zero-plane displacement height d). Eq. (A3.30) for the bulk canopy boundary layer resistances is based on the experimentally determined equation for a resistance exerted by a single leaf for many species (Goudriaan, 1977), and the assumption that individual resistances act in parallel. The coefficients C_1, C_2 and C_3 (depending of the total leaf-area index and canopy type) in the last three equations are calculated for each vegetation type and for different values of leaf-area index.

The formulation of the sensible heat transfer pathway in BATS is similar to that in SiB2 but the aerodynamic resistance formulations differ. Thus, the bulk canopy boundary layer resistances is given by:

$$r_b = \frac{1}{L_{SAI}} r_{al} \tag{A3.33}$$

where L_{SAI} is the sum of the leaf area index and stem area index, and r_{al} is the aerodynamic resistance for a leaf, defined as:

$$r_{al} = \frac{(D_f)^{1/2}}{0.01 L_{SAI}} \frac{1}{(u_{cas})^{1/2}} \tag{A3.34}$$

Here D_f is the characteristic dimension of the canopy in the wind direction. The quantity u_{cas} is the wind speed within the canopy air space, calculated from the wind speed at the reference level, u_r, and from the momentum drag coefficient, C_D, as $u_{cas} = (C_D)^{1/2} u_r$. The aerodynamic resistance between the ground and canopy air space, r_d, and the aerodynamic resistance between the canopy air space and the reference height, r_a, are given as:

$$r_d = \frac{1}{C_{D,soil} u_{cas}} \tag{A3.35}$$

$$r_a = \frac{1}{C_D u_a} \tag{A3.36}$$

where $C_{D,soil} = 0.004$ is the drag coefficient of soil. The variable u_a is expressed in term of the wind speed within the canopy air space, u_{cas}, and the wind speed at the reference level, u_r:

$$u_a = (1 - A_V) u_{cas} + A_v (z_{o,c} u_{cas} + (1 - z_{o,c})) u_r \tag{A3.37}.$$

where $z_{o,c}$ is the canopy roughness length and A_v is area fraction of the vegetation.

In CLASS (Verseghy et al., 1993), sensible heat flux from the ground under the canopy is set to be zero under stable conditions, and under unstable conditions, the Deardorff (1972) equation for free convection is used:

$$H = 1.9 \times 10^{-3} \rho_a c_p (T_s - T_c)(T_s' - T_c')^{1/3} \tag{A3.38}$$

where T_c and T_s are the actual and T_c' and T_s' are the virtual temperatures of canopy and ground surface under the canopy. The heat flux from the canopy to the reference level is:

$$H = \rho_a c_p \frac{(T_c - T_r)}{r_a} \tag{A3.39}$$

with the aerodynamic resistance r_a calculated as:

$$r_a = \frac{1}{C_H u_r} \tag{A3.40}.$$

The bulk transfer coefficient for heat and water vapor C_H differs from drag coefficient C_D used to describe momentum transfer and is given by:

$$C_H = \left(\frac{k}{\ln((z_r - d)/z_{o,H})} \right) \left(\frac{k}{\ln((z_r - d)/z_o)} \right) \Phi \tag{A3.41}$$

where $z_{o,H}$ is the roughness length for heat, which is obtained from the momentum roughness length z_o, i.e. $z_{o,H} = z_o / 2$, for trees, $z_{o,H} = z_o / 7$ for crops, $z_{o,H} = z_o / 12$ for grass, and $z_{o,H} = z_o / 3$ for bare soil.

Equations (3.39) and (3.40) are also used in ISBA, though unlike CLASS, which has prognostic equations for the canopy as well as for the ground temperature, in ISBA there is only one energy balance equation for the whole surface soil/vegetation system, resulting in only one (composite) surface soil/vegetation temperature. As a result, heat and mass transfers between the surface and atmosphere in ISBA are related to this temperature.

A3.3. Latent heat fluxes

Formulation of latent heat flux involves some additional problems compared to the sensible heat flux formulation because it should include all processes that limit evapotranspiration. In addition, there are different sources of water vapour on the land surface, which behave in very different way.

A typical equation describing evapotranspiration from the land-surface in second-generation models is:

$$\lambda E = \frac{(e_*(T_s) - e_r)}{r_{aer} + r_s} \frac{\rho_a c_p}{\gamma} \qquad \text{(A3.42)}$$

where λE is latent heat flux (λ-latent heat of vaporization, E-evapotranspiration), $e_*(T_s)$ is the saturated water vapor pressure at the surface temperature, T_s, e_r is the water vapor pressure at the reference level, γ is the psychometric constant and r_{aer} is the aerodynamic resistance. The remaining term, r_s, is the surface resistance, representing resistance to water evaporating from bare soil and through stomata. This

equation differs fundamentally from the equation used in first-generation LSMs that is:

$$\lambda E = \beta \frac{(e_*(T_s) - e_r)}{r_{aer}} \frac{\rho_a c_p}{\gamma} \qquad \text{(A3.43)}$$

where the resistance, r_s, has been omitted and a function describing the moisture availability β has been added (Pitman, 2003). The β -function is formulated to vary from 1 (freely available soil moisture) to 0 (dry soil condition) and this simple parameterization attempts to describe the full complexity of the surface resistance term. Fig. A3 illustrates the transfer pathways for latent heat as conceptualized in first generation land-surface models and in SiB2, one of the more sophisticated LSMs. The resistance terms shown in Fig. A3b are: (i) the aerodynamic resistance for water vapour transfer between the ground and canopy air space, denoted as r_d; (ii) the aerodynamic resistance between the canopy air space and the reference height, r_a; (iii) the aerodynamic resistance between canopy surface and canopy air space, r_b; (iv) the resistance to transfer of water through pores in the soil surface, r_{soil}; and (v) the resistance to water evaporating through plant stomata, r_c.

Most of the current LSMs describe separately bare soil evaporation, canopy transpiration through stomata, evaporation from water and snow intercepted by the canopy, and evaporation from snow intercepted by the soil surface. Evaporation from lakes typically is not done in the land surface model developed for use in climate models. The correct calculation of lake evaporation requires inclusion of an extra temperature for the lake surface, i.e. a separate energy balance equation, as well as the accounting mixing within the lake.

A3.3.1. Bare soil evaporation

Evaporation from bare soil is governed by (i) the molecular diffusion from the water in the soil pores up to the surface-atmosphere interface and (ii) laminar and

turbulent exchange in the air above the soil (Mahfouf and Noilhan, 1991). The first process involves a soil resistance (r_{soil}) depending on the soil type and relative humidity of the air in the soil pores while the second one can be described using aerodynamic resistance concepts. An accurate description of bare soil evaporation requires the soil model to have several layers in the top 5 cm of the soil (Mahfouf and Noilhan, 1991). In the LSMs designed for use in climate models, the typical depth of the first soil layer is a few cm, which is too coarse resolution to define explicitly the molecular diffusion of the water vapour from the water trapped in the soil pores.

The bulk parameterization approaches (α -type, β -type) and demand-supply method are commonly used in LSMs to parameterize bare soil evaporation. In α -methods, evaporation is modeled as a bulk transfer of water vapour between the surface-atmosphere interface and a reference height. These methods are based on the soil water content in the top layer of soil. In β -methods, evaporation is a fraction (β) of the water vapour bulk transfer between air in the soil pores (close to the water in soil) and the reference height. The β -method requires specification of the relative humidity of the air in the soil pores. In demand-supply methods, evaporation proceeds at the potential rate except for a diffusion limited maximum evaporation.

In SiB2 (see Fig. A3b), where β -methodology is used, evaporation from the bare soil is described by:

$$\lambda E_g = \left(\frac{h e_*(T_s) - e_{cas}}{r_{soil} + r_d} \right) \frac{\rho_a c_p}{\gamma} \qquad \text{(A3.44)}$$

where e_{cas} is the water vapour pressure in canopy air space and h is the relative humidity of the air in the soil pores defined as:

$$h = \exp\left(\frac{\psi g}{R T_s}\right) \qquad \text{(A3.45)}$$

Here ψ is the soil water potential in the top layer of soil and R is the gas constant. The soil resistance, r_{soil}, is an empirical term that can be derived from surface flux observations. Verseghy (1991) also used this methodology and the same formulation

for h. In the ISBA model, where the α-formulation is used, the evaporation from bare ground is defined as:

$$E_g = \rho_a C_H u_r (h_u q_*(T_s) - q_r) \tag{A3.46}$$

where C_H is the heat (water vapour) bulk transfer coefficient, $q_*(T_s)$ is the saturated specific humidity at T_s (surface temperature) and q_r is the specific humidity at the reference height. The quantity h_u is the relative humidity at the soil-atmosphere interface, which is a function of the moisture content, w_s, in the top layer of soil, given as:

$$h_u = \begin{cases} \frac{1}{2}\left[1 - \cos(\frac{w_s}{w_{fc}}\pi)\right], & w_s < w_{fc} \\ 1, & w_s \geq w_{fc} \end{cases} \tag{A3.47}$$

where w_{fc} is the volumetric soil water content at the field capacity. In BATS, the demand-supply approach is used. The actual evaporation is the lesser of the potential evaporation (atmospheric demand) and the maximum rate at which water can diffuse upward to a dry surface (soil supply):

$$E = \min(E_p, E_o) \tag{A3.48}$$

where $E_p = \rho_a C_D u_r (q_*(T_s) - q_r)$ is the potential evaporation and E_o is the diffusion-limited maximum evaporation. E_o is determined from the results of the multi-layer soil model integration, dimensional analysis and physical reasoning (Dickinson, 1984; Dickinson et al., 1993) and is given by:

$$E_o = E_{\max} s_s \bar{s} \tag{A3.49}.$$

Here $E_{\max}$ is the function of the saturation soil water potential, saturation hydraulic conductivity and soil porosity and s_s is the ratio of the surface soil layer water content to its maximum amount. The quantity $\bar{s}$ is expressed as $\bar{s} = s_s^{b-b_f-1} s_r^{3+b}$, where s_r is the ratio of the root zone soil layer water content to its maximum amount, b is a nondimensional parameter depending on soil texture (taken from Clapp and

Hornberger, 1978) and b_f is a function of the saturated hydraulic conductivity and parameter b.

A3.3.2. Wet canopy evaporation and dry canopy transpiration

The wet part of the canopy, covered by a thin film of water, evaporates at the potential rate shortly after a precipitation event or deposition of dew (Deardorff, 1978). In order to establish how long evaporation from the canopy can continue at the potential rate, a predictive equation for the intercepted water is required. In addition, the wet fraction of the canopy must be also specified.

The wet canopy evaporation in SiB2 is described as:

$$\lambda E_{ci} = f_{cw} \frac{(e_*(T_c) - e_{cas})}{2r_b} \frac{\rho_a c_p}{\gamma} \qquad \text{(A3.50).}$$

Here r_b is the aerodynamic resistance between canopy surface and canopy air space, f_{cw} is the canopy wet fraction, defined as $f_{cw} = (M_{cw} + M_{cs})/S_c$, where $(M_{cw} + M_{cs})$ is amount of water and snow intercepted on the canopy, and S_c is the maximum amount of water and snow the canopy can hold. The quantity S_c is a function of a number of factors (precipitation intensity, wind speed, etc.) but it is usually expressed as a function of the total leaf area index only (in SiB2, $S_c = 0.1L_T$). In Eq. (A3.50), the resistance, r_b, is doubled because it is assumed that water vapour exchange occurs from only one side of the leaf. BATS and CLASS use the same equation for canopy wet fraction, f_{cw} (except $S_c = 0.2L_T$ in CLASS), while ISBA use the Deardorff (1978) formulation ($f_{cw} = \left((M_{cw} + M_{cs})/S_c\right)^{2/3}$.

When the moisture stored on the canopy has been evaporated, transpiration of water from vegetation through stomata takes place. Transpiration is a complex process controlled by leaf photosynthesis and its modelling is very difficult. The rate of water extraction from the soil is parameterized in such a way that it can be

determined from the fractional volume of roots and the soil moisture potential (content) in the rooting zone of the soil. Usually, the fractional root volume is parameterized as an exponential function of soil depth below a given threshold, which coefficients depend on the canopy type. For the resistance of canopy leaves to transpiration, the assumption that leaf resistances act in parallel is usually made and the resistance of the whole canopy is expressed as:

$$\frac{1}{r_c} = \frac{L_T}{r_{st}} \tag{A3.51}$$

where r_{st} is the resistance of a single leaf and L_T is the leaf area index. The last equation is commonly called a "big leaf" model, since it represents the whole canopy as a single big leaf of resistance r_c (bulk stomatal resistance).

The variation in r_{st} can be caused by a variety of environmental factors that may act upon the canopy to produce stress. As a response to the stress, the stomata tend to close in order to prevent excessive transpiration, thus leading to an increase in r_{st}. The second-generation LSMs commonly use the Jarvis (1976) empirical model as a basis for bulk stomatal resistance formulation. The general form of the model of Jarvis (1976) is:

$$r_{st} = r_{st}^{*} F_1 F_2 F_3 F_4 F_5 \tag{A3.52}$$

where r_{st}^{*} is an unstressed (minima) resistance. The functions F_1, F_2, F_3, F_4 and F_5 describe the r_{st} dependence on the radiation, soil moisture, vapour pressure deficit, temperature and CO_2 concentration, respectively. Details of the functional forms of each of F_1 to F_5 can be found in Dickinson et al. (1986), Sellers et al. (1986) Noilhan and Platon (1989), and Verseghy et al. (1993). In summary little agreement exists concerning the functional forms of each of F_1 to F_5. Moreover, a large number of parameters are required for estimation of these functions, all of which are highly empirical and defined from a very sparse collection of measurements.

In the late 1990s, the semi-empirical photosynthesis-conductance (resistance) models, developed by plant physiologists (see Collatz et al., 1992), have been introduced in some LSMs (e.g., Sellers et al., 1996 and Dickinson et al., 1998). Leaf conductance (inverse of resistance) in these models is given as:

$$g_{st} = \frac{1}{r_{st}} = m\frac{A_n h_s}{c_s} + b \qquad \text{(A3.53)}$$

where A_n is the leaf assimilation rate, c_s is the partial pressure of CO_2 at the leaf surface, h_s is the relative humidity at the leaf surface and m is an empirical coefficient and b is the minimum stomatal conductance. Sellers et al. (1992) derived methods to scale up these leaf-level models in order to describe vegetation canopy processes at regional scale using satellite data. In this way, so-called third generation LSMs were born. As discussed in IPCC (2001), biology and atmospheric physics in these models are combined in an economical way requiring fewer parameters than their empirical predecessors.

A4. Surface energy balance and soil and/or canopy temperature

Calculation of the latent and sensible heat fluxes at the S-V-A interfaces requires, among others, knowledge of the surface soil and canopy temperature. Determination of this is based on the surface energy balance equations applied to the upper thin soil layer and to the canopy layer, or to the composite surface soil-vegetation layer. In the first case, two temperatures are determined: the surface soil layer temperature and canopy temperature. In the second case, only one surface temperature is obtained and is representative of the whole surface soil-vegetation system.

Many LSMs use a so-called force-restore method (Deardorff, 1978) to formulate the prognostic equation for the surface soil temperature. In the following paragraphs, some basic ideas of this method are presented.

Neglecting the horizontal heat transfer in soil, the conservation equation for a homogeneous soil in the absence of phase change of the soil water is given by:

$$\frac{\partial T_g(z,t)}{\partial t} = -\frac{1}{C_g}\frac{\partial}{\partial z}F(z,t) \qquad \text{(A4.1)}$$

where C_g is the volumetric heat capacity of the soil and $F(z,t)$ is the vertical heat flux in soil.

Assuming that the soil surface is heated in a simple periodic way we can write:

$$T_g(0,t) = \overline{T_g} + a_o \sin\omega t \qquad \text{(A4.2).}$$

Here $\overline{T_g}$ is the mean soil temperature and $a_o = a(z=0)$ is the amplitude of the temperature oscillation at the surface with angular frequency $\omega = 2\pi/\tau$ (τ is the oscillation period). Defining now the vertical heat flux in soil as:

$$F(z,t) = -\chi_g \frac{\partial T_g(z,t)}{\partial z} \qquad \text{(A4.3)}$$

where χ_g is the thermal conductivity of the soil and using Eq. (A4.1), the soil heat diffusion equation can be obtained as:

$$\frac{\partial T_g(z,t)}{\partial t} = k\frac{\partial^2 T_g(z,t)}{\partial z^2} \qquad \text{(A4.4)}$$

where $k = \chi_g / C_g$ is the thermal diffusivity of the soil. Assuming that the amplitude of the temperature oscillation tends to zero when $z \to \infty$ and using Eq. (A4.2), the solution of the soil heat diffusion equation is:

$$T_g(z,t) = a_o \exp\left(-z/d\sqrt{2}\right)\sin\left(\omega t - z/d\sqrt{2}\right), \qquad \text{(A4.5)}$$

where $d = \sqrt{\chi_g \tau / 2\pi C_g}$. As can be seen from Eq. (A4.5), the amplitude of the temperature oscillation is reduced by a factor of e^{-1} of its surface value at a depth of

$d\sqrt{2}$ (e-folding depth of the temperature wave). Bhumralkar (1975) proposed the temperature of the thin surface soil layer, with a depth $\delta << d$, be computed and used as the soil surface temperature (i.e. $T_g(\delta,t) \approx T_g(0,t) = T_s$). Integrating Eq. (A4.1) from the ground $z = 0$ to a depth δ and assuming C_g is constant gives the prognostic equation for $T_g(\delta,t)$:

$$C_g \delta \frac{\partial T_g(\delta,t)}{\partial t} = F(0,t) - F(\delta,t) \qquad \text{(A4.6)}.$$

Here $F(0,t) = G_o = R_n - H - \lambda E$ is the energy flux at the surface and $F(\delta,t)$ is the vertical soil heat flux at depth δ that can be derived from Eqs. (A4.3) and (A4.5). In this way, the following equation is obtained:

$$C_g\left(\delta + \sqrt{\frac{\chi_g}{2\omega C_g}}\right)\frac{\partial T_g(\delta,t)}{\partial t} = \underbrace{R_n - H - \lambda E}_{G_o} - \sqrt{\frac{\omega C_g \chi_g}{2}}\left(T_g(\delta,t) - \overline{T}_g\right) \qquad \text{(A4.7)}.$$

The above equation is used by Bhumralkar (1975) to compute the surface soil layer temperature. Using the condition $\delta << d$, we can neglect δ and Eq. (A4.7) becomes:

$$\frac{\partial T_s}{\partial t} = 2\sqrt{\frac{\pi}{\chi_g \tau C_g}} G_o - \frac{2\pi}{\tau}(T_s - \overline{T}_g) \qquad \text{(A4.8)}$$

that is Deardorff's (1978) force-restore equation. The first term on the right-hand side represents the diurnal forcing of T_s by the surface heat flux G_o, and the second term tends to restore T_s to the mean soil temperature $\overline{T}_g$. Therefore, the force-restore method requires additional information about the restore temperature $\overline{T}_g$ and its formulation differs between LSMs. Usually, $\overline{T}_g$ is obtained from a second prognostic equation for temperature related to the deeper subsurface soil layer. The coefficient $2\sqrt{\frac{\pi}{\chi_g \tau\ C_g}} = C_G$ in Eq. (A4.8) describes the thermal properties of the soil and depends on the soil texture and the soil moisture.

In ISBA (version implemented within the Météo-France Climate Model ARPEGE, Mahfouf et al., 1995) the following force-restore equations are used:

$$\frac{\partial T_s}{\partial t} = C_T(R_n - H - \lambda E) - \frac{2\pi}{\tau_1}(T_s - \overline{T}_g) \qquad \text{(A4.9)}$$

$$\frac{\partial \overline{T}_g}{\partial t} = \frac{1}{\tau_1}(T_s - \overline{T}_g) - \frac{2\pi}{\tau_2}(\overline{T}_g - T_{c\lim}) \qquad \text{(A4.10)}$$

where T_s corresponds to the composite surface soil-vegetation layer, C_T is a combined thermal coefficient for soil and vegetation, $\tau_1 = 1$ day, $\tau_2 = 20$ day, $T_{c\lim}$ is the climatological deep soil temperature (updated with the time constant $\tau_2 = 20$ day), toward which the mean temperature $\overline{T}_g$ is restored. The coefficient C_T is given by:

$$C_T = \left(\frac{1 - A_v}{C_G} + \frac{A_v}{C_v}\right)^{-1} \qquad \text{(A4.11)}$$

where, A_v is the vegetation fraction, $C_v (= 10^{-3}\ \mathrm{Km^2J^{-1}})$ is the thermal coefficient for vegetation and $C_G = 2\sqrt{\frac{\pi}{\chi_g \tau C_g}}$ (note that for bare ground conditions $C_T = C_G$, and Eq. (A4.9) becomes the same as Eq. (A4.8). The dependence of the soil thermal coefficient, C_G, on soil texture and water content is given as:

$$C_G = C_{Gsat}\left(\frac{w_{sat}}{w_2}\right)^{b/2\log 10} \qquad \text{(A4.12)}$$

where coefficient b depend on soil texture, w_2 is the total soil volumetric water content, w_{sat} is its value at saturation (maximum amount of water that a given soil can hold). The variables w_{sat}, C_{Gsat} and the coefficient b, which are different for each soil texture are taken from Clapp and Hornberger (1978).

In the recent force-restore version of ISBA (Bonne et al., 2000), where the contribution of water phase change is included, the prognostic equations for soil temperature are:

$$\frac{\partial T_s}{\partial t} = C_T^*\left[(R_n - H - \lambda E - \lambda_f(S_m - \phi_{wi\_s})\right] - \frac{2\pi}{\tau_1}(T_s - \overline{T}_g) \qquad \text{(A4.13)}$$

$$\frac{\partial \overline{T}_g}{\partial t} = \frac{1}{\tau_1}(T_s - \overline{T}_g) + C_G^* \lambda_f \phi_{wi\_2} \qquad \text{(A4.14).}$$

Here C_T^* and C_G^* are corresponding thermal coefficients. The quantity $\lambda_f(S_m - \phi_{wi\_s})$ is phase change term (λ_f is latent heat of melting (freezing), S_m is snowmelt rate, ϕ_{wi_s} is the rate of surface soil ice freezing or melting, and ϕ_{wi_2} is the rate of soil ice freezing or melting in the total soil layer. The temperature T_s in the Eq. (A4.13) corresponds to the composite surface soil-vegetation-snow temperature and the thermal coefficient, C_T^*, includes also the thermal effect of soil ice and snow:

$$C_T^* = \frac{1}{\frac{(1-A_v)(1-A_{snow})}{C_G^*} + \frac{(1-A_v)A_{snow}}{C_{snow}} + \frac{A_v}{C_v}} \qquad \text{(A4.15)}$$

where A_{snow} is the snow fraction. C_G^* in Eqs. (A4.14) and (A4.15) is the composite thermal coefficient for soil and is given as:

$$C_G^* = (1 - w_{i,2})\min(C_{Gwilt}, C_{Gsat}(\frac{w_{sat,2}}{w_2})^{b/2\ln 10}) + w_{i,2}C_I \qquad \text{(A4.16)}$$

where $w_{i,2}$ is total ice volumetric content, $C_I = 2(\pi / \chi_{ice}\rho_{ice}c_{ice}\tau_1)^{1/2}$ is the thermal coefficient for ice in the soil, (c_{ice}-ice specific heat, χ_{ice}-ice thermal conductivity, ρ_{ice}-ice density) and C_{Gsat} and C_{Gwilt} are the thermal soil coefficients at saturation and wilting point water content (amount of soil water below which it is assumed that plants are unable to pump water from the root zone to stomatal cells), respectively. The asterisk superscript in the above equations is introduced to denote the coefficients and terms that have been modified relative to the model presented by Noilhan and Platon (1989) to allow the inclusion of soil ice.

The prognostic equations for soil temperature in BATS and SiB are also based on the force-restore method. Dickinson (1988) generalized the force-restore treatment for heterogeneous soil layer (when snow and soil co-exist) and this is included in

BATS (Dickinson, 1993). The prognostic equations for surface and subsurface soil layer temperature (that is identified with the annual temperature wave) in BATS are:

$$(1+F_{CT1})\frac{\partial T_s}{\partial t} = C_T^{'}(R_n - H - \lambda E - \lambda_f S_m) - \frac{2\pi}{\tau_1}(T_s - \overline{T}_g) \qquad (4.17)$$

$$(1+F_{CT2})\frac{\partial \overline{T}_g}{\partial t} = \frac{2\pi}{\tau_a}(\frac{d_a}{d_d} + c_3 T_3) - \frac{2\pi}{\tau_a}\overline{T}_g(\frac{d_a}{d_d} + c_3) \qquad (4.18)$$

where $\tau_a = 365\,\text{days}$, d_a and d_d are e-folding depths of the annual and diurnal temperature wave that are weighted averages according to the snow depth. The thermal coefficient of the composite surface soil-snow layer, $C_T^{'}$, is given as:

$$C_T^{'} = (1-f_{snow})\underbrace{2(\frac{\pi}{\tau_1 \chi_g C_g})^{1/2}}_{C_G} + f_{snow}\underbrace{2(\frac{\pi}{\tau_1 \chi_{snow} C_{snow}})^{1/2}}_{C_{snow}} \qquad (4.19)$$

where f_{snow} is a function of the fraction snow cover. The coefficient F_{CT1} and F_{CT2} parameterize the contribution of the latent heat of freezing from the surface and subsurface soil layers:

$$F_{CT1} = \frac{\sqrt{2}\lambda_f (W_s - F_{rs})}{\rho_{ice} c_{ice} \Delta T Z_s} \qquad (4.20)$$

where W_s is the surface soil water (in meters) and F_{rs} is the fraction of upper layer soil water that does not freeze, Z_s is the depth of upper soil layer (10 cm) and $\Delta T = 4\,K$ (it is assumed that water freezes uniformly between 0 C and -4 C). The coefficient F_{CT2} for the subsurface soil layer is parameterized in the same manner.

In many LSMs, the soil temperature is solved by discretization of the heat diffusion equation, for example CLASS (Verseghy, 1991), the ECMWF LSM (Viterbo and Beljaars, 1995), LEAF (Avissar and Pielke, 1989) and VIC (Liang et al., 1994). The soil in these models are discretized by three or more layers. For example, the prognostic equation for the surface soil temperature in the case of three soil layers is:

$$C_{g1}\frac{\partial T_s}{\partial t} = \frac{G_o - G_1}{d_o} \tag{A4.21}$$

where C_{g1} is the volumetric heat capacity of the surface soil layer, d_o is its depth, and G_o is the heat flux into the surface soil layer. The quantity G_1 is the heat flux into the second layer, which has a depth of d_1 and mean temperature T_1:

$$G_1 = -\chi_{g1}\frac{T_s - T_1}{0.5(d_o + d_1)} \tag{A4.22}$$

The temperature of the second layer, T_1, is governed by a prognostic equation similar to (4.21), with the heat flux G_2, evaluated from the temperature of the second and third layer.

The temperature of the vegetation canopy in these models is calculated from a separate energy balance equation. This means that sensible and latent heat fluxes as well as the radiative flux at the canopy surface are calculated also. For example, in CLASS, the canopy temperature is calculated by an iterative solution of the canopy energy balance equation:

$$c_c\frac{\partial T_c}{\partial t} = R_{n,c} - H_c - \lambda E_c + S_c \tag{A4.23}$$

where $R_{n,c}$ is the net radiation at the canopy surface, H_c and λE_c are the canopy sensible and latent heat fluxes, S_c is the energy transfer due to water phase changes on the canopy and c_c is the effective heat capacity of the canopy (a weighted average of the vegetation heat capacity and the heat capacity of the water and snow stored on the canopy).

A5. Surface water balance

A5.1. Prognostic equations for soil moisture

Water and energy fluxes at the land surface are closely linked to the amount of available soil moisture. First-generation LSMs tended to include a single layer for simulation of soil moisture. Following Manabe (1969), the prognostic equation for soil moisture in these models is:

$$\frac{\partial W}{\partial t} = P + S_m - E - R \qquad \text{(A5.1)}$$

where W is the soil moisture content (in mm) of the single soil layer, P is precipitation rate, E is the evaporation, S_m is the snowmelt rate, and R is the runoff rate. Soil moisture holding capacity, W_{sat}, was prescribed and any excess of W over W_{sat} is taken to be the runoff. In second generation LSMs, the calculation of soil moisture is usually performed by soil discretization into two or more layers. Deardorff (1978) extended the force-restore method developed for soil temperature calculation to soil moisture. He proposed two prognostic equations, one for surface soil moisture and the other for bulk soil moisture:

$$\frac{\partial w_s}{\partial t} = \frac{C_1}{\rho_w d_1}\left[(1 - A_v)P + S_m - E_b - R_s)\right] - C_2 \frac{w_s - w_2}{\tau_1} \qquad \text{(A5.2)}$$

$$\frac{\partial w_2}{\partial t} = \frac{1}{\rho_w d_2}\left[(1 - A_v)P + S_m - E_b - E_{tr} - R_2\right] \qquad \text{(A5.3).}$$

Here C_1 and C_2 are dimensionless force-restore coefficients, A_v is the area fraction of the vegetation, w_s is the volumetric water content (m^3m^{-3}) in the surface layer, w_2 is the bulk volumetric water content of the soil, d_1 is the superficial soil layer depth (the depth to which the diurnal moisture cycle extends), d_2 is the total soil depth that includes the vegetation root zone, E_b is bare soil evaporation rate, E_{tr} is

the transpiration rate from root zone layer, R_s is the surface runoff and R_2 is the total soil runoff. Runoff occurs when w_s or w_2 exceeds the saturation value. Deardorff parameterized the force-restore coefficients empirically using Jackson (1973) data that are strictly applicable to only one kind of soil.

Many second-generation LSMs use the force-restore method to describe the soil moisture regime (e.g., ISBA, PLACE (Wetzel and Chang, 1988) and CSIRO (Kowalczyk et al., 1991)). However, the formulation of the force-restore coefficients varies between the models. In ISBA, for example, the parameterization of these coefficients is based on the integrations of a more detailed one-dimensional (1D) model. Soil temperature and water profiles in this 1D model are solved by discretization of the diffusion equation for heat transfer and Richards (1931) equation for movement of water in the unsaturated soil in 26 layers.

In order to improve the soil moisture calculation in ISBA, some other modifications of the Deardorff (1978) soil moisture equation were made: Noilhan and Platon (1989) replaced the restore water content (mean volumetric water content), w_2, in Eq. (A5.2) by w_{seq} that is an equilibrium value of surface moisture attained when gravity balances the capillarity forces (i.e., $\partial\psi / \partial z = 1$, where ψ is soil water potential). Mahfouf et al. (1995) modified the prognostic equation for the mean volumetric water content, w_2, in order to include deep drainage by gravity at the lower soil boundary that was neglected in Noilhan and Platon (1989):

$$\frac{\partial w_2}{\partial t} = \left(\frac{1}{\rho_w d_2}\right)(P_g - E_b - E_{tr} - R_2) - \frac{C_3}{\tau_1}\max(0,(w_2 - w_{fc})) \qquad \text{(A5.4)}$$

where P_g is the flux of liquid water reaching the soil surface, the coefficient C_3 characterized the velocity at which the water profile is restored to the field capacity, w_{fc} (it is assumed that w_{fc} corresponds to the hydraulic conductivity of 0.1 mm/day).

In recent version of ISBA (Boone et al., 2000) where the soil ice is included, the prognostic equations for liquid (w_s and w_2) and frozen (w_{sf} and w_{2f}) moisture content are given as:

$$\frac{\partial w_s}{\partial t} = \frac{C_1^*}{d_1 \rho_w}\left[(1-A_v)P - E_b + R_r + S_m\right] - \frac{1}{d_1 \rho_w}\left(\phi_{wi\_s} + R_s^*\right) - \frac{C_2^*}{\tau_1}(w_s - w_{seq}^*) \quad \text{(A5.5)}$$

$$\frac{\partial w_2}{\partial t} = \frac{1}{d_2 \rho_w}\left[(1-A_v)P - E_b - E_{tr} + R_r + S_m - \phi_{wi\_2} - R_2^*\right] - \frac{C_3}{\tau_1}\max(0, w_2 - w_{fc}^*) \quad \text{(A5.6)}$$

$$\frac{\partial w_{sf}}{\partial t} = \frac{1}{d_1 \rho_w}(\phi_{wi\_s} - E_{bi}) \quad \text{(A5.7)}$$

$$\frac{\partial w_{2f}}{\partial t} = \frac{1}{(d_2 - d_1)\rho_w}\phi_{wi\_2} \quad \text{(A5.8)}$$

where R_r is a canopy drip rate, E_{bi} is the bare soil sublimation, R_s^* and R_2^* are the surface soil runoff and total soil runoff, respectively, occurring when w_s or w_2 exceeds the saturation value, ϕ_{wi_s} is the rate of surface soil ice freezing or melting, and ϕ_{wi_2} is the rate of soil ice freezing or melting in the total soil layer.

Many LSMs such as SiB, BATS, CLASS, SSiB, MOSAIC (Koster and Suarez, 1992) and BASE (Desborough and Pitman, 1998) use three or more soil layers to compute the soil water content profile. The vertical transfer of water between soil layers in these models is usually based on Darcy's law (Darcy and Bazin, 1865), which describes the hydraulic diffusion and gravitational drainage of water in the soil and is given as:

$$Q = k\left(\frac{\partial \psi}{\partial z} + 1\right) \quad \text{(A5.9)}$$

where hydraulic conductivity, k, and soil water potential, ψ, both depend on soil moisture. The expressions provided by Clapp and Hornberger (1978), which describe these dependences are commonly used in LSMs, largely due to their simplicity:

$$\psi = \psi_{sat}(\frac{w}{w_{sat}})^{-b} \tag{A5.10}$$

$$k = k_{sat}(\frac{w}{w_{sat}})^{2b+3} \tag{A5.11}$$

where saturated hydraulic conductivity, k_{sat}, saturated soil water potential, ψ_{sat}, and coefficient b depend on soil type. The tabulated values of b, ψ_{sat}, k_{sat} and w_{sat} for the 11 soil classes of the U.S. Department of Agriculture (USDA) soil classification are provided by Clapp and Hornberger (1978) and Cosby et al. (1984), and are based on measurements over a large number of samples.

The governing equations for soil moisture in SiB are:

$$\frac{\partial w_1}{\partial t} = \frac{1}{d_1}(I - Q_{1,2} - \frac{1}{\rho_w}E_b) \tag{A5.12}$$

$$\frac{\partial w_2}{\partial t} = \frac{1}{d_2}(Q_{1,2} - Q_{2,3} - \frac{1}{\rho_w}E_{tr}) \tag{A5.13}$$

$$\frac{\partial w_3}{\partial t} = \frac{1}{d_3}(Q_{2,3} - Q_3) \tag{A5.14}$$

where w_i is the volumetric water content in the layer i, I is the infiltration of precipitation into the upper soil moisture reservoir, $Q_{i,i+1}$ is water flux between the layers i and $i+1$ and Q_3 is the gravitational drainage out of the bottom of the soil column (subsurface runoff). Infiltration is defined as a difference between the water reaching the soil surface (canopy can store a fraction of the precipitation) and surface runoff. The surface runoff is parameterized as the saturation excess of the surface soil layer, taking into account spatial variability of convective precipitation. It is assumed that convective rainfall is spatially distributed according to a simple exponential function, with a coefficient that can be adjusted to represent large-scale (spatially uniform) precipitation. Subsurface runoff is parameterized as:

$$Q_3 = f(\overline{T}_g)\left(\sin\varphi k_{sat}\left(\frac{w_3}{w_{sat}}\right)^{2b+3} + 0.001\frac{w_3 d_3}{\tau_1}\right) \qquad \text{(A5.15)}$$

where the factor $f(\overline{T}_g)$ is the function of the deep soil temperature, allowing for a progressive reduction in soil hydraulic conductivity as the soil freezes, and φ is the local slope angle. The subsurface runoff (base flow) together with the surface runoff creates the total runoff.

CLASS also uses Darcy's equations to evaluate fluxes between the layers. Water infiltration into the upper soil layer in CLASS is treated as a downward propagating square wave (Mein and Larson, 1973). When the infiltration capacity is exceeded, water is allowed to pond on the surface up to a maximum surface retention capacity, which varies according to the land cover. The overflow of the surface retention capacity is assumed to be surface runoff. The subsurface runoff refers to the drainage of water out of the soil column and is parameterized as:

$$Q_3 = k_{sat}\left(\frac{w_3}{w_{sat}}\right)^{2b+3} \qquad \text{(A5.16)}$$

In BATS, the prognostic equations for soil moisture are:

$$\frac{\partial W_s}{\partial t} = P(1-A_v) - R_s + \Gamma_{w1} - G_{w1} - \beta E_{tr} - E + D_o + S_m \qquad \text{(A5.17)}$$

$$\frac{\partial W_r}{\partial t} = P(1-A_v) - R_s + \Gamma_{w2} - G_{w2} - E_{tr} - E + D_o + S_m \qquad \text{(A5.18)}$$

$$\frac{\partial W_t}{\partial t} = P(1-A_v) - R_s - R_{base} - E_{tr} - E + D_o + S_m \qquad \text{(A5.19)}$$

where W_s is the amount of surface soil water (in meters), W_r is the water amount in the rooting zone of the soil, and W_t is the total water amount in the soil. Further, R_s is the surface runoff, R_{base} is drainage out of the modeled soil, $\Gamma_{w1(2)}$ is the capillary movement of water between the soil layers, $G_{w1(2)}$ is the gravitational drainage between the soil layers, D_o is rate of water dripping from canopy, S_m is the rate of

snow melt and β is the fraction of transpiration from the top soil layer. The surface runoff is defined as:

$$R_s = \gamma \max(0, P(1 - A_v) + D_o - E) \qquad \text{(A5.20).}$$

Here $\gamma = \min\left(1, \left(\frac{s_s + s_r}{2}\right)^m\right)$, where $m = \begin{cases} 1, T_g < 273.16K \\ 4, T_g \geq 273.16K \end{cases}$. The quantity s_s is the ratio of the soil water in the surface soil layer to its maximum amount, and s_r is the ratio of the soil water in the root zone layer to its maximum amount. Internal soil water fluxes in BATS are governed by the capillary movement of the water and gravitational drainage and are parameterized based on the multilayer soil model integrations. The gravitational drainage of soil water from the soil lower boundary to underlying ground water (base flow) is given as:

$$R_{base} = K_D s_t^{2b+3} \qquad \text{(A5.21)}$$

where K_D is an adjustable constant (4×10^{-4} mm/s, by default) The total runoff is defined as:

$$R_{tot} = R_s + R_{base} + R_{excess} \qquad \text{(A5.22).}$$

Here, R_{excess} is the saturation excess from the total soil layer.

A5.2. Prognostic equations for canopy intercepted water

Precipitation arriving at the vegetation canopy is either intercepted by the foliage or falls though gaps in the canopy to the ground. As a result the precipitation input in the soil is reduced. Therefore, the effects of canopy interception should be included in LSMs. This is done by carrying an equation for amount of the water residing on the foliage:

$$\frac{\partial M_{ci}}{\partial t} = A_v P - E_{ci} - D_o \qquad \text{(A5.23)}$$

where M_{ci} is the amount of water (snow) intercepted on the canopy, E_{ci} is wet canopy evaporation (discussed in section 3.3.2) and D_o is the canopy drip rate. In some LSMs (e.g., SiB), allowance is made for precipitation attenuation through the canopy, i.e. an attenuation factor is included in the first term on the right of Eq. (A5.23). The maximum water amount that can be stored on the canopy is expressed as a function of the total leaf area index (see section 3.3.2). Effects of the spatial variability of the rainfall over the grid area on the canopy interception is taken into account in some models by describing the local precipitation rate (over a fraction of grid area) by a given probability distribution function to reduce interception.

A6. Snow cover in Land Surface Models

The most important properties of snow with respect to climate are its high albedo, low thermal conductivity and roughness length and ability to store water within the hydrological cycle. Many LSMs (e.x., BATS, SiB, ISBA, SSIB) parameterize snow as part of the upper soil layer for thermal processes (composite snow modelling) and as a separate layer for hydrological processes. Models such as CLASS (Verseghy, 1991) and BASE (Desborough and Pitman, 1998) simulate snow as a discrete layer for both thermal and hydrological processes. In recent years, many authors included a multi-layer snow scheme within their LSMs (e.x., ISBA-ES, Habets et al., 2003).

As discussed by Dickinson et al. (1993) and Yang et al. (1997), the most important conceptual errors in the composite soil-snow models occur during times of snowmelt or rainfall on a snow pack. In nature snowmelt or rainfall on a snow pack percolates through the snow pack and may refreeze. In the composite soil-snow models water on the snow surface is placed directly into the soil. Melting at the bottom of the snow pack due to heat conducted from the ground also cannot be taken

into account. On the contrary, when the snow cover is represented as a separate layer these processes can be modeled. In CLASS, for example, melting of the snow pack appears if the solution of the surface energy balance equation results in a value of temperature greater than 0°C. The energy available for snowmelt (estimated by setting the surface temperature back to 0°C and recalculating surface energy fluxes) is used to melt the layer of snow from the top of the pack. If the snow-layer temperature is below 0°C, the melted snow percolates into the pack and refreezes, releasing latent heat and increasing the snow-layer temperature and density until the snow temperature reaches 0°C. Thereafter, melt-water infiltrates or ponds on the soil surface. Melting of snow pack can occur also by conduction of heat from the soil underlaying the snow pack, if snow temperature raises above zero. In this case, melt-water is supplied directly to the soil surface.

It is well known that snow albedo, fractional snow cover, and their interplay have a large effect on the amount of solar radiation absorbed by the surface. Theoretically, snow albedo depends on grain size, snow density, and the rate of growth of snow grains that is a complicated function of water vapour movement, the initial snowflake geometry, and freeze-thaw cycles (Verseghy, 1991). However, computational expense does not allow the inclusion of the full physics of snow processes in climate models. A variety of methods for the parameterization of snow albedo within the LSMs have been used. For example, in CLASS and ISBA albedo is expressed as a function of snow age, while in BATS, it is a function of age and solar zenith angle. Some models have fixed values of snow albedo (e.x., BUCKET, Robock et al., 1995). The fractional snow cover is parameterized either as a linear function of snow depth (e.g., SSIB) or as a linear function below a threshold of 10 cm (e.g., CLASS). In ISBA, BATS and BASE the fractional snow cover is expressed as:

$$F_{snow} = \frac{d_{snow}}{d_{snow} + cz_{o.c}} \qquad \text{(A6.1)}$$

where d_{snow} is snow depth, $z_{o,c}$ is the roughness of vegetation canopy and c is a constant. The thermal conductivity of snow is expressed as a linear, quadratic or exponential function of the snow density, the specification of which also differs between models (fixed value or exponential/linear function of time), with the value usually between 100 and 350 kg/m^3. In general, the way in which snow is modeled deserves more attention and remains a significant limitation in current LSMs.

A7. Validation and intercomparison of Land Surface Models

Any land surface parameterization scheme designed for use in climate models should be validated whenever possible against observed data in order to assess the degree of its physical realism. Numerous field experiments have been done over the last years with the objective of evaluating current LSMs and improving our understanding of the processes at the S-V-A interface: HAPEX-MOBILHY (André et al., 1986), FIFE (Sellers et al., 1988), BOREAS (Sellers et al., 1997), CABAUW (Beljaars and Bosveld, 1997) etc. The comparison between LSMs developed worldwide by different modelling groups is undertaken within the Project for Intercomparison of Land-Surface Parameterization Schemes (PILPS). This project was initiated in 1992 and its goal is to understand any differences found in the behavior of LSMs (Henderson-Sellers et al., 1995).

PILPS consist of four phases. Phase 1 of PILPS has been focused on local (point) evaluations of LSMs. The models are driven using atmospheric forcing generated from a GCM for two grid points, representative of a tropical forest and a mid-latitude grassland (Pitman et al., 1993). In Phase 2, LSMs have been driven using observed meteorological data (off-line simulation). Data from CABAUW were used in PILPS-2a (Chen et al., 1997) and HAPEX-MOBILHY in PILPS-2b (Shao and Henderson-Sellers, 1996), where LSM simulations were performed for one year

at the local scale. In PILPS-2d, LSM simulations over Valdai (Russia) were performed and evaluated at the local scale but for multi-year period (Schlosser et al., 2000). The first attempt by PILPS to address LSMs behavior at a regional (a river basin) scale, at 1° x 1° spatial resolution, and in multi-year time scales was undertaken in PILPS-2c (Wood et al., 1998) where the simulated hydrology over the southern Central-Plains of the US were evaluated using a river routing model and observed river discharge. PILPS-2e (Lettenmaier and Bowling, 2000) is similar to phase 2c, except that the river basins are located at relatively high latitude (Torne-Kalix rivers in northern Scandinavia; Mackenzie River in Canada; Lena River in Russia), and hence river-flows are primarily controlled by snowmelt and soil freeze-thaw. In phase 3, land surface models are evaluated as an interactive component of the atmospheric GCMs participating in the Atmospheric Model Intercomparison Project (AMIP, Gates 1992), which offers a first step toward evaluating the behavior of land surface schemes within fully coupled ocean-atmosphere global climate models (PILPS phase 4, Henderson –Sellers et al., 1995).

Following the PILPS approach, in recent years, the Rhône-Aggregation (Rhône-AGG) land surface scheme intercomparison has been undertaken (Boone et al., 2004). In the Rhône model domain, the atmospheric forcing and river network is at a significantly higher spatial resolution (8 km x 8 km), allowing the effects of spatial resolution change on LSM simulations to be examined.

To get an idea about differences in surface energy and water fluxes simulated by different models, some of the results from PILPS-2c, PILPS-2e and Rhône-AGG are presented in the following paragraphs.

Liang et al. (1998) analyzed simulations over the Red and Arkansas River basins for the period 1980-1986, which were performed with 16 LSMs that participated in PILPS-2c. As can be seen from Fig. A4, where simulated energy fluxes are compared, the net radiation, absorbed solar radiation and surface temperature generally agree among the models. The sensible heat fluxes have larger differences

among the models than the latent heat fluxes (the maximum difference of the latent heat flux is about three times smaller than that of sensible heat flux), and the ground heat fluxes show the largest variations among the energy components.

Fig. A5 shows the averaged annual cycle of the simulated evapotranspiration by the PILPS-2c models against the atmospheric water budget estimated evapotranspiration. Generally, the models tended to underestimate evapotranspiration in summer and overestimate it in winter. The average annual cycle of the runoff (see Fig. A6) show that the models produce quite different mean seasonal runoff, but in general have the minimum runoff occurring in the summer.

The partitioning of total runoff into surface and subsurface runoff for each of the 16 PILPS-2c models, averaged over the years 1980-1986, are shown in Fig. A7. The runoff from the Cogley (1991) climatology and from the naturalized streamflow data are also shown. As can be seen, the total runoff is dominated by subsurface drainage for some models (e.g., BASE). Others are dominated by surface runoff (e.g., BUCK, which is a standard Manabe's model, and CLASS), while some models have a more balanced division of surface and drainage runoff (e.g., BATS and SSiB). By comparing the predicted streamflow from PILPS-2c models to naturalized steamflow (not shown here), Liang et al. (1998) concluded that the models with a significant surface runoff production have more realistic hydrograph timing (subsurface-dominated models generally have their peak streamflow 2 to 7 days later than the naturalized streamflow). On the contrary, the models with subsurface-dominated production have more realistic behavior during the low-flow period (July-September).

Model-derived seasonal cycle of the soil moisture storage tendencies (see Fig. A8) are qualitatively similar to that inferred from observations (dashed line in Fig. A8), but most models do not predict the decrease in April soil moisture storage.

The performances of the LSMs in high-latitude environments, where the snow cover and small available net radiation dominate the surface energy and water fluxes, are presented by results obtained from simulations over Torne and Kalix River basins in northern Scandinavia (PILPS 2e). Fig. A9 shows the basin snow water equivalent

(SWE) averaged over 10 years for 21 LSMs (mean March SWE is used as a surrogate for maximum annual accumulation). As can be seen, there are large differences in predicted SWE among models.

Comparing Fig. A9 to Fig. A10, where mean annual sensible and latent heat flux are shown, we can see that the models with large latent heat flux and negative sensible heat flux tend to have the smallest snow accumulation. Note that annual sensible heat flux is the net result of a positive sensible heat flux (away from the surface) in spring and summer and a negative sensible heat flux during the fall and winter.

In Fig. A11, the mean annual basin sublimation and snowmelt is presented. As can be seen, sublimation varies widely among the models, ranging from small negative amounts to about 100 mm (the snowmelt presented in Fig. A11 is calculated as the difference between the prescribed snowfall and the simulated sublimation, assuming that the mean annual change in snow storage is negligible). The comparison of Fig. A11 to Fig. A10 shows that the models that have large amounts of sublimation generally have a negative sensible heat flux.

The simulated annual runoff over the Torne-Kalix river basin, as well as its partitioning into surface and subsurface runoff is presented in Fig. A12. The total runoff varies among the models from 301 to 481 mm, while the observed value is 403 mm. It is largely controlled by the snow amount, i.e. the models with high SWE tend to have the highest annual runoff. The mean annual cycles of the runoff (see Fig. A13) are characterized by the strong snowmelt peak in May and June, followed by a gradual recession during the summer and fall. In winter, runoff is small because snowmelt is negligible and most of the precipitation is stored in the snowpack. In conclusion, all models capture the broad dynamics of snowmelt and runoff over the catchments, but there are large differences in simulated snow accumulation and ablation, turbulent fluxes and streamflow.

In the Rhône-AGG experiment, 3-year simulations with 15 LSMs were performed. The obtained intermodel scatter of simulated energy and water budget

components is typical of differences previously found in other intercomparison studies. Boone et al. (2004) highlight that most of the LSMs simulate similar total evapotranspiration and runoff but the partitioning between the various components varies greatly. The averaged total soil moisture is significantly different between the LSMs (ranging from 0.1 to 1 m) but the monthly storage changes are similar when averaged over the entire basin. The LSMs having explicit snow schemes demonstrate better snow simulation compared to those with simpler composite schemes. Composite snow schemes generally simulate too much snowmelt before the observed springtime discharge peak (peak runoff generally occurs 2-4 weeks early).

The sensitivity of LSMs to the spatial resolution change is examined by running Rhône-AGG models at 8-km resolution, at 1° x 1° resolution (GCM grid box) and at ½°x ½°resolution (regional climate model grid box). The sensitivity varies widely among the models, although the trends tend to be similar for most of them. The variable most strongly affected by scaling is SWE, which is reduced by 25%-60% when moving from 8 km x 8km resolution to the 1°x1° resolution. Several variables behave reasonably well such as latent heat flux, soil moisture and subsurface runoff (total relative differences were generally less than 10%). Surface runoff is significantly decreased in most LSMs primarily because of the upscaling of the precipitation forcing. This result emphasizes the need for implementation of subgrid precipitation algorithms in large-scale LSM applications (Boone et al., 2004).

The assigning of simulation differences to specific parameterization differences within the experiments such as PILPS is often very difficult because of the complexity of current LSMs as well as the non-linearity of the many of the land-surface processes. Even in an experiment where meteorological forcing and many of the land surface characteristics are prescribed, the non-linearity of land-surface processes causes small differences in model parameterization to lead to large differences in model outputs. One solution to this problem is to conduct experiments within a more controlled environment where each aspect of the parameterization can be isolated. This approach has been proposed by Koster and Suarez (1994) and by

Desborough (1997, 1999). They developed the CHAmeleon Surface Model (CHASM), which has the ability to operate within a variety of configurations, where land surface parameters and other aspects of land surface parameterization are treated identically. Table 1 summarizes the CHASM experimental configurations in Desborough's (1999) study. The simplest of CHASM modes (SIMPA) resemble to that of the standard Manabe (1969) model (M69), having a single surface energy balance, single evaporation flux, and no surface resistance and stability correction. The next configuration (SIMP) is similar to the SIMPA except it includes the stability correction. The intermediate RS mode is obtained by adding temporally invariant surface resistance (r_s) to the SIMP, the RS-I mode has an additional explicit parameterization of canopy interception and the RS-GI mode includes bare ground evaporation. The last two configurations (SLAM-1T and SLAM) are the most complex, having explicit parameterization for canopy resistance, canopy interception and bare ground evapotranspiration. The SLAM-1T mode resolves only a single surface energy balance equation for the composite soil-canopy-snow surface, while the SLAM land surface is divided into bare ground-snow surface and vegetation surface, where each has its own energy balance equation.

Figure 14 shows how SIMP-A, SIMP and SLAM evaporation compares to that of all PILPS models for two sites: TRF (Tropical Forest Site, Pitman et al., 1993) and HAP (Hapex-Mobilhy, Shao and Henderson-Sellers, 1996). As can be seen, in TRF the stability-corrected SIMP mode (thick dashed line in Fig. A14) behaves more like the complex PILPS (unmarked thin lines) and SLAM (thick solid line) models than like M69 (indicated by a star). However, removing SIMP's stability correction has much less effect on HAP.

The simulations from intermediate RS, RS-I, RS-GI and SLAM-1T modes are used to examine geographic and sub-annual temporal variability aspects of evaporation parameterizations. As discussed by Desborough (1999), the largest sensitivity to the evaporation parameterization is seen at the daily time scale. Fig.

A15 compares daily average evaporation in each of the RS, RS-I, RS-GI simulations to that in SLAM-1T. The surface resistance, r_s, in RS, RS-I, RS-GI was previously calibrated in order to obtain the same annual evaporation as in SLAM-1T. It should be noted that the calibrated r_s values vary considerably across the sites, indicating the presence of geographic information in the SLAM-1T parameterization. The left panels in Fig. A15 indicate how daily evaporation is altered when temporal variations in canopy resistance are removed from SLAM-1T, the middle panels show also the effect of removing bare ground evaporation and the panels on the right show what happens when explicit interception is also removed. Daily averaged evaporation in the simpler RS mode is quite different from that of SLAM-1T, even with calibrated annual evaporation.

A8. Conclusion and point of view

Numerous investigations have demonstrated that simulated climate by General Circulation Models (GCMs) and Regional Climate Models (RCMs) are sensitive to the formulation of land surface processes. Modifying land surface properties such as albedo and roughness length has significant impacts on simulated large-scale atmospheric circulation, evaporation and precipitation. Similar effects appear when the parameterization of surface hydrology is altered or whether vegetation is included or not within a land surface scheme. As a result of a general recognition of the importance of land surface processes in climate modelling, LSMs have evolved from very simple first generation LSMs based on Manabe's (1969) (MAN69) approach to fairly sophisticated second and third generation models, that include an explicit representation of vegetation.

Incorporation of biophysics and a multilayer representation of soil thermal and hydrological regimes into the second-generation LSMs made them more realistic than

the first-generation models. Improvement of the simulated continental hydrometeorology is shown in many studies in which the simulations produced by a biophysical model coupled to a GCM are compared to the simulations produced by a bucket hydrology model coupled to the same GCM (Sato et al., 1989, Verseghy et al., 1996, Viterbo and Beljaars, 1996). Continental evaporation calculated by biophysical LSMs was consistently lower compared to the non-biophysical simulations, mainly because of the inclusion of stomatal resistance in the biophysical LSMs. As a consequence, reduced and more realistic continental precipitation fields are simulated. Similarly, in the offline intercomparison experiments of PILPS, it was found that the standard MAN69 model behaves in an anomalous way compared to the other models, producing significantly larger evaporation rates and smoller sensible heat fluxes. However, LSMs participating in the PILPS project, as well as in the recent Rhône-AGG project, showed a wide range of behavior despite using the same atmospheric forcing and land surface parameters. Attempts were made in these projects to relate simulation differences to specific parameterization differences but these efforts were sometimes unsuccessful because of the large number of potential sources of these differences. In addition, due to non-linearity of the land-surface processes small differences in model parameterizations can lead to large differences in model output. Thus, the sources of variability in LSM behavior are not fully resolved. The problems were identified also with identically named parameters having different effective meanings in each LSM.

The appropriate level of complexity of land-surface models for use in climate models and the relative usefulness of MAN69 and Deardorff's (1978) approaches are still unresolved issues. Both basic approaches in land surface modeling continue to coexist. Desborough (1999) showed that a simple surface energy balance parameterization with a constant surface resistance is as appropriate as a more complex parameterization for simulations of the annual, monthly and seasonally averaged evapotranspiration. However, complex aspects of canopy interception, bare ground evaporation and canopy resistance contain substantial geographic and daily

functionality that are not present in the simpler parameterizations. LSM performance must be ultimately assessed by how well observations are reproduced. The only way ahead to develop and improve parameterization is validation and comparison with observations. The impact of "improved" parameterizations on climate simulations should be assessed taking into account statistical significance of the induced changes. It is also important to compare simulated land surface climatology with observations over a range of climate conditions and for different surface types. Both coupled and offline simulations are required in order to improve our understanding of the feedback mechanisms acting between the atmosphere and underlaying surface.

Many problems in land-surface modelling remain to be addressed. The parameterization of subgrid spatial variability of soil type, vegetation characteristics and topography and their impact on surface turbulent and radiative fluxes and near-surface hydrology needs to be improved. The implementation and validation of different averaging schemes (aggregation rules) used to define *effective* parameters over large areas is required. The development and improvement of existing methods accounting for subgrid effects on certain land surface variables are also important. A probability distribution function should be applied to certain LSM variables (such as soil moisture) and to the atmospheric forcing variables (such as precipitation). Alternatively, the so-called mosaic (tile) approach proposed by Koster and Suarez (1992), which has the advantage of explicitly representing very distinct surface types and the surface properties assigned to each tile, can be used, but it is computationally more expensive compared to the *effective* surface treatment.

Effort is also required to improve the realism of vertical soil water transfer and to describe the effects of within grid cell horizontal transfer of soil water. The parameterization of surface and subsurface runoff in current LSMs, as well as snow processes, must also be improved. The available global land cover data sets (providing a global time-series of vegetation and soil parameters) designed for use in LSMs need to be further improved.

Finally, it should be mentioned that the climate community now needs LSMs able to provide the internally consistent carbon balance to be performed along with conventional surface water and energy balance calculation. Furthermore, some land surface modeling groups are now working on development of the interactive vegetation models that will be able to simulate changes in vegetation parameters and carbon cycle variables in response to climate change (IPCC, 2001).

Acknowledgement

The author is deeply grateful to Dr David Plummer for helpful comments on the manuscript.

References

André, J.-C., J.-P. Goutorbe, and A. Perrier, 1986: HAPEX-MOBILHY: A hydrologic atmospheric experiment for the study of water budget and evaporation flux at the climatic scale. *Bull. Amer. Meteor. Soc.*, **67**, 138-144.

Avissar, R., and R.A. Pielke, 1989: A parametrization of heterogeneous land surfaces for atmospheric numerical models and its impact on regional meteorology. *Mon. Wea. Rev.*, **117**, 2113-2136.

Beljaars, A. C. M., and F. C. Bosveld, 1997: Cabauw data for the validation of land surface parameterization schemes. *J. Climate*, **10**, 1172-1193.

Boone, A., V. Masson, T. Meyers, and J. Noilhan, 2000: The influence of the inclusion of soil freezing on simulations by a soil-vegetation-atmosphere transfer scheme. *J. Appl. Meteor.*, **39**, 1544-1569.

Boone A., F. Habets, J. Noilhan, D. Clark, P. Dirmeyer, S. Fox, Y. Gusev, I. Haddeland, R. Koster, D. Lohmann, S. Mahanama, K. Mitchell, O. Nasonova, G.-Y. Niu, A. Pitman, J. Polcher, A. B. Shmakin, K. Tanaka, B. Van Den Hurk, S. Verant, D. Verseghy, P. Viterbo, and Z.-Y. Yang, 2004: The Rhone-Aggregation Land Surface Scheme Intercomparison Project: An Overview. *J. Climate,* **17**, 187-208.

Bowling, L., D. Lettenmaier, B. Nijssen, J. Polcher, R. Koster, D. Lohmann, 2003: Simulation of high-latitude hydrological processes in the Torne-Kalix basin: PILPS Phase 2(e) 3: Equivalent model representation and sensitivity experiments. *Global and Plan. Change*, **38**, 55-71.

Bhumralkar, C.M., 1975: Numerical experiments on the computation of ground surface temperature in an atmospheric general circulation model. *J. Appl. Meteorol.* 14, 1246–1258.

Carson, D.J., 1982: Current parameterization of land surface processes in Atmospheric General Circulation models. Land surface processes in atmospheric general

circulation models. Cambridge University Press, 67-108.

Charney, J.G., 1975: Dynamics of deserts and droughts over the Sahel. *Quart. J. Roy. Meteor. Soc.*, **101**, 193-202.

Chen, T. H., A. Henderson-Sellers, P. C. D. Milly, A. J. Pitman, A. C. M. Beljaars, J. Polcher, F. Abramopoulos, A. Boone, S. Chang, F. Chen, Y. Dai, C. E. Desborough, R. E. Dickinson, L. Duemenil, M. Ek, J. R. Garratt, N. Gedney, Y. M. Gusev, J. Kim, R. Koster, E. Kowalczyk, K. Laval, J. Lean, D. Lettenmaier, X. Liang, J-F. Mahfouf, H.-T. Mengelkamp, K. Mitchell, O. N. Nasonova, J. Noilhan, A. Robock, C. Rosenzweig, J. Schaake, C. A. Schlosser, J.-P. Schulz, Y. Shao, A. B. Shmakin, D. L. Verseghy, P. Wetzel, E. F. Wood, Y. Xue, Z.-L. Yang, and Q. Zeng, 1997: Cabauw experimental results from the project for intercomparison of landsurface schemes (PILPS). *J. Climate*, **10**, 1194-1215.

Clapp, R.B. and G.M. Hornberger, 1978: Empirical equations for some hydraulic properties. *Water Resour. Res.*, **14**: 601-604.

Cogley, J., 1991: GGHYDRO-global hydrographic data release 2.0. Trent Climate Note 91-1. Trent University.

Cosby, B.J., G.M. Hornberger, R.B. Clapp and T.R. Ginn, 1984: A statistical exploration of the relationships of soil moisture characteristics to the physical properties of the soils. *Water Resour. Res.*, **20**, 682-696.

Collatz, G.J., M. Ribas-Carbo, and J.A. Berry, 1991: A coupled photosynthesis-stomatal conductance model for leaves of C4 plants. *Australian Journal of Plant Physiology*, **19**, 519-539.

Darcy, H.P.G., and H. Bazin, 1865: Recherches Hydrauliques. Imprimerie Nationale, Paris, France.

Deardorff J. W., 1972: Parameterization of the planetary boundary layer for use in general circulation models. *Mon. Wea. Rev.*, **100**, 93-106.

Deardorff, J.W., 1978: Efficient prediction of ground surface temperature and moisture, with inclusion of a layer of vegetation. *J. Geophys. Res.*, **83**, 1889-1903.

Desborough, C.E., and A.J. Pitman, 1998: The BASE land surface model. *Global and Plan. Change*, **19**, 3-18.

Desborough, C. E., 1999: Surface energy balance complexity in GCM land surface models. *Climate Dynamics*, **15**, 389-403.

Dickinson, R.E., 1983: Land surface processes and climate –Surfaces albedos and energy balance. *Advances in Geophysics*, **25**, Academic Press, 305-353.

Dickinson, R.E., 1988: The force-restore model for surface temperatures and its generalizations. *J. Climate*, **1**, 1086-1097.

Dickinson, R.E., A. Henderson-Sellers, and P.J. Kennedy, 1993: Biosphere-atmosphere transfer scheme (BATS) Version 1e as coupled to the NCAR Community Climate Model. NCAR Technical Note, NCAR/TN-387+STR, 72pp.

Dickinson, R.E., A. Henderson-Sellers, P.J. Kennedy, and M.F. Wilson, 1986: Biosphere-atmosphere transfer scheme (BATS) for the NCAR community model. NCAR Technical Note, NCAR/TN-275+STR, 69 pp.

Dickinson, R.E., M. Shaikh, R. Bryant, and L. Graumlich, 1998: Interactive canopies for a climate model. *J. Climate*, **11**, 2823-2836.

Entekhabi, D., and P. Eagleson, 1989: Land surface hydrology parameterization for atmospheric general circulation models including subgrid scale spatial variability. *J. Climate,* **2,** 816–832.

Flamiglietti, J. S., and E. F. Wood, 1994: Multiscale modeling of spatially variable water and energy balance processes. *Water Resour. Res.,* **30,** 3061–3078.

Gates, W.L., 1992: The atmospheric model intercomparison project. *Bull. Am. Meteorol. Soc.*, **73**, 1962-1970.

Garratt, J.R., 1992: The Atmospheric Boundary Layer. Cambridge University Press, 684 pp.

Garratt J.R., 1993: Sensitivity of climate simulation to land-surface and atmospheric boundary-layer treatments. A review. *J. Climate,* **6**, 419-448.

Goudriaan, J., 1977: Crop Micrometeorology. A simulation study. Wageningen Center for Agricultural Publishing and documentation, 249 pp.

Habets, F., A. Boone, and J. Noilhan, 2003: Simulation of a Scandinavian basin using the diffusion transfer version of ISBA. *Global and Plan. Change*, **38**, 137-149.

Hack, J.J., B.A. Boville, B.P. Briegleb, J.T. Kiehl, P.J. Rasch, and D.L. Williamson, 1993: Description of the NCAR Community Climate Model (CCM2). NCAR Tech. Note, NCAR/TN-382+STR, National Center for Atmospheric Research, Boulder, CO, 108 pp.

Henderson-Sellers, A., A. Pitman, P. Love, P. Irannejad, and T. Chen, 1995: The project of intercomparison of land-surface parameterization schemes (PILPS): Phases 2 and 3. *Bull. Amer. Meteor. Soc.*, **94**, 489-503.

Holloway, J. L., Jr., and S. Manabe, 1971: Simulation of climate by a global general circulation model, I. Hydrologic cycle and heat balance. *Mon. Wea. Rev.*, **99**, 335-370.

IPCC, 2001: Climate Change 2001: The Scientific Basis: Physical Climate Processes and Feedbacks. Cambridge University Press, Cambridge, 881 pp.

Jackson, R.D., 1973: Diurnal changes in soil water content during drying. *Field Soil Water Regime*, Soil Sci. Soc. Of Amer., 37-55.

Jarvis, P.G., 1976: The interpretation of the variations in leaf water potential and stomatal conductance found in canopies in the field. *Phil. Trans. Roy. Soc. London,* **B273**, 593-610.

Koster R.D., and M.J. Suarez, 1992: Modelling the land surface boundary in climate models as a composite of independent vegetation stands. *J. Geophys. Res.*, **97**, 2697-2715.

Koster, R.D., and M.J. Suarez, 1994: The components of an SVAT scheme and their effects on a GCM's hydrological cycle. *Adv. Water Res.*, **17**, 61-78.

Koster, R.D., and M.J. Suarez, 1992: Energy and water balance calculations in the Mosaic LSM, NASA Tech. Memo. 104606 (9), 76 pp.

Kowalczyk, E.A., J.R. Garratt, and P.B. Krnmmel, 1991: A soil-canopy scheme for use in a numerical model of the atmosphere--lD stand-alone model. CSIRO, DAR, Tech. Pap., 23, 56 pp.

Lean, J., and D.A. Warrilow, 1989: Simulation of the regional climate impact of Amazon deforestation. *Nature*, **342,** 411-413.

Lettenmaier, D. P., and L. Bowling, 2000: Arctic model intercomparison study initiated. *GEWEX News*, WCRP, **10**, 8-10.

Liang, X., D.P. Lettenmaier, E.F. Wood, and S.J. Burges, 1994: A simple hydrologically based model of land surface water and energy fluxes for general circulation models. *J. Geophys. Res.*, **99,** 14 415–14 428.

Liang, X., E. F. Wood, and D. Lettenmaier, 1996: One-dimensional statistical dynamic representation of subgrid spatial variability of precipitation in the two-layer variable infiltration capacity model. *J. Geophys. Res.*, **101,** 21 403–21 422.

Liang, X., E Wood, D. Lettenmaier, D. Lohmann, A. Boone, S. Chang, F. Chen, Y. Dai, C. Desborough, R. Dickinson, Q. Duan, M. Ek, Y. Gusev, F. Habets, P. Irannejad, R. Koster, K. Mitchell, O. Nasonova, J. Noilhan, J. Schaake, A. Schlosser, Y. Shao, A. Shmakin, D. Verseghy, K. Warrach, P. Wetzel, Y. Xue, Z.-L. Yang, and Q. Zeng, 1998: The Project for Intercomparison of Land-surface Parameterization Schemes (PILPS) phase 2(c) Red-Arkansas River basin experiment: 2. Spatial and temporal analysis of energy fluxes. *Global and Plan. Change*, **19**, 137-159.

Lohmann, D., D. Lettenmaier, X. Liang, E. Wood, A. Boone, S. Chang, F. Chen, Y. Dai, C. Desborough, R. Dickinson, Q. Duan, M. Ek, Y. Gusev, F. Habets, P. Irannejad, R. Koster, K. Mitchell, O. Nasonova, J. Noilhan, J. Schaake, A. Schlosser, Y. Shao, A. Shmakin, D. Verseghy, K. Warrach, P. Wetzel, Y. Xue, Z.-L. Yang, and Q. Zeng, 1998: The Project for Intercomparison of Land-surface Parameterization Schemes (PILPS) phase 2(c) Red-Arkansas River basin experiment: 3. Spatial and temporal analysis of water fluxes, *Global and Plan. Change*, **19**, 161-179.

Manabe, S., 1969: The atmospheric circulation and the hydrology of the earth's surface. *Mon. Wea. Rev.*, **97**, 739-774.

Mahfouf, J.-F., and J. Noilhan, 1991: Comparative study of various formulations of

evaporation from bare soil using in situ data. *J. Appl. Meteorol.,* **9**, 351-362.

Mahfouf, J-F., A.O. Manzi, J. Noilhan., H. Giordani, and M. Déqué, 1995: The land surface scheme ISBA within the Météo-France climate model ARPEGE. Part I: Implementation and preliminare results. *J Climate*, **8**, 2039-2057.

Mahfouf, J.-F. and J. Noilhan, 1996: Inclusion of gravitational drainage in a land surface scheme based on the force-restore method. *J. Appl. Meteor.*, **35**, 987-992.

Mein, R. G., and C. L. Larson. 1973: Modeling infiltration during a steady rain. *Water Resourc. Res*. 9, 384-394.

Meador , W.E., and W.R. Weaver, 1980: Two-stream approximations to radiative transfer in planetary atmospheres: A unifield description of existing methods and a new improvement. *J. Atmos. Sci.*, **37**, 630-643.

McFarlane, N.A., G.J. Boer, J.-P. Blanchet, and M. Lazare, 1992: The Canadian Climate Centre Second-Generation General Circulation Model and Its Equilibrium Climate. *J. Climate*, **5**, 1013-1044.

Mintz, Y., 1984: The sensitivity of numerically simulated climates to land-surface boundary conditions. *Global Climate*, J. Houghton, Ed., 79-105.

Monin A. S. and A.M. Obukhov, 1951: Main characteristics of the turbulent mixing in the atmospheric surface layer, *Trudy Geophys.*, **24**, 153–187.

Monteith, J.L., 1973: Principles of Environmental Physics. Edward Arnold Ltd., 242 pp.

Noilhan, J., and S. Planton, 1989: A simple parameterization of land surface processes for meteorological models. *Mon. Wea. Rev.,* **117,** 536–549.

Nijssen, B., L. Bowling, D. Lettenmaier, D. Clark, M. E. Maayar, R. Essery, S. Goers, Y. Gusev, F. Habets, B. van den Hurk, J. Jin, D. Kahan, D. Lohmann, X. Ma, S. Mahanama, D. Mocko, O. Nasonova, G.-Y. Niu, P. Samuelsson, A. Shmakin, K. Takata, D. Verseghy, P. Viterbo, Y. Xa, Y. Xue, and Z.-L. Yang, 2003: Simulation of high latitude hydrological processes in the Torne-Kalix basin:

PILPS Phase 2(e) 2: Comparison of model results with observations. *Global and Plan. Change*, **38**, 31-53.

Pitman, A.J., Z.L. Yang, J.G. Cogley, and A. Henderson-Sellers, 1991: Description of bare essentials of surface transfer for the Bureau of Meteorology Research Centre AGCM. BMRC Res. Rep., 32, 117 pp.

Pitman, A.J., and C. Desborough, 1996: Brief description of bare essentials of surface transfer and results from simulations with the HAPEX-MOBILHY data. *Global Plan. Change*, **13**, 135-143.

Pitman, A.J., 2003: The evolution of, and revolution in, land surface schemes designed for climate models: Review. *Int. J. Climatology*, **23**, 479-510.

Possey, J. W., and D. F. Clapp, 1964: Global distribution of normal surface albedo. *Geofis. Int.*, **4**, 33-48.

Richards, L.A., 1931: Capillary conduction of liquids through porous mediums. *Physics*, **1**, 318-333.

Robock, A., Vinnikov, K.Y., Schlosser, C.A., Speranskaya, N.A. and Xue, Y., 1995. Use of Russian soil moisture and meteorological observations to validate soil moisture simulations with biosphere and bucket models. *J. Climate*, **8**, 15-35.

Sato, N., P.J. Sellers, D.A. Randall, E. K. Schneider, J.Shukla, J.L. Kinter III, Y.-Y. Hou, and E. Albertazzi, 1989: Effect of implementation of the Simple Biosphere Model (SiB) in general a circulation model. *J. Atmos. Sci.,* **46**, 2757-2782.

Sellers, P.J., Y. Mintz, Y.C. Sud, and A. Dalcher, 1986: A simple biosphere model (SiB) for use within general circulation models. *J. Atmos. Sci.*, **43**, 505-531.

Sellers, P. J., F. G. Hall, G. Asrar, D. E. Strebel, and R. E. Murphy, 1988: The first ISLSCP Field Experiment (FIFE). *Bull. Amer. Meteor. Soc.*, **69**, 22-27.

Sellers, P. J., J.A. Berry, G.J. Collatz, C.B. Field, and F.G. Hall, 1992: Canopy reflectance, photosynthesis, and transpiration. III. A reanalysis using improved leaf models and new canopy integration scheme. *Remote Sensing of the Environment*, **42**, 187-216.

Sellers, P.J., G.J. Collatz, J.A. Berry, C.B. Field, D.A. Dazlich, C. Zhang, G.D.Collelo, and L. Bounoua, 1996: A revised land surface parameterization (SiB2) for atmospheric GCMs. Part I: Model formulation. *J. Climate.*, **9**, 676–705.

Sellers, P.J., F.G. Hall, R.D. Kelly, A. Black, D. Baldocchi, J. Berry, M. Ryan, K.J. Ranson, P.M. Crill, D.P. Lettenmaier, H. Margolis, J. Cihlar, J. Newcomer, D. Fitzjarrald, P.G. Jarvis, S.T. Gower, D. Halliwell, D. Williams, B. Goodison, D.E. Wickland, and F.E. Guertin, 1997: BOREAS in 1997: Experiment Overview, Scientific Results and Future Directions. *Journal of Geophysical Research,* **102,** 28 731-28 770.

Shao, Y., and A. Henderson-Sellers, 1996: Validation of soil moisture simulation in land surface parameterization schemes with HAPEX data. *Global and Plan. Change*, **13**, 11-46.

Schlosser, C. A., A. G. Slater, A. Robock, A. J. Pitman, K. Y. Vinnkov, A. Henderson-Sellers, N. A. Speranskaya, K. Mitchell, A. Boone, H. Braden, F. Chen, P. Cox, P. de Rosnay, C. E. Desborough, R. E. Dickinson, Y.-J. Dai, Q. Duan, J. Entin, P. Etchevers, N. Gedney, Y. M. Gusev, F. Habets, J. Kim, V. Koren, E. Kowalczyk, O. N. Nasonova, J. Noilhan, J. Schaake, A. B. Shmakin, T. G. Smirnova, D. Verseghy, P. Wetzel, Y. Xue, and Z.-L. Yang, 2000: Simulations of a boreal grassland hydrology at Valdai, Russia: PILPS Phase 2(d). *Mon. Wea. Rev.*, **128**, 301-321.

Stull, R.B., 1988: An Introduction to Boundary Layer Meteorology. Cambrige University Press, 684 pp.

Sud, Y.C., J. Shukla, and Y. Mintz, 1986 : Influence of land-surface on circulation and rainfall in a tropical model. *Quart. J. Roy. Met. Soc.,* **103**, 29-46.

Thom, A.S., 1971: Momentum absorption by vegetation. *Quart. J. Roy. Meteor. Soc.,* **110**, 1143-1163.

Verseghy, D.L., 1991: CLASS - A Canadian land surface scheme for GCMs. Part I: Soil model. *Int. J. Climatol.,* **11**, 111–133.

Verseghy, D.L., N.A. McFarlane, and M. Lazare, 1993: CLASS - A Canadian land surface scheme for GCMs. Part II: Vegetation model and coupled runs. *Int. J. Climatol.* **3**, 347–370.

Verseghy, D.L., 1996: Local climates simulated by two generation of Canadian GCM Land Surface Schemes. *Atmos.-Ocean*, **34**, 435-456.

Viterbo, P., and A.C.M. Beljaars, 1995: An improved land surface parameterization scheme in the ECMWF model and its validation. *J. Climate*, **8**, 2716-2748.

Wetzel, P., and A. Boone, 1995: A parameterization for land- atmosphere-cloud exchange (PLACE): documentation and testing a detailed process model of the partly cloudy boundary layer over heterogeneous land. *J. Climate*, **8**, 1810-1837.

Wood, E. F., D. Lettenmaier, X. Liang, D. Lohmann, A. Boone, S. Chang, F. Chen, Y. Dai, C. Desborough, Q. Duan, M. Ek, Y. Gusev, F. Habets, P. Irannejad, R. Koster, O. Nasanova, J. Noilhan, J. Schaake, A. Schlosser, Y. Shao, A. Shmakin, D. Verseghy, J. Wang, K. Warrach, P. Wetzel, Y. Xue, Z.-L. Yang, and Q. Zeng, 1998: The Project for Intercomparison of Land-Surface Parameterization Schemes (PILPS) Phase-2c Red-Arkansas River Basin experiment: 3. experiment description and summary intercomparisons. *Global and Plan. Change*, **19**, 115-135.

Xue, Y., P. Sellers, J. Kinter, and J. Shukla, 1991: A simplified biosphere model for climate studies. *J. Climate,* **4,** 345–364.

Xue, Y., F.J. Zeng, and C.A. Schlosser, 1996: SSiB and its sensitivity to soil properties-a case study using HAPEX-Mobilhy data. *Global Plan. Change*, **13**, 183-194.

Yang, Z.-L., and R.E. Dickinson, 1996: Description of the Biosphere-Atmosphere Transfer Scheme (BATS) for the Soil Moisture Workshop and evaluation of its performance. *Global Plan. Change*, **13**, 117-134.

Table A1. Summary of CHASM's experimental configurations (Desborough, 1999).

Surface mode	Stability correction	Surface resistance	Canopy interception	Bare ground evaporation	Canopy resistance	Temperature differentiation
SIMP-A	–	–	–	–	–	–
SIMP	✓	–	–	–	–	–
RS	✓	✓	–	–	–	–
RS-I	✓	✓	✓	–	–	–
RS-GI	✓	✓	✓	✓	–	–
SLAM-1 T	✓	✓	✓	✓	✓	-
SLAM	✓	✓	✓	✓	✓	✓

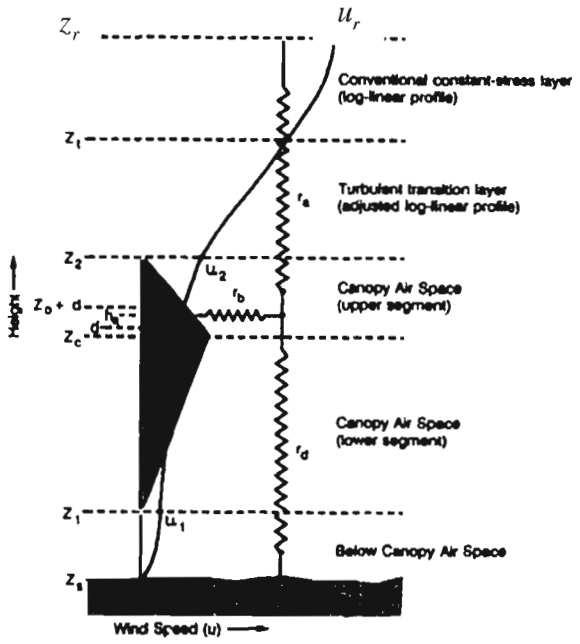

Fig. A1. Turbulent transfer regimes considered in SiB2 (modified from Sellers et al., 1996): z_1-height of canopy bottom, z_2- height of canopy top, z_c- inflection height for leaf-area density, z_s- ground roughness length, z_r- reference height, z_o- canopy roughness length, d- canopy zero plane displacement height, h_a- water vapour and sensible heat source height, u_1, u_2 and u_r- wind velocity at z_1, z_2 and z_r, respectively, r_d-aerodynamic resistance for heat (vapour) transfer between the ground and canopy air space, r_a-aerodynamic resistance between the canopy air space and the reference height, and r_b- aerodynamic resistance between the canopy surface and canopy air space.

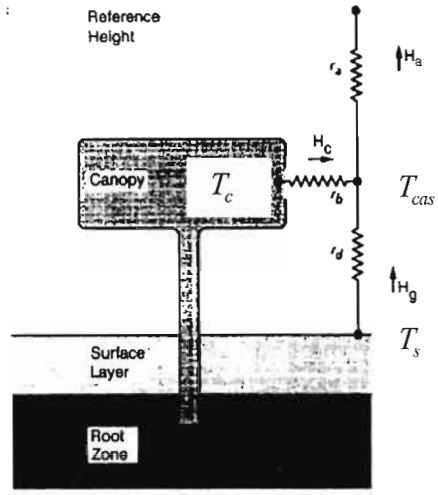

Fig. A2. Transfer pathways for sensible heat as conceptualised in SiB2 (modified from Sellers et al., 1996).

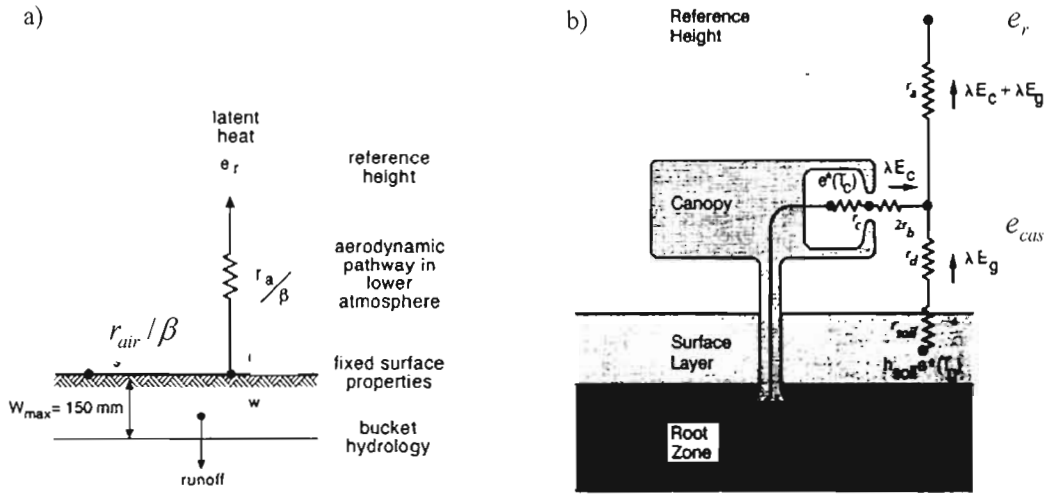

Fig. A3. Transfer pathways for latent heat as conceptualized in the first-generation LSMs, modified from Pitman (2003) (a) and in SiB2, modified from Sellers et al. (1996) (b).

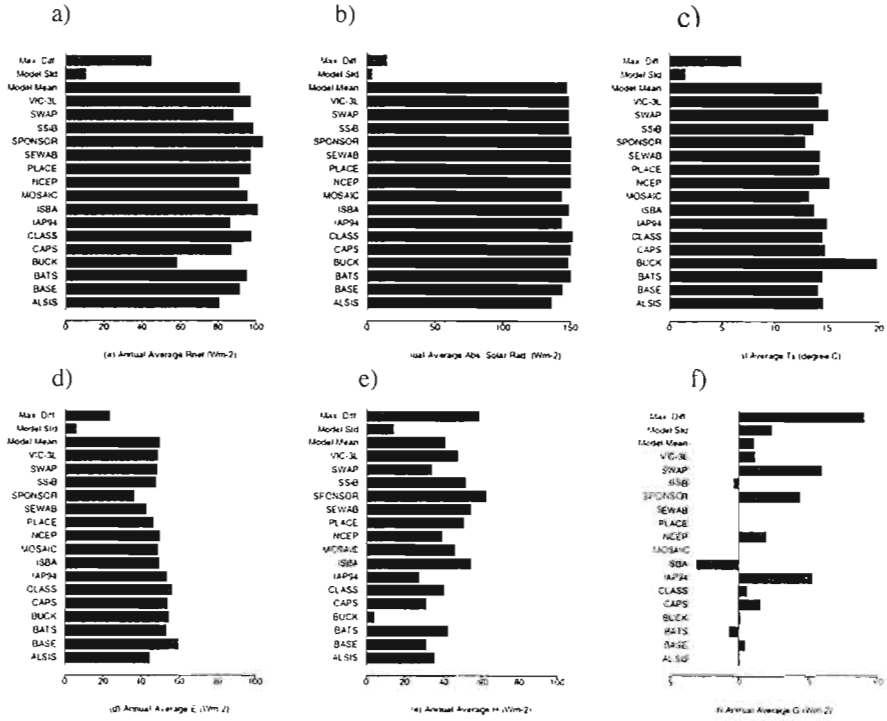

Fig.A4. Annual average (1980–1986) model-simulated net radiation (a), absorbed solar radiation (b), surface temperature (c), latent (d), sensible (e), and ground heat flux (f) over the Red-Arkansas River basin (Liang et al., 1998).

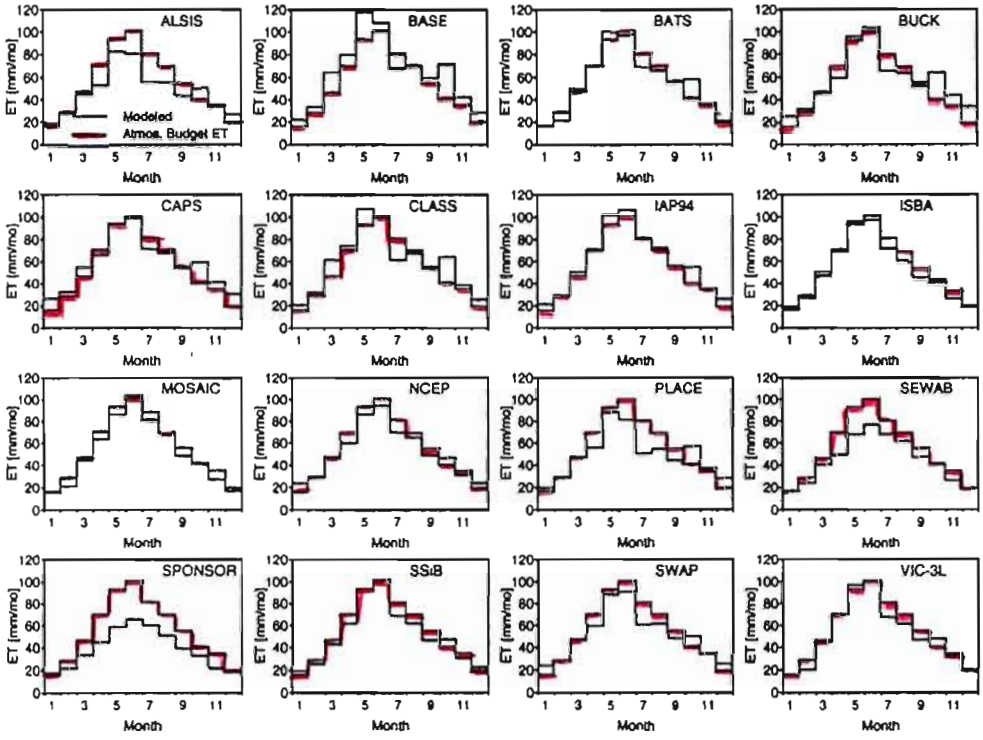

Fig. A5. Mean monthly evapotranspiration (1980–1986) over the Red-Arkansas River basin (Lohmann et al., 1998).

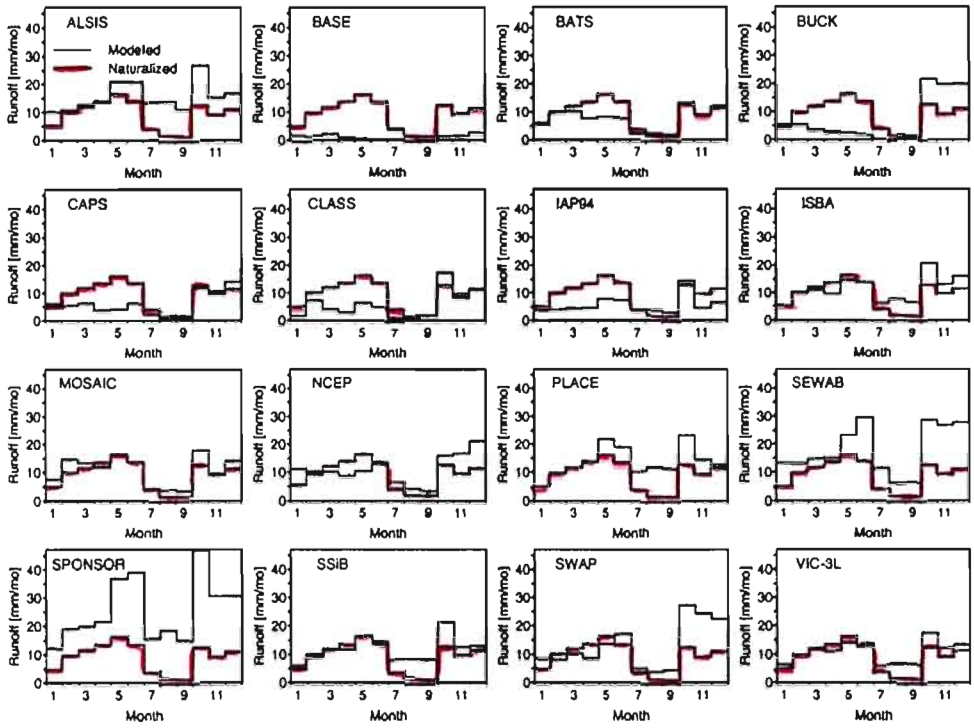

Fig. A6. Mean monthly runoff (1980–1986) over the Arkansas and Red River basins routed to respective basin outlets, compared to observed monthly mean naturalized streamflows summed at basin outlets (Lohmann et al., 1998).

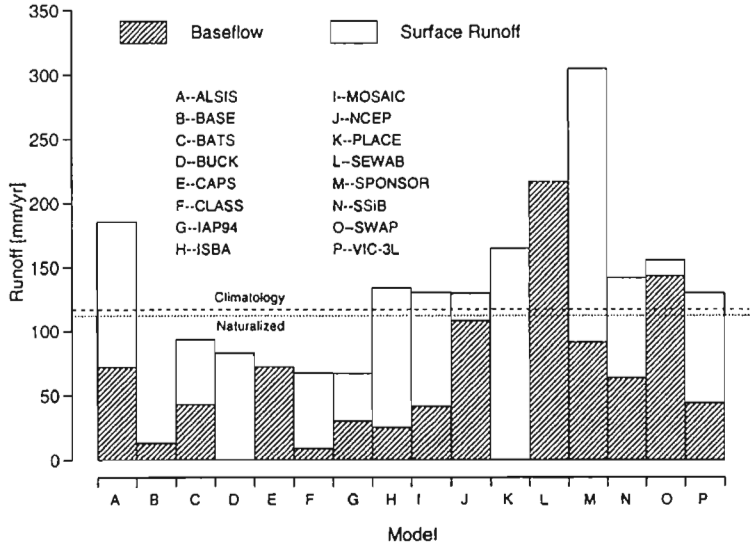

Fig. A7. Model partitioning of runoff into surface and subsurface runoff, averaged over the years 1980–1986. Also shown are the runoff from the Cogley (1991) climatology and from the naturalized streamflow data (Lohmann et al., 1998).

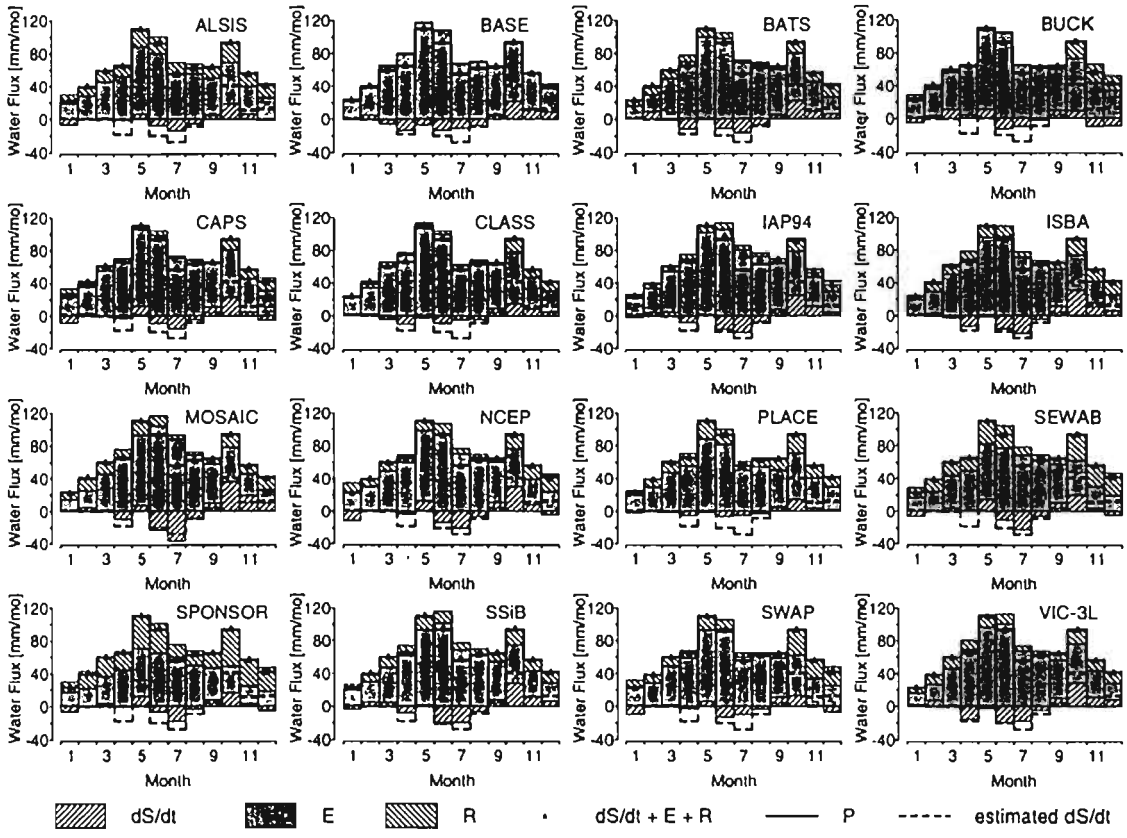

Fig. A8. Mean monthly (1980–1986) water balances: soil moisture tendency (dS/dt), evapotranspiration (E), runoff (R), precipitation (P) (Lohmann et al., 1998).

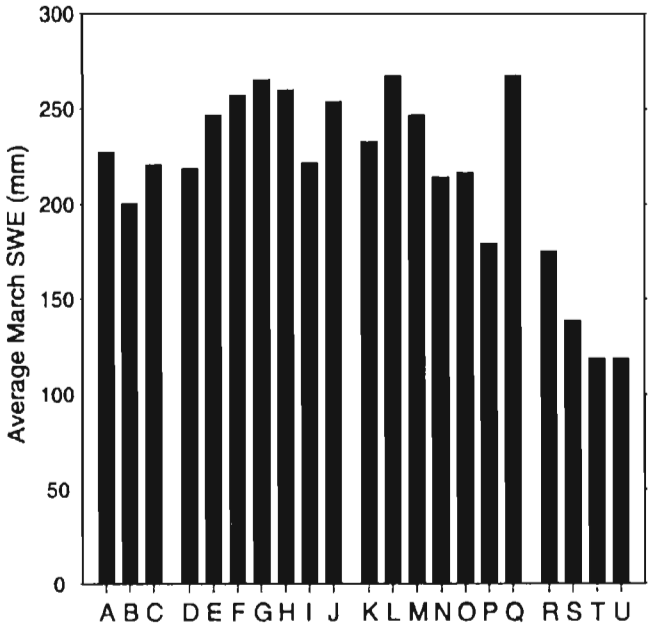

Model Name	Model Identifier
SPONSOR	A
RCA	B
IHAS	C
SEWAB	D
ISBA	E
NSIPP	F
CLASS	G
IBIS	H
CHASM	I
VIC	J
MATSIRO	K
HY-SSiB	L
VISA	M
SAST	N
MECMWF	O
NOAH	P
SWAP	Q
SSiB	R
ECMWF	S
MOSES	T
MOSES-CEH	U

Fig. A9. Basin average snow water equivalent (SWE) for March (surrogate for maximum) for the period (1989–1998) (left panel) and model identifiers (right panel) (Bowling et al., 2003)

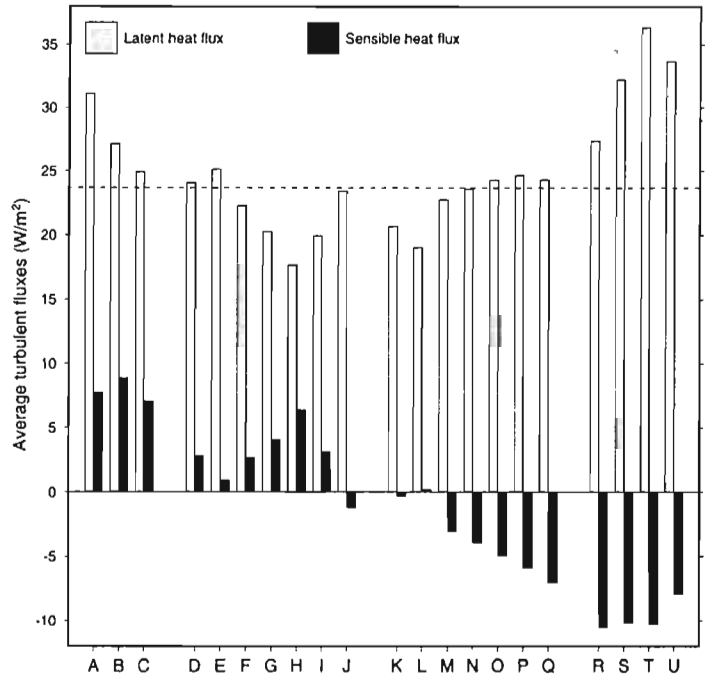

Fig. A10. Mean annual basin-wide turbulent heat fluxes. The dashed line shows the water balance based estimate of the latent heat flux over the basin (Nijssen et al., 2003). Model identifiers are the same as in Fig. 9.

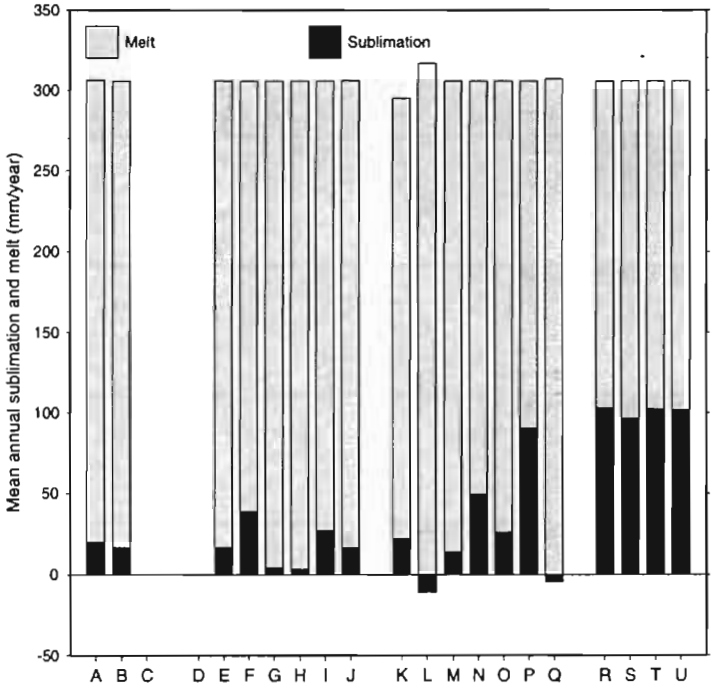

Fig. A11. Mean annual basin-wide sublimation and melt (Nijssen et al., 2003). Model identifiers are the same as in Fig. 9.

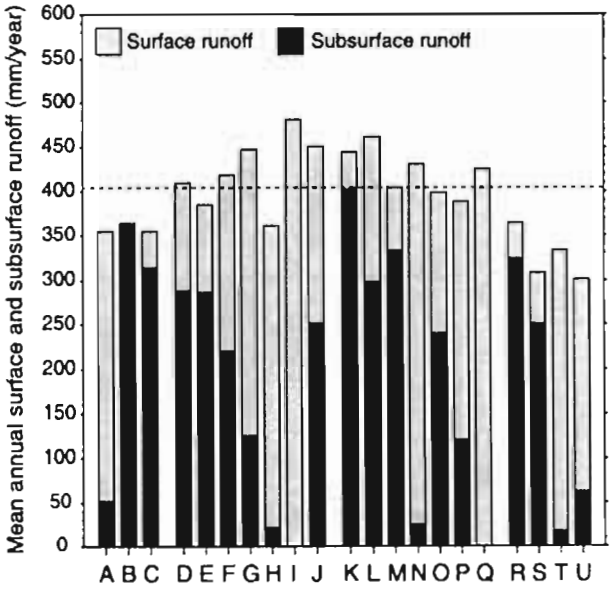

Fig. A12. Total basin mean annual surface and subsurface runoff. The dashed horizontal line represents mean annual runoff at the mouths of the Torne and Kalix Rivers combined (Nijssen et al., 2003). Model identifiers are the same as in Fig. 9.

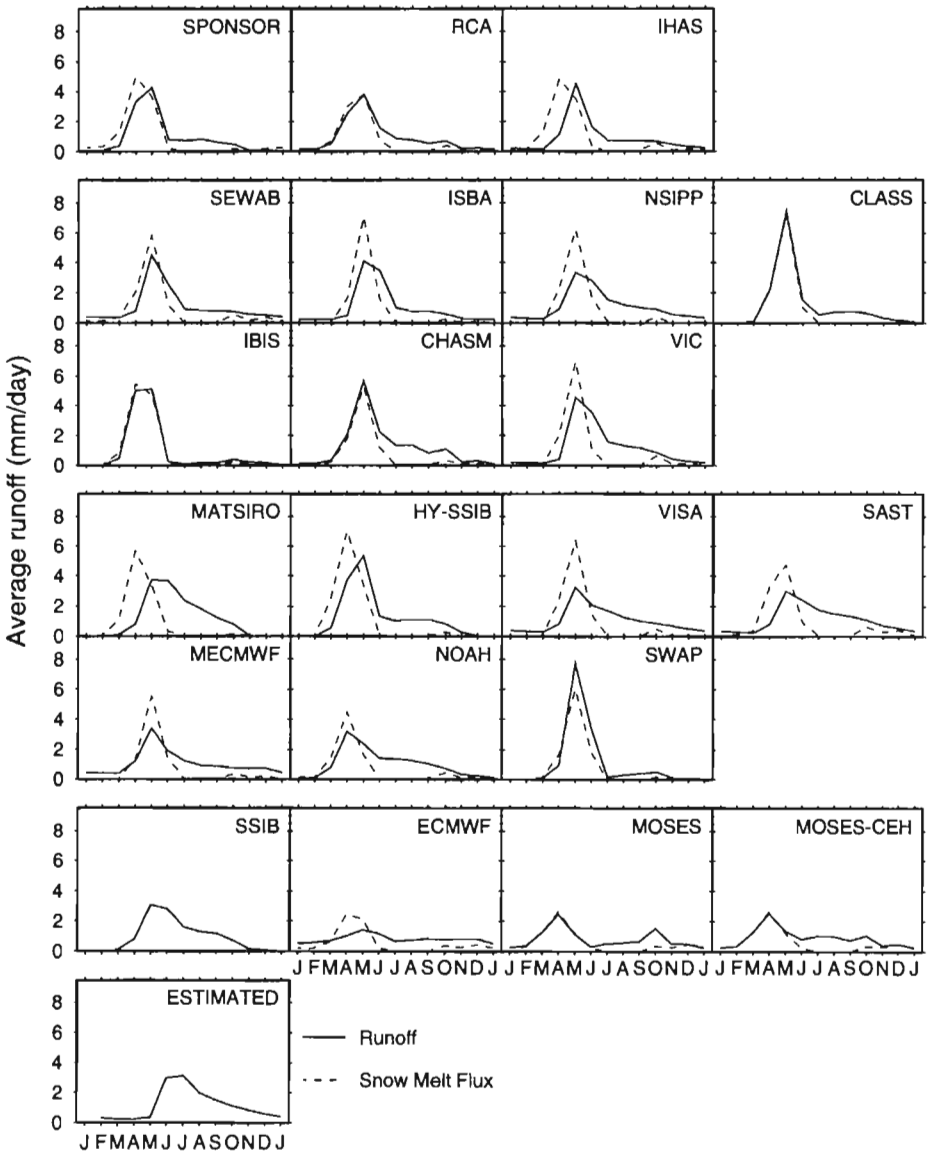

Fig. A13. Total mean monthly runoff (not routed streamflow) and mean monthly snow melt flux (Bowling et al., 2003).

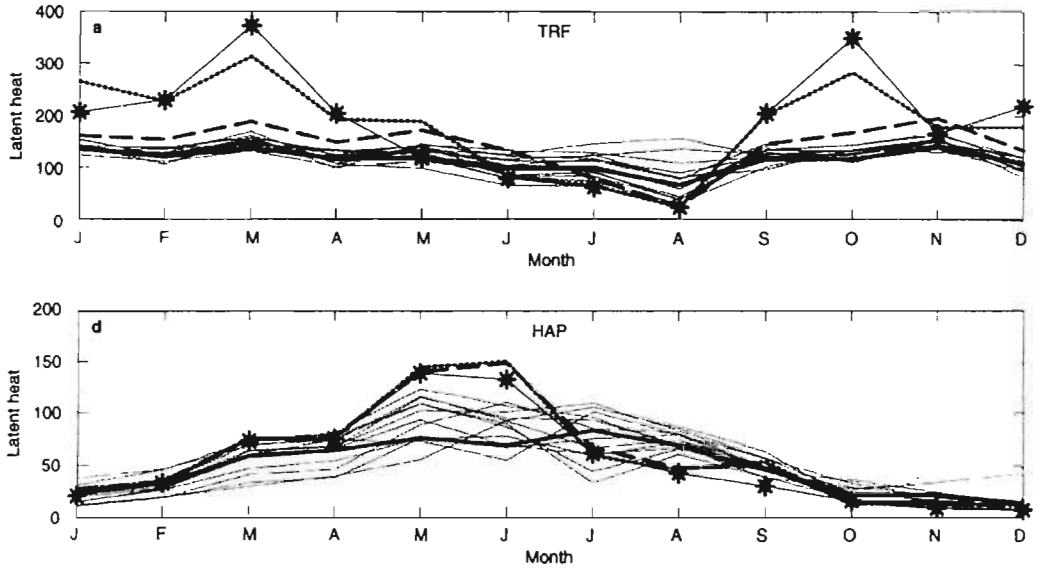

Fig. A14. Monthly evaporation cycles for CHASM's SLAM and SIMP modes compared to results from the corresponding PILPS experiments for (TRF a) and HAP (b). A thick solid line is used for SLAM, a thick dashed line for SIMP with an aerodynamic stability correction and a thick dotted line for SIMP without a stability correction (SIMP-A). M69-PILPS simulations are indicated by stars (*) and the simulations of other PILPS models are represented as unmarked thin lines (Desborough, 1999).

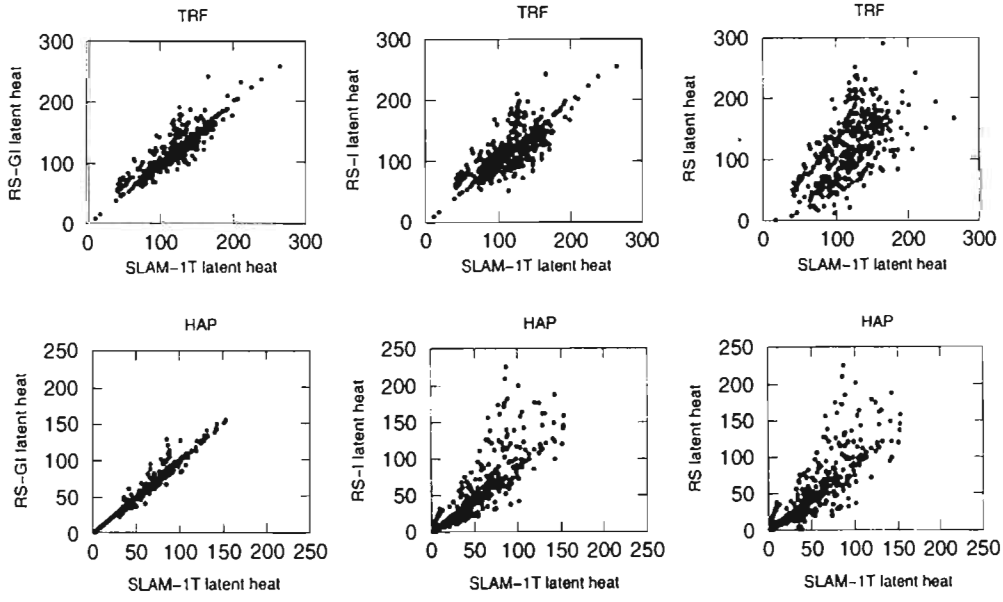

Fig. A15. Daily evaporation for TRF (a) and HAP (b) in CHASM's RS-GI, RS-I and RS calibrated constant surface resistance modes compared to corresponding values in simulations with SLAM-1T (Desborough, 1999).